

TECHNISCHE UNIVERSITÄT MÜNCHEN  
WACKER-Lehrstuhl für Makromolekulare Chemie

# Surface Chemistry of Silicon Nanocrystals: Influence on Properties and Applications

**Arzu Angı**

Vollständiger Abdruck der von der Fakultät für Chemie der Technischen Universität München zur Erlangung des akademischen Grades eines

**Doktors der Naturwissenschaften**

genehmigten Dissertation.

Vorsitzender:

Prof. Dr. Ulrich K. Heiz

Prüfer der Dissertation:

Prof. Dr. Dr. h.c. Bernhard Rieger

Prof. Dr. Tom Nilges

Prof. Dr. Mita Dasog (schriftliche Beurteilung)

Prof. Dr. Klaus Köhler (mündliche Prüfung)

Die Dissertation wurde am 26.06.2018 bei der Technischen Universität München eingereicht und durch die Fakultät für Chemie am 17.07.2018 angenommen.

*“Herhangi bir zorluk önünde kaldığım zaman benim yaptığım iş şudur: Vaziyeti iyice tespit etmek, sonra bu vaziyet karşısında alınacak tedbirin ne olduğuna karar vermek. Akıl ve mantığın halledemeyeceği mesele yoktur.”*

*1924*

*M. Kemal Atatürk*

*“When I encounter with a difficulty, what I do is the following: To analyze and determine the situation thoroughly, and then to decide which measures to be taken under these circumstances. There is no issue that reason and logic cannot overcome.”*

*1924*

*M. Kemal Atatürk*

## Acknowledgements

First and foremost, I am grateful to *Prof. Bernhard Rieger* for giving me the chance to be a part of his group. He granted me unlimited freedom while offering support whenever I needed. I deeply appreciate his style which helped me to develop both scientifically and personally.

I am especially thankful to *Prof. Oded Millo* for his valuable contributions to my research. He played an extremely important role on my PhD project to be successful. I would like to thank *Prof. Jonathan Veinot*, he was always available for discussions related to silicon nanocrystals and gave me important insights. He introduced me to very important people, such as *Prof. Millo* and *Prof. Meldrum*. Many thanks to *Prof. Al Meldrum* for his contributions and kind support on PL dynamics. I would like to thank *Prof. Job Boekhoven* for adopting me into his group, being extremely patient with me and introducing me dissipative self-assembly and biology related concepts.

My PhD projects were all about collaborations. During these projects, I had the chance to work with great people such as *Raphael Grötsch*, *Regina Sinelnikov*, *Marius Loch*, *Simon Pfaehler* and *Hendrik Heenen*. I was privileged to have my friends as my collaboration partners, I would like to thank them all for their valuable contributions and the fun we had together.

I would like to thank all members of WACKER-Chair of Macromolecular Chemistry for the nice working atmosphere. Many thanks to *Dr. Carsten Troll*, *Dr. Sergei Vagin* and *Ms. Annette Bauer* for their friendly support on organizational matters.

I am thankful to all members of *AK Boekhoven* for accepting me as an honorary member. It was always so much fun to meet you for lunch breaks.

I would like to thank all members of our “Nanocrew”, starting from *Frank Deubel* (who brought me in), *Julian Kehrle* (for teaching me everything from scratch including which direction is argon, which one is vacuum), *Tobias Helbich* (for the joy he brings and his valuable support as a lab mate) and *Marc Kloberg* (he is the future!). I especially thank *Ignaz Höhle* for his support during my PhD.

Finally, I would like to thank my brother Argun who shares all with me with his incredible sense of humor, no matter how far away we are. Also, many thanks to my dear parents for guiding us always to the right and the best; believing, understanding and supporting us all the time, giving the best advices possible and having fun with us. We are the luckiest to have you.

## Contents

<b>1</b>	<b>Abstract of the Dissertation.....</b>	<b>1</b>
<b>2</b>	<b>Introduction .....</b>	<b>8</b>
<b>3</b>	<b>Theoretical Background .....</b>	<b>11</b>
<b>3.1</b>	<b>Synthesis of Silicon Nanocrystals.....</b>	<b>11</b>
3.1.1	Physical Methods.....	11
3.1.2	Gas-phase Methods .....	12
3.1.3	Solution-phase Methods .....	13
3.1.4	Solid-state Methods .....	14
<b>3.2</b>	<b>Surface Functionalization of Silicon Nanocrystals.....</b>	<b>17</b>
3.2.1	Surface Functionalization of Halogen-Terminated SiNCs.....	17
3.2.2	Surface Functionalization of Hydride-Terminated SiNCs .....	17
<b>3.3</b>	<b>Properties of Silicon Nanocrystals .....</b>	<b>22</b>
3.3.1	Physical Properties .....	22
3.3.2	Biological Properties .....	26
<b>3.4</b>	<b>Applications of Silicon Nanocrystals .....</b>	<b>28</b>
3.4.1	Sensors.....	28
3.4.2	Solar Cells .....	29
3.4.3	Biomedical Applications .....	31
3.4.4	Light Emitting Diodes .....	32
<b>4</b>	<b>Manuscripts .....</b>	<b>34</b>
<b>4.1</b>	<b>Functionalization of Hydride-Terminated Photoluminescent Silicon Nanocrystals with Organolithium Reagents.....</b>	<b>35</b>
<b>4.2</b>	<b>Photoluminescence through In-Gap States in Phenylacetylene Functionalized Silicon Nanocrystals .....</b>	<b>50</b>
<b>4.3</b>	<b>The Influence of Conjugated Alkynyl(aryl) Surface Groups on the Optical Properties of Silicon Nanocrystals: Photoluminescence through In-Gap States.....</b>	<b>62</b>
<b>4.4</b>	<b>The Influence of Surface Functionalization Methods on the Performance of Silicon Nanocrystal LEDs .....</b>	<b>95</b>
<b>4.5</b>	<b>Dissipative Self-Assembly of Photoluminescent Silicon Nanocrystals.....</b>	<b>109</b>
<b>5</b>	<b>Summary and Outlook .....</b>	<b>141</b>
	<b>Bibliography.....</b>	<b>144</b>

## Table of Abbreviations

4-DDB	4-decylbenzene diazonium tetrafluoroborate
AIBN	azobisisobutyronitrile
ATP	adenosine triphosphate
BP	benzoyl peroxide (BP).
CB	conduction band
DBTJ	double-barrier tunnel junction
DLS	dynamic light scattering
DNT	dinitrotoluene
DSA	dissipative self-assembly
EBL	electron blocking layer
EDC	1-ethyl-3-(3-dimethylaminopropyl) carbodiimide
EL	electroluminescence
EQE	external quantum efficiency
ETL	hole transport layer
FRET	Förster resonance energy transfer
FTIR	Fourier-transform infrared
FWHM	full-width at half maximum
HBL	hole blocking layer
HF	hydrofluoric acid
HOMO	highest occupied molecular orbital
HPLC	high-pressure liquid chromatography
HS	hydrosilylation
HSQ	hydrogen silsesquioxane
HTL	hole transport layer
IQE	internal quantum efficiency

IR	infrared
ITO	indium tin oxide
LED	light emitting diode
LUMO	lowest unoccupied molecular orbital
MEG	multiple excitation generation
MES	2-(n-morpholino)ethanesulfonic acid
NHS	n-hydroxysuccinimide
nm	nanometer
OLR	organolithium reagents
P3HT	poly(3-hexylthiophene)
PBS	phosphate-buffered saline
PEDOT:PSS	poly(3,4-ethylenedioxythiophene)–poly(styrenesulfonate)
PL	photoluminescence
PolyTPD	poly[N,N'-bis(4-butylphenyl)-N,N'-bisphenylbenzidine]
QD	quantum dot
QY	quantum yield
SEM	scanning electron microscope
SiNC	silicon nanocrystal
STM	scanning tunneling microscopy
STS	scanning tunneling spectroscopy
TEM	transmission electron microscopy
TEOS	tetraethyl orthosilicate
TGA	thermogravimetric analysis
TNT	trinitrotoluene
TOAB	tetraoctylammoniumbromide
UV/VIS	ultraviolet/visible
VB	valence band
WF	work function

# 1 Abstract of the Dissertation

Silicon nanocrystals (SiNCs) gained significant attention in recent years due to their intriguing properties that are not shown by their bulk counterparts.<sup>1</sup> When the dimensions of SiNCs are reduced below the Bohr radius of an exciton in silicon ( $\sim 4.5$  nm),<sup>2</sup> they exhibit photoluminescence (PL) at energies tunable by the SiNC size<sup>3,4</sup> and surface chemistry.<sup>5-7</sup> In addition, SiNCs offer several advantages such as the elemental abundance of silicon, bio-compatibility<sup>8</sup> and low-toxicity.<sup>9</sup> Therefore, SiNCs are a promising material for several applications including light emitting diodes (LEDs),<sup>10</sup> solar cells,<sup>11</sup> sensors<sup>12</sup> and photoluminescent biomarkers.<sup>8</sup>

Most of the common synthetic routes to prepare SiNCs result in a hydride-terminated surface.<sup>13</sup> The hydride-terminated surface is prone to rapid oxidation under ambient conditions, which influences the chemical and optoelectronic properties of SiNCs. Therefore, SiNCs are commonly functionalized with long chain alkyl moieties through hydrosilylation reaction to protect their surface from oxidation and render them dispersible in various solvents.<sup>14,15</sup> Despite being successful to inhibit oxidation, these surface groups have limited utility for controlling the optical properties of SiNCs.<sup>16,17</sup> Moreover, long chain alkyl surface groups form insulating layers, which may hinder the charge transport properties of SiNCs and result in lower efficiencies in optoelectronic applications.<sup>18,19</sup> In this regard, aromatic molecules (*i.e.*, aryl, alkynyl(aryl)) are a promising alternative class of surface groups. These molecules, when in direct conjugation with the core of SiNCs, are expected to facilitate charge transfer to and from SiNCs.<sup>20</sup> However, due to the reaction mechanism of the hydrosilylation reaction, which involves the addition of a surface Si – H bond to an unsaturated C – C bond of an alkene or alkyne molecule, aryl and alkynyl(aryl) molecules cannot be directly grafted to the SiNCs' surface *via* this method (Figure 1, left).<sup>21</sup> Considering the limitations of the hydrosilylation reaction, developing alternative methods

to decorate the surface of SiNCs with functional surface groups, which have the potential to tune SiNCs' properties, is an important target.

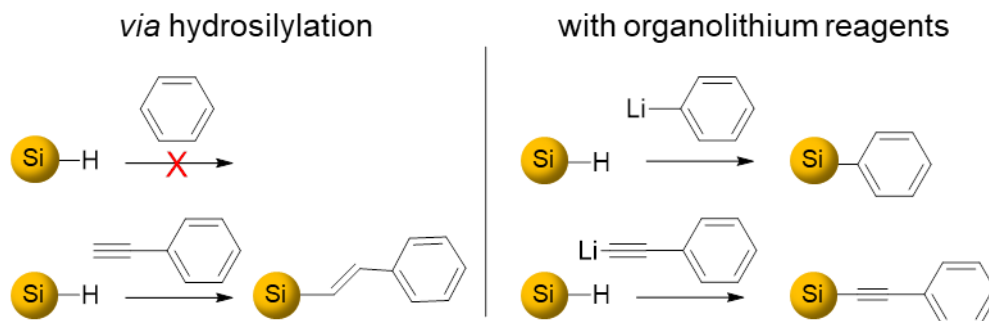


**Figure 1.** Reactions of aryl and alkynyl(aryl) molecules with SiNCs *via* hydrosilylation (left) and with lithiated compounds (right).

Reactivity of organometallic reagents towards silanes to form Si – C bonds *via* Si – Si bond cleavage has long been known.<sup>22</sup> Similarly, organolithium and Grignard reagents were shown to react with hydride-terminated porous silicon, leading to functionalization of the surface with alkyl, aryl and alkynyl(aryl) groups.<sup>23,24</sup> The proposed reaction mechanism involves the cleavage of Si – Si bonds due to the attack of the organolithium reagent, followed by the formation of neighboring Si – C bonds and Si – Li surface species. The reactive Si – Li group can be quenched by electrophiles, such as protons.<sup>23</sup> With this motivation, we chose organolithium and Grignard reagents to react with photoluminescent SiNCs ( $d \sim 3$  nm) to establish an alternative surface functionalization route. As a result, we achieved the efficient functionalization of hydride-terminated SiNCs with aryl (*i.e.*, phenyl) and alkynyl(aryl) (*i.e.*, phenylacetylene) molecules for the first time (Figure 1, right). Even though the surface chemistry of SiNCs is expected to be different than molecular silane chemistry due to large steric hindrance of the surface, this result showed that organolithium reagents can react with silicon atoms on the SiNC surface in a fashion similar to the case of disilanes and porous silicon. These results were summarized in the publication “Functionalization of Hydride-Terminated Photoluminescent Silicon Nanocrystals with Organolithium Reagents” published in *Chemistry - A European Journal*.<sup>25</sup>

Interestingly, we observed that the PL maximum of phenylacetylene functionalized SiNCs red-shifted by  $\sim 50$  nm with respect to their hexyl and phenyl counterparts (Figure 2).



Elucidating the mechanism leading to this phenomenon is of great interest since it may provide insights into the influence of conjugated surface groups on the SiNC electronic structure and optoelectronic properties. Understanding this relationship is of crucial importance in order to tune the optoelectronic response of SiNCs for targeted high-efficiency applications.

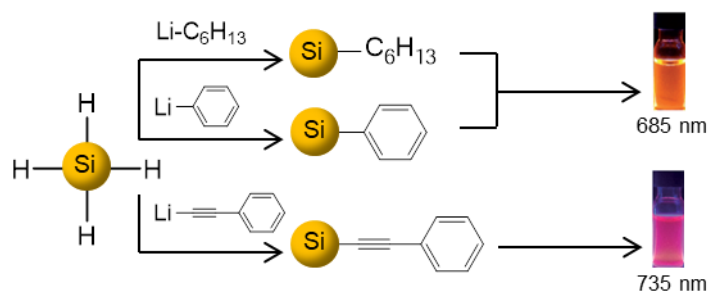


**Figure 2.** The influence of different surface groups on the PL maximum of SiNCs. Phenylacetylene surface groups caused a red shift in PL for ~50 nm with respect to hexyl and phenyl counterparts.<sup>26</sup> Adopted from reference 26 with permission from The Royal Society of Chemistry.

With the aim of understanding the influence of phenylacetylene surface groups on the PL emission of SiNCs, we performed an analysis combining optical spectroscopic methods with scanning tunneling microscopy/spectroscopy (STM/STS). This combination is crucial, as optical measurements alone cannot unambiguously determine the initial and final states associated with optical transitions. As a result, the influence of the surface groups on the electronic structure of SiNCs cannot be deduced from optical spectroscopic methods; utilization of complementary techniques is required.<sup>3</sup> STS provides information regarding the electronic density of states (DOS) by mapping the conduction band (CB) and valence band (VB) states independently. Therefore, the single-particle (rather than excitonic) band gap can be evaluated directly.<sup>27</sup> We studied hexyl, phenyl and phenylacetylene functionalized SiNCs *via* STM/STS in collaboration with Prof. Oded Millo from The Hebrew University of Jerusalem. Our analysis on functionalized SiNCs showed the presence of a new state within the band gap of SiNCs, only with phenylacetylene surface groups. Therefore, we attributed the observed PL shift for phenylacetylene functionalized SiNCs to a transition *via* this in-gap state, which reduced the effective band gap for recombination. These observations showed that organolithium reagents, reacting with the

SiNC surface in a fashion resembling to molecular chemistry, can influence optical properties of SiNCs as the surface silicon atoms are associated with a band gap structure. To the best of our knowledge, this is the first time that an in-gap state, intentionally introduced *via* surface functionalization, has been observed by STS in SiNCs. These findings were published in *Nanoscale* with the title “Photoluminescence through In-Gap States in Phenylacetylene Functionalized Silicon Nanocrystals” in 2016.<sup>26</sup>

Upon observing the presence of in-gap states with phenylacetylene surface groups, new questions arose: (1) Can other alkynyl(aryl) molecules also induce the formation of the in-gap states? (2) Can this principle be used to tune the PL maximum of SiNCs? (3) Why do only alkynyl(aryl) surface groups induce the formation of in-gap states while directly grafted aryl groups have no apparent impact? With the aim of answering these questions, we prepared and characterized SiNCs functionalized with several alkynyl(aryl) molecules such as phenylacetylene, 2-ethynyl naphthalene and 2-ethynyl-5-hexylthiophene. We observed that PL emission could be tuned between 685-800 nm with these surface groups. No change in PL maximum was observed with their aryl counterparts (*e.g.*, phenyl, naphthalene and 2-hexylthiophene). Importantly, tunneling spectra showed the presence of in-gap states only for SiNCs functionalized with alkynyl(aryl) groups, which induced a red-shift in PL.

To understand the underlying principles behind these observations, *ab-initio* calculations were performed in collaboration with Hendrik Hennen from Prof Reuter’s group. It is important to note that the modelling of SiNCs with large conjugated surface groups is highly challenging and computationally impractical. Therefore, our analysis was performed on model Si<sub>10</sub>H<sub>16</sub>, Si<sub>14</sub>H<sub>20</sub> and Si<sub>26</sub>H<sub>32</sub> diamond structures. The results suggested that the in-gap states originate as interface states from excited electronic antibonding ( $\pi^*$ ) states located on the alkynyl bond ( $-\text{Si}-\text{C}\equiv\text{C}$ ) which strongly couple to the SiNC. These outcomes provided a likely mechanism for the PL shifts, which were observed only with alkynyl(aryl) surface groups and not with their aryl counterparts: Excitation of the SiNC core states is followed by a non-radiative relaxation to a bright  $\pi^*$  in-gap state, which are conjugated with the alkynyl(aryl) moiety. A subsequent transition to the ground state then accounts for the red-shifted PL (Figure 3). The presented results demonstrate the possibility

of utilizing alkynyl(aryl) molecules to manipulate the electronic structure and the optical properties of SiNCs systematically, which may enhance the performance of SiNCs in semiconductor devices. These outcomes resulted in a further publication in *Nanotechnology* in 2018 entitled: “The Influence of Conjugated Alkynyl(aryl) Surface Groups on the Optical Properties of Silicon Nanocrystals: Photoluminescence through In-Gap States”.<sup>28</sup>

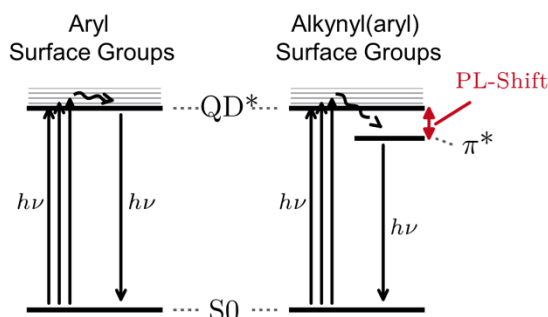


**Figure 3.** Schematic depiction of the mechanism of absorption/emission for aryl (left) and alkynyl(aryl) (right) functionalized SiNCs. Absorption of a photon ( $h\nu$ ) leads to a transition from the ground state  $S_0$  to the excited state  $QD^*$ . In the case of aryl groups, following deexcitation occurs from the  $QD^*$  state. With alkynyl(aryl) surface groups, first a non-radiative relaxation (wiggly lines) to the alkynyl(aryl) antibonding state ( $\pi^*$ ) takes place, followed by recombination from this  $\pi^*$  state.<sup>28</sup> Reproduced from ref. 28 with permission.

One of the important areas of application for SiNCs is hybrid organic/inorganic LEDs. Several groups demonstrated SiNC-based LEDs (Si-LEDs) with various device architectures to achieve higher efficiencies. However, despite the undeniable impact of the surface chemistry on the SiNC properties, the influence of different surface characteristics on Si-LED efficiency has not been studied in detail. Almost in every case, SiNCs functionalized with long alkyl chains *via* thermally initiated hydrosilylation were utilized.<sup>29–31</sup> Thermal hydrosilylation poses disadvantages such as oligomerization of surface groups, which yields uncontrolled surface coverage.<sup>15</sup> In contrast, surface functionalization with organolithium reagents ensure monolayer coverage due to its reaction mechanism. Besides, Si – H moieties on the surface of SiNCs are not consumed in this reaction, which could act as a “gate” for charge transfer to and from SiNCs. Therefore, we wanted to assess the influence of surface characteristics obtained *via* hydrosilylation and with organolithium reagents on the efficiency of Si-LEDs. For this purpose, Si-LEDs were built with hexyl functionalized SiNCs prepared *via* each method and fully characterized in

collaboration with Marius Loch from Prof. Lugli's chair. Our analysis showed that devices utilizing SiNCs functionalized with organolithium reagents consistently exhibited lower turn-on voltages, higher luminance and external quantum efficiencies compared to those obtained from the hydrosilylation method (Figure 4). These improvements were attributed to the lower density and monolayer surface coverage of the SiNCs obtained by the organolithium reagents method, as well as their higher absolute quantum yield based on detailed characterization of these SiNCs. Our results published in *Nanoscale* in 2018 with the title "The Influence of Surface Functionalization Methods on the Performance of Silicon Nanocrystal LEDs" underline, once more, the tremendous potential of utilizing surface chemistry to influence SiNC properties and concomitantly the efficiencies of SiNC-based devices.<sup>32</sup>

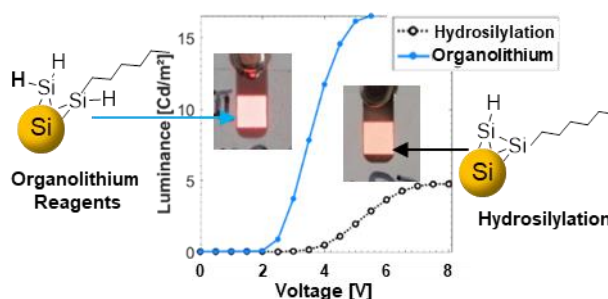


**Figure 4.** Luminance vs voltage trends for Si-LEDs built with SiNCs functionalized *via* hydrosilylation and organolithium reagents. Photographs of functional devices are given in the inset.<sup>32</sup> Adopted from ref. 32 with permission from The Royal Society of Chemistry.

SiNCs are promising candidates for a diverse range of applications in part due to their tunable PL, bio-compatibility and low toxicity. However, the explored material properties in these applications are static and do not evolve over time or adapt to changes in the surroundings.<sup>33</sup> Autonomously evolving materials are desired, especially in the context of biomaterials. In dissipative supramolecular materials, self-assembly of precursors is driven by a chemical reaction network that irreversibly consumes a chemical fuel. Like living materials, the properties of the emerging structures are controlled by the kinetics of the underlying chemical reaction network.<sup>33,34</sup> If the transient properties obtained through dissipative self-assembly (DSA) can be coupled to the intrinsic characteristics of SiNCs, this could pave the way to novel biomedical applications. With this motivation, we tested

the utility of SiNCs in a DSA system in collaboration with Raphael Grötsch from Prof. Boekhoven's group. We successfully induced DSA of SiNCs by adding a chemical fuel, which was followed by disassembly as the system ran out of the fuel (Figure 5). We could control the lifetime of the assemblies by the amount of fuel added and induce the assembly-disassembly process multiple times on the same batch of SiNCs. We also demonstrated that this platform could be used to control the delayed uptake of the nanocrystals by mammalian cells. This principle can potentially be utilized to achieve time-delayed drug delivery systems, which simultaneously offer the possibility for bioimaging, if the surface of SiNCs is loaded with therapeutics. The manuscript based on these results is currently under peer-review to be published in *Angewandte Chemie Int. Ed.*

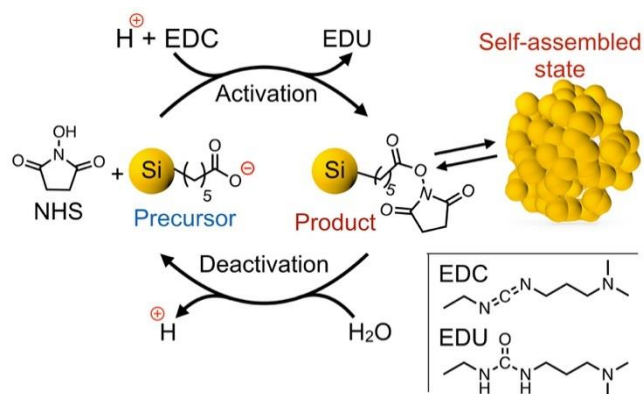


**Figure 5.** Schematic representation of the chemical reaction network. Carboxylate surface groups on the SiNCs reacted with EDC and NHS to form a transient NHS ester. The loss of surface charges induced the temporary self-assembly of SiNCs.

## 2 Introduction

Nanotechnology has gained significant attention since the 1960's, when its concepts were first discussed.<sup>35</sup> The discovery of revolutionary nanomaterials such as fullerenes,<sup>36</sup> carbon nanotubes<sup>37</sup> and colloidal nanoparticles<sup>38,39</sup> completely changed the way material properties are described. This is because properties of materials in the nanoscale are not solely determined by their composition but also by their size.<sup>40</sup> The quantum confinement effect is one of the most prominent phenomena that explains the size-dependent properties of nanomaterials.<sup>41</sup> In addition to size, the surface chemistry of nanomaterials also plays an important role in determining the properties of nanomaterials, due to their high surface to volume ratio.<sup>42</sup>

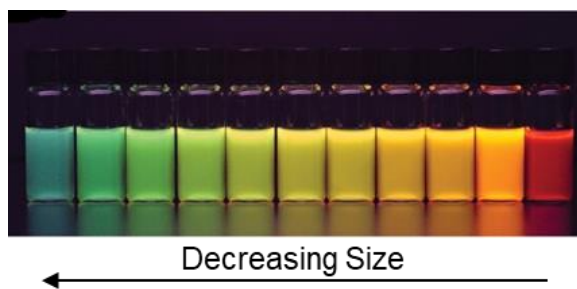


**Figure 6.** Fluorescence image of vials containing QDs of decreasing size (right to left) showing emissions covering the entire visible-to-near-IR wavelength range. Reprinted from ref. 43 with permission.

Semiconductor nanoparticles, or quantum dots (QDs), in the size regime of a few nanometers, constitute an important class of nanomaterials. They display size-dependent optical absorption and emission with high quantum yield (QY).<sup>43</sup> These properties result from confinement of charge carriers into nanoscale physical dimensions of the particles. As a result, quantum confinement leads to disruption of the continuous energy bands of a bulk material and formation of discrete energy levels in all confined dimensions. When the size of a QD is reduced to approach the Bohr radius of an electrostatically bound electron-hole

pair, the quantum confinement effect becomes more prominent and an increase in band gap is observed while the absorption and emission blue-shift.<sup>39,44,45</sup> This phenomenon makes it possible to prepare QDs with emissions across the visible to near-IR range of the electromagnetic spectrum, as a function of their size (Figure 6).<sup>43,46</sup>

Size-dependent band gap of QDs was first demonstrated by the pioneering work of Louis Brus and his co-workers in the early 1980's.<sup>38,39</sup> Following this, tremendous research efforts, both in experimental and theoretical fields, have focused on these materials with the aim of understanding their structures and properties. The most extensively studied QDs are group II–VI (*e.g.*, CdS, CdSe, CdTe), III–V (*e.g.*, InP, InAs, GaAs), and IV–VI (*e.g.*, PbS, PbSe) compounds, mostly due to facile synthetic routes developed, which offer high purity QD in tangible amounts with narrow size distributions.<sup>47</sup> Based on their unique optoelectronic properties, their utility in several applications such as solar cells,<sup>48</sup> LEDs,<sup>49</sup> sensors,<sup>50,51</sup> bioimaging,<sup>43,52</sup> lasing<sup>53</sup> and liquid crystals<sup>54</sup> were investigated. Despite their enormous potential, the main drawback of these materials is the presence of toxic heavy metals. Legislations limiting or banning the use of toxic heavy metals in consumer products hamper their development.<sup>1,55</sup> Therefore, the emphasis was shifted to the development of non-toxic and abundant alternatives.

Silicon, despite being the workhorse element of the microelectronics industry, is an indirect semiconductor in its bulk form which has poor optical utility.<sup>56</sup> However, the discovery of efficient room-temperature PL from porous silicon by Canham revealed nanostructured silicon as a promising alternative to traditional QDs.<sup>57</sup> SiNCs offer several advantages such as elemental abundance of silicon, size- and surface-tunable PL, biocompatibility, low-toxicity, well-established surface chemistry and compatibility with existing electronics industry.<sup>5,9,58</sup> In the last two decades, significant progress in terms of synthesis and characterization of SiNCs was achieved.<sup>13</sup> Several prototype applications of SiNCs have been demonstrated including in photovoltaics,<sup>59</sup> LEDs,<sup>10</sup> sensors,<sup>12</sup> and bioimaging.<sup>60</sup> However, despite the vast-amount of research efforts focused on SiNCs, crucial issues such as the influence of surface chemistry on optical response of SiNCs are still not completely understood.<sup>42</sup> A better understanding of fundamental mechanisms is

necessary to enable tailoring of SiNCs' properties and to improve their performance in future applications.



## 3 Theoretical Background

This chapter provides a summary of synthesis and surface functionalization methods for SiNCs. Physical and biological properties of SiNCs are reviewed and an overview on their applications is given.

### 3.1 Synthesis of Silicon Nanocrystals

Numerous methods have been developed for the synthesis of SiNCs with different size, shape and surface characteristics. These methods can be classified as physical, gas-phase, solution-phase and solid-state methods.

#### 3.1.1 Physical Methods

Several top-down approaches were employed for the preparation of SiNCs including ball milling, etching of bulk silicon, laser ablation and ion implantation. Švrček *et al.* described the synthesis of SiNCs with sizes smaller than 10 nm *via* ball milling. Despite yielding tangible amounts, the obtained SiNCs exhibited only weak PL emission, which was attributed to non-radiative recombination pathways by amorphous defects formed during the milling process.<sup>61</sup> By utilizing an improved procedure, which combines ball milling with simultaneous surface functionalization, Heintz *et al.* reported the synthesis of SiNCs ( $d < 4$  nm) that exhibited blue PL with high quantum yields.<sup>62</sup> The main drawbacks of this method are the poor control over size and its high cost, since it involves crushing high quality silicon wafers.<sup>63</sup>

Electrochemical etching of bulk silicon in HF electrolytes yields porous silicon which emits PL under UV irradiation. This was the method through which efficient emission from silicon was achieved for the first time by Canham.<sup>57</sup> Sailor *et al.* showed for the first time that the ultrasonication of porous silicon yields luminescent dispersions of SiNCs.<sup>64</sup> SiNCs

with size-tunable emission from blue to red were obtained by controlled etching of silicon wafers<sup>65</sup> and crystalline silicon powders.<sup>66</sup> The main shortcoming of this method is the low yield of SiNCs.

In the laser ablation technique, silicon nanoclusters are obtained by etching silicon wafers or rods by a laser beam in a vacuum chamber equipped with a helium flow. Collisions between the helium carrier gas and the silicon plasma cool down the particles and yield them as heterogeneous nucleation sites.<sup>67,68</sup> Photoluminescent, crystalline silicon nanoclusters of different sizes between 1 and 5 nm were obtained by controlling experimental parameters. Size selection was achieved by relying on different time-of-flight of differently sized clusters.<sup>68</sup> Despite these advancements, the lack of widespread use of this technique is due to the fact that it does not allow direct control over particle size.<sup>63</sup>

Ion implantation involves bombarding of silicon ions into a host material and subsequent annealing to form Si nanoclusters. Photoluminescent SiNCs embedded in silica glass<sup>69</sup> and SiO<sub>2</sub><sup>70,71</sup> were synthesized *via* implantation of Si<sup>+</sup> ions. These materials offer an advantageous platform for the study of the optical properties of the SiNCs, as they are embedded in a host material and thus protected from surface oxidation.<sup>69</sup> LEDs utilizing SiNCs embedded in SiO<sub>2</sub> synthesized *via* ion implantation were demonstrated.<sup>72</sup>

### 3.1.2 Gas-phase Methods

Gas-phase methods offer size tunability and narrower size distributions while yielding surface passivated SiNCs. The most prominent gas phase methods can be listed as laser pyrolysis and plasma synthesis.

Laser pyrolysis is one of the most powerful tools to synthesize free-standing SiNCs. In this method, SiNCs are prepared *via* decomposition of silanes under inert atmosphere which is induced by high temperatures achieved by a laser beam. Initially, the obtained SiNCs showed strong PL only after etching with HF, which resulted in very low yields. Li *et al.* improved this technique by synthesizing larger Si nanoclusters *via* CO<sub>2</sub> laser in an aerosol reactor, followed by controlled etching with HF and HNO<sub>3</sub> mixture to achieve hourly yield up to 200 mg.<sup>73,74</sup> Controlled etching of SiNCs resulted in size-tunable emission covering the whole visible spectrum with QY in the range of 2 – 15%.<sup>73,75</sup>

In the non-thermal plasma synthesis of SiNCs, hot electrons in the plasma lead to an effective dissociation of silicon precursors, such as silanes.<sup>76,77</sup> As a result, unsaturated silane clusters ( $\text{Si}_n\text{H}_m$ ) having positive electron affinities are yielded, which easily attract electrons to form negative ions.<sup>78</sup> These negative clusters are electrostatically trapped in the plasma and act as seeds for particle nucleation.<sup>77</sup> One of the advantages of the plasma synthesis is the fact that the resulting SiNCs are negatively charged in plasma, which prevents agglomeration and reduces their size distribution.<sup>77</sup> Kortshagen and co-workers were able to prepare SiNCs exhibiting significantly high QY up to 60% by utilizing plasma synthesis.<sup>79</sup>

### 3.1.3 Solution-phase Methods

There are several well-established solution-phase methods to synthesize free-standing SiNCs in good yields (Figure 7). Compatibility of these methods with conventional bench-top chemical techniques is advantageous. However, the main disadvantage is the lack of tunability of the emission wavelength, as these solution-phase techniques yield SiNCs that exhibit only blue PL, irrespective of their size.<sup>42</sup>

Synthesis of SiNCs *via* reduction of silane precursors was first demonstrated by Heath *et al.* in 1992.<sup>80</sup> In this method, simultaneous reduction of  $\text{SiCl}_4$  and  $\text{RSiCl}_3$  ( $\text{R}=\text{H}$  or *n*-octyl) by sodium at high pressure (>100 atm) and temperature (385 °C) conditions for 3 to 7 days yielded SiNCs. The synthesis with trichlorosilane yielded a highly polydisperse sample, whereas with octyltrichlorosilane the size distribution was limited to  $5.5 \pm 2.5$  nm, as octyl groups act as a surface capping agent.<sup>80</sup> Several variations of this method were reported, including the use of sodium naphthalene ( $\text{NaC}_{10}\text{H}_8$ ) to reduce  $\text{SiCl}_4$ <sup>81</sup> or reducing tetraethylorthosilicate (TEOS) with sodium.<sup>82</sup> To achieve the synthesis of SiNCs with narrow size distribution, surfactant molecules such as tetraoctylammoniumbromide (TOAB) were utilized as demonstrated by Wilcoxon *et al.*<sup>83</sup> and Tilley *et al.*<sup>84</sup> Despite being successful in reducing the size distribution, this strategy suffers from the difficulty to remove the surfactants from the reaction mixture.

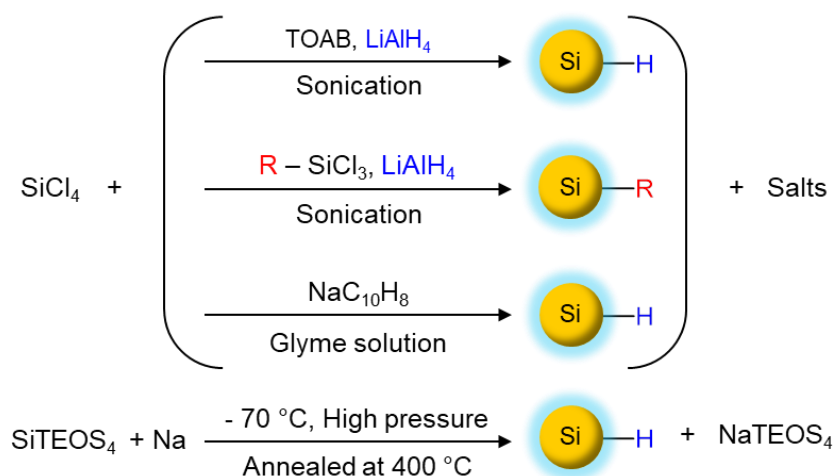


**Figure 7.** Summary of synthesis routes through precursor reduction in solution.<sup>13</sup> Adopted from ref. 13 with permission from The Royal Society of Chemistry.

Zintl salts ( $\text{ASi}$ ;  $\text{A} = \text{Na}, \text{K}, \text{Mg}$ ) obtained from the high temperature reaction of metals with elemental silicon have been shown to yield SiNCs by reacting with silicon halides,<sup>85–89</sup> bromine<sup>90</sup> or ammonium bromide<sup>91</sup> in glyme solutions. These synthetic routes yield SiNCs with halogen-terminated surfaces (Figure 8).

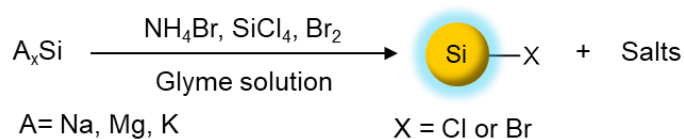


**Figure 8.** Synthetic routes based on Zintl salts for the preparation of SiNCs.<sup>13</sup> Adopted from ref. 13 with permission from The Royal Society of Chemistry.

### 3.1.4 Solid-state Methods

#### Disproportionation of Silicon Rich Oxides

Thermal annealing of silicon rich oxide precursors ( $\text{SiO}_x$ ,  $x < 2$ ) at elevated temperatures yields SiNCs embedded in a  $\text{SiO}_2$  matrix through a disproportionation reaction. Liu *et al.* demonstrated the synthesis of free-standing SiNCs by annealing commercially available amorphous  $\text{SiO}_x$  ( $x < 2$ ) powder at elevated temperatures (900 –

1000 °C) under an inert atmosphere. Free-standing, hydride-terminated SiNCs were obtained upon etching the oxide layer with HF.<sup>92,93</sup>

Veinot and co-workers developed an improved variation of this approach utilizing thermal disproportionation of commercially available hydrogen silsesquioxane (HSQ).<sup>94</sup> HSQ ( $\text{HSiO}_{1.5}$ )<sub>n</sub> can also be synthesized in large quantities and high purity by controlled hydrolysis of  $\text{HSiCl}_3$ .<sup>95</sup> Although HSQ utilized for SiNC synthesis is mistakenly described as a cage-like molecule with the formula  $\text{H}_8\text{Si}_8\text{O}_{12}$  in the literature, it is important to note that the polymeric form was used in all cases.<sup>96</sup>

In this method, thermolysis of HSQ at temperatures above 1100 °C under a slightly reducing atmosphere (95%  $\text{N}_2$ , 5%  $\text{H}_2$ ) yields SiNCs in a  $\text{SiO}_2$  matrix.<sup>94</sup> During this process, rearrangement of the HSQ network and formation of  $\text{SiH}_4$  take place at temperatures between 250 – 350 °C. Between 350 – 450 °C, additional thermal dissociation of Si – H bonds leads the formation of elemental Si (Figure 9).<sup>94,97</sup>

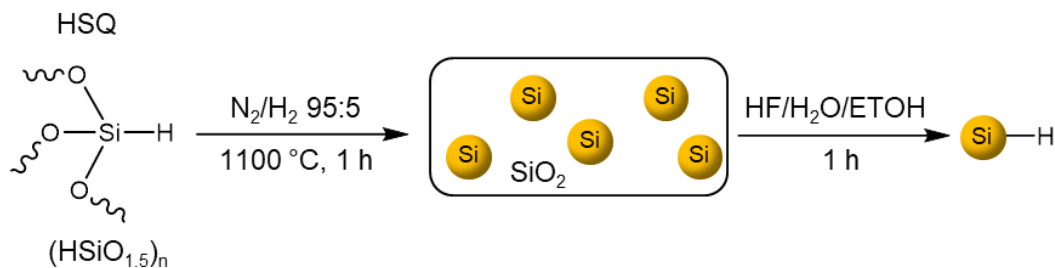


**Figure 9.** Synthesis of SiNCs with an average diameter of 3 nm *via* the thermal disproportion of HSQ and subsequent liberation to obtain freestanding, hydride-terminated SiNCs by etching with HF.

One of the advantages of this approach is that it offers control over size<sup>98</sup> and shape<sup>99</sup> of the resulting SiNCs. The size of SiNCs could be tuned between  $3 \pm 0.3$  nm and  $13 \pm 2.4$  nm, at reaction temperatures 1000 and 1350 °C, respectively.<sup>98</sup> Yang *et al.* showed that post annealing of SiNC/ $\text{SiO}_2$  composite at high temperatures yield SiNCs in cubic geometries.<sup>99</sup>

After thermal disproportionation of HSQ, hydride-terminated SiNCs are obtained by etching this composite with an ethanolic HF solution followed by extraction into toluene. Resulting SiNCs show size-dependent emission between yellow to NIR (600 – 1060 nm),<sup>98</sup> whereas blue or green emission could not be achieved without further surface

functionalization. The SiNCs studied in this work were synthesized through thermal disproportionation of HSQ.

The mechanism of etching the  $\text{SiO}_2$  matrix to liberate hydride-terminated, free-standing SiNCs was investigated. The oxide layer contains species such as silanol ( $\text{Si-OH}$ ) and bridged oxides ( $\text{Si-O-Si}$ ). Due to high electronegativity difference between silicon and oxygen atoms, the nature of  $\text{Si-O}$  bond is highly ionic. Therefore, partially positively polarized silicon attracts nucleophilic attack from  $\text{HF}$ , yielding a  $\text{Si-F}$  bond. Acidic conditions facilitate this reaction by protonating oxygen atoms, thus making them better leaving groups.<sup>100,101</sup> Upon oxide removal, a fluorine terminated silicon surface is formed. The highly ionic nature of the  $\text{Si-F}$  bond polarizes the silicon back-bond allowing the insertion of  $\text{HF}$  into the  $\text{Si-Si}$  bond. It leads to fluorination of the surface silicon and hydrogenation of the second-layer silicon. This sequence is completed with the removal of the surface silicon atom as  $\text{SiF}_4$ , and formation of the hydride-terminated surface as the kinetic product (Figure 10).<sup>102</sup> Fluorine terminated surface would be expected to be more stable based on the fact that the  $\text{Si-F}$  bond strength (138.4 kcal/mol) is much higher than that of  $\text{Si-H}$  (80.4 kcal/mol). This indicates that kinetic, rather than thermodynamic conditions, are responsible for hydride passivation of the silicon surface.<sup>103</sup>

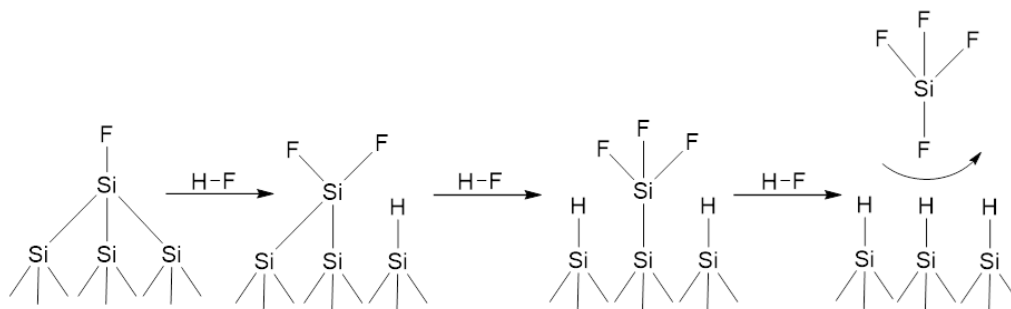


**Figure 10.** Suggested mechanism for hydride-termination of silicon surface upon  $\text{HF}$  etching.<sup>102</sup>

## 3.2 Surface Functionalization of Silicon Nanocrystals

The surface of SiNCs is prone to rapid oxidation under ambient conditions, which influences their chemical and optical properties.<sup>104</sup> Therefore, SiNC surfaces are commonly passivated with organic groups through stable covalent bonds. Functionalization with surface groups having different steric properties and polarities is also utilized to render SiNCs dispersible in various solvents. Optical and electronic properties of SiNCs can be tuned by controlling their surface chemistry.<sup>5,105</sup> Thus, functionalization of SiNCs with proper surface groups is crucial to facilitate their utilization in targeted applications.

Most of the surface functionalization methods of SiNCs were built on the in-depth knowledge of surface chemistry on bulk and porous silicon as demonstrated by Chidsey,<sup>106</sup> Buriak<sup>21</sup> and Sailor,<sup>23,24</sup> among others.

### 3.2.1 Surface Functionalization of Halogen-Terminated SiNCs

Synthetic methods involving Zintl salts yield SiNCs with reactive halogen-terminated surfaces.<sup>81,85,86,88</sup> Owing to the strong electrophilicity of the Si – X bond (Si – Cl, Si – Br), nucleophilic substitution reactions with organometallic compounds<sup>86,87</sup> and alcohols<sup>107</sup> could be demonstrated. Si – O bonds form when alcohols react with the halogen-terminated SiNC surface.<sup>107</sup> Stable Si – C bonds form when these SiNCs are reacted with organolithium and Grignard reagents.<sup>86,87</sup>

### 3.2.2 Surface Functionalization of Hydride-Terminated SiNCs

Hydrosilylation is, without a doubt, the most employed method to functionalize hydride-terminated SiNCs through stable Si – C bonds. This reaction can be initiated by

UV/white light irradiation, at elevated temperatures, with radical initiators, metal catalysts or Lewis acids.

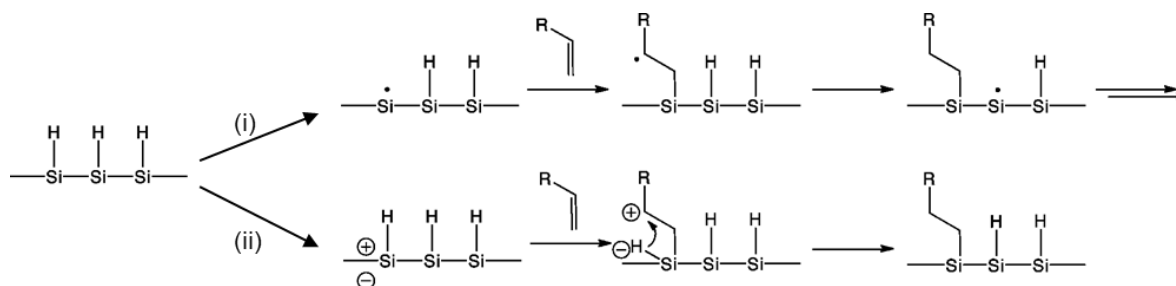


**Figure 11.** Accepted reaction mechanisms for hydrosilylation reaction: i) free radical mechanism initiated thermally or in the presence of radical initiators. ii) Exciton mediated mechanism for nanostructured silicon surfaces under photochemical conditions.<sup>108</sup> Adapted with permission from ref. 108. Copyright 2011 American Chemical Society.

### Photo-Initiated Hydrosilylation

Hydrosilylation can be initiated by UV or white light irradiation at room temperature. In the case for nanostructured silicon an excitonic mechanism is proposed in which an unbound exciton induced by light absorption results in a positive surface charge (Figure 11, ii).<sup>109</sup> This charged surface reacts with an alkene to form a Si – C bond, generating a neighboring carbocation. The carbocation can abstract a hydride from an adjacent Si – H group, which yields a covalently bound alkyl group on the surface.<sup>109</sup> Size-dependent reactivity of this reaction supports this mechanism, since SiNCs larger than 5 nm are inefficient.<sup>108</sup> Besides, the energy of white light would not be enough to induce the homolytic cleavage of Si – H bonds to start the radical initiated hydrosilylation.<sup>110</sup> Interestingly, SiNCs functionalized using photochemical hydrosilylation showed higher QYs compared to thermal hydrosilylation.<sup>111</sup>

### Thermally Initiated Hydrosilylation

For thermally initiated hydrosilylation reactions a radical mechanism is proposed (Figure 11, i). Si – H bonds are homolytically cleaved at elevated temperatures ( $T > 150\text{ }^{\circ}\text{C}$ ) to yield surface silicon radicals. These radicals react with the unsaturated terminal C – C



bonds of alkenes or alkynes. Once initiated, it is suggested that the reaction propagates *via* a surface chain reaction similar to that proposed for bulk systems.<sup>15,112</sup> Thermally initiated hydrosilylation is used commonly to functionalize SiNCs due to its simplicity and high degree of surface coverage, which helps protecting the SiNCs against oxidation. However, due to the required elevated reaction temperatures, only the molecules with high boiling points (thus, longer chain alkyls) can be grafted to the SiNC surface. In addition, oligomerization of unsaturated molecules which yields undefined multilayer surface coverage was also reported.<sup>15</sup> These surface groups may form an insulating barrier and be disadvantageous for optoelectronic applications by hindering charge transport.<sup>18</sup>

### **Hydrosilylation with Radical Initiators**

Hydrosilylation can also be initiated with traditional radical initiators such as azobisisobutyronitrile (AIBN) and benzoyl peroxide (BP).<sup>14</sup> These reactions take place at the decomposition temperatures of the initiators (60 °C for AIBN and 75 °C for BP). Therefore, the range of possible surface groups increases.<sup>14</sup>

Room temperature hydrosilylation with diazonium salts as initiators was demonstrated by Höhlein *et al.* Efficient surface functionalization was achieved in short reaction times (2 hours) with diverse surface group tolerance, with the exception of molecules containing acidic protons such as alcohols or amines.<sup>113</sup> In a follow up work, diaryliodonium salts were also shown as efficient initiators for hydrosilylation reaction. Interestingly, in this study hydride-terminated SiNCs were shown to act as co-initiators with diaryliodonium salts to initiate cationic ring opening polymerization.<sup>114</sup>

Recently, it was demonstrated that XeF<sub>2</sub> and PCl<sub>5</sub> can act as radical initiators for the hydrosilylation reaction.<sup>115,116</sup> The proposed mechanism suggests that surface silyl radicals are formed as these compounds cleave Si – Si bonds.<sup>115,116</sup> SiNCs were functionalized instantaneously when XeF<sub>2</sub> was utilized.<sup>115</sup> Exceptionally high absolute QYs (up to 60 – 70%) were achieved through this method, which was tentatively attributed to removal of dark surface defect states.<sup>115,116</sup>

## Hydrosilylation Initiated with Metal and Lewis Acid Catalysts

Room temperature hydrosilylation can also be initiated by utilizing metal ( $\text{H}_2\text{PtCl}_6$ )<sup>117,118</sup> and Lewis acid ( $\text{BH}_3\cdot\text{THF}$ )<sup>119</sup> catalysts. However, in comparison to thermal hydrosilylation, lower surface coverages are achieved with these initiators. In addition, platinum catalysts are costly and trace metal impurities may adversely affect the optical response of SiNCs.<sup>120,121</sup>

## Plasma-Assisted Hydrosilylation

Plasma assisted hydrosilylation appears as a valuable alternative to solution phase approaches.<sup>122</sup> In this technique, SiNCs synthesized *via* plasma induced deposition of silane gasses are transferred by a stream of argon gas to a second chamber, in which an aerosol of unsaturated organic molecules targeted for surface functionalization is injected.<sup>77,123</sup> The main advantage of plasma-assisted hydrosilylation over other techniques is that SiNCs are not exposed to air or moisture at any step. Besides, low boiling point, short-chain alkenes such as ethylene can also be grafted to SiNC surface.<sup>124</sup>

## Two-step Surface Functionalization Reactions Involving Halogenation

Surface functionalization of hydride-terminated SiNCs has also been achieved by first halogenating their surface and subsequently reacting them with nucleophiles, such as organolithium and Grignard reagents, amines, and alcohols (Figure 12).<sup>5,105,125</sup> This principle was demonstrated first by Rogozhina *et al.*, where ultrasmall (1 nm) SiNCs were chlorinated by  $\text{Cl}_2$  and further functionalized with butylamine through Si – N bonds. These SiNCs kept their bright blue emission, which red-shifted by 40 nm after functionalization.<sup>125</sup> Later, Dasog *et al.* performed chlorination, bromination and iodination of hydride-terminated SiNCs with  $\text{PCl}_5$ ,  $\text{Br}_2$  and  $\text{I}_2$ , respectively. These treatments resulted in etching of silicon surface and PL quenching. However, upon subsequent reaction with Grignard reagents, PL was recovered. Interestingly, previously chlorinated SiNCs exhibited blue emission whereas iodinated SiNCs emitted yellow, irrespective of SiNC size. Only the SiNCs which were brominated in the first step maintained their core emission.<sup>105</sup> Bell *et al.*

used *n*-bromosuccinimide (NBS) as the bromination reagent and functionalized the SiNCs with alcohols through Si – O bonds.<sup>126</sup>

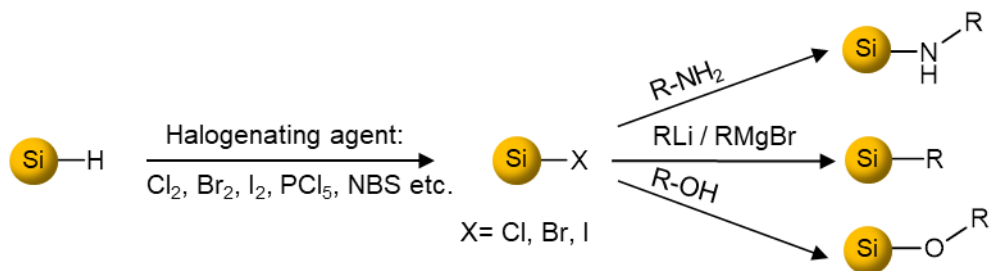


**Figure 12.** 2-step surface functionalization of hydride-terminated SiNCs with nucleophiles obtained *via* halogenation.<sup>13</sup> Adopted from ref. 13 with permission from The Royal Society of Chemistry.

## 3.3 Properties of Silicon Nanocrystals

### 3.3.1 Physical Properties

Bulk silicon is an indirect band gap semiconductor. In indirect band gap materials, the lowest point of the conduction band and the highest point of the valence band occur at different wavevectors ( $k$ -vector) in the Brillouin zone (Figure 13, i).<sup>56</sup> During radiative recombination, an electron excited to the conduction band recombines with a hole from the valence band, and its energy is released in the form of a photon. In this process, both energy and crystal momentum need to be conserved. Therefore, in an indirect band gap semiconductor, this process can only occur in a phonon-mediated fashion, where the phonon momentum is equal to the difference between electron and hole momentum. The probability of phonon-electron coupling is low; as a result, under standard conditions, radiative recombination is less efficient in indirect band gap materials.<sup>127</sup> The indirect character of the band gap of bulk silicon explains its low optical utility. However, strong emission at room temperature from nanocrystalline and porous silicon suggests a different band structure exists in nano-regime.<sup>57,128–130</sup>

In line with Heisenberg's uncertainty principle, the confinement of electron-hole pairs in nanoscale dimensions of the nanocrystal leads to increased uncertainty for the crystal momentum and broadening of the exciton wavevector in the  $k$ -space. As a result, the tails of electron and hole wavefunctions overlap, allowing for an increased probability for a non-phonon assisted direct transition, which is described as "quasi-direct" recombination (Figure 13, iii). An increased contribution of zero-phonon to phonon-assisted transitions with decreasing crystal size was observed.<sup>131,132</sup> This suggests that smaller nanocrystals have more "quasi-direct" character. Transition from indirect to more direct band gap can also be observed by the decrease in radiative lifetime. In bulk silicon, longer lifetimes in the

range of milliseconds are found, due to slow phonon-assisted processes.<sup>133</sup> In the case of SiNCs, microsecond lifetimes are observed.<sup>134</sup>

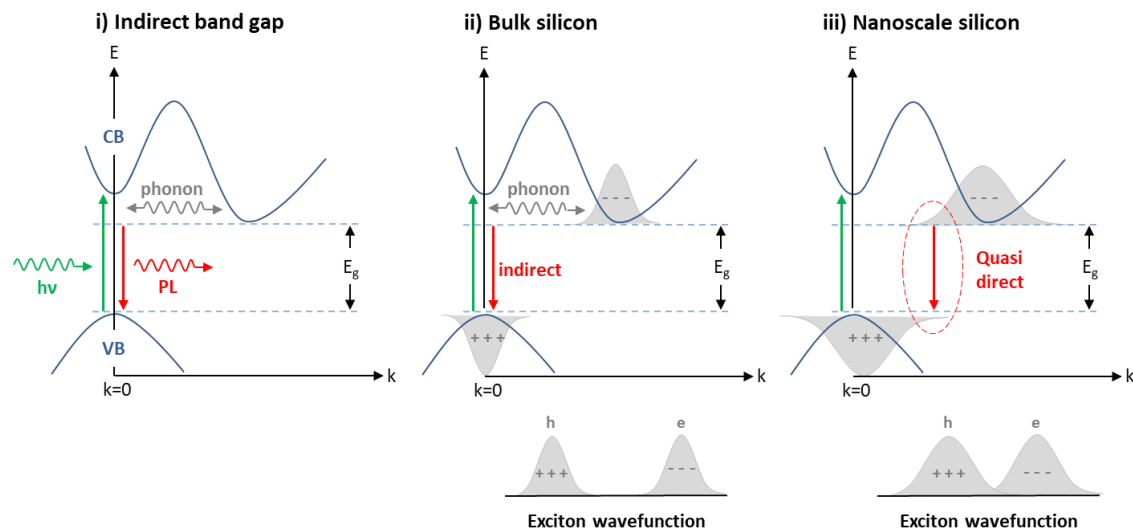


**Figure 13.** i) Depiction of the band structure of an indirect band gap semiconductor. Lowest point of the conduction band (CB) and the highest point of the valence band (VB) occur at different  $k$ -vectors. Radiative combination requires phonon assisted transitions. Broadening of exciton wavefunction in iii) nanoscale silicon with respect to ii) bulk silicon leads to a “quasi-direct” character.

Overall, the nature of the radiative decay of SiNCs is still debated. While some publications report a quasi-direct electronic transition, others suggest that core-states still remain highly indirect based on long-lived PL of SiNCs.<sup>42</sup> Size and surface chemistry are the two important factors influencing the optical response of SiNCs.

### Effect of SiNC Size

The quantum confinement (QC) effect accounts for the size-dependent optical properties of SiNCs by describing the change in the energetic band structure of a material when its size is reduced from bulk to nanoscale. More specifically, as the size of a material is reduced, quantization of continuous DOS and an increase in band gap take place which cause a blue-shift both in absorption and emission of the nanocrystal.<sup>39,41</sup> This principle offer the possibility of tuning the emission wavelength of a QD by decreasing its size.<sup>3</sup> There are several theoretical models including effective mass approximation (EMA) to

correlate SiNC size with band gap energy.<sup>40,135</sup> However such approximations fail to describe complex experimental observations on the PL emission maximum and PL dynamics.

The synthetic routes employed to prepare SiNCs influence the PL characteristics of SiNCs. SiNCs synthesized through HSQ method and non-thermal plasma exhibit size-dependent emission.<sup>58,98</sup> Non-thermal plasma remains as the only method capable of producing SiNCs with emissions cover the full visible spectrum based on the SiNC size.<sup>58</sup> However, Wen *et al.* described a tunability limit at 590 nm, and stated that PL emission cannot be further blue-shifted by reducing the size of the SiNCs. He attributed emission at smaller wavelengths to take place through surface related states, rather than quantum confined core states.<sup>4</sup> In general, SiNCs obtained *via* non-thermal plasma and HSQ method exhibit microsecond lifetimes, which reflects the indirect nature of the transitions. However, nanosecond life times were also observed for these SiNCs in some cases, which were attributed to surface defects due to oxidation.<sup>111</sup>

On the other hand, SiNCs prepared through solution-based synthetic routes exhibit blue emission and nanosecond lifetimes irrespective of their size.<sup>86,89,90,118,136</sup> This blue emission was attributed to occur due to nitrogen based impurities involved in such synthetic routes.<sup>137</sup>

The size of SiNCs also influences their QY, which is defined as the number of photons emitted per photons absorbed. It was reported that the QY of SiNCs decreases with decreasing SiNC size.<sup>134</sup> This trend was explained by an increased number of non-radiative pathways due to surface defects and disruption of crystallinity in the case of small SiNCs.<sup>134</sup> It was also argued that as the size of the SiNCs decreases, the probability for charge carriers to combine outside of the nanocrystals increases which leads to non-radiative decay.<sup>138</sup>

### **Effect of SiNC Surface**

Atoms and molecules grafted to the SiNC surface play an important role in determining the optical properties of SiNCs. It is assumed that hydrogen has a negligible effect on the optical properties of SiNCs, therefore hydride-terminated SiNCs are taken as a

reference.<sup>139</sup> PL energy is not influenced by  $sp^3$  hybridized carbon chains (*i.e.*, alkyl).<sup>16,17</sup> In addition, microsecond lifetime is maintained with such surface groups, suggesting the emission through core-states remains.<sup>5</sup>

Even though SiNCs' surface is passivated with organic molecules, the surface can still be oxidized as a complete surface coverage can never be achieved.<sup>140</sup> The influence of surface oxidation on the PL of SiNCs is not been completely understood due to controversial results observed in different systems. Some groups reported blue-shifts in emission upon oxidation, while others observed red-shifts.<sup>71,141,142</sup> Similarly, oxidation caused a decrease in QY in some studies,<sup>143</sup> while the opposite effect was also observed by others.<sup>144</sup>

Surface functionalization of SiNCs with nitrogen containing ligands yields PL in the blue region associated with nanosecond lifetimes.<sup>137</sup> The origin of this observation was attributed to a charge transfer state due to p-type doping by nitrogen as suggested by scanning tunneling spectroscopy.<sup>3,145</sup> More interestingly, when SiNCs are functionalized with aryl amines through Si – N bonds, the PL wavelength can be tuned between blue (carbazole, tetrahydrocarbazole),<sup>146</sup> green (diphenylamine),<sup>5</sup> yellow (1,2,3,4-tetrahydrocarbazol-4-one)<sup>147</sup> and to orange (aniline).<sup>146</sup>

Functionalization of SiNCs with conjugated molecules attached to the surface *via*  $sp^2$  carbon atoms is expected to enhance the rate of electron transfer to and from SiNCs.<sup>20</sup> Several groups reported that the PL maximum and associated lifetimes are influenced with aromatic surface groups. For example, Le *et al.* functionalized SiNCs with octyl, styryl and 4-ethynylstyryl molecules. An increase in QY and decrease in lifetimes were observed as the conjugation length increased. The authors suggested that a more direct band gap character is facilitated due to strong electronic interaction between the core and surface groups.<sup>148</sup> Surface functionalization of SiNCs with 4-ethynyl-N,N-bis(4-methoxyphenyl)aniline resulted a red-shift in emission relative to decyl functionalized counterparts. These authors stated that to be able to tune the optical response of SiNCs, Type-II alignment between the HOMO-LUMO levels of SiNCs and surface groups and a conjugated bridge in between are required. In Type-II level alignment, the HOMO of the surface group should lie between the energy levels of the HOMO and LUMO of the SiNC.

In this case, a charge transfer state is established and the observed red-shift was attributed to delocalization of electron density from the SiNC to the surface ligands.<sup>6,149</sup>

Functionalization of SiNCs with conjugated fluorescent dyes is another approach to induce charge transfer to SiNCs. In these cases, charge carriers were transferred to SiNCs from aromatic surface groups excited by UV sources.<sup>150–152</sup>

As summarized here, despite intensive research efforts focused on SiNCs during the past decades, the influence of size and surface on the optical response of SiNCs is highly debated and still not completely understood.

### 3.3.2 Biological Properties

Cytotoxicity and bio-compatibility of a material are the two fundamental criteria for biomedical applications. Several groups reported low cytotoxicity and bio-compatibility of SiNCs both *in-vitro*<sup>136,153</sup> and *in-vivo*.<sup>9,154</sup>

Cytotoxicity of SiNCs has been shown to depend on both their size<sup>153</sup> and surface functionalization.<sup>136,153</sup> Zuilhof *et al.* studied the size-dependent toxicity by comparing 1.6 nm and 3.5 nm SiNCs. They found that smaller SiNCs were more toxic due to increased surface area.<sup>153</sup> Tilley *et al.* found that epoxide functionalized SiNCs were nearly twice as toxic as diol and amine functionalized counterparts. Oxidative stress within the cells created by the highly reactive nature of epoxide groups was proposed as the rationale.<sup>136</sup> Zuilhof *et al.* showed that surface groups which carry a positive charge (*e.g.*, amines) were more toxic than neutral (*e.g.*, azide) and negatively charged (*e.g.*, carboxylic acid) species.<sup>153</sup> These studies clearly show that in order to achieve successful development of biomedical applications utilizing SiNCs, it is crucial to appropriately design their size and surface chemistry.

Bio-compatibility of SiNCs within living systems was studied by several *in-vivo* studies. For example, Liu *et al.* performed *in-vivo* toxicity tests on mice and monkeys and found no signs of toxicity at a dose of 200 mg/kg over a three month period. However, in the case of mice, SiNCs did not seem to degrade as expected. Elevated levels of silicon were detected in the liver and spleen, in contrast to tests with monkeys.<sup>9</sup> Kauzlarich and co-workers showed that SiNCs were rapidly cleared from the bloodstream of mice by renal



filtration, however elevated levels of silicon were found in the kidneys several months after the initial injection.<sup>154</sup> These results show the importance of multi-animal toxicity tests.

## 3.4 Applications of Silicon Nanocrystals

The unique properties of SiNCs, which are tunable by controlling their size and surface chemistry, make them highly suitable for several applications including sensors,<sup>12</sup> solar cells,<sup>59</sup> bioimaging,<sup>155</sup> and LEDs.<sup>10</sup>

### 3.4.1 Sensors

SiNCs have appeared as a low-toxic alternative to traditional QDs in the last years, for building a photoluminescent sensing platform to detect nitroaromatics,<sup>156</sup> metal cations<sup>157-159</sup> and biologically relevant molecules. Sensing of the substances mostly occur *via* quenching of PL through different mechanisms such as electron transfer, fluorescence resonance energy transfer (FRET) or photocurrent generation.<sup>12</sup>

Veinot and co-workers employed red emitting dodecyl functionalized SiNC in a paper based sensor to detect nitroaromatics, nitroamines and nitrate esters, relevant to explosives.<sup>156</sup> Regular filter paper was dip coated with SiNCs and subsequently treated with respective nitrocompounds in solution or as solid which resulted in PL quenching. Detection limit for dinitrotoluene (DNT) was found as low as 0.34 mM in solution or 18 ng in solid. The quenching mechanism was suggested to occur *via* an electron transfer.<sup>12</sup> In a following work, blue emitting 3-aminopropyl functionalized SiNCs were utilized to detect nitroaromatic molecules, as well. In that case, the detection limit for trinitrotoluene (TNT) was determined as 1 nM in solution, where quenching was proposed to take place through FRET that is facilitated by surface bound amine groups.<sup>160</sup>

Metal cations in the aquatic environment and biological systems are a substantial problem due to their deleterious effects on the ecosystem and human health, depending on the dose and toxicity.<sup>161</sup> Use of QDs (*e.g.*, CdSe) to detect metal ions has been extensively studied.<sup>161,162</sup> However, as it is irrational to use toxic metal based sensors to sense toxic

materials, SiNCs appear as a promising choice. Relying on this motivation, blue-emitting SiNCs were utilized to detect  $\text{Hg}^{2+}$ ,  $\text{Cu}^{2+}$  and  $\text{Cr}^{4+}$  ions.<sup>157-159</sup>

Several contributions also showed that sensing of biologically relevant molecules such as glucose,<sup>163</sup> dopamine,<sup>164</sup> ethanol,<sup>165</sup> antibiotics<sup>166</sup> and pesticides<sup>167</sup> is feasible with SiNCs.

### 3.4.2 Solar Cells

Currently, around 90% of all solar panels in use are based on silicon.<sup>168</sup> Favorable properties of bulk silicon, including its 1.1 eV band gap which is optimal for capturing the solar spectrum using a single junction device, together with natural abundance and availability of large high purity single crystals explain this dominance.<sup>168</sup> Currently, the highest photovoltaic conversion energy accomplished is near 26%.<sup>169</sup> This is very close to the 30% theoretical maximum efficiency limit for crystalline silicon solar cells (Shockley-Queisser limit), which underlines that only limited progress can be expected in the future.<sup>170</sup> Several different strategies exploiting unique properties of SiNCs can be utilized to overcome the Shockley-Queisser limit, as discussed in following sub-chapters.

#### SiNCs as Down-Shifters for Solar Cells

For bulk crystalline silicon solar cells, internal quantum efficiency (IQE) is higher with photons having a longer wavelength (500-1000 nm).<sup>59</sup> As SiNCs absorb short wavelength photons and emit in the visible-red region with high QYs, they can be utilized as down-shifters in silicon solar cell designs to achieve more efficient utilization of the short wavelength part of the solar spectrum. In this way, maximization of the number of photons reaching the solar cell with energies leading the highest internal quantum efficiency (IQE) is intended.<sup>59</sup> Pi *et al.* showed that spin coated SiNCs synthesized *via* non-thermal plasma on the solar cell surface resulted an increase in power-conversion efficiency up to 4% which corresponded to 0.6% increase in overall solar cell efficiency.<sup>171</sup> It is important to note that only the efficiency of a solar cell with a poor performance in the UV-blue region can be improved with this approach.<sup>172</sup>

## **Multi-layer Tandem Solar Cells**

In multi-layer tandem solar cells, materials with different band gaps are stacked together to utilize a broader spectrum of sun light. Due to the quantum confinement effect, the band gap of SiNCs is tunable by controlling their size. Therefore, tandem solar cells consisting solely of silicon of different sizes can be built.<sup>59</sup> This approach was demonstrated by Green in a two-junction solar cell based on phosphorous doped SiNCs and crystalline silicon.<sup>173</sup>

## **Hot Carrier Solar Cells and Multiple Exciton Generation in SiNCs**

In a solar cell, when the incident photon has energy larger than the bandgap, excitons with excess energy (hot carriers) are formed. These carriers relax to band edges while losing the excess energy in the form of heat. This thermalization reduces the number of carriers which could be separated through the p-n junction.<sup>174</sup> Hot carrier solar cells aim to increase the efficiency of solar cells by extracting these hot carriers before they lose their energy.<sup>59</sup> Due to quantization and widening the distance of the energy levels in SiNCs, relaxation of the energy carriers is slower than bulk silicon.<sup>59</sup> Therefore, SiNCs can potentially be beneficial in hot carrier solar cells as demonstrated by Aliberti,<sup>175</sup> Shrestha,<sup>176</sup> Conibeer<sup>177</sup> and Saeed.<sup>178</sup>

Multiple excitation generation (MEG) defines the concept that when an excitation with energy at least two times larger than the band gap is absorbed, it can have an increased probability to split into multiple excitons, instead of losing the excess energy in the form of heat. It has been shown that SiNCs are capable of generating multiple excitations.<sup>179,180</sup> If these multiple excitons can be extracted from SiNCs successfully, this could potentially improve the efficiency of the solar cells by reducing thermal losses.<sup>59,179</sup> Hot carrier solar cells and MEG underline the potential of SiNCs for photovoltaic applications.

## **Inorganic/Organic Hybrid Solar Cells**

Hybrid solar cells based on mixtures of conjugated polymers and inorganic semiconductor nanocrystals are attractive because they may combine the desirable

properties of both materials. Hybrid solar cells based on SiNCs and poly(3-hexylthiophene) (P3HT) were demonstrated. Smaller SiNCs (26 nm vs 4 nm) and P3HT polymers with high regioregularity showed better performance.<sup>181</sup> However, low efficiencies in the order of 1% resulted which were attributed to limited charge transfer from SiNCs.<sup>182,183</sup> Annealing of the SiNC/P3HT layer and HF etching of SiNCs to remove oxide shell and surface defects prior to blending were found beneficial to increase charge transport.<sup>184</sup> In addition, agglomeration of SiNCs and formation of inhomogeneous films were reported as problems causing lower yields, which could be improved by functionalizing the surface of SiNCs with appropriate molecules.<sup>185</sup>

### 3.4.3 Biomedical Applications

For a material to be successfully integrated into biomedical applications, it should offer good bio-compatibility, low-toxicity, stable emission and high QYs. SiNCs are a promising candidate owing to their favorable properties including their low-toxicity, strong resistance to photobleaching, and range of emission colors available.<sup>9,60</sup> Utilization of SiNCs have been explored for two important biomedical fields, bioimaging and drug delivery.

Several groups studied *in-vitro* bioimaging with SiNCs soluble in aqueous media. For example, poly(acrylic acid) functionalized red-, and amine functionalized blue emitting SiNCs were tested for different cell lines and demonstrated higher resistance to photobleaching than the commonly used organic dyes.<sup>118,186</sup> Alsharif *et al.* reported that cellular uptake of alkyl-functionalized SiNCs by malignant human cells is significantly faster than normal cells.<sup>187</sup>

Surfaces of SiNCs were functionalized with bio-functional moieties to be able to target specific cell types or locations. For example, SiNCs encapsulated in phospholipid micelles were used to image pancreatic cancer cells and showed improved targeting, photo- and pH stability compared to alkyl functionalized SiNCs.<sup>8</sup> Dasog *et al.* demonstrated that mannose and alanine functionalized SiNCs are taken up by human breast cancer cells, whereas pentanoic acid terminated SiNCs were not.<sup>188</sup> He and co-workers coupled antibodies to the surface of SiNCs and achieved the imaging of specific organelles of the cells due to specific antibody conjugation.<sup>189-191</sup> These results underline the significant impact of the

surface chemistry on the properties of SiNCs. Prasad and co-workers demonstrated long term (40 hours) *in-vivo* imaging with SiNCs encapsulated in protein terminated micelles, for the first time. They could also performed multicolor imaging where red and yellow emissions were clearly resolved.<sup>192</sup>

SiNCs used for bioimaging applications are generally excited by UV sources which may lead to autofluorescence from biological tissue and phototoxicity.<sup>193,194</sup> Two-photon excitation was proposed as a potential solution.<sup>193,194</sup> A different approach aiming to take advantage of emission lifetime differences between autofluorescence and SiNC PL in a time-gated imaging was also demonstrated.<sup>195</sup>

Platforms that combine bioimaging and drug delivery can also be designed. He and co-workers demonstrated this concept by loading poly(methacrylic acid) functionalized SiNCs' surface with a commonly used cancer drug (DOX) and performed simultaneous *in-vivo* imaging and chemotherapy. Treated mouse subjects with cancer survived for at least 30 days after the treatment, whereas untreated subjects died in a matter of days.<sup>196</sup> This study was the first step towards multifunctional SiNCs, creating a tremendous scope for simultaneous medical imaging and treatment.

#### **3.4.4 Light Emitting Diodes**

The basic working principle of LEDs involves the creation of charge carriers by an active emissive material, in response to an external current applied through a p-n junction. Upon recombination of the electron-hole pairs, energy is released in the form of a photon with the energy equal to the band gap of the active material. Several groups described electrically stimulated light emission, electroluminescence, from SiNCs and proposed LEDs with different device architectures.

The first reports on electroluminescence (EL) of SiNCs were based on SiNCs incorporated into nonconductive matrices such as oxides and nitrides.<sup>197,198</sup> Holmes and Kortshagen demonstrated that SiNCs can be incorporated into organic light-emitting diodes (OLEDs). In hybrid nanocrystal-OLEDs, a NC emissive layer is sandwiched between organic charge transport layers.<sup>29</sup> In their first report, Cheng *et al.* utilized dodecyne functionalized SiNCs (d ~ 5 nm) synthesized *via* non-thermal plasma to achieve infrared

EL at 868 nm and external quantum efficiency (EQE) of 0.6%.<sup>29</sup> Higher SiNC ratio in the thin film resulted in a decrease in current and increase in drive voltage, suggesting that the devices become more resistive.<sup>29</sup> In a follow up paper, these authors carefully chose electron and hole blocking layers with favorable energy levels to improve charge carrier injection and confinement in the SiNC layer. Resulting devices exhibited significantly increased the EQE of the devices up to 8.6%, which is the highest efficiency reported for Si-LEDs so far.<sup>199</sup> However, this high EQE was criticized by Ozin, who stated that this value was measured under conditions where there was no visible emission from the devices. He also claimed that at voltages above device turn-on, where the luminance reaches 1 cd/m<sup>2</sup>, the EQE values reported by Cheng *et al.* were comparable to the previously reported EQE values below 1%.<sup>18</sup>

In the same year, Ozin and co-workers utilized decyl functionalized SiNCs (d~3 nm) synthesized in a sol-gel route to build LEDs emitting at 645 nm with EQE of 0.7%.<sup>30</sup> They attributed the low efficiency to both low absolute QY of SiNCs and the insulating nature of the SiNC surface groups and SiNC thin films.<sup>30</sup> Therefore, they functionalized SiNCs with allylbenzene molecules with the aim of reducing resistivity of the SiNC surface groups and increasing electronic coupling between SiNCs in the emissive layer.<sup>18</sup> Maier-Flaig *et al.* achieved to build yellow and red LEDs by using very monodisperse size-separated SiNCs and achieved higher EQE up to 1.1%.<sup>10</sup> They also found that the polydispersity of SiNCs contribute to device failure modes and result in shorter operational lifetimes.<sup>200</sup>

Despite extensive studies on SiNC-LEDs to improve their efficiency, intrinsic resistance and reduced charge transfer of the SiNC layer remains as the main challenge.<sup>29,30</sup> Surface chemistry of SiNCs, employed charge blocking layers and fabrication technologies need to be tailored for satisfactory efficiency levels.

## 4 Manuscripts

In this chapter, manuscripts of the publications for the fulfillment of the doctorate degree are included. Before each contribution, a preface is given where the aims of the research project are discussed and the impact of the results is stated.

### Contents

<b>4.1</b> Functionalization of Hydride-Terminated Photoluminescent Silicon Nanocrystals with Organolithium Reagents .....	35
<b>4.2</b> Photoluminescence through In-Gap States in Phenylacetylene Functionalized Silicon Nanocrystals.....	50
<b>4.3</b> The Influence of Conjugated Alkynyl(aryl) Surface Groups on the Optical Properties of Silicon Nanocrystals: Photoluminescence through In-Gap States.....	62
<b>4.4</b> The Influence of Surface Functionalization Methods on the Performance of Silicon Nanocrystal LEDs.....	95
<b>4.5</b> Dissipative Self-Assembly of Photoluminescent Silicon Nanocrystals.....	109



## 4.1 Functionalization of Hydride-Terminated Photoluminescent Silicon Nanocrystals with Organolithium Reagents

Hydride-terminated SiNCs are frequently functionalized with long alkyl chains through hydrosilylation to protect the surface from oxidation and achieve colloidal stability in various solvents.<sup>14</sup> The mechanism of hydrosilylation, which involves the addition of a Si – H bond to an unsaturated C – C bond of terminal alkenes/alkynes, does not allow the grafting of aryl and alkynyl(aryl) molecules directly to the SiNC surface (Figure 14). Unlike long chain alkyl groups, which may create an insulating layer,<sup>18</sup> these conjugated aromatic molecules are expected to facilitate charge transfer to or from SiNCs which may be beneficial for optoelectronic applications.<sup>20</sup>

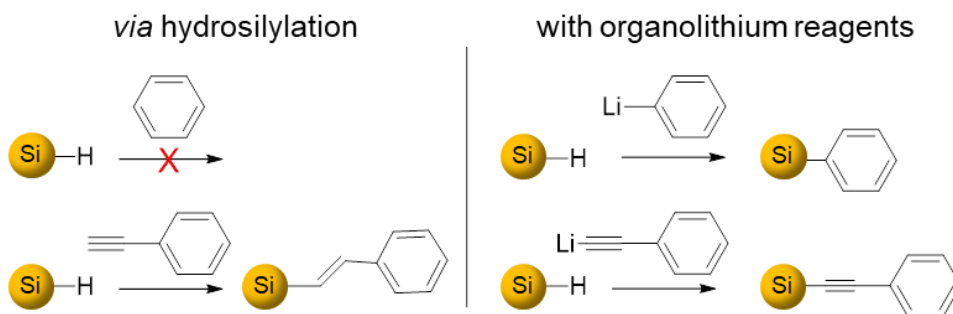


**Figure 14.** Reaction of hydride-terminated SiNCs with phenyl and phenylacetylene *via* hydrosilylation (left) and lithiated compounds (right).

In this work, we utilized organolithium and Grignard reagents to functionalize hydride-terminated SiNCs. The suggested mechanism of this reaction involves the cleavage of Si – Si bonds upon nucleophilic attack from the organolithium reagent. As a result, Si – C bonds are formed neighboring Si – Li groups. The reactive Si – Li groups can be quenched with nucleophiles to terminate the reaction.<sup>23,24</sup> This method is able to functionalize SiNCs at room temperature and in short reaction times, while ensuring monolayer coverage. This reaction allowed direct grafting of aryl (*e.g.*, phenyl, 2-hexylthiophene) and alkynyl(aryl) (*e.g.*, phenylacetylene) groups to SiNC surface, for the first time. These results showed that the organolithium reagents react with surface Si atoms in a fashion similar to molecular silanes. Interestingly, while no change in PL was observed with aryl groups with respect to alkyl counterparts, the PL of phenylacetylene functionalized SiNCs red-shifted for ~50 nm.

**Manuscript:**

**Functionalization of Hydride-Terminated Photoluminescent Silicon Nanocrystals with Organolithium Reagents**

<b>Status</b>	Published on December 22, 2014
<b>Journal</b>	<i>Chemistry - A European Journal</i> , 2015, Volume 21, 2755-2758.
<b>Publisher</b>	John Wiley and Sons
<b>DOI</b>	10.1002/chem.201405555
<b>Authors</b>	Ignaz M. D. Höhle,† Arzu Angi,† Regina Sinelnikov, Jonathan G. C. Veinot, Bernhard Rieger

† These authors contributed equally to this work.

Reprinted with the permission of *Chemistry - A European Journal* with the license number 4367100922442.

## Surfaces and Interfaces | Hot Paper |

## Functionalization of Hydride-Terminated Photoluminescent Silicon Nanocrystals with Organolithium Reagents

Ignaz M. D. Höhle, [a] Arzu Angi, [a] Regina Sinelnikov, [b] Jonathan G. C. Veinot, [b] and Bernhard Rieger\* [a]

**Abstract:** Hydride-terminated photoluminescent silicon nanocrystals (SiNCs) were functionalized with organolithium compounds. The reaction is proposed to proceed through cleavage of Si–Si bonds and formation of a Si–Li surface species. The method yields colloiddally stabilized SiNCs at room temperature with short reaction times. SiNCs with mixed surface functionalities can be prepared in an easy two-step reaction by this method by quenching of the Si–Li group with electrophiles or by addressing free Si–H groups on the surface with a hydrosilylation reaction.

Nanomaterials have gained great interest in recent years due to differing properties in contrast to their bulk material counterparts, such as size-dependent optical properties, for example, photoluminescence. Silicon nanocrystals (SiNCs) are of special interest, because they are comparably non-toxic in contrast to often used heavy metal-containing materials and therefore biocompatible.<sup>[1]</sup> In addition, the abundance of silicon makes it a promising precursor for the production of low-cost nanomaterials. A variety of applications have been realized by using SiNCs including solar cells, photoluminescent biomarkers, and light-emitting diodes (LEDs).<sup>[1–3]</sup>

Due to the high surface-to-volume ratio of nanomaterials, the control over their surface chemistry is of crucial importance. This is especially true for SiNCs, because silicon is oxidized under ambient conditions by water or oxygen. Also, different surface groups influence the photoluminescence of SiNCs.<sup>[4,5]</sup> In addition, a surface functionalization is needed to render the SiNCs soluble in various solvents. Finding new ways to modify and protect the surface of SiNCs is therefore an attractive target.

[a] I. M. D. Höhle, A. Angi, Prof. B. Rieger  
Wacker-Lehrstuhl für Makromolekulare Chemie  
Technische Universität München  
Lichtenbergstrasse 4, 85747 Garching (Germany)  
E-mail: rieger@tum.de

[b] R. Sinelnikov, Prof. J. G. C. Veinot  
Department of Chemistry, University of Alberta  
Edmonton, Alberta, T6G 2G2 (Canada)

[\*] These authors contributed equally to this work.

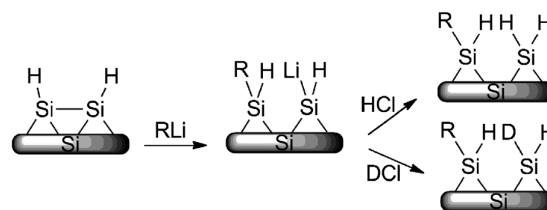
Supporting information for this article is available on the WWW under <http://dx.doi.org/10.1002/chem.201405555>. It contains detailed experimental procedures, as well as further FTIR, DLS, PL, TGA, NMR, and HR TEM data.

The most common synthetic ways form SiNCs with a silicon hydride (Si–H)-terminated surface.<sup>[6–9]</sup> To functionalize these SiNCs, the hydrosilylation reaction is normally used. A compound with a double or triple bond forms a covalent Si–C bond through addition reaction with the Si–H surface group. The hydrosilylation can be induced thermally, by UV irradiation, radical initiators, or Lewis acids.<sup>[8,10–12]</sup> A drawback of the hydrosilylation reaction is that no aryl- or alkynyl-groups can be bound directly to the SiNCs surface. However, these groups with conjugated  $\pi$ -systems could be promising for application in electronic devices, because they might offer the possibility of charge transfer from or to the SiNCs.

SiNCs can be synthesized with a halogen (Si–X, X = Br, Cl) instead of a hydrogen-terminated surface as well.<sup>[13,14]</sup> These SiNCs offer a different reactivity, because the Si–X bond can be attacked by nucleophiles including organometallic compounds. This reaction path allows the functionalization of SiNCs with conjugated molecules, such as phenyl groups. The halogen-terminated surface itself, however, alters the properties of the SiNCs, and up to date, only blue photoluminescent SiNCs have been reported in contrast to the full visible spectrum with hydride-terminated SiNCs.<sup>[15]</sup>

Organolithium compounds and Grignard reagents can also react directly with silicon surfaces, without the presence of hydrolyzable groups. This was shown on porous silicon (p-Si), a form of silicon with a very high, nanostructured surface area.<sup>[16,17]</sup> The mechanism is believed to proceed by breaking of Si–Si bonds and therefore formation of a Si–C bond and a Si–Li surface species (Scheme 1). The reactive Si–Li group is quenched during the workup with electrophiles, such as protons or deuterons.

Herein, we report that hydride-terminated SiNCs react with organolithium compounds at room temperature by breaking of Si–Si bonds. The SiNCs were functionalized with a variety of organolithium reagents and form colloiddally stabilized disper-



**Scheme 1.** Reactivity of organolithium reagents towards nanostructured silicon surfaces.

sions. Also, SiNCs with mixed surface functionalities are formed by quenching the reaction with various electrophiles or by addressing free Si–H groups through hydrosilylation reaction with 1-dodecene.

The H-terminated SiNCs used in this work have an average diameter of around 3–4 nm and were prepared by pyrolysis of hydrogen silsesquioxane (HSQ) at 1100 °C for 1 h in an atmosphere consisting of 5% hydrogen and 95% nitrogen.<sup>[6]</sup> Under these conditions, SiNCs were formed incorporated into a silica matrix. The SiNCs were liberated by etching the composite with HF and final extraction in toluene.

SiNCs obtained by etching 300 mg Si/SiO<sub>2</sub> composite were dispersed in a 0.1 M solution of *n*-hexyllithium in toluene and stirred at room temperature for 2 h (Figure 1 A). The reaction was quenched by methanol, acidified with HCl, and the functionalized SiNCs were further purified by two antisolvent precipitation steps from toluene with methanol.

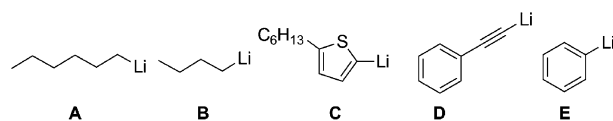


**Figure 1.** Organolithium reagents used for the functionalization of SiNCs. A) *n*-hexyllithium; B) *n*-butyllithium; C) (5-hexyl-2-thienyl)lithium; D) lithium phenylacetylide; and E) phenyllithium.

The unfunctionalized, hydride-terminated SiNCs form a turbid yellow dispersion in toluene and showed only the distinctive Si–H bands at 2099, 906, and 665 cm<sup>-1</sup> in the IR spectrum (Figure 2 A). After reaction with *n*-hexyllithium, additional strong C–H bands at 2900 and 1450 cm<sup>-1</sup> from surface-bound

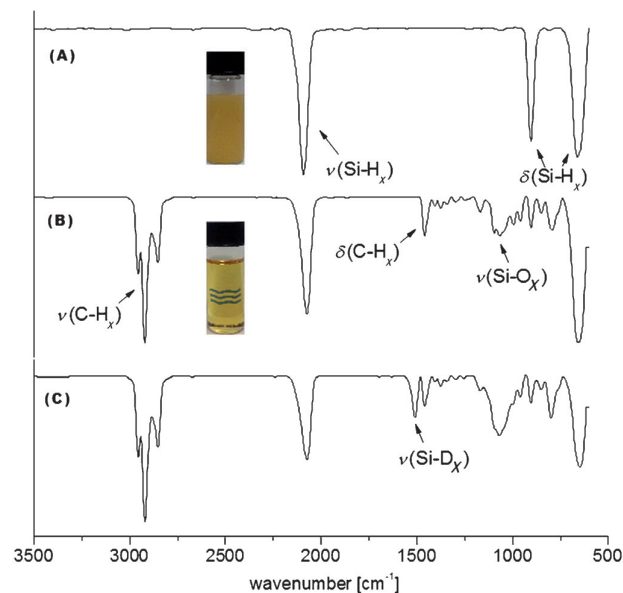


**Figure 2.** FTIR spectra of A) freshly etched SiNCs; B) functionalized with *n*-hexyllithium and HCl used for workup; C) functionalized with *n*-hexyllithium and DCl used for workup.

alkyl chains were visible (Figure 2 B). The functionalization was sufficient to stabilize the SiNCs colloiddally, which is apparent by the formation of a clear SiNCs dispersion. Minor surface oxidation of the SiNCs was observed, evident from the Si–O band at 1050 cm<sup>-1</sup>.

To prove the postulated mechanism by formation of a Si–Li group is also accurate for SiNCs, the quenching was also performed with deuterated methanol, acidified with DCl. A FTIR band at 1510 cm<sup>-1</sup> was observed after this reaction, which can be assigned to a Si–D bond (Figure 2 C). A control experiment, in which unfunctionalized SiNCs were treated with DCl, did not indicate any formation of Si–D bonds (Figure S2 in the Supporting Information).

Hexylmagnesiumbromide was also tested to check the reactivity of Grignard reagents towards SiNCs. The same reactivity compared to organolithium compounds was found, but the surface coverage seems to be lower, because only comparably weak alkyl bands were visible in the FTIR spectra (Figure S3 in the Supporting Information), and the functionalized SiNCs were poorly dispersible in toluene. Therefore, further reactions were conducted only with organolithium reagents.

To show a broad applicability of the reaction, the organolithium reagents *n*-butyllithium, (5-hexyl-2-thienyl)lithium, lithium phenylacetylide, and phenyllithium (Figure 1 B–E) were tested for the functionalization of SiNCs. The reaction procedure was the same as that described with *n*-hexyllithium. In every case, colloiddally stabilized dispersions were formed, and the functionalized SiNCs showed IR bands of the respective surface groups (Figure 3 A–D).

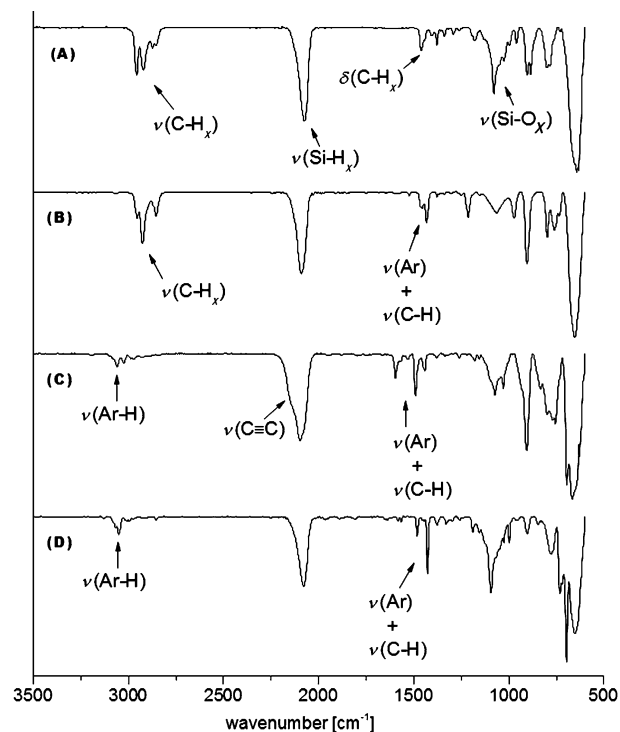
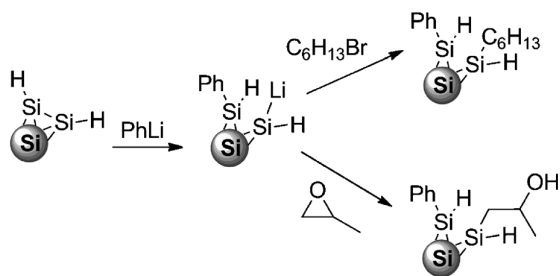


**Figure 3.** FTIR spectra of SiNCs functionalized with A) *n*-butyllithium; B) (5-hexyl-2-thienyl)lithium; C) lithium phenylacetylide; and D) phenyllithium.



**Scheme 2.** Reaction of SiNCs with phenyllithium and quenching of the surface Si-Li group with 1-bromohexane (top) and propylene oxide (bottom).

For the quenching of the silyl anions during the workup, other electrophiles than protons can be used. This was shown by Kim and Laibinis and Song and Sailor, for example, with acyl chlorides on porous silicon.<sup>[16,17]</sup> We wanted to determine whether less reactive electrophiles are also suitable for this reaction. Therefore, 1-bromohexane and propylene oxide were used as quenching reagents (Scheme 2).

The SiNCs were functionalized with phenyllithium in the described way and the reaction mixture was cooled to  $-78^{\circ}\text{C}$  before adding 20 equivalents of the respective quenching reagent. The dispersion was then warmed to room temperature, and the following purification was performed by three precipitation/centrifugation cycles from toluene and methanol. In the FTIR spectra additional C-H bands were visible for the 1-bromohexane-functionalized SiNCs (Figure 4A), and a broad C-OH band at  $3400\text{ cm}^{-1}$  for the SiNCs reacted with propylene oxide, which indicates that the quenching was successful (Figure 4B).

Because the Si-H groups of the SiNCs are not consumed during the reaction with organolithium reagents, they should be available for further functionalization, such as hydrosilyla-

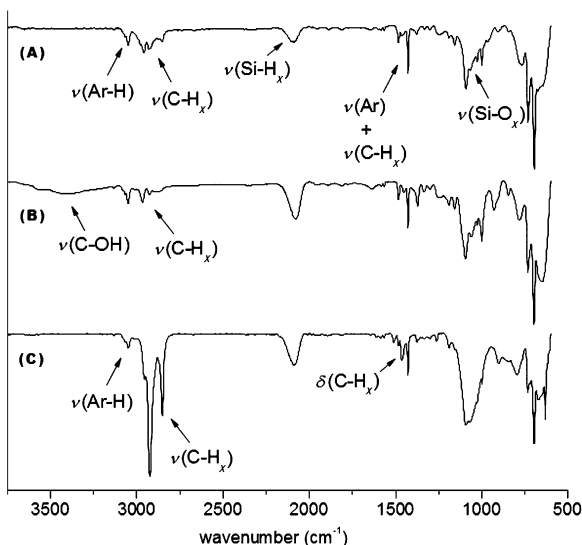
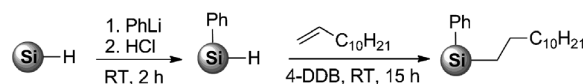


**Figure 4.** FTIR spectra of SiNC functionalized with A) phenyllithium and quenched with 1-bromohexane; B) phenyllithium and quenched with propylene oxide; and C) phenyllithium followed by hydrosilylation of 1-dodecene initiated with 4-DDB.



**Scheme 3.** Functionalization of SiNCs with PhLi followed by 4-decylbenzene diazonium tetrafluoroborate (4-DDB) initiated hydrosilylation of dodecene.

tion reactions (Scheme 3). This hypothesis was tested with SiNCs that were first reacted with phenyl lithium and after the workup resuspended in 3 mL of a 1 M solution of 1-dodecene in toluene. The hydrosilylation reaction was started with the addition of 4-decylbenzene diazonium tetrafluoroborate (4-DDB) as radical initiator and stirred overnight.<sup>[12]</sup> Purification of the functionalized SiNCs was performed by three antisolvent precipitations from toluene with methanol/ethanol. The FTIR spectrum clearly showed additional C-H bands from surface-bound dodecyl groups next to the aromatic bands from the phenyl rings on the surface (Figure 4C). Bands of Si-H were still present; however, this is expected, because a complete coverage by hydrosilylation cannot be achieved due to steric hindrance.<sup>[18]</sup>

Dynamic light scattering (DLS) measurements were conducted of the functionalized SiNCs (Table 1). Hydrodynamic radii

**Table 1.** DLS data of the SiNCs with different surface functionalities dispersed in toluene.

Reagent	Hydrodynamic radius [nm]	Polydispersity [%]
<i>n</i> -butyllithium	2.2	41.1
<i>n</i> -hexyllithium	2.3	35.9
(5-hexyl-2-thienyl)lithium	3.2	42.1
lithium phenylacetylide	2.5	41.5
phenyllithium	2.1	22.4
phenyllithium and 1-dodecene	2.8	34.4
phenyllithium and 1-bromohexane	2.3	16.5
phenyllithium and propylene oxide	362.8	20.6

between 2.1 and 3.2 nm are consistent with values reported in literature of SiNCs functionalized by hydrosilylation, and indicate that the SiNCs do not agglomerate in the solvent.<sup>[10]</sup> The only exception are SiNCs functionalized with phenyllithium and quenched with propylene oxide, which have a hydrodynamic radius over 300 nm. The free hydroxide groups on the surface could render the SiNC surface more polar, which then would be reasonable to cause the formation of agglomerates in toluene.

The photoluminescence (PL) maxima of the functionalized SiNCs were found at  $\lambda = 690\text{ nm}$  except for SiNCs with phenylacetylene surface groups, in which it is redshifted to 740 nm (Figure 5). The cause of this shift is not known to us, but it has been reported before that the photoluminescence of porous silicon is influenced by covalently bound phenylacetylene groups.<sup>[17]</sup> However, Song et al. described only a weakening of the photoluminescence, not a shift of the emission wavelength. This matter will be subject to further investigations.

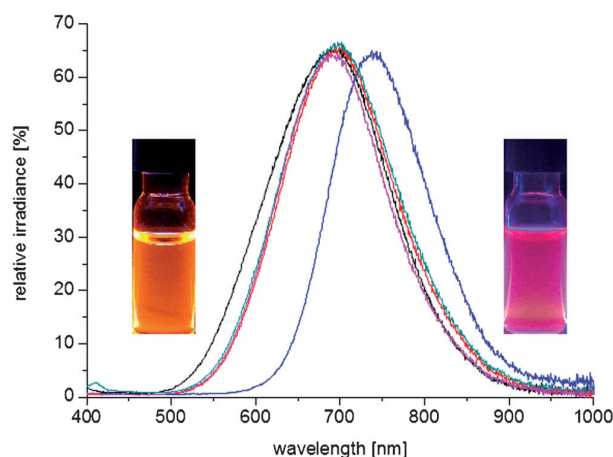


**Figure 5.** PL spectra of SiNCs functionalized with *n*-hexyllithium (green), (5-hexyl-2-thienyl)lithium (black), phenyllithium (red), *n*-butyllithium (magenta), and lithium phenylacetylide (blue). Dispersion of SiNC with hexyl surface groups (left) and phenylacetylene surface groups (right) under  $\lambda = 365$  nm UV radiation.

In summary, we report that SiNCs with a hydride surface can be functionalized with organolithium compounds. The reaction was performed at room temperature with short reaction times and the functionalized SiNCs form colloiddally stable dispersions. The proposed mechanism proceeds through breaking of Si–Si bonds and formation of surface Si–Li species. SiNCs with mixed surface functionalities can be obtained when the Si–Li groups are quenched with various electrophiles or if free Si–H groups on the SiNC are addressed through hydrosilylation reaction in a following step.

## Acknowledgements

R.S. and J.G.C.V. acknowledge funding from the Natural Sciences and Engineering Research Council of Canada (NSERC), Canada Foundation for Innovation (CFI), Alberta Science and Research Investment Program (ASRIP), and University of Alberta Department of Chemistry. Kai Cui from the National Institute

for Nanotechnologie (NINT) is thanked for HR TEM measurements. I.M.D.H., A.A., and R.S. are grateful for scholarships from the Fonds der Chemischen Industrie (FCI), the Deutscher Akademischer Austauschdienst (DAAD) & Turkish Education Foundation (TEV) and Alberta Innovates Technology Futures (AITF), respectively.

**Keywords:** nanoparticles • organometallic compounds • silicon • surface chemistry

- [1] J. Liu, F. Erogbogbo, K.-T. Yong, L. Ye, J. Liu, R. Hu, H. Chen, Y. Hu, Y. Yang, J. Yang, *ACS Nano* **2013**, *7*, 7303–7310.
- [2] K.-Y. Cheng, R. Anthony, U. R. Kortshagen, R. J. Holmes, *Nano Lett.* **2010**, *10*, 1154–1157.
- [3] C. Liu, Z. C. Holman, U. R. Kortshagen, *Nano Lett.* **2009**, *9*, 449.
- [4] K. Dohnalová, T. Gregorkiewicz, K. Kúsová, *J. Phys. Condens. Matter* **2014**, *26*, 173201.
- [5] M. Dasog, G. B. De Los Reyes, L. V. Titova, F. Hegmann, J. G. C. Veinot, *ACS Nano* **2014**, *8*, 9636–9648.
- [6] C. M. Hessel, E. J. Henderson, J. G. C. Veinot, *Chem. Mater.* **2006**, *18*, 6139–6146.
- [7] X. Li, Y. He, S. S. Talukdar, M. T. Swihart, *Langmuir* **2013**, *29*, 8490–8496.
- [8] R. D. Tilley, J. H. Warner, K. Yamamoto, I. Matsui, H. Fujimori, *Chem. Commun.* **2005**, 1833–1835.
- [9] J. L. Heinrich, C. L. Curns, G. M. Credo, K. L. Kavanagh, M. J. Sailor, *Science* **1992**, *255*, 66–68.
- [10] J. A. Kelly, J. G. C. Veinot, *ACS Nano* **2010**, *4*, 4645–4656.
- [11] J. Nelles, D. Sendor, A. Ebbbers, F. M. Petrat, H. Wiggers, C. Schulz, U. Simon, *Colloid Polym. Sci.* **2007**, *285*, 729–736.
- [12] I. M. D. Höhlein, J. Kehrle, T. Helbich, Z. Yang, J. G. C. Veinot, B. Rieger, *Chem. Eur. J.* **2014**, *20*, 4212–4216.
- [13] C. Yang, R. A. Bley, S. M. Kauzlarich, H. W. H. Lee, G. R. Delgado, *J. Am. Chem. Soc.* **1999**, *121*, 5191–5195.
- [14] J. Zou, R. K. Baldwin, K. a. Pettigrew, S. M. Kauzlarich, *Nano Lett.* **2004**, *4*, 1181–1186.
- [15] X. Cheng, S. B. Lowe, P. J. Reece, J. J. Gooding, *Chem. Soc. Rev.* **2014**, *43*, 2680–2700.
- [16] N. Y. Kim, P. E. Laibinis, *J. Am. Chem. Soc.* **1998**, *120*, 4516–4517.
- [17] J. H. Song, M. J. Sailor, *J. Am. Chem. Soc.* **1998**, *120*, 2376–2381.
- [18] L. Scheres, B. Rijkse, M. Giesbers, H. Zuilhof, *Langmuir* **2011**, *27*, 972–980.

Received: October 7, 2014

Published online on December 22, 2014

# CHEMISTRY

## A European Journal

### Supporting Information

© Copyright Wiley-VCH Verlag GmbH & Co. KGaA, 69451 Weinheim, 2015

#### **Functionalization of Hydride-Terminated Photoluminescent Silicon Nanocrystals with Organolithium Reagents**

Ignaz M. D. Höhle<sup>[a]</sup>, Arzu Angl<sup>[a]</sup>, Regina Sinelnikov<sup>[b]</sup>, Jonathan G. C. Veinot<sup>[b]</sup> and Bernhard Rieger<sup>\*[a]</sup>

chem\_201405555\_sm\_miscellaneous\_information.pdf

## Table of Contents

1	General information.....	2
2	Synthetic procedures.....	2
2.1	Synthesis of Hydrogen Silsesquioxane (HSQ).....	2
2.2	Preparation of oxide-embedded silicon nanocrystals.....	2
2.3	Liberation of SiNCs .....	2
2.4	Synthesis of lithium phenylacetylide and (5-hexyl-2-thienyl)lithium .....	3
2.5	Functionalization of SiNCs with organometallic reagents.....	3
2.6	Quenching with 1-bromohexane .....	3
2.7	Quenching with propylene oxide .....	3
2.8	Two-step functionalization of SiNCs via hydrosilylation.....	3
3	Analytical data .....	4
3.1	Nuclear Magnetic Resonance Spectroscopy (NMR) .....	4
3.2	Fourier Transform Infrared Spectroscopy (FTIR) .....	5
3.3	Photoluminescence Spectra (PL) .....	6
3.4	Thermogravimetric analysis (TGA).....	6
3.5	Dynamic light scattering (DLS) .....	7
3.6	High Resolution Transmission Electron Microscopy (HR-TEM) .....	8



## 1 General information

All reactants and reagents were purchased from Sigma-Aldrich and used without further purification if not stated otherwise. Phenyllithium was bought as a 1.8 M solution in dibutyl ether, hexyllithium as 2.3 M solution in hexane, butyllithium as 2.5 M solution in hexane and hexylmagnesiumbromide as 2.0 M solution in diethylether. Dry toluene and THF was obtained from a MBraun SPS 800 solvent purification system.

FTIR spectra were measured with a *Bruker Vertex 70 FTIR* using a *Platinum ATR* from *Bruker*. Nuclear magnetic resonance (NMR) spectra were measured on a *ARX-300* from *Bruker* in deuterated chloroform at 300 K. Photoluminescence (PL) spectra were taken with an *AVA-Spec 2048* from *Avantes* using a *Prizmatix (LED Current controller)* as light source. Dynamic light scattering measurements were made with a *Dyna Pro NanoStar* from *Wyatt* with toluene as solvent. TGA-analysis was performed with a *Netzsch TG 209 F1 Libramachine* at a heating rate of 10 K/min in an argon flow of 20 mL/min (Ar 4.8) in platinum pans. HR-TEM measurements were performed on a JEM-2200FS TEM with 200kV field emission gun.

## 2 Synthetic procedures

### 2.1 Synthesis of Hydrogen Silsesquioxane (HSQ)

The HSQ was prepared following a literature procedure.<sup>[1]</sup> To a mixture of sulfuric acid (22.7 g) and fuming sulfuric acid (13.9 g), Toluene (45 ml) was added via a dropping funnel for 10 min and stirred for additional 20 min. To the yellow, biphasic solution,  $\text{HSiCl}_3$  (21.5 g, 0.16 mol) dissolved in 110 ml Toluene was added over the course of several hours. Subsequently, the upper layer was separated, washed thrice with sulfuric acid 50 % (w/w) and stirred over night over  $\text{MgSO}_4$  and  $\text{CaCO}_3$ . After filtration, the solvent was removed *in vacuo* giving a colorless solid.

EA:    calculated Si: 52.90%, H: 1.90%                    found Si: 51.18 %, H: 1.88%

### 2.2 Preparation of oxide-embedded silicon nanocrystals

HSQ (7 g) was placed in a quartz reaction boat, transferred to a *Nabertherm RD 30/200/11* oven with quartz working tube and heated from ambient to a peak processing temperature of 1100 °C at 18 °C/min in a slightly reducing atmosphere (5%  $\text{H}_2$ /95%  $\text{N}_2$ ). The sample was maintained at the peak processing temperature for 1 h. Upon cooling to room temperature, the resulting amber solid was ground into a fine brown powder using mortar and pestle to remove large particles. Further grinding was achieved via shaking the powder dispersed in ethanol for 24h with high-purity silica beads using a *WAB Turbula mixer*. The resulting SiNC/SiO<sub>2</sub> composite was dried *in vacuo* and the powder stored in glass vials.

### 2.3 Liberation of SiNCs

Hydride-terminated SiNCs were liberated from the SiNC/SiO<sub>2</sub> composites using HF etching. First, 0.30 g of the ground SiNC/SiO<sub>2</sub> composite was transferred to a ethylene-tetrafluoroethylene (ETFE) beaker equipped with a Teflon-coated stir bar. Ethanol (3 mL) and water (3 mL) were then added under mechanical stirring to form a brown suspension, followed by 3 mL of 49% HF aqueous solution. After

1 h of etching in subdued light, the suspension appeared yellow. Hydride-terminated SiNCs were subsequently extracted from the aqueous layer into ca. 30 mL of toluene by multiple (i.e.,  $3 \times 10$  mL) extractions. The SiNC toluene suspension was transferred to ETFE-centrifuge tubes, and the SiNCs were isolated by centrifugation at 5000 rpm.

## 2.4 Synthesis of lithium phenylacetylide and (5-hexyl-2-thienyl)lithium

2-hexylthiophene was synthesized following literature procedures.<sup>[2]</sup> Phenyllithium or 2-hexylthiophene respectively (15 mmol) is dissolved in 9 ml THF and *n*-butyllithium (2.5 M in hexanes, 6 ml, 15 mmol) is added to the reaction flask dropwise in 1 hour at  $-78^{\circ}\text{C}$ . Upon the completion of the addition the reaction mixture is stirred for 15 more minutes, then it is brought to room temperature. The product is obtained as a clear black or yellow solution. The solution is degassed and stored in the schlenk flask in a cool place.

## 2.5 Functionalization of SiNCs with organometallic reagents

Hydride terminated Si-NCs, obtained by etching 300 mg Si/SiO<sub>2</sub> composite, are dispersed in 2 ml of a degassed solution of the organolithium reagents. The organolithium reagents used for this study are diluted with toluene to form 0.1 M solutions. The mixture is stirred for 2 h and afterwards poured into methanol (5 ml) acidified with HCl conc. (0.2 ml) or deuterated methanol and DCl conc. respectively. The formed precipitate is centrifuged at 9000 rpm for 10 min and the sediment is redispersed in minimal amount of toluene. The precipitation-centrifugation-redispersion step is performed two more times from methanol and toluene. Finally the functionalized SiNCs are dispersed in toluene, filtered through a 0.45  $\mu\text{m}$  PTFE syringe filter and stored in vials for further use.

For the functionalization with hexylmagnesiumbromide, the same procedure was used but the solvent was changed to a 1:1 mixture of toluene and diethyl ether.

## 2.6 Quenching with 1-bromohexane

SiNCs from 300 mg etched Si/SiO<sub>2</sub> are reacted with phenyllithium as described above. After 5 h, the reaction mixture is cooled to  $-78^{\circ}\text{C}$  and 1-bromohexane (0.56 ml, 4.0 mmol) is added. After 10 min, the dispersion is warmed to room temperature and stirred for further 2.5 h. Subsequently, the functionalized SiNCs are purified by three precipitation/centrifugation/redispersion steps with 1:1 ethanol/methanol and toluene. Finally the functionalized SiNCs are dispersed in toluene, filtered through a 0.45  $\mu\text{m}$  PTFE syringe filter and stored in vials for further use.

## 2.7 Quenching with propylene oxide

SiNCs from 300 mg etched Si/SiO<sub>2</sub> are reacted with phenyllithium as described above. After 5 h, the reaction mixture is cooled to  $-78^{\circ}\text{C}$  and propylene oxide (0.28 ml, 4.0 mmol) is added. After 30 min, the dispersion is warmed to room temperature and stirred for further 90 min. Subsequently, the solvent and excess propylene oxide is evaporated *in vacuo* and the residue redispersed in 1 ml of toluene. Purification is performed *via* three precipitation/centrifugation/redispersion steps with 1:1 ethanol/methanol and toluene. Finally the functionalized SiNCs are dispersed in toluene, filtered through a 0.45  $\mu\text{m}$  PTFE syringe filter and stored in vials for further use.

## 2.8 Two-step functionalization of SiNCs via hydrosilylation

Dry phenyllithium functionalized Si-NCs are resuspended in a mixture of toluene (3 ml) and 1-dodecene (0.66 ml, 3.0 mmol). The clear dispersion is degassed three times *via* freeze-pump-thaw cycles. 4-decylbenzene diazonium tetrafluoroborate (5 mg, 15.3  $\mu\text{mol}$ ) is added to start the

hydrosilylation and the reaction is stirred overnight. Purification of the functionalized SiNCs is performed by precipitation from a 1:1 mixture of ethanol and methanol (5 ml), centrifugation and redispersion in toluene. This cycle is repeated three times and the SiNCs are filtered afterwards through a 0.45  $\mu\text{m}$  PTFE syringe filter and stored in vials for further use.

### 3 Analytical data

#### 3.1 Nuclear Magnetic Resonance Spectroscopy (NMR)

NMR spectra of SiNCs functionalized with *n*-hexyllithium are in accordance with published spectra of SiNCs functionalized with alkyl chains via hydrosilylation.<sup>[3]</sup> The  $\text{CH}_2$ -group directly bound to SiNC surface (F) is expected to appear around 0.5 ppm.<sup>[4]</sup> However with SiNCs in the size range of a few nanometers, this group is commonly not observed.<sup>[3,5,6]</sup> A possible explanation is that the signals cannot be detected due to a broadening induced by anisotropic effects and a prolonged relaxation time since the molecules cannot move freely on the SiNC surface.

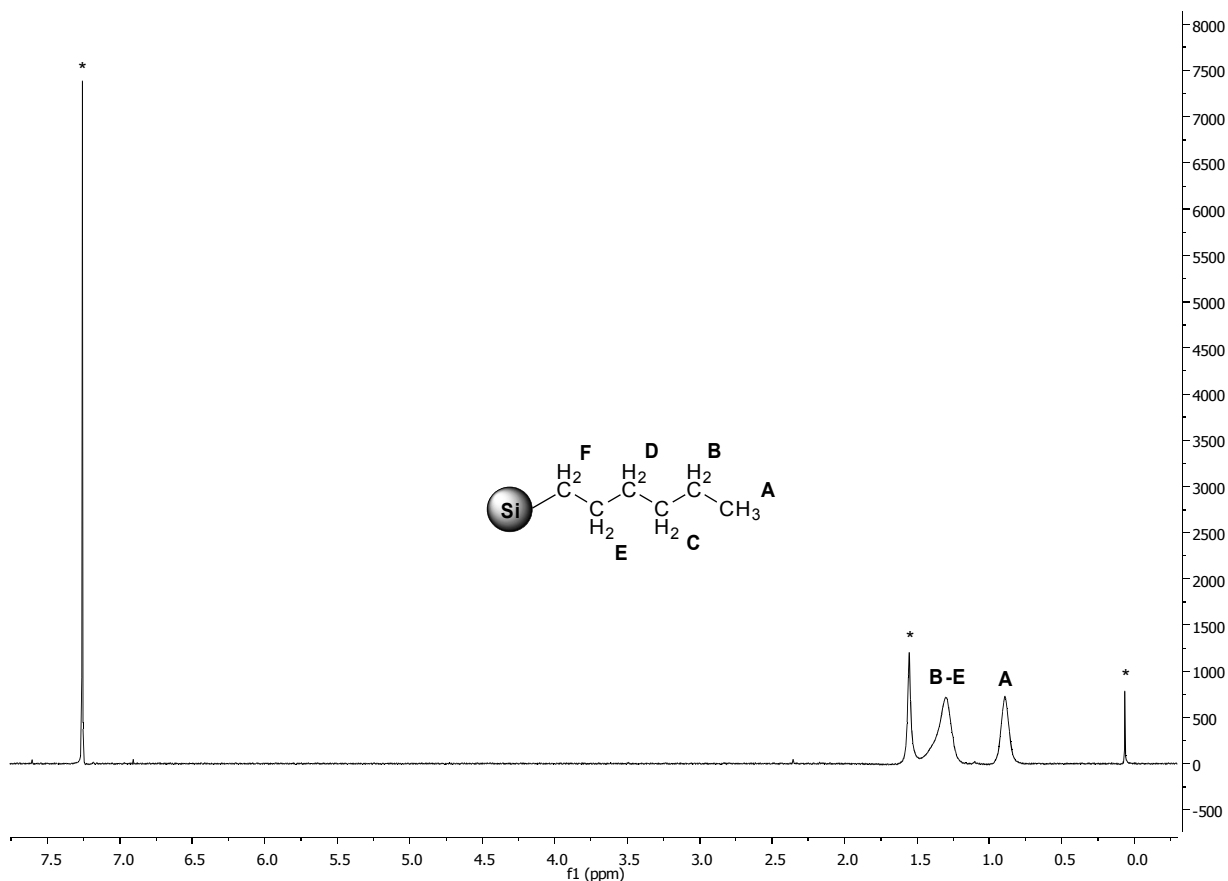


**Figure S1:** NMR spectrum of SiNCs functionalized with *n*-hexyllithium. Signals from the solvent are marked with an asterisk.

### 3.2 Fourier Transform Infrared Spectroscopy (FTIR)

A control experiment was conducted to rule out that the formation of Si–D groups is due to a proton/deuteron exchange *via* deprotonation of the SiNC surface. H-terminated SiNCs were treated with deuterated methanol, acidified with DCl, in the same manner as described above for the workup of SiNCs functionalized with organolithium reagents. No Si–D bands are visible which indicates that the Si–D surface groups are indeed formed via quenching of the Si–Li surface species (Figure S2).

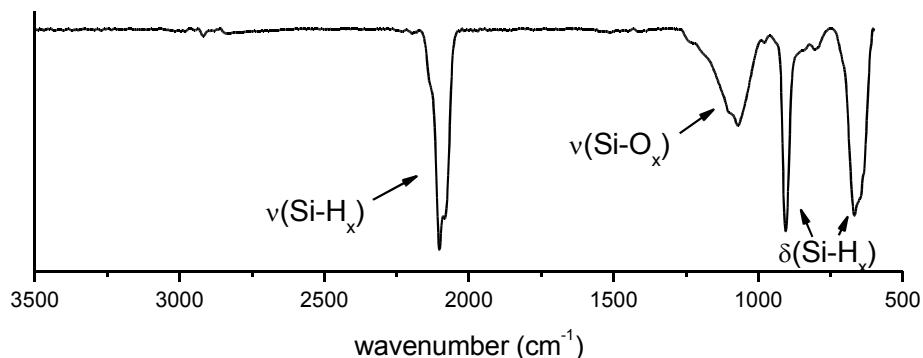


**Figure S2.** FTIR spectrum of H-terminated SiNCs treated with deuterated methanol and DCl.

SiNCs were reacted with hexylmagnesiumbromide analogous to the organolithium reagents. However the colloidal stabilization of the SiNCs was not as good as with hexyllithium so that the dispersion with the functionalized SiNCs was still turbid and could not be filtered through a 0.45  $\mu\text{m}$  PTFE filter. Also the FTIR shows bands of the surface bound hexyl groups with a lesser intensity (Figure S3). This could be due to the in general higher reactivity of organolithium compounds compared to Grignard reagents.

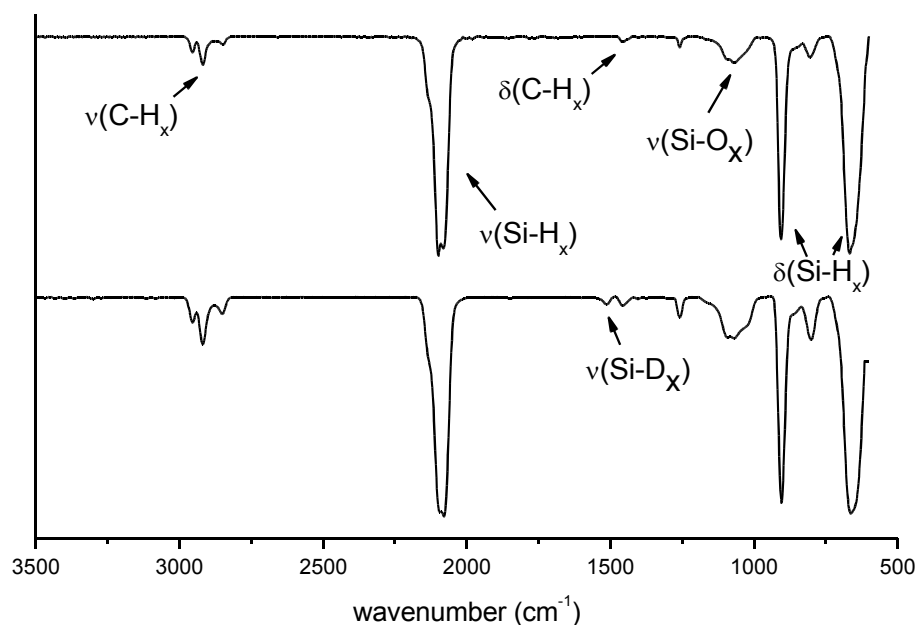


**Figure S3.** FTIR spectrum of SiNCs functionalized with hexylmagnesiumbromide.

### 3.3 Photoluminescence Spectra (PL)

SiNCs reacted with phenyllithium and quenched with 1-bromohexane or propylene oxide and SiNCs reacted first with phenyllithium and afterwards with dodecene also show PL maxima at 690 nm (Figure S4).

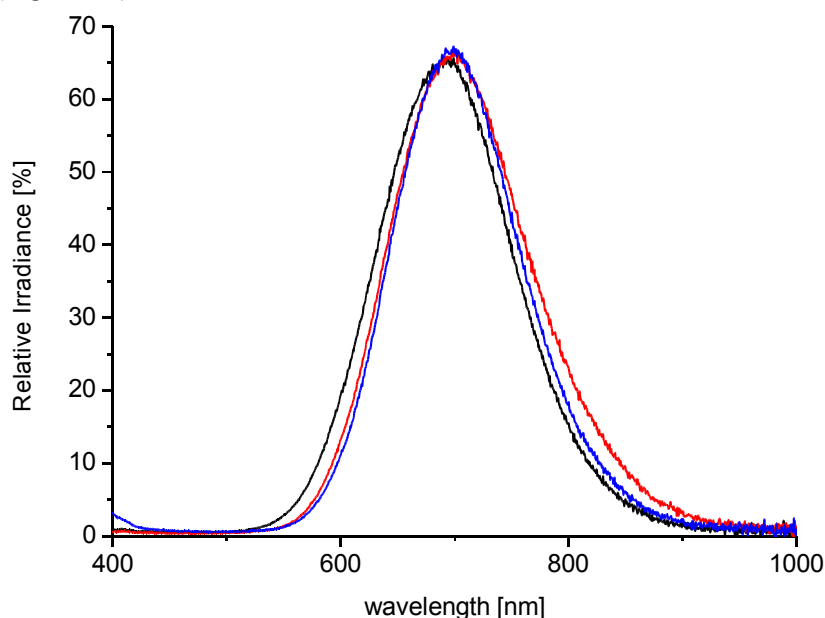


**Figure S4.** PL data of SiNCs functionalized with phenyllithium and dodecene (black), phenyllithium and 1-bromohexane (red) and phenyllithium and propylene oxide (blue) .

### 3.4 Thermogravimetric analysis (TGA)

To obtain a semiquantitative understanding of the amount of organic groups bound on the SiNCs, thermogravimetric (TG) analysis was performed of the SiNCs functionalized with organolithium reagents (Figure S5).

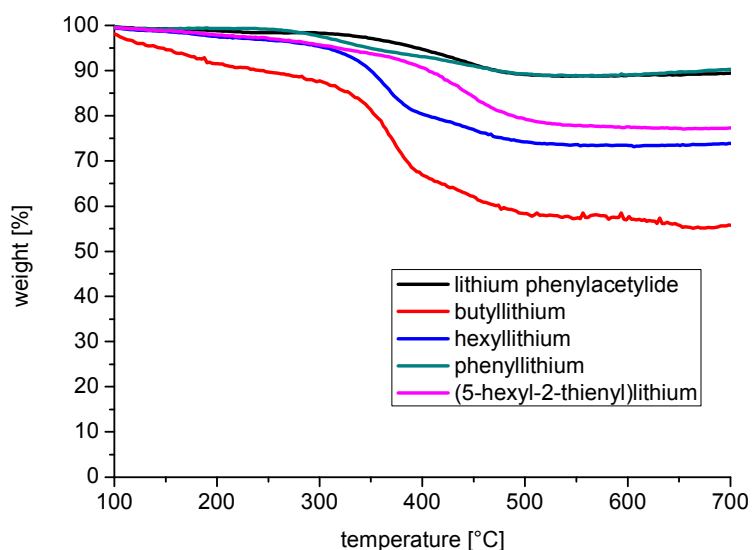


**Figure S5.** TG analysis of SiNCs functionalized with organolithium compounds.

The weightloss via TG was divided by the molecular weight of the bound surface groups to get comparable values (Table S1). The data suggests that the coverage with the aromatic organolithium reagents is similar for each compound. However the coverage with the aliphatic organolithium reagent hexyllithium is higher by a factor of around 2-2.5 and for the smaller butyllithium by a factor of 4-5. It can be assumed therefore that sterical issues are the main factor for the difference in surface coverage.

**Table S1.** TG data from SiNCs functionalized with organolithium compounds

Reagent	Weightloss [%]	Molecular weight [g/mol]	Weightloss/Molecular weight
<i>n</i> -butyllithium	38.0	57.1	0.67
<i>n</i> -hexyllithium	27.4	85.2	0.32
(5-hexyl-2-thienyl)lithium	23.8	167.3	0.14
lithiumphenylacetylide	11.8	101.1	0.12
phenyllithium	12.1	77.1	0.16

### 3.5 Dynamic light scattering (DLS)

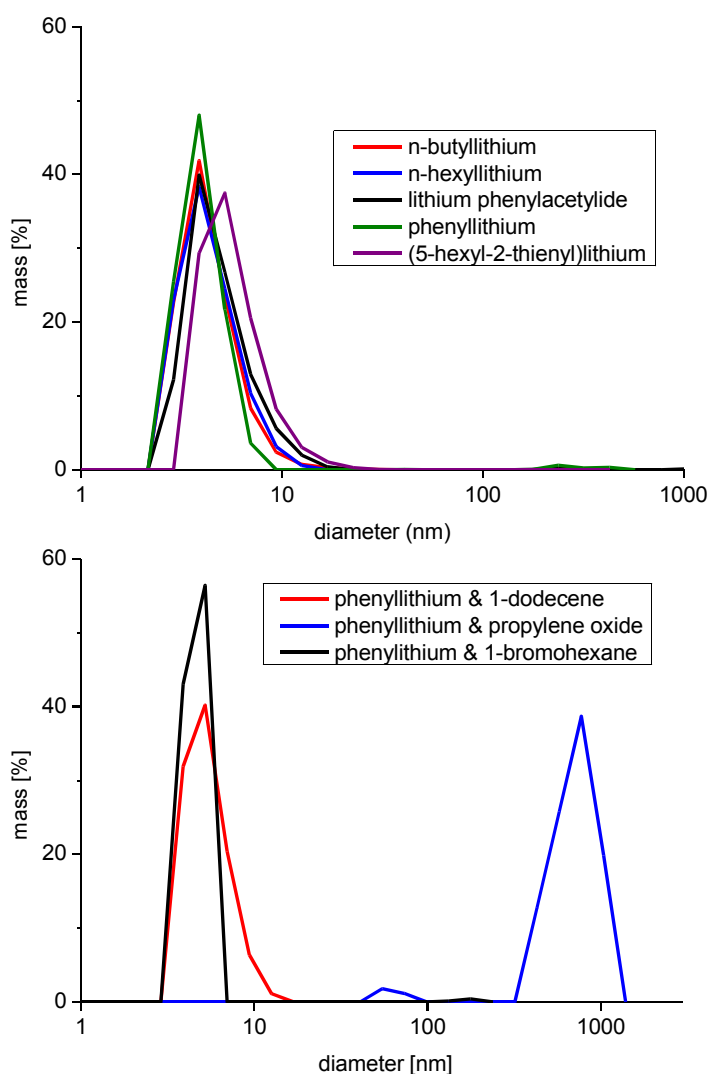


**Figure S6:** DLS data of the SiNCs functionalized with *n*-butyllithium, *n*-hexyllithium, lithium phenylacetylide, phenyllithium and (5-hexyl-2-thienyl)lithium (top) and SiNCs reacted with phenyllithium and 1-dodecene, propylene oxide and 1-bromohexane in a second step (bottom).

### 3.6 High Resolution Transmission Electron Microscopy (HR-TEM)

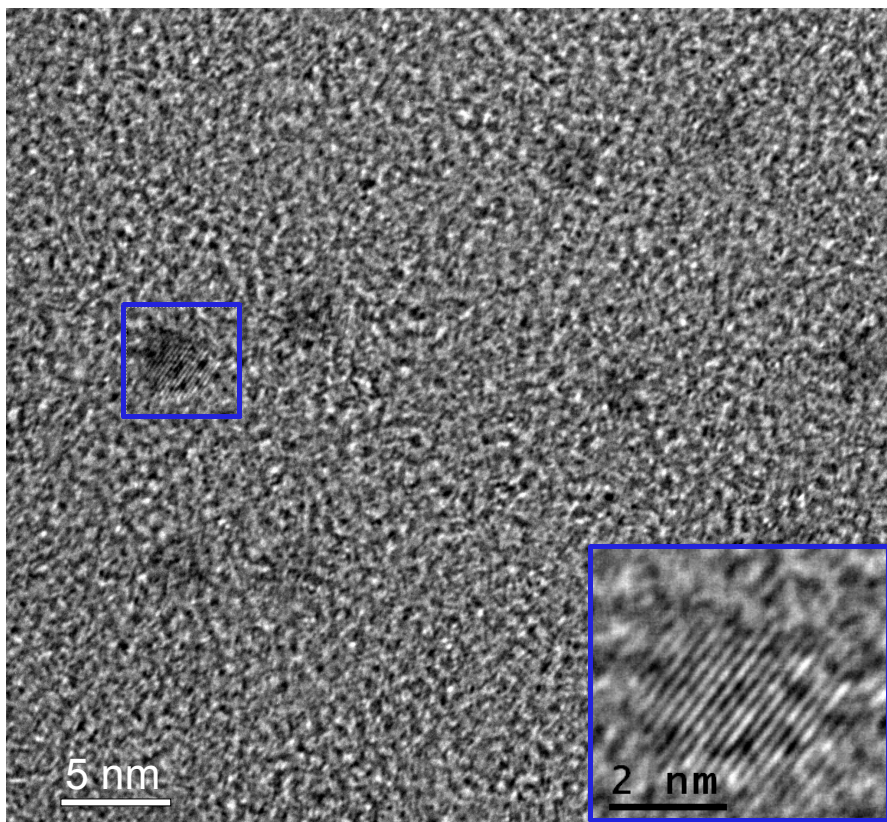


**Figure S7:** HR-TEM picture of SiNCs functionalized with *n*-hexyllithium. The lattice fringes of the crystals are clearly visible (blue box).

#### Literature

- [1] H. M. Bank, M. E. Cifuentes, E. M. Theresa, *United States Pat.* **1991**, 5.010.159.
- [2] C. Xia, X. Fan, J. Locklin, R. C. Advincula, *Org. Lett.* **2002**, 4, 2067–2070.
- [3] F. Hua, M. T. Swihart, E. Ruckenstein, *Langmuir* **2005**, 21, 6054–62.
- [4] J. M. J. Paulusse, M. W. F. Nielen, H. Zuilhof, *Chem. Mater.* **2012**, 4311–4318.
- [5] N. Shirahata, M. R. Linford, S. Furumi, L. Pei, Y. Sakka, R. J. Gates, M. C. Asplund, *Chem. Commun. (Camb)*. **2009**, 4684–6.
- [6] J. H. Ahire, Q. Wang, P. R. Coxon, G. Malhotra, R. Brydson, R. Chen, Y. Chao, *ACS Appl. Mater. Interfaces* **2012**, 4, 3285–92.

## 4.2 Photoluminescence through In-Gap States in Phenylacetylene Functionalized Silicon Nanocrystals

Surface chemistry plays an important role in controlling optical properties of SiNCs.<sup>5,7</sup> In our previous work, we presented the surface functionalization of SiNCs with hexyl, phenyl and phenylacetylene groups by using organolithium reagents. Upon surface functionalization, we observed that the PL maximum of phenylacetylene functionalized SiNCs red-shifted for ~50 nm, with respect to hexyl and phenyl functionalized counterparts.<sup>25</sup> Elucidating the mechanism leading to this phenomenon is of great interest because it may provide insights into the influence of conjugated surface groups on the SiNC electronic structure and optoelectronic properties.

This work aimed to explain the mechanism behind the observed red-shift with phenylacetylene functionalized SiNCs. Therefore, a detailed analysis on hexyl, phenyl and phenylacetylene functionalized SiNCs was performed combining optical spectroscopy and scanning tunneling microscopy/spectroscopy (STM/STS). This combination is crucial, as optical measurements alone cannot unambiguously determine the initial and final states associated with optical transitions. As a result, utilization of complementary techniques is required.<sup>3</sup> STM/STS is one of the most effective tools for studying the electronic structure of single colloidal semiconductor NCs. The main advantage of this approach over optical methods is that STS provides information regarding the electronic density of states (DOS) by mapping the conduction band (CB) and valence band (VB) states independently. Therefore, the single-particle (rather than excitonic) band gap can be evaluated directly.<sup>27</sup>

Only for phenylacetylene functionalized SiNCs, STS analysis revealed the presence of an in-gap state close to the CB-edge. The PL shift to a lower energy was attributed to a transition *via* this in-gap state, which reduce the effective band gap for recombination. To the best of our knowledge, this is the first time that an in-gap state, intentionally introduced *via* surface functionalization, has been observed by STS for SiNCs.



**Manuscript:**

**Photoluminescence through In-Gap States in Phenylacetylene  
Functionalized Silicon Nanocrystals**

<b>Status</b>	Published on March 17, 2016
<b>Journal</b>	<i>Nanoscale</i> , 2016, Volume 8, 7849-7853.
<b>Publisher</b>	Royal Society of Chemistry
<b>DOI</b>	10.1039/C6NR01435F
<b>Authors</b>	Arzu Angi, Regina Sinelnikov, Al Meldrum, Jonathan G. C. Veinot, Isacc Balberg, Doron Azulay, Oded Millo, Bernhard Rieger

Angi *et al.* *Nanoscale*, **2016**, 8, 7849-7853. – Reproduced by permission of The Royal Society of Chemistry.



Cite this: *Nanoscale*, 2016, **8**, 7849

Received 19th February 2016,  
Accepted 16th March 2016

DOI: 10.1039/c6nr01435f

www.rsc.org/nanoscale

## Photoluminescence through in-gap states in phenylacetylene functionalized silicon nanocrystals†

Arzu Angi,<sup>a</sup> Regina Sinelnikov,<sup>b</sup> Al Meldrum,<sup>c</sup> Jonathan G. C. Veinot,<sup>b</sup> Isacc Balberg,<sup>d</sup> Doron Azulay,<sup>d</sup> Oded Millo\*<sup>d</sup> and Bernhard Rieger\*<sup>a</sup>

**Optoelectronic properties of Si nanocrystals (SiNCs) were studied by combining scanning tunneling spectroscopy (STS) and optical measurements. The photoluminescence (PL) of phenylacetylene functionalized SiNCs red shifts relative to hexyl- and phenyl-capped counterparts, whereas the absorption spectra and the band gaps extracted from STS are similar for all surface groups. However, an in-gap state near the conduction band edge was detected by STS only for the phenylacetylene terminated SiNCs, which can account for the PL shift *via* relaxation across this state.**

Silicon nanocrystals (SiNCs) have gained significant interest in recent years due to their intriguing properties that are not exhibited by their bulk counterparts. When the dimensions of SiNCs are reduced below the Bohr radius of an exciton in Si (~4.5 nm),<sup>1</sup> they photoluminesce at energies that are tunable by defining the SiNC size<sup>2–4</sup> and surface functionalization.<sup>5–8</sup> This, in combination with their low toxicity,<sup>9</sup> biocompatibility<sup>10</sup> and elemental abundance of Si, makes SiNCs a promising material for several applications including LEDs,<sup>11</sup> solar cells,<sup>12</sup> sensors<sup>13</sup> and photoluminescent biomarkers.<sup>10</sup>

The surface chemistry of SiNCs can have a significant impact on their optoelectronic properties.<sup>5</sup> For instance, SiNC photoluminescence has been tuned across the visible spectrum by changing surface groups (*i.e.*, amine, phosphine, oxide and acetal) without altering the NC size.<sup>14</sup> In this context, controlling surface characteristics *via* surface functionalization is essential to make SiNCs useful in optoelectronic applications by preserving and/or controlling their properties.

Recently, we presented the surface functionalization of hydride terminated SiNCs with organolithium reagents.<sup>15</sup> This method offers, for the first time, the opportunity to bind aryl and alkynyl groups, such as phenyl and phenylacetylene, directly to the hydride terminated SiNC surface while ensuring monolayer coverage. Subsequent to the functionalization, we observed that SiNC PL was influenced by the surface group identity. For phenylacetylene functionalized SiNCs, the PL maximum red-shifted to ~735 nm, compared to hexyl and phenyl functionalized SiNCs which emitted at ~685 nm (Fig. 1).<sup>15,16</sup> Elucidating the mechanism leading to this phenomenon is of great interest because it may provide insights into the influence of conjugated surface groups on SiNC electronic structures and optoelectronic properties.

In this work, we present a detailed analysis of the optoelectronic properties of hexyl, phenyl and phenylacetylene functionalized SiNCs with an attempt to explain the PL red-shift observed with phenylacetylene surface groups by utilizing PL and UV-Vis spectroscopy, excited state lifetime measurements and scanning tunneling microscopy/spectroscopy (STM/STS). STS results show that the band gap of the SiNCs is nearly independent of these three surface groups studied. However, for SiNCs functionalized with phenylacetylene, the tunneling spectra reveal the formation of an in-gap state close to the conduction band edge of SiNCs. The PL shift to a lower energy can be attributed to a transition *via* this in-gap state, which reduces the apparent band gap for recombination. To the best

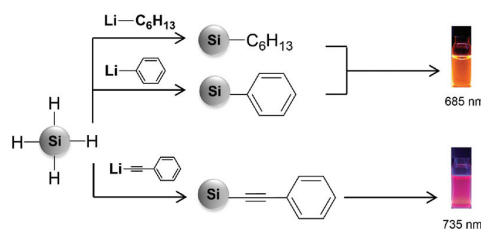


Fig. 1 Influence of hexyl, phenyl and phenylacetylene groups on PL emission of SiNCs.

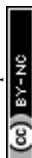
<sup>a</sup>WACKER-Lehrstuhl für Makromolekulare Chemie, Technische Universität München, Lichtenbergstrasse 4, 85747 Garching, Germany. E-mail: rieger@tum.de

<sup>b</sup>Department of Chemistry, University of Alberta, 11227 Saskatchewan Drive, Edmonton, Alberta, Canada T6G 2G2

<sup>c</sup>Department of Physics, University of Alberta, Edmonton, Alberta T6G 2G2, Canada

<sup>d</sup>Racah Institute of Physics, The Hebrew University of Jerusalem, Jerusalem 91904, Israel. E-mail: milode@mail.huji.ac.il

† Electronic supplementary information (ESI) available: Detailed experimental procedures, additional HR-TEM images and PL lifetime data. See DOI: 10.1039/c6nr01435f



of our knowledge, this is the first time that an in-gap state, intentionally introduced *via* surface functionalization, has been observed by STS for SiNCs.

The SiNCs used in this work were synthesized by thermolysis of hydrogen silsesquioxane (HSQ) at 1100 °C for 1 hour under an atmosphere consisting of 5% hydrogen and 95% nitrogen.<sup>17</sup> This procedure yields SiNCs in a silica-like matrix. Freestanding, hydride terminated SiNCs are obtained by etching the composite with ethanolic HF and final extraction into toluene.

Surface functionalization was performed by dispersing SiNCs, freshly etched from a 300 mg Si/SiO<sub>2</sub> composite, in 2 mL 0.1 M solution of the organolithium reagent in toluene and stirring overnight at room temperature. The reaction was quenched upon addition of an acidified methanol-ethanol mixture, and the functionalized SiNCs were further purified by two antisolvent precipitation–dispersion steps.

FT-IR spectroscopy was utilized to confirm the surface functionalization. The freshly etched, hydride terminated SiNCs showed only Si–H bands in the IR spectrum at 2100, 906, and 660 cm<sup>-1</sup>, without any indication of oxidation (Fig. 2A). For the SiNCs functionalized with *n*-hexyllithium, strong C–H and C–C stretching bands appeared at *ca.* 2900 and 1450 cm<sup>-1</sup>, respectively (Fig. 2B). In the case of phenyl and phenylacetylene functionalized SiNCs, the IR spectra displayed aromatic C–H stretching modes between 3020 and 3085 cm<sup>-1</sup> and aromatic C–C stretching peaks at 1595, 1490 and 1442 cm<sup>-1</sup>, together with aromatic overtones between

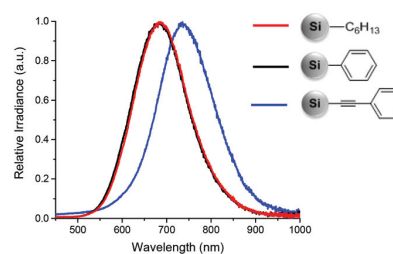


Fig. 3 PL spectra of SiNCs functionalized with *n*-hexyllithium (red), phenyllithium (black) and lithium phenylacetylide (blue).

1600 and 2000 cm<sup>-1</sup> (Fig. 2C and D). For phenylacetylene functionalized SiNCs, an asymmetric C≡C alkyne stretching band was observed at 2150 cm<sup>-1</sup> as a shoulder on Si–H stretching at 2100 cm<sup>-1</sup>. In every case, only a minor surface oxidation was evidenced, by the Si–O band at 1050 cm<sup>-1</sup>.

The PL spectra show that both hexyl and phenyl functionalized SiNCs emit at around 685 nm. However, when the SiNCs are functionalized with phenylacetylene, the PL maximum redshifts to 735 nm, (Fig. 3) despite the particle size remaining constant.

The influence of surface-bonded molecules on the optical properties of SiNCs is a complex issue. Surface groups can modify the optical transitions of NCs by introducing additional surface states and defects.<sup>14,18</sup> In general, size dependent, red/NIR PL emission accompanied by an excited life-time in the range of microseconds, dominantly originates from quantum confined band gap emission.<sup>19</sup> In our study, observed PL decay curves (ESI Fig. S1†) were strongly non-exponential. The decay traces were fit with a log-normal lifetime distribution,<sup>20</sup> which is applicable for ensembles of SiNCs.<sup>21</sup> From the fitting parameters, we extracted a mean lifetime of 89.6, 79.7, and 102.1 μs for the hexyl, phenyl and phenylacetylene functionalized SiNCs, respectively. Since red PL, together with μs excited-state lifetime was observed, the PL is considered to be through a band gap transition.<sup>7,19</sup>

In several reports, shifts in PL emission maxima of SiNCs induced by different surface groups were observed together with changes in UV-Vis absorption.<sup>6,18</sup> In the present work, even though the PL wavelength of phenylacetylene functionalized SiNCs appears at a lower energy, the absorption spectra obtained for hexyl, phenyl and phenylacetylene did not show any significant difference in the absorption edge (Fig. 4).

This, as well as direct evaluation (TEM and STM) of the NC size (*vide infra*) rule out the possibility that the difference in PL spectra arises from an effective reduction of the SiNC diameter upon treatment with phenyllithium or hexyllithium reagents or to a different dielectric confinement effect<sup>22</sup> in phenylacetylene functionalized SiNCs. If this was the case, these effects should contribute equally to the PL and absorption spectra leading to changes in both.

Difficulties associated with interpreting the optical spectroscopy data (PL and absorption) measured on SiNCs and relating them to the intrinsic level electronic structure are

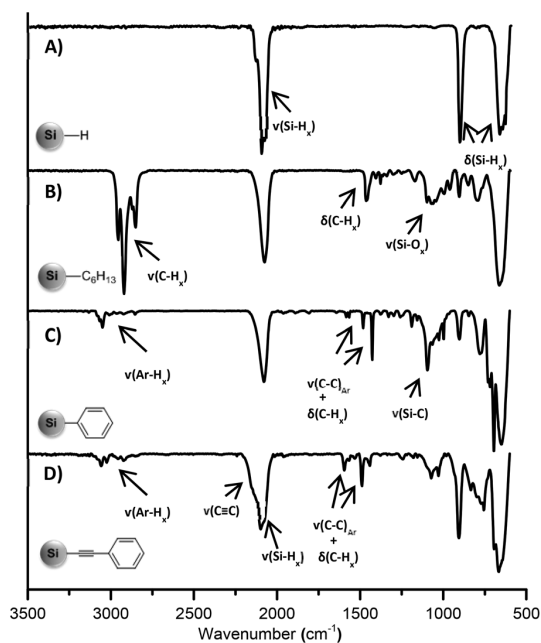


Fig. 2 FT-IR spectra of (A) hydride terminated SiNCs; SiNCs functionalized with (B) *n*-hexyllithium; (C) phenyllithium; (D) lithium phenylacetylide.



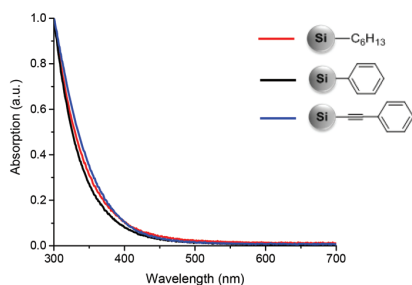


Fig. 4 UV-Vis spectra of SiNCs functionalized with *n*-hexyllithium (red), phenyllithium (black) and lithium phenylacetylide (blue). Absorption is normalized at 300 nm.

common.<sup>3,23,24</sup> These challenges primarily stem from the fact that optical measurements alone cannot unambiguously determine the initial and final states associated with the excitation/recombination transitions. In particular, the influence of the surface groups on PL emission and the electronic structure of SiNCs cannot be deduced by optical spectroscopy. Clearly, complementary methods are required if the origin of the PL red-shift seen for the phenylacetylene functionalized SiNCs is to be elucidated.

STM/STS is one of the most effective tools for studying the electronic structure/properties of single colloidal semiconductor NCs.<sup>3,25</sup> The main advantage of this approach over optical methods is STS provides information regarding the electronic density of states (DOS) by mapping the conduction band (CB) and valence band (VB) states independently. Therefore the single-particle (rather than excitonic) band gap can be evaluated directly.<sup>26</sup> In addition, and most significant for our present work, the tunneling spectra can reveal in-gap states associated with either surface or NC-bulk defects.<sup>27,28</sup> Such states are usually not observed in absorption measurements due to their very small absorption cross-sections.

STM images and a topographic cross-section taken on one of the isolated hexyl functionalized SiNCs, whose electronic structure was examined, are shown in Fig. 5A and B. All images were acquired with a set bias of 2.2 eV (well above the CB edge where the DOS of the SiNC is appreciable) and a set current of 0.2 nA. Under these conditions, the cross-section height corresponds well to the diameter of the SiNC, yielding in this case (and all other SiNCs presented here) a mean size of  $\sim 3$  nm. Further experimental details regarding the STM-STs measurements are given in the ESI.† TEM images of SiNCs functionalized with *n*-hexyllithium also reveal the average diameter of SiNCs around 3 nm (Fig. 5C). In the HR-TEM image, crystal lattice fringes are clearly seen (Fig. 5D).

Tunneling spectra measured on isolated SiNCs are shown for all three different surface functionalities together with the corresponding STM topography images and cross-sections in the insets (Fig. 6). Band gaps are deduced directly from the STS data from the energy difference between the VB and CB edges. For each band, the edge is defined here as the mid-value between the position of the first peak (or shoulder) and

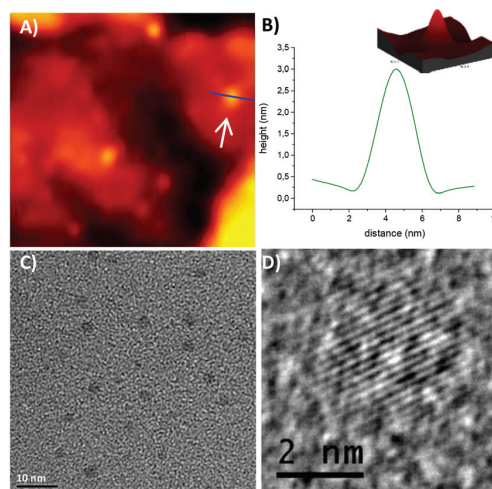
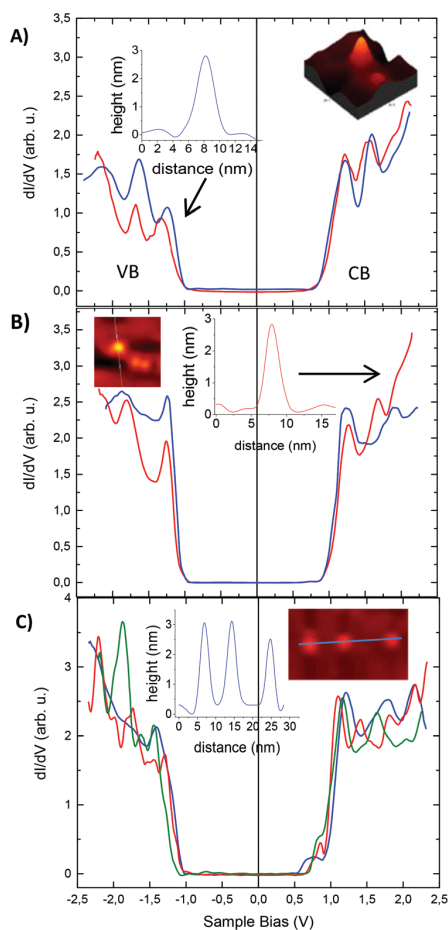


Fig. 5 (A) STM image ( $150 \times 150 \text{ nm}^2$ ) showing isolated SiNCs functionalized with *n*-hexyllithium; (B) STM topographic image of a single SiNC marked by the white arrow in (A) and a cross-section taken along the blue line. (C) TEM image of *n*-hexyllithium functionalized Si-NCs with an average diameter of 3 nm; (D) HR-TEM image of 3 nm SiNCs functionalized with *n*-hexyllithium, lattice-fringes are clearly observable. Both methods verify a 3 nm average size of the SiNCs.

the onset of detectable DOS.<sup>29</sup> This method affords band gaps of hexyl and phenyl functionalized SiNCs of  $2.1 \pm 0.1$  eV. Note that the band gap values obtained by STS are larger than exciton band gaps determined by PL maxima (685 nm = 1.81 eV). The reason for that is predominantly three-fold. First, the electron-hole Coulomb interaction that is incorporated in the optical (excitonic) gap does not play a role in the fundamental single-particle gap measured by STS.<sup>26,30</sup> Second, the tunneling spectra are measured in the double-barrier tunnel junction configuration and thus the apparent gap is broadened due to the effect of voltage division between the two tunnel barriers involved; the tip-SiNC and the SiNC-substrate junctions.<sup>26</sup> Third, the polarization energy associated with electron tunneling through the SiNC also contributed to the widening of the measured gap.<sup>31</sup> We note that the STS-extracted gaps found here are somewhat larger than those reported in ref. 3. This may be due to the different ligands used here, which may affect the latter two factors.

In the case of phenylacetylene functionalized SiNCs, the band gap is still in the range  $2.1 \pm 0.1$  eV, in spite of the red-shifted PL. However, an in-gap state close to the CB-edge of the SiNCs is clearly observed in their tunneling spectra (Fig. 6C). This observation was very robust and detected in every measurement acquired for these NCs. The separation of the in-gap state from the CB-edge varied between 140 meV (red and green curves in Fig. 6C) and 190 meV (blue curve), where most spectra showed  $\sim 160$  meV separation. These values are in the range of, yet somewhat larger than, the PL red-shift ( $\sim 130$  meV). The slight enlargement may be due to the afore-





**Fig. 6** Tunneling spectra measured on  $\sim 3$  nm SiNCs functionalized with (A) *n*-hexyllithium; (B) phenyllithium; (C) lithium phenylacetylide. The insets show some of the NCs and the corresponding cross-section on which the spectra were acquired. The extracted band gaps of the SiNCs are all around 2.1 eV, except for the green curve in (C) which was measured on the smaller, rightmost, NC. Importantly, the spectra measured on the phenylacetylene-capped SiNCs (in C) exhibit in-gap states close to the CB-edge.

mentioned voltage division effect. After observing the in-gap state introduced by the phenylacetylene surface groups, along with the independence of the STS gap on surface functionalization, we suggest that the shift of PL to lower energy can be accounted for by a transition across this state, which reduces the apparent band gap for recombination.

Direct covalent bonding of a  $\pi$ -conjugated molecule to a silicon atom can efficiently reduce its HOMO–LUMO gap because of the  $\sigma^*-\pi^*$  conjugation between the Si core and the bonded conjugated molecule.<sup>32</sup> The formation of states near band edges was theoretically expected to be the reason for the narrowing of the band gap.<sup>33</sup> Such a conjugation between the Si core and the surface bound conjugated molecule can enhance the optical absorption of SiNCs at longer wavelengths which is highly desired for light harvesting applications. In

contrast, no change in UV-Vis absorption was observed in the present system; this may result from the comparatively short conjugation length of phenylacetylene, and the corresponding small cross-section for photon absorption through these states. The effect of different conjugated surface groups with varied conjugation lengths on the optoelectronic properties and light harvesting efficiencies of SiNCs is under investigation.

## Conclusions

In summary, we utilized STM/STS in combination with optical measurements to study the optoelectronic properties of hexyl, phenyl and phenylacetylene functionalized Si-NCs. PL emission of phenylacetylene functionalized SiNCs red-shifts for around 50 nm relative to hexyl- and phenyl-capped Si-NCs. No significant difference was observed in the band gaps deduced from STS and UV-Vis absorption measurements on Si-NCs terminated with these three different surface groups. However, for phenylacetylene functionalized SiNCs, the tunneling spectra revealed an in-gap state close to the CB edge. The lowering in PL emission energy can be attributed to a transition across this state, which reduces the apparent band gap for the recombination process. These results expand the understanding of the influence of the surface groups on the electronic structure of SiNCs and can lead to the control of the properties utilized in optoelectronic devices.

## Acknowledgements

B. R., J. G. C. V. and A. M. acknowledge the funding from DFG IRTG (2022) and NSERC CREATE programs for Alberta/TU München International Graduate School. J. G. C. V. and A. M. thank the NSERC DG program for continued generous support. A. A. is grateful for the scholarship from Studienstiftung des Deutschen Volkes. R. S. acknowledges the funding from AITF. O. M. and I. B. acknowledge support of the Harry de Jur Chair in Applied Science (O. M.), the Enrique Berman Chair in Solar Energy Research (I. B.) and the Focal Technology Area program within the Israel National Nanotechnology Initiative. Ignaz Höhle is thanked for valuable discussions. Kai Cui is thanked for assistance with HR-TEM measurements.

## Notes and references

- 1 E. G. Barbagiovanni, D. J. Lockwood, P. J. Simpson and L. V. Goncharova, *J. Appl. Phys.*, 2012, **111**, 34307.
- 2 G. Ledoux, O. Guillois, D. Porterat, C. Reynaud, F. Huisken, B. Kohn and V. Paillard, *Phys. Rev. B: Condens. Matter*, 2000, **62**, 15942–15951.
- 3 O. Wolf, M. Dasog, Z. Yang, I. Balberg, J. G. C. Veinot and O. Millo, *Nano Lett.*, 2013, **13**, 2516–2521.



- 4 X. Wen, P. Zhang, T. A. Smith, R. J. Anthony, U. R. Kortshagen, P. Yu, Y. Feng, S. Shrestha, G. Coniber and S. Huang, *Sci. Rep.*, 2015, **5**, 12469.
- 5 K. Dohnalová, T. Gregorkiewicz and K. Kúsová, *J. Phys.: Condens. Matter*, 2014, **26**, 173201.
- 6 T. Zhou, R. T. Anderson, H. Li, J. Bell, Y. Yang, B. P. Gorman, S. Pylypenko, M. T. Lusk and A. Sellinger, *Nano Lett.*, 2015, **15**, 3657–3663.
- 7 M. Dasog and J. G. C. Veinot, *Phys. Status Solidi B*, 2014, **251**, 2216–2220.
- 8 M. Dasog, J. Kehrle, B. Rieger and J. G. C. Veinot, *Angew. Chem., Int. Ed.*, 2016, **55**, 2322–2339.
- 9 J. Liu, F. Erogbogbo, K.-T. Yong, L. Ye, J. Liu, R. Hu, H. Chen, Y. Hu, Y. Yang, J. Yang, I. Roy, N. A. Karker, M. T. Swihart and P. N. Prasad, *ACS Nano*, 2013, **7**, 7303–7310.
- 10 F. Erogbogbo, K.-T. Yong, I. Roy, G. Xu, P. N. Prasad and M. T. Swihart, *ACS Nano*, 2008, **2**, 873–878.
- 11 F. Maier-Flaig, J. Rinck, M. Stephan, T. Bockrocker, M. Bruns, C. Kübel, A. K. Powell, G. A. Ozin and U. Lemmer, *Nano Lett.*, 2013, **13**, 475–480.
- 12 M. Dutta, L. Thirugnanam, P. van Trinh and N. Fukata, *ACS Nano*, 2015, **9**, 6891–6899.
- 13 C. M. Gonzalez, M. Iqbal, M. Dasog, D. G. Piercey, R. Lockwood, T. M. Klapötke and J. G. C. Veinot, *Nanoscale*, 2014, **6**, 2608–2612.
- 14 M. Dasog, G. B. De los Reyes, L. V. Titova, V. Lyubov, F. A. Hegmann and J. G. C. Veinot, *ACS Nano*, 2014, **8**, 9636–9648.
- 15 I. M. D. Höhle, A. Angi, R. Sinelnikov, J. G. C. Veinot and B. Rieger, *Chem. – Eur. J.*, 2015, **21**, 2755–2758.
- 16 I. M. D. Höhle, J. Kehrle, T. K. Purkait, J. G. C. Veinot and B. Rieger, *Nanoscale*, 2015, **7**, 914–918.
- 17 C. M. Hessel, E. J. Henderson and J. G. C. Veinot, *Chem. Mater.*, 2006, **18**, 6139–6146.
- 18 M. X. Dung, D. D. Tung, S. Jeong and H.-D. Jeong, *Chem. – Asian J.*, 2013, **8**, 653–664.
- 19 V. A. Belyakov, V. A. Burdov, R. Lockwood and A. Meldrum, *Adv. Opt. Technol.*, 2008, 1–32.
- 20 A. F. van Driel, I. S. Nikolaev, P. Vergeer, P. Lodahl, D. Vanmaekelbergh and W. L. Vos, *Phys. Rev. B: Condens. Matter*, 2007, **75**, 35329.
- 21 A. Nguyen, C. M. Gonzalez, R. Sinelnikov, W. Newman, S. Sun, R. Lockwood, J. G. C. Veinot and A. Meldrum, *Nanotechnology*, 2016, **27**, 105501.
- 22 T. Takagahara, *Phys. Rev. B: Condens. Matter*, 1993, **47**, 4569–4584.
- 23 M. Dasog, Z. Yang, S. Regli, T. M. Atkins, A. Faramus, M. P. Singh, E. Muthuswamy, S. M. Kauzlarich, R. D. Tilley and J. G. C. Veinot, *ACS Nano*, 2013, **7**, 2676–2685.
- 24 M. V. Wolkin, J. Jorner, P. M. Fauchet, G. Allan and C. Delerue, *Phys. Rev. Lett.*, 1999, **82**, 197–200.
- 25 B. Marsen, M. Lonfat, P. Scheier and K. Sattler, *Phys. Rev. B: Condens. Matter*, 2000, **62**, 6892–6895.
- 26 U. Banin and O. Millo, *Annu. Rev. Phys. Chem.*, 2003, **54**, 465–492.
- 27 D. Steiner, T. Mokari, U. Banin and O. Millo, *Phys. Rev. Lett.*, 2005, **95**, 56805.
- 28 Y. Bekenstein, K. Vinokurov, S. Keren-Zur, I. Hadar, Y. Schilt, U. Raviv, O. Millo and U. Banin, *Nano Lett.*, 2014, **14**, 1349–1353.
- 29 O. Millo, I. Balberg, D. Azulay, T. K. Purkait, A. K. Swarnakar, E. Rivard and J. G. C. Veinot, *J. Phys. Chem. Lett.*, 2015, **6**, 3396–3402.
- 30 A. Franceschetti and A. Zunger, *Phys. Rev. B: Condens. Matter*, 2000, **62**, 2614–2623.
- 31 E. P. A. M. Bakkers, Z. Hens, A. Zunger, A. Franceschetti, L. P. Kouwenhoven, L. Gurevich and D. Vanmaekelbergh, *Nano Lett.*, 2001, **1**, 551–556.
- 32 J.-K. Choi, S. Jang, K.-J. Kim, H. Sohn and H.-D. Jeong, *J. Am. Chem. Soc.*, 2011, **133**, 7764–7785.
- 33 R. Wang, X. Pi and D. Yang, *J. Phys. Chem. C*, 2012, **116**, 19434–19443.



# Supplementary Information

## Photoluminescence Through In-gap States in Phenylacetylene Functionalized Silicon Nanocrystals

Arzu Angı, Regina Sinelnikov, Al Meldrum, Jonathan G. C. Veinot, Isacc Balberg,  
Doron Azulay ,Oded Millo\* and Bernhard Rieger\*

### Table of Contents

<b>1. General Information</b> .....	1
1.1. Chemicals.....	1
1.2. Instruments and Measurement Details.....	1
<b>2. Synthetic Procedures</b> .....	1
2.1. Preparation of oxide-embedded silicon nanocrystals.....	1
2.2. Liberation of Hydride Terminated SiNCs .....	2
2.3. Synthesis of Lithium Phenylacetylide .....	2
2.4. Functionalization of SiNCs with Organometallic Reagents .....	2
<b>3. Analytical Data</b> .....	3
3.1. PL Decay Lifetime .....	3
3.2. HR-TEM.....	3
<b>References</b> .....	4

# 1. General Information

## 1.1. Chemicals

All reactants and reagents were purchased from Sigma-Aldrich and used without further purification if not stated otherwise. Phenyllithium was bought as a 1.8 M solution in dibutyl ether, *n*-hexyllithium as 2.3 M solution in hexane, *n*-butyllithium as 2.5 M solution in hexane. Dry toluene and THF was obtained from a MBraun SPS 800 solvent purification system.

## 1.2. Instruments and Measurement Details

**FTIR spectra** were measured with a *Bruker Vertex 70 FTIR* using a *Platinum ATR* from *Bruker*. **Photoluminescence (PL) spectra** were taken with an *AVA-Spec 2048* from *Avantes* using a *Prizmatix (LED Current controller)* as light source. Samples were excited with a 365 nm source.

**HR-TEM** measurements were performed on a *JEM-2200FS TEM* with 200 kV field emission gun. Samples of SiNCs were drop-casted onto a lacey carbon grid and the solvent was evaporated in vacuum.

**UV-Vis Spectroscopy** was performed with a *Varian Cary 50 Scan Spectrometer*. (Wavelength region: 200-800 nm.)

**PL life-time decay measurements** were performed by a 445 nm CW diode laser, sent through an *Isomet IMDD-T110L-1.5 acousto-optic modulator (AOM)* operated at a frequency of 200 Hz. The PL lifetime decays were collected by a *Becker-Hickl PMC-100* photon-counting PMT.

For **STM measurements**, SiNCs were spin cast from a toluene solution onto atomically flat flame-annealed Au(111) substrates. All measurements were performed at room temperature, using Pt-Ir tips. Tunneling current-voltage (I-V) characteristics were acquired after positioning the STM tip above individual NCs, realizing a double barrier tunnel junction (DBTJ) configuration<sup>1</sup> and momentarily disabling the feedback loop. In general, care was taken to retract the tip as far as possible from the NC, so the applied tip-substrate voltage would fall mainly on the tip-NC junction rather than on the NC-substrate junction whose properties (capacitance and tunneling resistance) are determined by the layer of organic capping ligands that cannot be modified during the STM measurement. This protocol reduces the voltage division induced broadening effects, and thus the measured gaps and level separations in general better correspond to the real SC gaps, although broadening on the order of 10% are still expected.<sup>1-4</sup> The  $dI/dV$ -V tunneling spectra, proportional to the local tunneling density of states (DOS), were numerically derived from the measured I-V curves. We have acquired the topographic images with a set sample-bias,  $V_s$ , of 2.2 V and set current  $I_s = 0.2$  nA. This bias value ensures tunneling to states well above the conduction band edge, where the DOS is rather large, thus the measured SiNC height corresponds well to the real height. The tunneling spectra (on the NCs) were measured with lower set bias, of  $V_s \cong 1.2$ -1.5 V, and  $I_s \cong 0.1$ -0.3 nA. These  $V_s$  values still ensure tunneling above the band edge (before disconnecting the feedback loop), yet being sensitive to the details of the DOS around the band edge.  $I_s$  was reduced as much as possible, to the lowest value that still allowed acquisition of smooth tunneling spectra, in order to retract the tip as much as possible from the NC (thus reducing the voltage division factor).

# 2. Synthetic Procedures

## 2.1. Preparation of Oxide-Embedded Silicon Nanocrystals

Polymeric hydrogen silsesquioxane (HSQ) was synthesized as described in a literature known procedure.<sup>5</sup> HSQ (7 g) was placed in a quartz reaction boat, transferred to a *Nabertherm RD 30/200/11* oven with quartz working tube and heated from ambient to a peak processing temperature of 1100 °C at 18 °C/min in a slightly reducing atmosphere (5% H<sub>2</sub>/95% N<sub>2</sub>). The sample was kept at the peak processing temperature for 1 h. Upon cooling to room temperature, the resulting amber solid was ground into a fine brown powder using a mortar and pestle to remove large particles. Further grinding was achieved via shaking the powder dispersed in



ethanol for 24h with high-purity silica beads using a *WAB Turbula mixer*. The resulting SiNC/SiO<sub>2</sub> composite was dried in vacuo and the powder stored in glass vials.

## **2.2. Liberation of Hydride Terminated SiNCs**

Hydride-terminated SiNCs were obtained by etching the SiNC/SiO<sub>2</sub> composite using HF. First, 300 mg of the ground SiNC/SiO<sub>2</sub> composite was transferred to a ethylene-tetrafluoroethylene (ETFE) beaker equipped with a Teflon-coated stir bar. Ethanol (3 mL) and water (3 mL) were then added, and it is stirred to form a brown suspension, followed by addition of 3 mL of 49% HF aqueous solution. After 30 min of etching in subdued light, the suspension appeared yellow. Hydride-terminated SiNCs were subsequently extracted from the aqueous layer into ca. 30 mL of toluene by multiple (i.e., 3 × 10 mL) extractions. The SiNC toluene suspension was transferred to ETFE-centrifuge tubes, and the SiNCs were isolated by centrifugation at 9000 rpm for 5 mins. To remove any residual water/ethanol, extracted particles dispersed in 5 ml dry toluene and centrifuged again.

## **2.3. Synthesis of Lithium Phenylacetylide**

Phenylacetylene (1.53 g, 15 mmol, 1 eq.) is dissolved in 9 ml THF and *n*-butyllithium (4.8 ml, 2.5 M in hexanes, 12 mmol, 0.8 eq.) is added to the reaction flask drop wise in 30 minutes at -78°C. Upon the completion of the addition, the reaction mixture is stirred for 15 more minutes, then it is brought to room temperature. The product is obtained as a clear yellow/orange solution. The solution is degassed and stored in a schlenk flask in a cool place.

## **2.4. Functionalization of SiNCs with Organometallic Reagents**

Hydride terminated Si-NCs, obtained by etching 300 mg Si/SiO<sub>2</sub> composite, are dispersed in 2 ml of a degassed solution of the organolithium reagents. The organolithium reagents used for this study are diluted with toluene to form 0.1 M solutions. The mixture is stirred for overnight. The reaction was terminated by precipitating functionalized SiNCs in 5 ml 1:1 ethanol-methanol mixture, acidified with HCl conc. (0.2 ml). Obtained SiNCs are centrifuged at 9000 rpm for 10 min and the sediment is redispersed in minimum amount of toluene. The precipitation-centrifugation-redispersion step is performed two more times from ethanol-methanol and toluene. Finally, functionalized SiNCs are dispersed in toluene and filtered through a 0.45 µm PTFE syringe filter.

### 3. Analytical Data

#### 3.1. PL Decay Lifetime

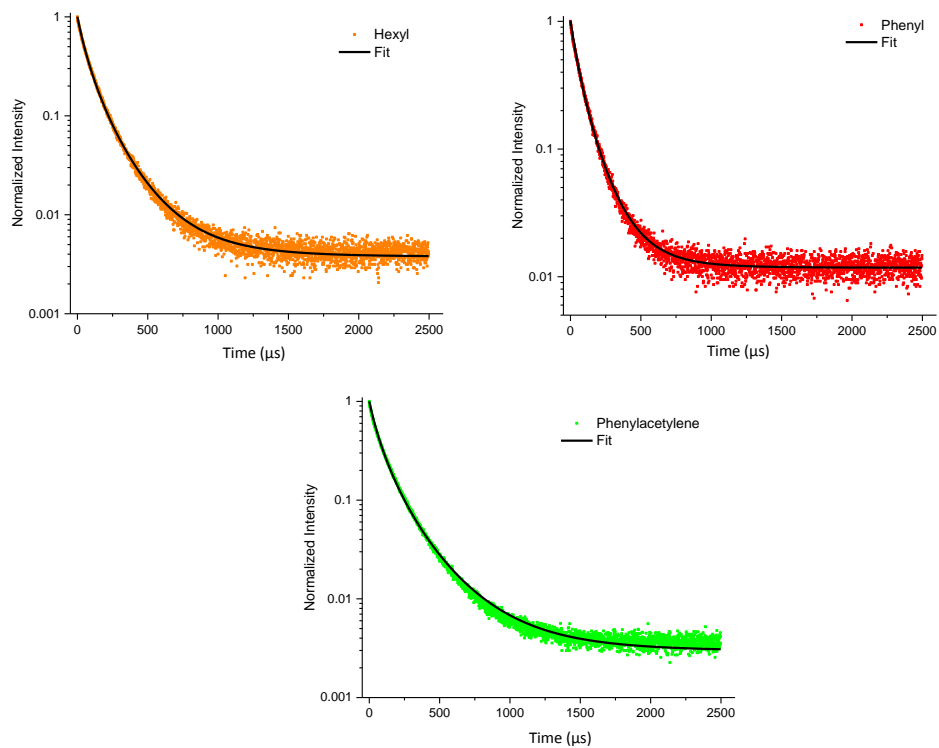


**Fig. S1** PL decay curves of SiNCs functionalized with *n*-hexyllithium (orange), phenyllithium (red) and lithium phenylacetylide (green). Black curves show the fitted curve with lognormal function.

#### 3.2. HR-TEM

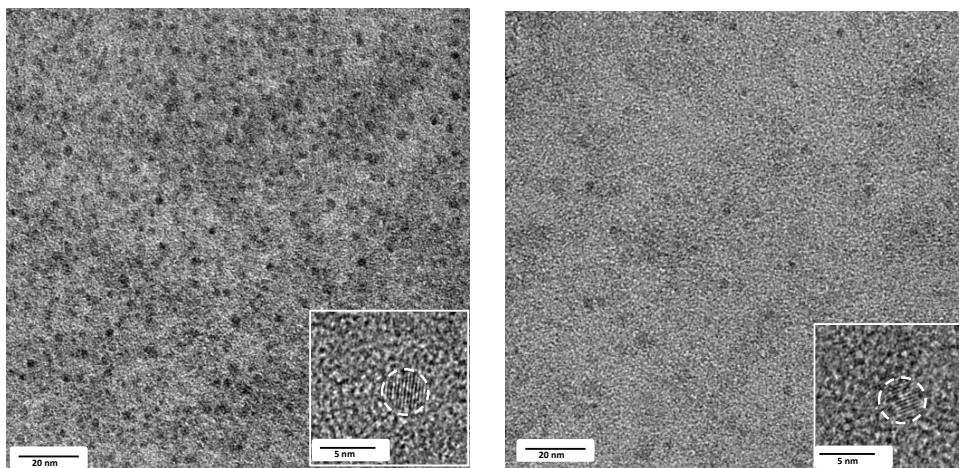


**Fig. S2** TEM image of SiNCs functionalized with phenyllithium (left) and lithium phenylacetylide (right). HR-TEM images showing crystal fringes are shown in insets.

## References

- 1 U. Banin and O. Millo, *Annu. Rev. of Phys. Chem.*, 2003, **54**, 465–492.
- 2 E. P. A. M. Bakkers, Z. Hens, A. Zunger, A. Franceschetti, L. P. Kouwenhoven, L. Gurevich, D. Vanmaekelbergh, *Nano Lett.*, 2001, **1**, 551–556.
- 3 E. P. A. M. Bakkers, D. Vanmaekelbergh, *Phys. Rev. B*, 2000, **62**, R7743-R7746.
- 4 U. Banin, Y. W. Cao, D. Katz, O. Millo, *Nature*, 1999, **400**, 542–544.
- 5 H. M. Bank, M. E. Cifuentes, E. M. Theresa, *United States Pat.*, 1991, 5.010.159.

### 4.3 The Influence of Conjugated Alkynyl(aryl) Surface Groups on the Optical Properties of Silicon Nanocrystals: Photoluminescence through In-Gap States

In our previous work, we presented that organolithium reagents offer a convenient way to tether conjugated aryl and alkynyl(aryl) molecules to the surface of hydride-terminated SiNCs.<sup>25</sup> Consequently, this technique allows the study of the influence of a previously inaccessible class of surface groups on the optical properties of SiNCs. In addition, we showed that phenylacetylene surface groups induce a red-shift in PL emission and formation of a new state within the band gap of SiNCs. The PL shift was then suggested to be associated with the emission through this in-gap state.<sup>32</sup>

These results were the first hints of the influence of conjugated surface groups on the optical properties of SiNCs. However, some questions remained unanswered including: (1) Do other alkynyl(aryl) molecules cause the formation of in-gap states and alter the PL of SiNCs? (2) Can this principle be applied to different alkynyl(aryl)s to tune the PL wavelength of SiNCs? (3) Why can only alkynyl(aryl) surface groups shift the PL while there is no impact from aryl groups?

In this work, we aimed to answer these questions by functionalizing SiNCs with different alkynyl(aryl) molecules and analyzing these SiNCs *via* STM/STS measurements. We observed that the PL of SiNCs could be tuned in the range 685-800 nm solely *via* surface functionalization with alkynyl(aryl) (phenylacetylene, 2-ethynyl naphthalene, 2-ethynyl-5-hexylthiophene) surface groups. On the other hand, aryl counterparts and alkynyl surface groups did not alter the PL maximum. STM/STS measurements performed on isolated single SiNCs showed the presence of in-gap states for every alkynyl(aryl) surface group studied. In this regard, the observed PL red-shifts were attributed to an emission pathway involving these in-gap states that decrease the effective band gap for recombination.

To gain a better understanding, *ab-initio* calculations on model Si clusters were performed. The results suggested that the in-gap states originate as interface states from excited electronic antibonding ( $\pi^*$ ) states, located on the alkynyl bond which strongly

couple to the SiNC. These outcomes provided a likely mechanism for the PL shifts, which were only observed with alkynyl(aryl) surface groups and not with aryl counterparts: Excitation of the SiNC core states is followed by non-radiative relaxation to bright  $\pi^*$  in-gap states which are conjugated with the alkynyl(aryl) moiety. A subsequent transition to the ground state then accounts for the red-shifted PL emission. The presented results demonstrate the possibility of specific conjugated surface groups to tune the electronic level structure and the optical properties of SiNCs systematically, which may be beneficial to improve the efficiency of SiNCs in semiconductor devices.


**Manuscript:**

**The Influence of Conjugated Alkynyl(aryl) Surface Groups on the Optical Properties of Silicon Nanocrystals: Photoluminescence through In-Gap States**

<b>Status</b>	Published June 25, 2018
<b>Journal</b>	<i>Nanotechnology</i> , 2018, Volume 29, 355705.
<b>Publisher</b>	IOP Publishing
<b>DOI</b>	10.1088/1361-6528/aac9ef
<b>Authors</b>	Arzu Angı, Regina Sinelnikov, Hendrik H. Heenen, Al Meldrum, Jonathan G. C. Veinot, Christoph Scheurer, Karsten Reuter, Or Ashkenazy, Doron Azulay, Isacc Balberg, Oded Millo, Bernhard Rieger

©IOP publishing. Reproduced with permission with the license number 4455200626376. All rights reserved.

# The influence of conjugated alkynyl(aryl) surface groups on the optical properties of silicon nanocrystals: photoluminescence through in-gap states

Arzu Angi<sup>1,2</sup> , Regina Sinelnikov<sup>3</sup> , Hendrik H Heenen<sup>4</sup> , Al Meldrum<sup>5</sup>, Jonathan G C Veinot<sup>3</sup> , Christoph Scheurer<sup>4</sup>, Karsten Reuter<sup>4</sup> , Or Ashkenazy<sup>6</sup>, Doron Azulay<sup>6,7</sup>, Isaac Balberg<sup>6</sup>, Oded Millo<sup>6,8</sup>  and Bernhard Rieger<sup>1,2,8</sup> 

<sup>1</sup> WACKER-Lehrstuhl für Makromolekulare Chemie, Technische Universität München, Lichtenbergstraße 4, D-85747, Germany

<sup>2</sup> Catalysis Research Center, Ernst-Otto-Fischer-Straße 1, D-85748 Garching, Germany

<sup>3</sup> Department of Chemistry, University of Alberta, 11227 Saskatchewan Drive, Edmonton, Alberta, T6G 2G2, Canada

<sup>4</sup> Chair for Theoretical Chemistry and Catalysis Research Center, Technische Universität München, Lichtenbergstrasse 4, D-85747 Garching, Germany

<sup>5</sup> Department of Physics, University of Alberta, Edmonton, Alberta T6G 2G2, Canada

<sup>6</sup> Racah Institute of Physics, The Hebrew University of Jerusalem, Jerusalem 91904, Israel

<sup>7</sup> Azrieli, Jerusalem College of Engineering, Jerusalem 9103501, Israel

E-mail: [rieger@tum.de](mailto:rieger@tum.de) and [milode@mail.huji.ac.il](mailto:milode@mail.huji.ac.il)

Received 9 April 2018, revised 23 May 2018

Accepted for publication 4 June 2018

Published 25 June 2018



CrossMark

## Abstract

Developing new methods, other than size and shape, for controlling the optoelectronic properties of semiconductor nanocrystals is a highly desired target. Here we demonstrate that the photoluminescence (PL) of silicon nanocrystals (SiNCs) can be tuned in the range 685–800 nm solely via surface functionalization with alkynyl(aryl) (phenylacetylene, 2-ethynyl-naphthalene, 2-ethynyl-5-hexylthiophene) surface groups. Scanning tunneling microscopy/spectroscopy on single nanocrystals revealed the formation of new in-gap states adjacent to the conduction band edge of the functionalized SiNCs. PL red-shifts were attributed to emission through these in-gap states, which reduce the effective band gap for the electron–hole recombination process. The observed in-gap states can be associated with new interface states formed via (–Si–C≡C–) bonds in combination with conjugated molecules as indicated by *ab initio* calculations. In contrast to alkynyl(aryl)s, the formation of in-gap states and shifts in PL maximum of the SiNCs were not observed with aryl (phenyl, naphthalene, 2-hexylthiophene) and alkynyl (1-dodecyne) surface groups. These outcomes show that surface functionalization with alkynyl(aryl) molecules is a valuable tool to control the electronic structure and optical properties of SiNCs via tuneable interface states, which may enhance the performance of SiNCs in semiconductor devices.

Supplementary material for this article is available [online](#)

<sup>8</sup> Authors to whom any correspondence should be addressed.

Keywords: silicon nanocrystals, photoluminescence, surface functionalization, conjugated surface groups, in-gap states, scanning tunneling microscopy/spectroscopy, quantum dots

(Some figures may appear in colour only in the online journal)

## Introduction

Following the discovery of efficient room temperature photoluminescence (PL) from porous silicon by Canham [1], nanostructured silicon became the focus of a tremendous research activity [2]. Silicon nanocrystals (SiNCs) exhibit size-dependent PL, arising from the quantum confinement effect. The emission wavelength can be tuned from infrared to visible by decreasing the size of the nanocrystals below the exciton Bohr radius of silicon ( $\sim 4.5$  nm) [3–6]. In addition to size, surface chemistry can also influence the optoelectronic properties of SiNCs [7–13]. Based on these properties, several prototype applications of SiNCs have been demonstrated including in photovoltaics [14–17], light emitting diodes [18–20], sensors [21, 22] and bio-imaging [23, 24].

Developing methods to tune the optical properties of SiNCs is important for these numerous potential applications. Significant efforts have been directed towards utilizing the surface chemistry as a promising strategy to control the optical properties of SiNCs [7–13]. However, in most of the cases, changes in the PL wavelength were proposed to rely on emission through surface states, impurities, defects or Förster resonance energy transfer from fluorophores [25] and were frequently elucidated with indirect methods (e.g., excited state lifetimes) [4, 8, 9, 26]. Reports providing direct experimental evidence for surface chemistry-induced alteration of the band structure [7] and the PL wavelength of SiNCs are rare [27].

We recently presented the surface functionalization of hydride-terminated SiNCs with organolithium reagents [28, 29]. This method provides a convenient way to tether conjugated aryl and alkynyl(aryl) molecules to the surface of SiNCs for the first time [30]. Consequently, it allows the study of the influence of a previously inaccessible class of surface groups on the optical properties of SiNCs. For example, we functionalized SiNCs with phenyl (aryl) and phenylacetylene (alkynyl(aryl)) groups. While the PL wavelength of SiNCs was not altered with phenyl functionalization, phenylacetylene surface groups caused a red-shift (i.e. shift to longer wavelengths) in PL for 50 nm. Concomitantly, scanning tunneling microscopy and spectroscopy (STM/STS) revealed the formation of a new state within the band gap of SiNCs, only with the phenylacetylene surface groups. The PL shift was then suggested to be associated with the emission through this in-gap state [7].

Several works presented that surface functionalization should influence density of states (DOS) of SiNCs especially at the band edges due to tails of projected density from strongly localized states in the surface layer [31, 32]. However, in these works, the states were not prominent enough to shift the band gap to smaller values despite having significant effects on PL dynamics, especially due to the indirect character of SiNCs [31–34]. To the best of our knowledge, an in-gap state

introduced by specific surface functionalization was experimentally observed by STM for the first time in our recent work on phenylacetylene functionalized SiNCs [7].

These results were the first hints of the influence of conjugated surface groups on the optical properties of SiNCs. However, some questions including (1) Do other alkynyl(aryl) molecules cause the formation of in-gap states and alter the PL of SiNCs? and (2) Can this principle be applied with different alkynyl(aryl)s to tune the PL wavelength of SiNCs? remained unanswered.

In this work, we aim to answer these questions by functionalizing SiNCs with different alkynyl(aryl) molecules and analyzing the functionalized SiNCs via STM/STS measurements in combination with optical spectroscopic methods. We observed that the PL maximum of SiNCs red-shifts by  $\sim 50$ ,  $\sim 65$ , and  $\sim 115$  nm with phenylacetylene, 2-ethynyl-naphthalene and 2-ethynyl-5-hexylthiophene alkynyl(aryl) surface groups, respectively. STM/STS measurements performed on isolated single SiNCs showed the presence of in-gap states for every alkynyl(aryl) surface group studied. In this regard, the observed PL red-shifts were attributed to an emission pathway involving these in-gap states that decrease the effective band gap for recombination. *Ab initio* calculations on model systems suggested that the in-gap states originate as interface states from excited electronic  $\pi^*$  states located on the alkynyl bond which strongly couple to the SiNC. We also observed that the aryl counterparts (phenyl, naphthalene, 2-hexylthiophene) and alkynyl (1-dodecyne) surface groups do not alter the PL maximum of SiNCs. The presented results demonstrate the possibility of utilizing alkynyl(aryl) molecules to manipulate the electronic level structure and the optical properties of SiNCs systematically, which may be beneficial for SiNC-based devices.

## Results and discussion

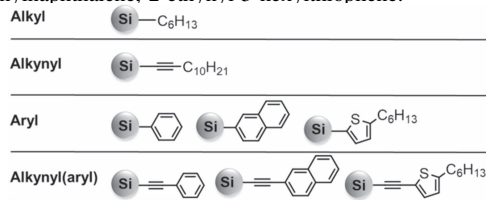
### *Surface functionalization of SiNCs with lithiated conjugated molecules*

Different alkynyl(aryl) groups (phenylacetylene, 2-ethynyl-naphthalene, 2-ethynyl-5-hexylthiophene) and their aryl counterparts (phenyl, naphthalene, 2-hexylthiophene) were studied. 1-dodecyne was utilized as a ‘control’ surface group, to study the influence of the alkynyl linkage without a subsequent aromatic group (table 1). SiNCs functionalized with 1-dodecyne, naphthalene, 2-ethynyl-naphthalene and 2-ethynyl-5-hexylthiophene molecules were not reported previously in the literature.

Fourier transform infrared (FTIR) spectroscopy was utilized to monitor the surface functionalization reactions. FTIR spectra of SiNCs functionalized with surface groups, previously not reported, are presented in figure 1. Hydride-terminated SiNCs show Si–H signals at  $\sim 2100$ , 906 and  $660\text{ cm}^{-1}$  without any sign of oxide (ESI figure S1(a) is



**Table 1.** Surface groups utilized to functionalize SiNCs: alkyl: hexyl; alkynyl: 1-dodecyne; aryl: (left to right) phenyl, naphthalene, 2-hexylthiophene; alkynyl(aryl): (left to right) phenylacetylene, 2-ethynyl-naphthalene, 2-ethynyl-5-hexylthiophene.



available online at [stacks.iop.org/NANO/29/355705/mmedia](https://stacks.iop.org/NANO/29/355705/mmedia). The spectrum of 1-dodecyne functionalized particles shows the characteristic alkyl peaks between  $2850$  and  $2955\text{ cm}^{-1}$  ( $\text{CH}_2$  and  $\text{CH}_3$   $\nu$ -stretching) and at  $\sim 1462$  and  $\sim 1378\text{ cm}^{-1}$  ( $\text{CH}$   $\delta$ -deformation) (figure 1(a)). For 2-ethynyl-5-hexylthiophene functionalized SiNCs, the bands correlated to aromatic C–H stretching at around  $3055\text{ cm}^{-1}$  and aromatic C–C stretching modes of the thiophene ring at  $1524$ ,  $1455$  and  $1432\text{ cm}^{-1}$  are observed (figure 1(b)). In the case of naphthalene and 2-ethynyl-naphthalene functionalized SiNCs, the spectra display aromatic C–H stretching modes between  $3010$ – $3080\text{ cm}^{-1}$  and aromatic C–C stretching peaks at  $1627$ ,  $1595$ ,  $1500$  and  $1432\text{ cm}^{-1}$  (figures 1(c), (d)). The asymmetric  $\text{C}\equiv\text{C}$  stretching signal characteristic for alkynes is observed at  $2150\text{ cm}^{-1}$  as a shoulder (marked by an arrow) on the Si–H stretching mode at  $\sim 2100\text{ cm}^{-1}$  in the spectra of 1-dodecyne, 2-ethynyl-5-hexylthiophene and 2-ethynyl-naphthalene functionalized SiNCs. In all spectra, only minor surface oxidation was observed, as evidenced by the Si–O band at  $1050\text{ cm}^{-1}$ . FTIR spectra of hexyl, phenyl, phenylacetylene and 2-hexylthiophene functionalized SiNCs are shown in ESI figure S1.

#### Optical properties of SiNCs functionalized with lithiated conjugated molecules

The PL peak-wavelength of the SiNC ensembles clearly depends on the identity of the surface groups (figure 2). Hexyl functionalized SiNCs emit at  $\sim 686\text{ nm}$ . With aryl surface groups, the PL peak-wavelength remains similar and is detected at  $684$ – $688\text{ nm}$  (table 2(a)). However, the PL wavelength red-shifts by  $\sim 50$ ,  $\sim 65$ , and  $\sim 115\text{ nm}$  for phenylacetylene, 2-ethynyl-naphthalene and 2-ethynyl-5-hexylthiophene groups, respectively (table 2(b)).

UV/VIS absorption spectroscopy was performed in order to compare the results with the PL maxima and the band gaps measured by STM (figure 3). Absorption spectra are difficult to measure due to small but unavoidable variations in the density of NCs in solution. Here the spectra were normalized (at  $240\text{ nm}$ ) in order to bring out any major differences in their shape. Similar absorption edges were observed for all SiNCs functionalized with alkyl, aryl and alkynyl groups. In the case of alkynyl(aryl) surface groups, a small shoulder is visible between  $\sim 300$  and  $400\text{ nm}$ . In the case of 2-ethynyl-5-hexylthiophene functionalized SiNCs, the shoulder appears more prominent and the absorption edge red-shifts by  $\sim 50\text{ nm}$  (red curve in figure 3). Alkynyl(aryl) molecules themselves do not have any significant

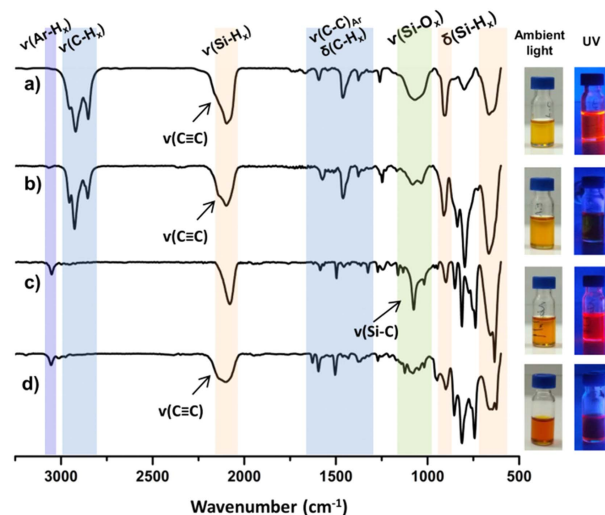


**Figure 1.** FTIR spectra of (a) 1-dodecyne, (b) 2-ethynyl-5-hexylthiophene, (c) naphthalene, (d) 2-ethynyl-naphthalene functionalized SiNCs. Right: images of SiNCs dispersed in toluene under ambient light and UV irradiation ( $365\text{ nm}$ ). Visible PL intensity qualitatively decreases with 2-ethynyl-naphthalene and 2-ethynyl-5-hexylthiophene functionalized SiNCs whose emission falls at the upper edge of the visible region.

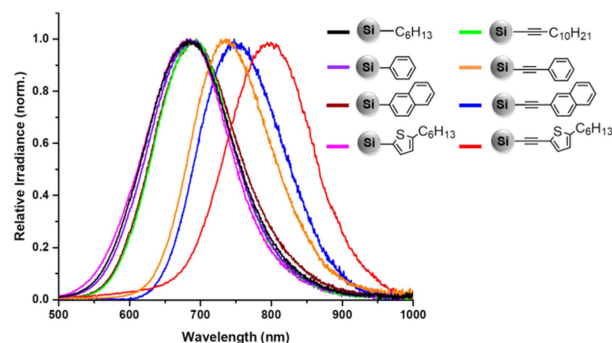


**Figure 2.** Normalized PL spectra of the SiNCs upon excitation at  $365\text{ nm}$ .

absorption peaks above  $\sim 300\text{ nm}$  (ESI figures S2 and S3). Therefore, the shoulder observed in the absorption spectra of alkynyl(aryl) functionalized SiNCs may be due to new states becoming optically active upon surface functionalization.

Excited state lifetime measurements on functionalized SiNCs were also performed. The non-exponential decay traces were fit using a log-normal lifetime distribution [35] which provides a good fit to the observed decay traces (ESI figure S4). The mean excited state lifetimes extracted from these fittings are in the microsecond regime for all samples investigated (ESI table S1) characteristic of a long-lived emission mechanism [36].

#### STM/STS analysis of isolated SiNCs

To investigate the influence of the alkynyl(aryl) surface groups on the electronic level structure of the SiNCs and in particular on the observed PL red-shifts, we present an

**Table 2.** Peak emission (in nm and eV) of functionalized SiNCs. Peak maxima were calculated via (skewed) Gaussian fitting of the raw PL data. The errors originating from the fits were reported.

(a) Surface functionalization	PL (nm)	PL (eV)
Phenyl	687 ± 0.1	1.80
Naphthalene	688 ± 0.1	1.80
2-hexylthiophene	684 ± 0.1	1.81
Hexyl	686 ± 0.2	1.81
1-dodecyne	687 ± 0.1	1.80
(b) Surface functionalization	PL (nm)	PL (eV)
Phenylacetylene	737 ± 0.1	1.68
2-ethynynaphthalene	751 ± 0.3	1.65
2-ethynyl-5-hexylthiophene	798 ± 0.4	1.55

analysis combining STM/STS measurements with the optical spectroscopy data. This combination is crucial for SiNCs, due to challenges associated with relating optical spectroscopy data to the SiNC electronic structure [37]. These difficulties arise primarily from limitations of the optical measurements to determine the initial and final states involved in the excitation and relaxation steps.

STM/STS overcomes this problem, as the electronic DOS is measured by mapping the conduction band (CB) and valence band (VB) independently [38–43]. This allows for a direct evaluation of the fundamental band gap of individual NCs, rather than the ensemble averaged excitonic band gap monitored via PL spectroscopy. In addition, STM/STS can provide information about in-gap states [7, 44] and monitor the effect of doping [38, 45]. However, it should be noted that there is also an inherent problem in STM tunneling spectroscopy of colloidal semiconductor NCs regarding the exact determination of the DOS, since the tunneling spectra depend on the STM current and bias settings, as detailed below.

Figures 4(b) and (d) show an STM image together with a topographic cross-section taken on one of the isolated 1-dodecyne functionalized SiNCs, from which tunneling spectra were obtained. In our work, STS/STM data was acquired from SiNCs deposited on an atomically flat Au (111) substrate by drop-casting from toluene. All measurements were performed at room temperature and ambient conditions, employing a home-built STM system with a Pt–Ir tip. For each sample, tunneling spectra were acquired from 4 to 6 SiNCs having the average size within the corresponding ensemble, as determined from transmission electron microscopy (TEM) (figures 4(a), (c) and see ESI figures S5, S6 for size distributions of SiNCs studied).

The same surface functionalization-dependent general behavior, namely, nearly the same band gap and the existence or absence of an in-gap state was observed for each SiNC measured within a given sample. We have also measured SiNCs of sizes lower or higher than the mean size, but also here, the appearance (or absence) of in-gap states in the spectra was independent on SiNC size, and depended only on the observation of a PL red-shift (or not) in the corresponding ensemble

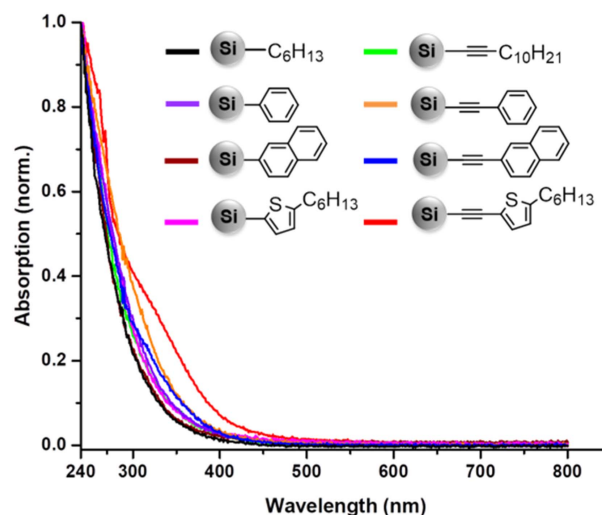


**Figure 3.** Normalized UV-vis absorption spectra of functionalized SiNCs in THF. The data was normalized at 240 nm.

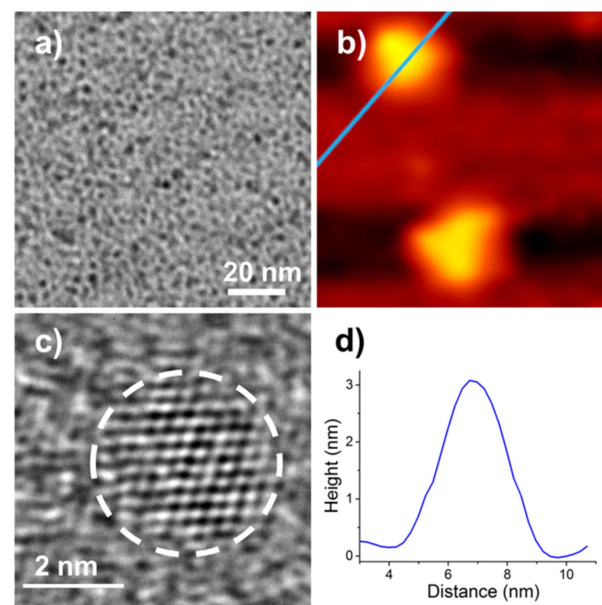


**Figure 4.** (a) Bright field TEM image of naphthalene functionalized SiNCs with an average diameter of  $3.0 \pm 0.2$  nm. TEM images and size distributions of SiNCs are given in ESI figures S5 and S6. (b) STM image showing two isolated SiNCs functionalized with 1-dodecyne; (c) HR-TEM image of a single SiNC functionalized with naphthalene. Lattice fringes are visible. (d) Cross-section of the SiNC taken along the blue line marked in (B). Both methods verify  $\sim 3$  nm average size of the SiNCs. Both methods verify 3 nm average size of the SiNCs.

sample. The only effect that could result from taking these data into account in our analysis is the widening of the STM-related error bar in tables 3 and 4 below by about 30 meV.

The tunneling spectra were obtained by positioning the STM tip over a single SiNC, forming a double-barrier tunnel junction (DBTJ) configuration [39, 41], after momentarily

**Table 3.** STS band gaps of SiNCs in comparison to PL emission energy.

Surface functionalization	Band gap (eV)	PL (eV)
Phenyl	$2.1 \pm 0.1$	1.80
Naphthalene	$2.2 \pm 0.1$	1.80
2-hexylthiophene	$2.0 \pm 0.2$	1.81
Hexyl	$2.1 \pm 0.1$	1.81
1-dodecyne	$2.0 \pm 0.1$	1.80

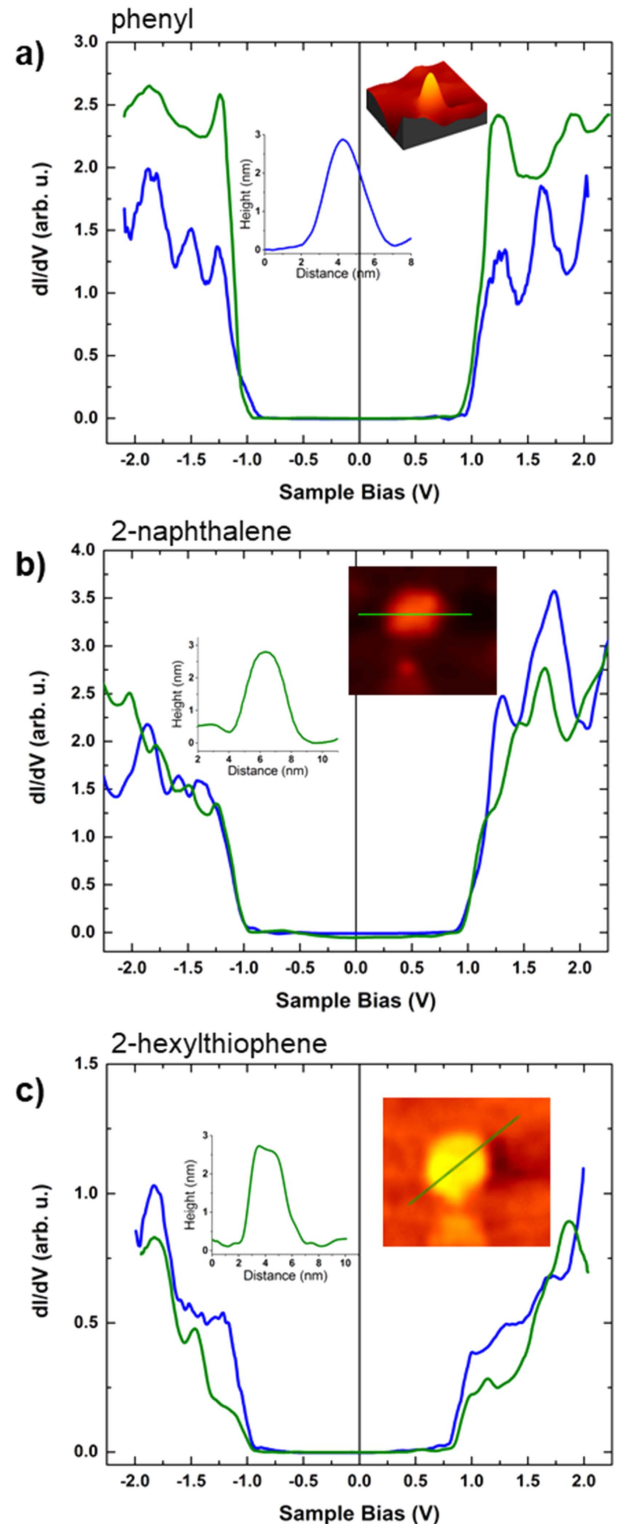
**Table 4.** STS band gaps and VB-in-gap energy separation of SiNCs in comparison to PL emission energy for the SiNCs having in-gap states.

Surface functionalization	Band gap (eV)	In-gap-VB (eV)	PL (eV)
Phenylacetylene	$2.1 \pm 0.1$	$1.88 \pm 0.1$	1.68
2-ethynyl-naphthalene	$2.1 \pm 0.2$	$1.85 \pm 0.2$	1.65
2-ethynyl-5-hexylthiophene	$1.8 \pm 0.1$	$1.62 \pm 0.1$	1.55

disabling the feedback circuit. In this configuration, the tunneling spectra strongly depend on the tip-NC distance, which affects both the capacitance of the corresponding junction,  $C_1$ , and the tunneling rate through it,  $\Gamma_1$ . These parameters are thus determined by the STM current (mainly) and bias settings, while those corresponding to the NC-substrate junction,  $C_2$  and  $\Gamma_2$ , are fixed for a given NC. The capacitance ratio between the affects the voltage-division induced broadening of the measured band gaps and level separations, by a factor of  $\eta = (1 + C_1/C_2)$ , while  $\Gamma_1/\Gamma_2$  determines the magnitude of charging effects, diminishing with increasing ratio [38, 39, 41, 44]. It should be noted, however, that taking these factors into account, good correspondence between calculated DOS or simulated spectra and measured tunneling spectra were achieved [42, 43]. In our present work, we took care to retract the tip as far as possible from the SiNC by using the lowest current setting possible (1 nA), and large bias voltages (2.2 V), just before disabling the feedback loop, thus eliminating charging effects and reducing  $\eta$  to  $\sim 1.1$ .

The tunneling  $dI/dV - V$  spectra of phenyl, naphthalene and 2-hexylthiophene functionalized SiNCs are shown in figure 5, together with corresponding STM topography images and cross-sections in the insets. In the spectra of SiNCs functionalized with aryl groups no in-gap spectral features are observed, i.e., they are similar to that of hexyl functionalized SiNCs (figure 7(a)).

In the tunneling spectra of alkynyl(aryl) functionalized SiNCs, the presence of in-gap states is observed as evidenced by a new peak appearing close to the CB edges, for every case, as demonstrated in figure 6 (in-gap states are highlighted with black circles). We note the positions of the peaks in the tunneling spectra did not depend on the lateral position of the STM tip over the SiNC, but their height did change. This is

**Figure 5.** Tunneling  $dI/dV - V$  spectra measured on SiNCs functionalized with (a) phenyl (b) naphthalene (c) 2-hexylthiophene. The two curves presented in each figure correspond to measurements obtained on two different SiNCs, where the inset shows a STM topography image and cross-section of one of them (color coded).

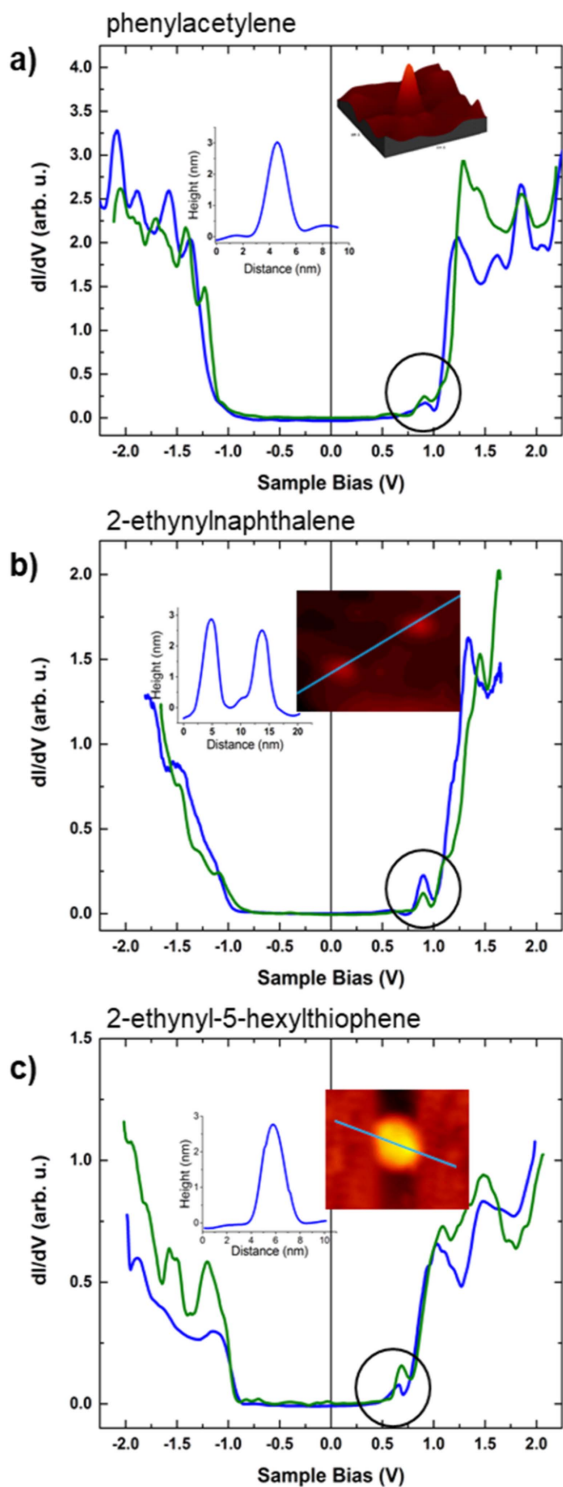


**Figure 6.** Tunneling  $dI/dV-V$  spectra measured on SiNCs functionalized with (a) phenylacetylene (b) 2-ethynynaphthalene (c) 2-ethynyl-5-hexylthiophene. The two curves presented in each figure correspond to measurements obtained on two different SiNCs, where the inset shows a STM topography image and cross-section of one of them (color coded). Black circles highlight the in-gap states introduced by the alkynyl(aryl) surface groups near the CB edge.

probably due to position-dependent coupling between the tip and the wavefunctions of the quantum-confined NC states.

It is important to note that in-gap states are detected for every surface group which causes a red-shift in the PL of SiNCs. Based on this observation, we attribute the observed PL red-shifts to emissions occurring from the in-gap states introduced by the surface groups, which reduce the effective band gap for electron-hole recombination.

For the SiNCs functionalized with 1-dodecyne, the tunneling spectra exhibit weak signals close to the CB (figure 7(b)). However, this spectral feature is not separated from the band edge in an appreciable manner and has a rather low spectral weight. We cannot rule out the possibility that this spectral feature is related to a tail of ligand-induced supra band gap states residing within the CB, but these could not be resolved in our spectra. Nevertheless, this observation further underlines our claim that PL red-shifts only occur when aromatic molecules are tethered to the SiNCs surface through alkynyl bonds, resulting prominent in-gap states well separated from the CB edge.

The fundamental (single particle) band gaps of the functionalized SiNCs were calculated directly from the STS data, by taking the energy difference between the VB and CB edges. The edge is defined as the midpoint between the first peak and the onset of detectable DOS. Tables 3 and 4 show the STS band gaps in comparison to the PL emission energies, together with the deviations associated with this calculation. For the alkynyl(aryl) functionalized SiNCs, where the PL emission is considered to be through the in-gap states, table 4 also summarizes the energy separations between the in-gap state and the VB-edge.

Our analysis reveals that the STS-extracted band gaps are rather similar for nearly all surface groups residing between 2.0 and 2.2 eV. 2-ethynyl-5-hexylthiophene functionalized SiNCs are the only exception of the system due to the smaller STS band gap ( $1.8 \pm 0.1$  eV) found. This observation is consistent with both the PL and UV-vis absorption spectroscopy data that also show smaller gaps for this sample (figures 2 and 3). The origin of this unique behavior is not clear to us, and may be related to a different dielectric confinement effect.

It is important to note, however, that the fundamental band gaps measured by STS are inherently larger than the excitonic band gaps determined by the PL maxima. This outcome stems mainly from three factors. First, the electron-hole Coulomb interaction which reduces the optical (excitonic) band gap, does not influence the STS band gap. Second, voltage-division effect between the tip-SiNC and SiNC-substrate tunnel barriers causes the widening of the measured STS band gap [39]. Third, the polarization (charging) energy related to electron tunneling through the SiNCs also causes a broadening of the measured values for the band gaps [39, 40]. Small deviations in STS band gaps of SiNCs functionalized with different molecules, despite their similar optical band gaps, can be explained as all these three factors are also influenced by the nature of surface groups.

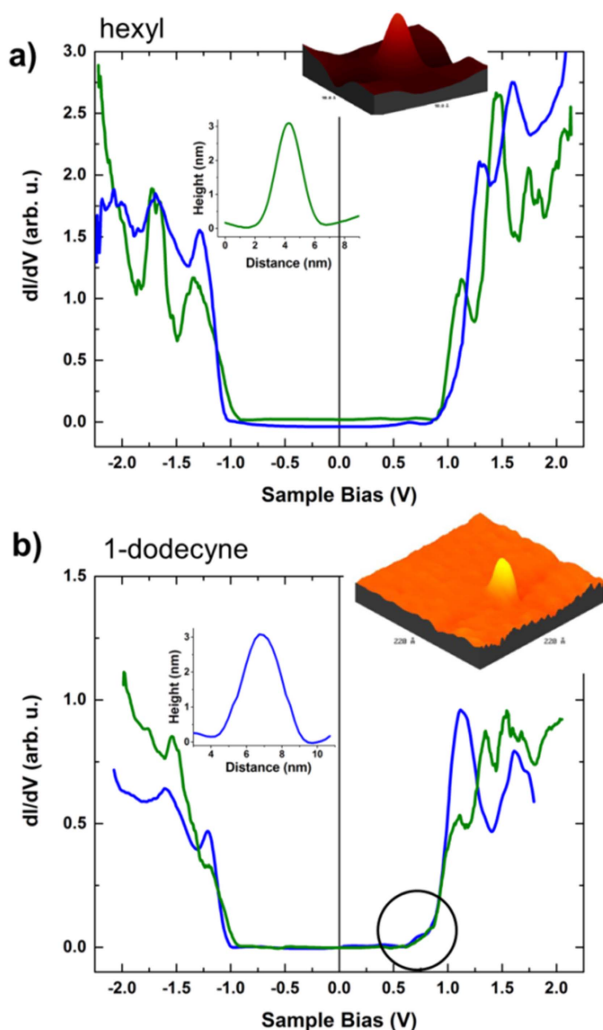


**Figure 7.** Tunneling  $dI/dV-V$  spectra measured on SiNCs functionalized with (A) hexyl and (B) 1-dodecyl. Measurements obtained on two different SiNCs are presented in each case. Corresponding STM topography image and cross-section of one of them are shown in the insets.

Over all, it is noteworthy that even if the STS band gaps are larger than the excitonic band gaps (*vide supra*), the observed trend of the VB-edge to in-gap state energy difference matches well to the degree of PL shifts seen with different alkynyl(aryl) surface groups. In the case of 2-ethynyl-5-hexylthiophene functionalized SiNCs, the observed PL shift is likely the result of a combined effect of recombination through the in-gap state and a smaller band gap.

#### Excited state calculations on model SiNCs

The observed red-shifts in PL maxima and the corresponding in-gap states in the tunneling spectra are possibly due to interface states afforded by the surface bonded alkynyl groups in combination with an extended conjugated molecule, which may result in strong coupling between the core and surface

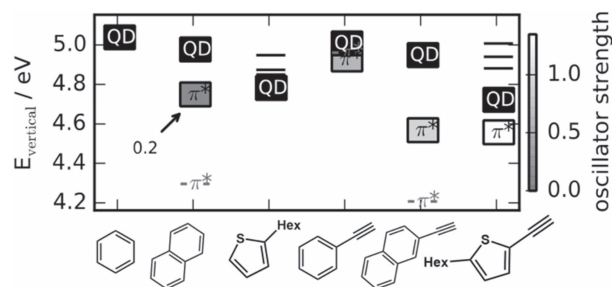


**Figure 8.** Relevant excited states for the  $\text{Si}_{26}\text{H}_{32}$  diamond model clusters functionalized with aryl and alkynyl(aryl) molecules (shown as x-axis). The antibonding quantum dot states with lowest energy are depicted as black blocks, others with black lines. Bright  $\pi^*$  states are depicted as boxes shaded according to their oscillator strength while dark  $\pi^*$  states (oscillator strength  $\ll 0.1$ ) are depicted by a dark gray  $\pi^*$  symbol.  $\pi^*$  states at higher energies than the QD states are not shown for clarity. Note, that the oscillator strength of the weakly bright  $\pi^*$  state of naphthalene is explicitly marked.

[44, 46]. In the case of aryl surface groups, the overlap of the C=C double bonds in aromatic rings with the electronic structure of the SiNCs seems not effective. In the case of 1-dodecyl, the conjugation length of the alkynyl group alone may not be sufficient to induce the PL shift and in-gap states.

To support this hypothesis we performed CC2 excited state calculations on model  $\text{Si}_{10}\text{H}_{16}$ ,  $\text{Si}_{14}\text{H}_{20}$  and  $\text{Si}_{26}\text{H}_{32}$  diamond structures. We attach the alkynyl(aryl) and aryl molecules to these model SiNCs and compute the first excited states as depicted in figure 8. Within these excited states, electronic transitions for deexcitation can be categorized as (1) from the confined quantum dot core states (QD) and (2) from antibonding  $\pi^*$  orbitals located on the aromatic surface group. In the  $\pi^*$  configuration we can differentiate optically active (bright) and inactive (dark) transitions based on the respective oscillator strengths—a dimensionless measure for the transition probability of absorption and emission.

In all model systems with alkynyl(aryl) groups, we observe a bright  $\pi^*$  state (white or light gray boxes, colored according to oscillator strengths in figure 8) appearing energetically below the first antibonding quantum dot (QD\*) state (black boxes). These bright  $\pi^*$  states consist of a transition to a distinctive antibonding  $\pi^*$  LUMO located on the alkynyl bond as depicted in figure 9. This antibonding alkynyl molecular orbital is conjugated with the extended  $\pi$ -orbitals of the aromatic molecule and couples with near-surface orbitals of the SiNC, thus mediating between the surface functionalization and the core.

In contrast, in the models with aryl surface groups  $\pi^*$  states are found only above the first QD\* state (figure 8). Only in the case of the naphthalene surface group,  $\pi^*$  states with weak oscillator strengths appears also below the first QD\* state. This exception can be attributed to an accidental degeneracy of  $\pi^*$  and QD\* states as an effect of the size-dependent band gap (see ESI for discussion) in our computational SiNC models of necessarily limited size.

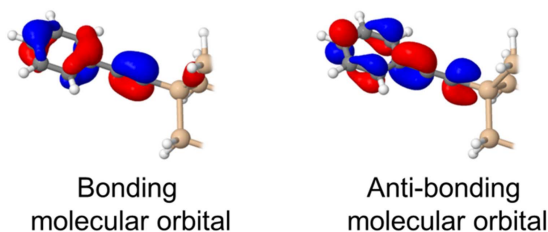


**Figure 9.** Bonding (left) and antibonding (right) molecular orbital of the alkyne bond for the phenylacetylene functionalization. The distinctive antibonding orbital is conjugated with the aromatic molecules and is the LUMO in all model clusters functionalized with alkyne(aryl) compounds.

The low-lying excited states of antibonding alkyne character provide a likely explanation for the in-gap states observed exclusively in the STM/STS spectra of the alkyne (aryl) compounds. Thus, a suggested mechanism for the observed PL red-shifts results: Excitation of the QD core states is followed by non-radiative relaxation to bright  $\pi^*$  interface states which are conjugated with the alkyne(aryl) moiety. This transfer likely occurs via an electronic barrier surpassing a second, dark  $\pi^*$  state also originating from the triple bond, which interacts directly with the SiNC states (see ESI for detailed discussion). A subsequent transition to the ground state then accounts for the red-shifted PL emission (figure 10). At the experimentally relevant SiNC sizes, absorption and emission into the QD core states likely occur via an indirect band gap [47–49] which accounts for long PL lifetimes. In contrast to that, in the small computational model clusters, a fast, direct emission via a bright  $\pi^*$  interface state could be expected. Notwithstanding, momentum conservation in transitions between excited QD core and interface states ( $k = 0$ ) still involves a necessary phonon scattering for large SiNCs. Such vibronic effects are not included in the current model as they would not change the qualitative picture which discriminates between alkyne(aryl) and aryl functionalizations. In both cases long PL lifetimes can be expected. These derive either from the indirect band gap of the SiNC in functionalizations without an in-gap state or from the electronic barrier originating from the mediating electronic states in combination with a necessary vibronic interaction during the transition from QD core to interface state in functionalizations with an in-gap state. A detailed theoretical analysis of these distributions is beyond the scope of our current computations.

The small model Si clusters used here can only approximate the large SiNCs. A more realistic analysis on 3 nm SiNCs functionalized with large aromatic surface groups is computationally impractical and would still suffer from insufficient knowledge about the detailed atomistic structure, size distributions and defects for the SiNCs [50].

Therefore, it is important to note that our current model offers a strictly qualitative explanation for the experimental observations. Despite these shortcomings and systematic size effects (see ESI), the appearance of bright, low-lying  $\pi^*$  states originating from the alkyne bond interface states is consistent over all cluster sizes studied and seems likely to persist for

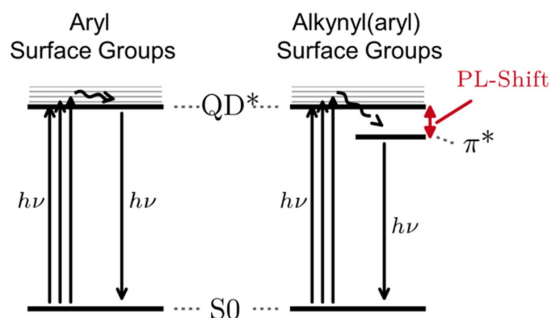


**Figure 10.** Schematic depiction of the mechanism of absorption/emission for aryl (left) and alkyne(aryl) (right) functionalized SiNCs. Absorption of a photon ( $h\nu$ ) leads to a transition from the ground state  $S_0$  to the excited state  $QD^*$ . In the case of aryl groups, following deexcitation occurs from the  $QD^*$  state. With alkyne(aryl) surface groups, first a non-radiative relaxation (wiggly lines) to the alkyne(aryl) state  $\pi^*$  takes place, followed by recombination from this  $\pi^*$  state.

larger SiNCs offering a plausible mechanism for observed red-shifts in PL emission with alkyne(aryl) surface groups.

## Conclusions

In conclusion, we studied the influence of alkyne(aryl) surface groups on the PL emission of SiNCs by utilizing STM/STS in combination with various optical spectroscopies. The PL wavelength of SiNCs functionalized with phenylacetylene, 2-ethynyl naphthalene and 2-ethynyl-5-hexylthiophene groups red-shifted by  $\sim 50$ ,  $\sim 65$  and  $\sim 115$  nm, respectively. STM/STS revealed the presence of in-gap states adjacent to the CB edge of the SiNCs with every alkyne(aryl) surface group studied. PL red-shifts were attributed to emissions through these in-gap states, which reduce the effective band gap for the electron–hole recombination process. The extent of the PL shift is influenced by the nature of the aromatic group. In vast contrast, when aryl and alkyne surface groups were attached to the SiNC surface, no change in the band structure or PL wavelength was observed.

Theoretical calculations suggest that the presence of interface states arising directly from the alkyne(aryl) bond plays a key role in the emission mechanism. The presented results clearly indicate the influence of the alkyne(aryl) surface groups on the optical properties of the SiNCs. They also demonstrate the possibility of utilizing simple conjugated aromatic molecules to manipulate the band structure and the PL of SiNCs, which may permit one to tune or enhance the performance of the SiNCs for the desired applications.

## Experimental

### General information and materials

All reactions were carried out under an argon atmosphere using standard Schlenk or glovebox techniques. All chemicals

were purchased from Sigma-Aldrich and used without further purification, unless stated otherwise. Phenyllithium (1.8 M, in dibutyl ether), *n*-hexyllithium (2.3 M, in hexane), *n*-butyllithium (2.5 M, in hexane) were used. Dry toluene, diethylether and THF were obtained from a MBraun SPS 800 solvent purification system with Argon 5.0 as the operating gas.

### Synthetic procedures

**Preparation of oxide-embedded silicon nanocrystals.** Polymeric hydrogen silsesquioxane (HSQ) was synthesized following a literature known procedure [51]. HSQ (7 g) was placed in a quartz reaction boat, transferred to a Nabertherm RD 30/200/11 furnace with quartz working tube and heated from ambient to a peak processing temperature of 1100 °C at 18 °C min<sup>-1</sup> in a slightly reducing atmosphere (5% H<sub>2</sub>/95% N<sub>2</sub>). The sample was kept at 1100 °C for 1 h. After cooling to room temperature, the resulting amber solid was ground into a fine brown powder using a mortar and pestle. The composite was further ground via shaking the powder dispersed in ethanol for 24 h with high-purity silica beads using a WAB Turbula mixer. The resulting SiNC/SiO<sub>2</sub> composite was dried *in vacuo* and the powder stored in glass vials.

**Liberation of hydride-terminated SiNCs.** 300 mg of the SiNC/SiO<sub>2</sub> composite was weighed into an ethylene-tetrafluoroethylene (ETFE) beaker equipped with a Teflon-coated stir bar. Ethanol (3 ml) and water (3 ml) were then added, and it is stirred to form a brown suspension, followed by addition of 3 ml of 49% HF aqueous solution. After 30 min of etching, the color of the suspension turns to yellow. Hydride-terminated SiNCs were subsequently extracted from the aqueous layer into ca. 30 ml of toluene by multiple (i.e., 3 × 10 ml) extractions. The SiNC toluene suspension was centrifuged in an ETFE-centrifuge tube at 9000 rpm for 5 min. To remove any residual water/ethanol, extracted particles dispersed in 5 ml dry toluene and centrifuged once more.

### Functionalization of SiNCs with organometallic reagents.

Hydride-terminated SiNCs, obtained by etching 300 mg Si/SiO<sub>2</sub> composite, are dispersed in 2 ml of a degassed dry toluene and transferred to a Schlenk flask equipped with a stir bar. The relative volume of the organolithium reagent yielding 0.2 mmol is added. Upon addition of the organolithium reagent the color of the reaction mixture turns dark brown. The mixture is degassed via three freeze-thaw cycles and stirred for overnight under argon atmosphere. To terminate the reaction, functionalized SiNCs were precipitated in 5 ml 1:1 ethanol-methanol mixture, acidified with HCl conc. (0.2 ml). Obtained SiNCs are centrifuged at 9000 rpm for 10 min and the sediment is redispersed in minimum amount of toluene. The precipitation-centrifugation-redispersion cycle is performed two more times from toluene and ethanol-methanol. Finally, functionalized

SiNCs are dispersed in toluene and filtered through a 0.45 μm PTFE syringe filter.

**Synthesis of conjugated organic molecules.** 2-ethynyl-naphthalene and 2-ethynyl-5-hexylthiophene were synthesized via a Sonogashira cross-coupling based on literature known procedures [52, 53]. The synthesis of 2-hexylthiophene was achieved via a Kumada coupling reaction [54]. Detailed experimental descriptions are given in the ESI.

### Lithiation of the conjugated organic molecules

**Lithiation of phenylacetylene, 1-dodecyne, 2-hexylthiophene, 2-ethynyl-5-hexylthiophene and 2-ethynyl-naphthalene.** The conjugated organic molecule (200 mg, 1 eq.) is dissolved in a predetermined amount of THF in a Schlenk flask, equipped with a stir bar and a septum. *n*-butyllithium (2.5 M in hexanes, 0.8 eq.) is added to the reaction flask drop wise in 15 min at -78 °C under an argon atmosphere. Upon the completion of the addition, the reaction mixture is stirred for 15 more minutes, and then it is brought to room temperature. The solution is degassed and stored in a Schlenk flask in a cool place. 1 M solutions were prepared with phenylacetylene, 2-hexylthiophene and 2-ethynyl-5-hexylthiophene. In the case of 1-dodecyne a 0.5 M solution was prepared.

**Lithiation of 2-bromonaphthalene.** 2-bromonaphthalene (200 mg, 0.97 mmol, 1 eq.) is dissolved in 1.4 ml of diethylether to yield a 0.5 M solution in a Schlenk flask, equipped with a stir bar and a septum. *n*-butyllithium (0.35 ml, 2.5 M in hexanes, 0.8 eq.) is added to the reaction flask drop wise in 15 min at -78 °C. Upon the completion of the addition, the reaction mixture is stirred for 15 more minutes, and then it is brought to room temperature. The solution is degassed and stored in a Schlenk flask in a cool place.

### Characterization

STM/STS data was acquired from SiNCs deposited on an atomically flat Au (111) substrate by drop-casting from toluene. All measurements were performed at room temperature and ambient conditions, employing a home-built STM system with a Pt-Ir tip. All STM images were obtained under a set bias of 2.2 V (well above the CB edge where the DOS of the SiNCs is noticeable) and set current of 1 nA. With these settings, the cross-section height is close to the actual diameter (~3 nm) of the SiNCs. The tunneling spectra were obtained by positioning the STM tip over a single SiNC, forming a DBTJ configuration, after momentarily disabling the feedback circuit. The above settings also ensure that the tip is retracted as far as possible from the NC, in order to minimize the broadening of band gaps resulting from the voltage-division effect.

FTIR spectra were collected with a Bruker Vertex 70 FTIR using a Platinum ATR from Bruker. PL spectra were measured with an AVA-Spec 2048 from Avantes using a Prizmatix (LED Current controller) as light source. Samples

were excited with a 365 nm source. The PL maxima were determined by fitting the raw data with a (skewed) Gaussian function. PL lifetime decay measurements were measured by a 351 nm excitation line from the Ar<sup>+</sup> laser, sent through an *Isomet IMDD-T110L-1.5* acousto-optic modulator operated at a frequency of 200 Hz. The PL lifetime decays were collected by a *Becker-Hickl PMC-100* photon-counting PMT. UV-vis Spectroscopy was performed with a *Varian Cary 50 Scan Spectrometer* within the range 200–800 nm. Bright field TEM images were obtained using a JEOL-2012 electron microscope equipped with LaB<sub>6</sub> filament and operated at an accelerating voltage of 200 kV. HR-TEM images were obtained by a *JEM-2200FS* TEM with 200 kV field emission gun. SiNCs were drop-casted onto a lacey carbon grid with a 300 μm diameter hole and the solvent was evaporated under vacuum. Particle size distribution was calculated by counting at least 200 particles using ImageJ software (Version 1.49).






#### CC2 calculations

CC2 calculations [55] for isolated model clusters were performed with the TURBOMOLE package [56, 57]. The employed def2-SV(P) basis set was benchmarked against an aug-cc-pVDZ basis set as shown in the SI. The molecular geometries were optimized on MP2 level until residual forces fell below 0.01 eV Å<sup>-1</sup>.

#### Acknowledgments

B Rieger, J G C Veinot and A Meldrum acknowledge the funding from the DFG IRTG (2022) and NSERC CREATE programs for Alberta/TU München International Graduate School. J G C Veinot and A Meldrum appreciate the continued generous support from the NSERC DG program. A Angi is thankful for the funding from Studienstiftung des Deutschen Volkes. R Sinelnikov acknowledges the funding from AITF. O Millo acknowledges funding from the ISF grant number 661/16 and the Harry de Jur Chair in Applied Science. I Balberg thanks the support from the Enrique Berman Chair in Solar Energy Research. Ignaz Höhle and Tobias Helbich are thanked for valuable discussions and corrections. Kai Cui is thanked for assistance with HR-TEM measurements.

#### ORCID iDs

Arzu Angi  <https://orcid.org/0000-0002-6722-7408>  
 Regina Sinelnikov  <https://orcid.org/0000-0001-6741-6017>  
 Hendrik H Heenen  <https://orcid.org/0000-0003-0696-8445>  
 Jonathan G C Veinot  <https://orcid.org/0000-0001-7511-510X>  
 Karsten Reuter  <https://orcid.org/0000-0001-8473-8659>  
 Oded Millo  <https://orcid.org/0000-0003-4377-0294>  
 Bernhard Rieger  <https://orcid.org/0000-0002-0023-884X>

#### References

- [1] Canham L T 1990 *Appl. Phys. Lett.* **57** 1046
- [2] Dasog M, Kehrle J, Rieger B and Veinot J G C 2016 *Angew. Chem., Int. Ed.* **55** 2322
- [3] Ledoux G, Guillois O, Porterat D, Reynaud C, Huisken F, Kohn B and Paillard V 2000 *Phys. Rev. B* **62** 15942
- [4] Wolf O, Dasog M, Yang Z, Balberg I, Veinot J G C and Millo O 2013 *Nano Lett.* **13** 2516
- [5] Hessel C M, Reid D, Panthani M G, Rasch M R, Goodfellow B W, Wei J, Fujii H, Akhavan V and Korgel B A 2012 *Chem. Mater.* **24** 393
- [6] Barbagioanni E G, Lockwood D J, Simpson P J and Goncharova L V 2012 *J. Appl. Phys.* **111** 34307
- [7] Angi A, Sinelnikov R, Meldrum A, Veinot J G C, Balberg I, Azulay D, Millo O and Rieger B 2016 *Nanoscale* **8** 7849
- [8] Dasog M, De los Reyes G B, Titova L V, Hegmann F A and Veinot J G C 2014 *ACS Nano* **8** 9636
- [9] Dasog M, Bader K and Veinot J G C 2015 *Chem. Mater.* **27** 1153
- [10] Ondic L et al 2014 *Nanoscale* **6** 3837
- [11] Fuzell J, Thibert A, Atkins T M, Dasog M, Busby E, Veinot J G C, Kauzlarich S M and Larsen D S 2013 *J. Phys. Chem. Lett.* **4** 3806
- [12] Botas A M P, Anthony R J, Wu J, Rowe D J, Silva N J O, Kortshagen U, Pereira R N and Ferreira R A S 2016 *Nanotechnology* **27** 325703
- [13] Wang R, Pi X and Yang D 2012 *J. Phys. Chem. C* **116** 19434
- [14] Svrcek V, Yamanari T, Mariotti D, Mitra S, Velusamy T and Matsubara K 2015 *Nanoscale* **7** 11566
- [15] Liu C-Y and Kortshagen U R 2012 *Nanoscale* **4** 3963
- [16] Dutta M, Thirugnanam L, van Trinh P and Fukata N 2015 *ACS Nano* **9** 6891
- [17] Liu C-Y, Holman Z C and Kortshagen U R 2009 *Nano Lett.* **9** 449
- [18] Maier-Flaig F, Rinck J, Stephan M, Bocksrocker T, Bruns M, Kübel C, Powell A K, Ozin G A and Lemmer U 2013 *Nano Lett.* **13** 475
- [19] Cheng K-Y, Anthony R, Kortshagen U R and Holmes R J 2010 *Nano Lett.* **10** 1154
- [20] Angi A, Loch M T, Sinelnikov R, Veinot J G C, Becherer M, Lugli P and Rieger B 2018 *Nanoscale* **10** 10337
- [21] Gonzalez C M, Iqbal M, Dasog M, Piercey D G, Lockwood R, Klapötke T M and Veinot J G C 2014 *Nanoscale* **6** 2608
- [22] Zhang J and Yu S-H 2014 *Nanoscale* **6** 4096
- [23] Fucikova A, Valenta J, Pelant I, Kalbacova M H, Broz A, Rezek B, Kromka A and Bakaeva Z 2014 *RSC Adv.* **4** 10334
- [24] Cheng X, Lowe S B, Reece P J and Gooding J J 2014 *Chem. Soc. Rev.* **43** 2680
- [25] Abdelhameed M, Martir D R, Chen S, Xu W Z, Oyeneye O O, Chakrabarti S, Zysman-Colman E and Charpentier P A 2018 *Sci. Rep.* **8** 3050
- [26] de los Reyes G B, Dasog M, Na M, Titova L V, Veinot J G C and Hegmann F A 2015 *Phys. Chem. Chem. Phys.* **17** 30125
- [27] Zhou T, Anderson R T, Li H, Bell J, Yang Y, Gorman B P, Pylypenko S, Lusk M T and Sellinger A 2015 *Nano Lett.* **15** 3657
- [28] Höhle I M D, Angi A, Sinelnikov R, Veinot J G C and Rieger B 2015 *Chem. Eur. J.* **21** 2755
- [29] Song J H and Sailor M J 1999 *Inorg. Chem.* **38** 1498
- [30] Song J H and Sailor M J 1998 *J. Am. Chem. Soc.* **120** 2376
- [31] Hapala P, Kúsová K, Pelant I and Jelínek P 2013 *Phys. Rev. B* **87** 195420
- [32] Brown S L, Miller J B, Anthony R J, Kortshagen U R, Kryjevski A and Hobbie E K 2017 *ACS Nano* **11** 1597



- [33] Wen X, Zhang P, Smith T A, Anthony R J, Kortshagen U R, Yu P, Feng Y, Shrestha S, Coniber G and Huang S 2015 *Sci. Rep.* **5** 12469
- [34] Miller J B, Dandu N, Velizhanin K A, Anthony R J, Kortshagen U R, Kroll D M, Kilina S and Hobbie E K 2015 *ACS Nano* **9** 9772
- [35] van Driel A F, Nikolaev I S, Vergeer P, Lodahl P, Vanmaekelbergh D and Vos W L 2007 *Phys. Rev. B* **75** 35329
- [36] Nguyen A, Gonzalez C M, Sinelnikov R, Newman W, Sun S, Lockwood R, Veinot J G C and Meldrum A 2016 *Nanotechnology* **27** 105501
- [37] Mustafeez W, Majumdar A, Vučković J and Salleo A 2014 *J. Appl. Phys.* **115** 103515
- [38] Banin U, Cao Y W, Katz D and Millo O 1999 *Nature* **400** 542
- [39] Banin U and Millo O 2003 *Annu. Rev. Phys. Chem.* **54** 465
- [40] Bakkers E P A M, Hens Z, Zunger A, Franceschetti A, Kouwenhoven L P, Gurevich L and Vanmaekelbergh D 2001 *Nano Lett.* **1** 551
- [41] Swart I, Liljeroth P and Vanmaekelbergh D 2016 *Chem. Rev.* **116** 11181
- [42] Wang T, Vaxenburg R, Liu W, Rupich S M, Lifshitz E, Efros A L, Talapin D V and Sibener S J 2015 *ACS Nano* **9** 725
- [43] Liljeroth P, van Zeijlman Emmichoven P A, Hickey S G, Weller H, Grandidier B, Allan G and Vanmaekelbergh D 2005 *Phys. Rev. Lett.* **95** 86801
- [44] Bekenstein Y, Vinokurov K, Keren-Zur S, Hadar I, Schilt Y, Raviv U, Millo O and Banin U 2014 *Nano Lett.* **14** 1349
- [45] Mocatta D, Cohen G, Schattner J, Millo O, Rabani E and Banin U 2011 *Science* **332** 77
- [46] Yang Z, de los Reyes G B, Titova L V, Sychugov I, Dasog M, Linnros J, Hegmann F A and Veinot J G C 2015 *ACS Photonics* **2** 595
- [47] Kelly J A and Veinot J G C 2010 *ACS Nano* **4** 4645
- [48] Li H, Wu Z, Zhou T, Sellinger A and Lusk M T 2014 *Phys. Chem. Chem. Phys.* **16** 19275
- [49] Lee B G, Luo J-W, Neale N R, Beard M C, Hiller D, Zacharias M, Stradins P and Zunger A 2016 *Nano Lett.* **16** 1583
- [50] Dohnalová K, Gregorkiewicz T and Kůsová K 2014 *J. Phys.: Condens. Matter* **26** 173201
- [51] Bank H M, Cifuentes M E and Theresa E M 1991 *US Patent Specification* 5.010.159
- [52] Hundertmark T, Littke A F, Buchwald S L and Fu G C 2000 *Org. Lett.* **2** 1729
- [53] Rondeau-Gagné S, Curutchet C, Grenier F, Scholes G D and Morin J-F 2010 *Tetrahedron* **66** 4230
- [54] Wex B, Jradi F M, Patra D and Kaafarani B R 2010 *Tetrahedron* **66** 8778
- [55] Hättig C and Köhn A 2002 *J. Chem. Phys.* **117** 6939
- [56] Ahlrichs R, Bär M, Häser M, Horn H and Kölmel C 1989 *Chem. Phys. Lett.* **162** 165
- [57] Treutler O and Ahlrichs R 1995 *J. Chem. Phys.* **102** 346

## Supporting Information:

# The Influence of Conjugated Alkynyl(aryl) Surface Groups on the Optical Properties of Silicon Nanocrystals: Photoluminescence through In-Gap States

Arzu Angi,<sup>a</sup> Regina Sinelnikov,<sup>b</sup> Hendrik H. Heenen,<sup>c</sup> Al Meldrum,<sup>d</sup> Jonathan G. C. Veinot,<sup>b</sup> Christoph Scheurer,<sup>c</sup> Karsten Reuter,<sup>c</sup> Or Ashkenazy,<sup>e</sup> Doron Azulay,<sup>e,f</sup> Isaac Balberg,<sup>e</sup> Oded Millo,<sup>e,\*</sup> and Bernhard Rieger<sup>a,\*</sup>

<sup>a</sup> WACKER-Lehrstuhl für Makromolekulare Chemie, Technische Universität München, Lichtenbergstraße 4, 85747; Catalysis Research Center, Ernst-Otto-Fischer-Straße 1, 85748 Garching, Germany.

<sup>b</sup> Department of Chemistry, University of Alberta, 11227 Saskatchewan Drive, Edmonton, Alberta, T6G 2G2, Canada .

<sup>c</sup> Chair for Theoretical Chemistry and Catalysis Research Center, Technische Universität München, Lichtenbergstrasse 4, D-85747 Garching, Germany.

<sup>d</sup> Department of Physics, University of Alberta, Edmonton, Alberta T6G 2G2, Canada.

<sup>e</sup> Racah Institute of Physics, The Hebrew University of Jerusalem, Jerusalem 91904, Israel.

<sup>f</sup> Azriely, Jerusalem College of Engineering, Jerusalem 9103501, Israel.

## Table of Contents

<b>1</b>	<b>Analytical Data.....</b>	<b>3</b>
1.1	FTIR Spectroscopy .....	3
1.2	UV-VIS Spectroscopy .....	4
1.3	Excited State Life-time Measurements .....	5
1.4	TEM Images .....	7
<b>2</b>	<b>CC2 Excited State Calculations for Model Silicon Nanoclusters .....</b>	<b>10</b>
<b>3</b>	<b>Synthesis of Conjugated Organic Molecules.....</b>	<b>16</b>
3.1	2-Ethynyl-naphthalene .....	16
3.2	2-Hexylthiophene .....	17
3.3	2-Ethynyl-5-Hexyl Thiophene .....	18

# Analytical Data

## FTIR Spectroscopy

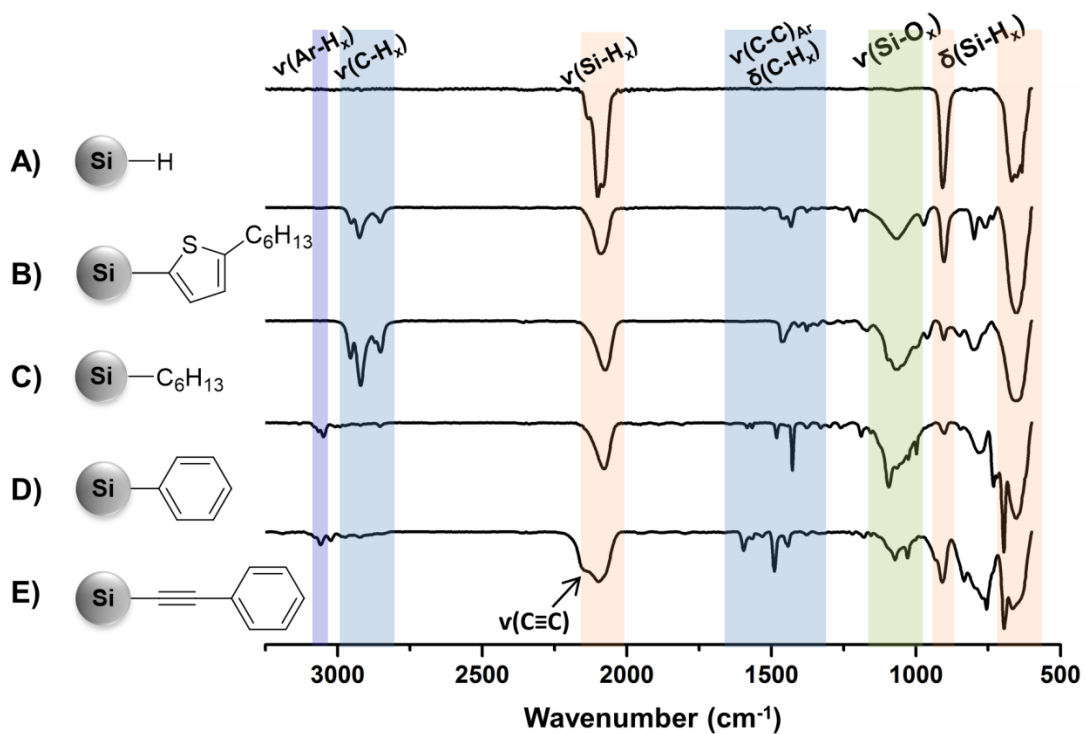


**Figure S1.** FTIR spectra of A) hydride terminated, B) 2-hexylthiophene, C) hexyl, D) phenyl and E) phenylacetylene functionalized SiNCs.

## UV-VIS Spectroscopy

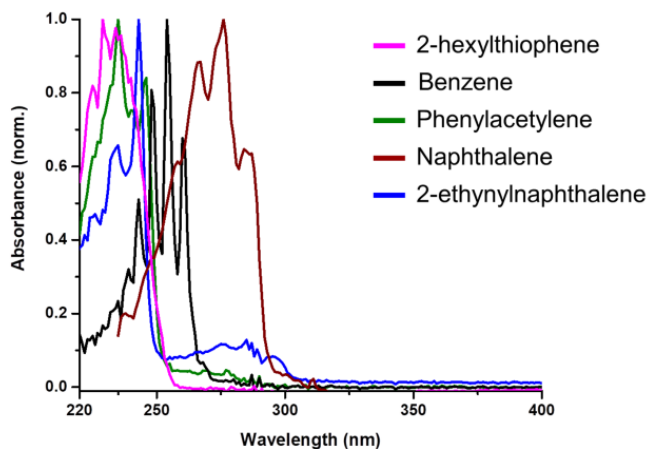


**Figure S2.** Normalized UV/VIS absorbance of the conjugated molecules in THF. It is important to note that these conjugated molecules do not absorb at 365 nm. PL of SiNCs was recorded upon excitation at 365 nm.

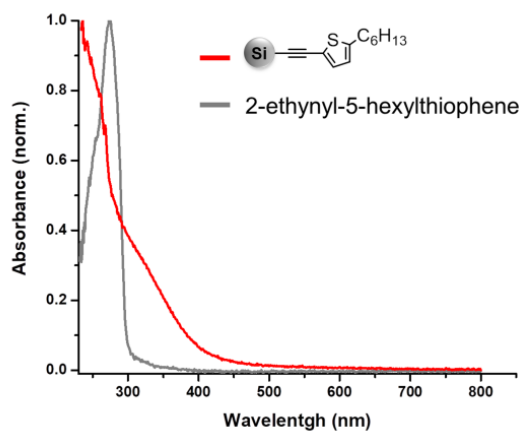


**Figure S3.** Normalized absorbance of 2-ethynyl-5-hexylthiophene molecule in comparison to the SiNCs functionalized with 2-ethynyl-5-hexylthiophene molecules in THF. The shoulder appearing between 300-500 nm in the absorbance of SiNCs is not caused by the absorption of the surface molecules.

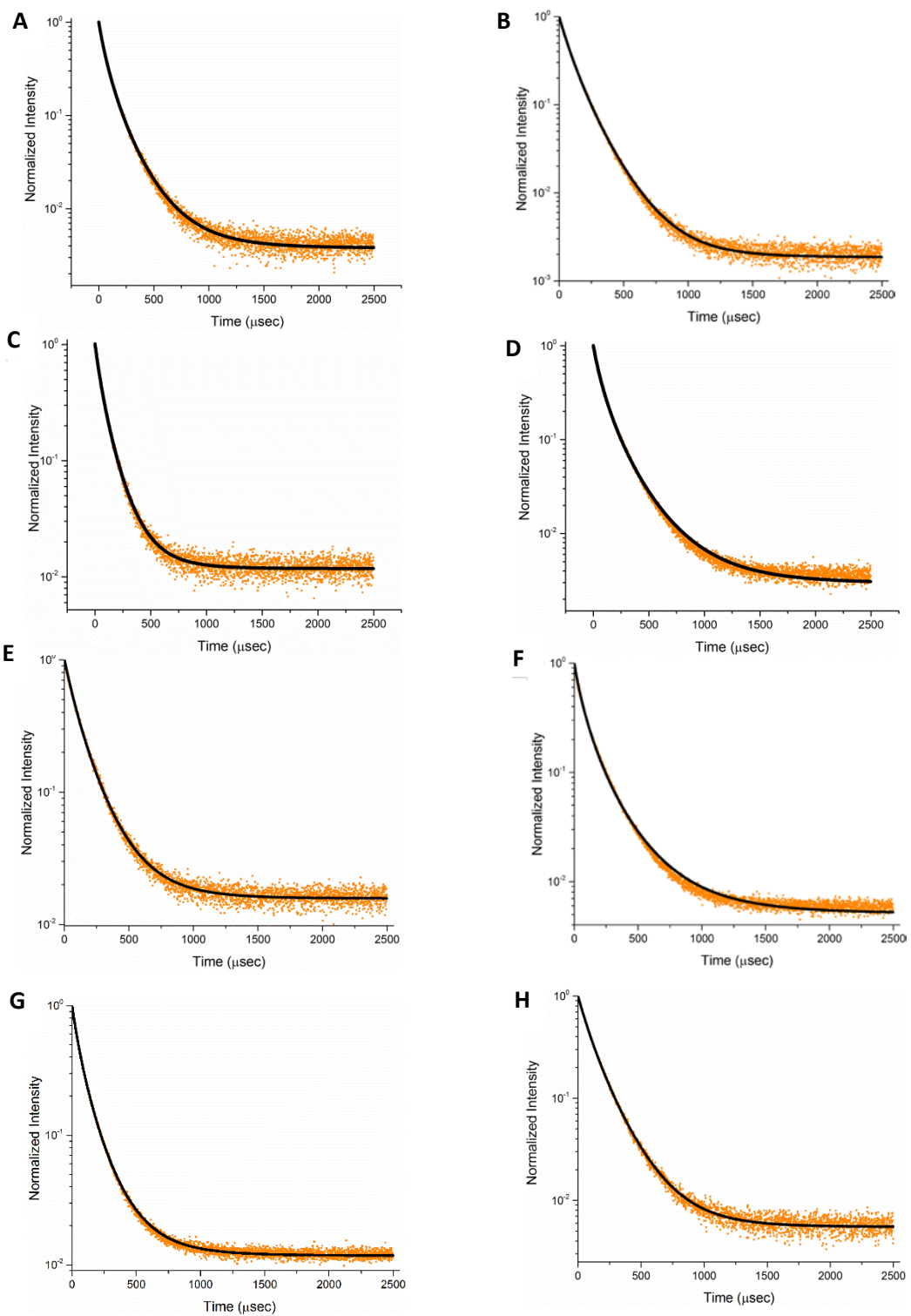
## Excited State Life-time Measurements

**Table S1.** Peak (*i.e.*, most common) excited state life-times extracted from fitting the raw data with lognormal function given by the standard decay rate probability distribution function

$$H(\Gamma) = \frac{1}{\Gamma} \cdot \frac{1}{\sigma\sqrt{2\pi}} \exp \left[ -\frac{(\ln\Gamma - \mu)^2}{2\sigma^2} \right],$$

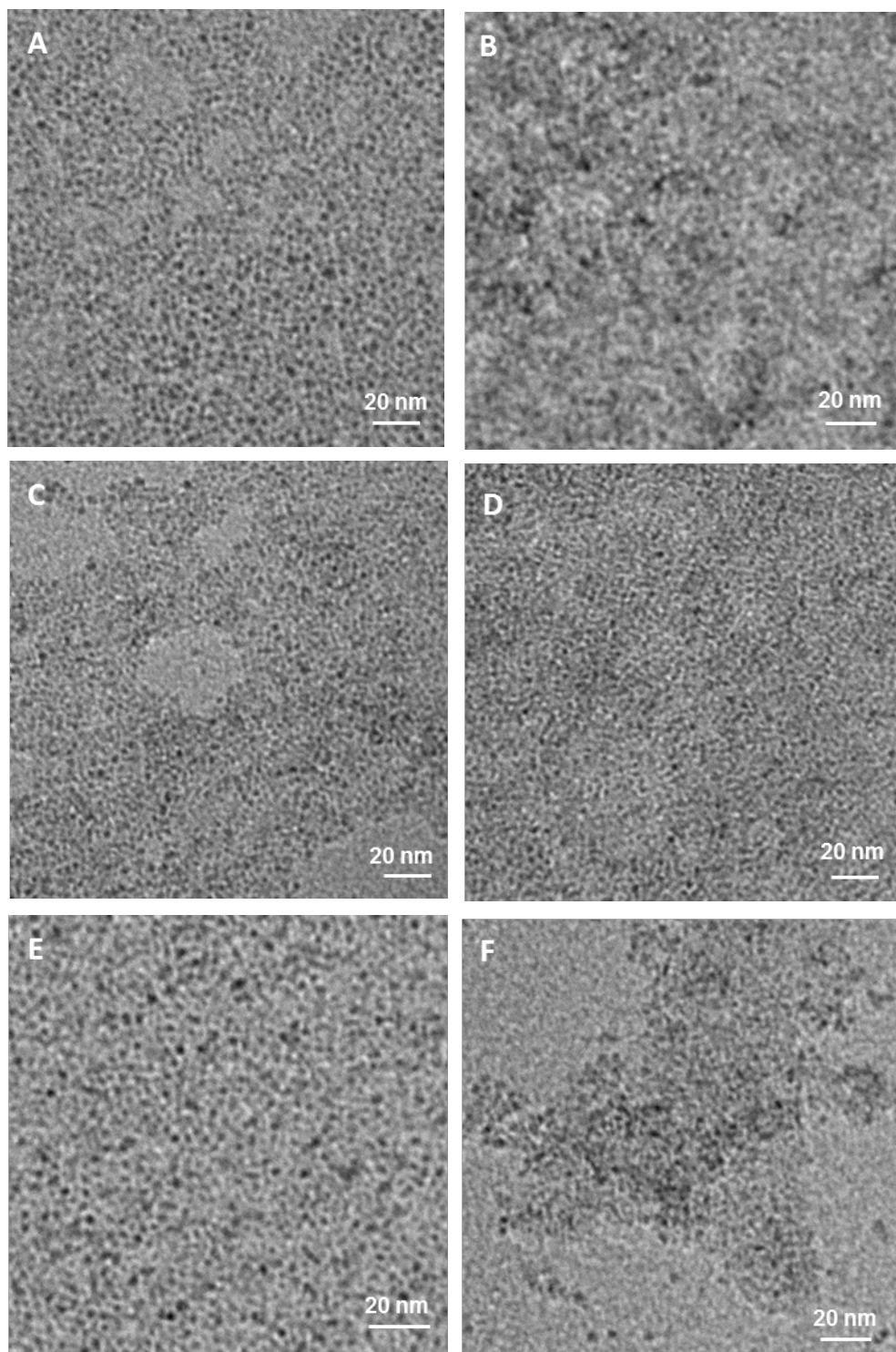
where  $\Gamma$  is the emission rate and  $\mu$  and  $\sigma$  are the location and scale parameters.

<b>Surface Functionalization</b>	<b><math>\tau</math> (<math>\mu\text{sec}</math>)</b>
Hexyl	110.6
1-Dodecyne	105.8
Phenyl	93.7
Phenylacetylene	129.7
Naphthalene	131.0
2-Ethynynaphthalene	127.4
2-Hexylthiophene	105.5
2-Ethynyl-5-hexylthiophene	134.3



**Figure S4** PL decay curves of SiNCs functionalized with A) hexyl, B) 1-dodecyne C) phenyl, D) phenylacetylene, E) naphthalene, F) 2-ethynynaphthalene, G) 2-hexylthiophene, H) 2-ethynyl-5-hexylthiophene. Black curves show the fitted curve with lognormal function.

## TEM Images





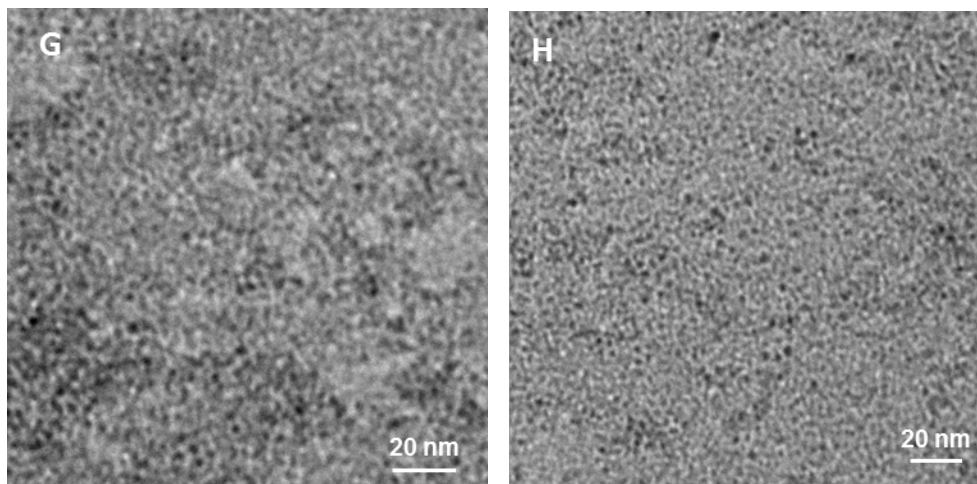


**Figure S5.** Bright field TEM images SiNCs functionalized with A) hexyl, B) 1-dodecyne, C) phenyl D) phenylacetylene E) naphthalene, F) 2-ethynyl-naphthalene, G) 2-hexylthiophene, H) 2-ethynyl-5-hexylthiophene.

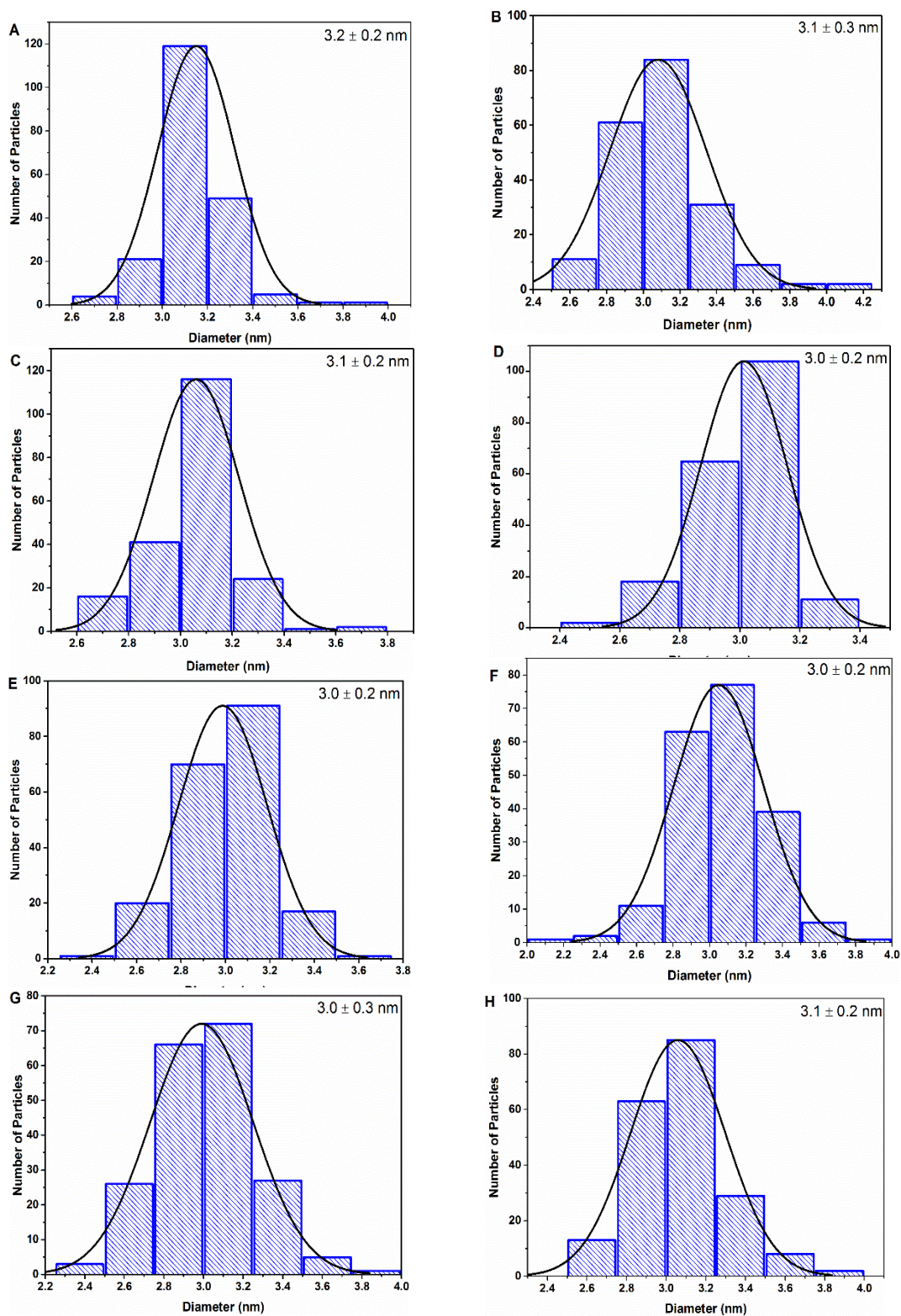


**Figure S6.** Size distributions of SiNCs functionalized with A) hexyl, B) 1-dodecyne, C) phenyl D) phenylacetylene E) naphthalene, F) 2-ethynynaphthalene, G) 2-hexylthiophene, H) 2-ethynyl-5-hexylthiophene.

## CC2 Excited State Calculations for Model Silicon Nanoclusters

**Size effects of R-Si<sub>x</sub>H<sub>y</sub> model clusters:** The CC2 excited state calculations of Si<sub>10</sub>H<sub>16</sub>, Si<sub>14</sub>H<sub>20</sub> and Si<sub>26</sub>H<sub>32</sub> diamond structures with attached alkynyl(aryl) molecules show low lying bright  $\pi^*$  interface states which are considered as the origin of the in-gap states observed in the STS spectra (see manuscript). The structural models are employed as an approximation to the experimentally studied SiNCs with average size of 3 nm which cannot be feasibly calculated at the same level of theory. To rationalize the viability and size persistence of the qualitative observations, we discuss the size effects associated with the model clusters.

**Table S2.** Vertical excitation energies in eV and oscillator strength (in parenthesis) of the first five excited states (S1-S5) for all calculated organic molecules on the diamond model clusters.

	Phenyl				
	S1	S2	S3	S4	S5
Si <sub>10</sub> H <sub>16</sub>	5.097 (0.001)	5.680 (0.001)	5.971 (0.582)	6.064 (0.002)	6.157 (0.024)
Si <sub>14</sub> H <sub>20</sub>	5.092 (0.001)	5.567 (0.000)	5.686 (0.019)	5.803 (0.006)	5.831 (0.183)
Si <sub>26</sub> H <sub>32</sub>	5.038 (0.003)	5.043 (0.045)	5.049 (0.002)	5.071 (0.004)	5.086 (0.015)
	Phenylacetylene				
	S1	S2	S3	S4	S5
Si <sub>10</sub> H <sub>16</sub>	4.971 (0.001)	5.271 (1.030)	5.532 (0.002)	5.646 (0.007)	5.761 (0.007)
Si <sub>14</sub> H <sub>20</sub>	4.969 (0.001)	5.230 (1.146)	5.491 (0.001)	5.534 (0.007)	5.638 (0.002)
Si <sub>26</sub> H <sub>32</sub>	4.926 (0.658)	4.961 (0.001)	5.008 (0.000)	5.024 (0.043)	5.033 (0.002)
	Naphthalene				
	S1	S2	S3	S4	S5
Si <sub>10</sub> H <sub>16</sub>	4.318 (0.002)	4.836 (0.093)	5.458 (0.000)	5.692 (2.228)	5.930 (0.002)
Si <sub>14</sub> H <sub>20</sub>	4.314 (0.002)	4.824 (0.101)	5.353 (0.000)	5.610 (2.033)	5.701 (0.000)
Si <sub>26</sub> H <sub>32</sub>	4.296 (0.002)	4.749 (0.223)	4.977 (0.012)	5.006 (0.001)	5.021 (0.000)
	2-ethynyl-naphthalene				
	S1	S2	S3	S4	S5
Si <sub>10</sub> H <sub>16</sub>	4.218 (0.002)	4.645 (0.526)	5.299 (1.587)	5.394 (0.002)	5.526 (0.004)
Si <sub>14</sub> H <sub>20</sub>	4.216 (0.002)	4.635 (0.616)	5.269 (1.657)	5.359 (0.001)	5.414 (0.005)
Si <sub>26</sub> H <sub>32</sub>	4.207 (0.003)	4.568 (0.963)	4.948 (0.001)	4.978 (0.031)	4.997 (0.214)
	2-hexylthiophene				
	S1	S2	S3	S4	S5
Si <sub>10</sub> H <sub>16</sub>	5.171 (0.058)	5.316 (0.543)	5.627 (0.162)	5.718 (0.010)	5.771 (0.027)
Si <sub>14</sub> H <sub>20</sub>	5.095 (0.001)	5.244 (0.684)	5.493 (0.001)	5.547 (0.003)	5.574 (0.052)
Si <sub>26</sub> H <sub>32</sub>	4.781 (0.101)	4.831 (0.296)	4.850 (0.001)	4.873 (0.003)	4.949 (0.000)
	2-ethynyl-5-hexylthiophene				
	S1	S2	S3	S4	S5
Si <sub>10</sub> H <sub>16</sub>	4.723 (1.064)	5.073 (0.002)	5.346 (0.000)	5.457 (0.104)	5.543 (0.003)
Si <sub>14</sub> H <sub>20</sub>	4.698 (1.196)	5.019 (0.001)	5.236 (0.000)	5.452 (0.109)	5.499 (0.001)
Si <sub>26</sub> H <sub>32</sub>	4.558 (1.349)	4.722 (0.001)	4.881 (0.012)	4.940 (0.000)	5.007 (0.000)

The main effect observed with increasing cluster size is a decreasing energy of the first appearing excited quantum dot (QD) state from 5.5 to 5.0 eV for the clusters Si<sub>10</sub>H<sub>16</sub>, Si<sub>14</sub>H<sub>20</sub> and Si<sub>26</sub>H<sub>32</sub> (compare Table S2 and S3). This QD state represents the conduction band edge in a macroscopic SiNC and therewith this trend indicates a closing band-gap. The electronic effect on the atomistic level is manifold as the energetic alignment among the occupied  $\pi$  bonding and  $\sigma$ (Si) bonding orbitals as well as the unoccupied  $\pi^*$  antibonding and QD orbitals changes rigorously. The influence on the electronic structure is described in the following.

**Table S3.** Character of the electronic transitions with their respective share in percentage (in parenthesis) of the first five excited states (S1-S5) for all calculated organic molecules on the diamond model clusters. All transitions with a contribution of above 5% are included, same-character transitions are summed for visibility.

Phenyl					
	S1	S2	S3	S4	S5
Si <sub>10</sub> H <sub>16</sub>	$\pi$ - $\pi^*$ (78)	$\pi$ -QD (92)	$\pi$ - $\pi^*$ (85)	$\pi$ -QD (74)	$\pi$ -QD (63)
Si <sub>14</sub> H <sub>20</sub>	$\pi$ - $\pi^*$ (76) $\pi$ -QD (7)	$\pi$ -QD (83)	$\sigma$ (Si)-QD (95)	$\sigma$ (Si)-QD (7) $\pi$ -QD (20)	$\sigma$ (Si)-QD (24) $\pi$ - $\pi^*$ (16) $\pi$ -QD (10)
Si <sub>26</sub> H <sub>32</sub>	$\sigma$ (Si)-QD (41) $\pi$ -QD (33)	$\pi$ -QD (35) $\pi$ - $\pi^*$ (19) $\sigma$ (Si)-QD (8)	$\sigma$ (Si)-QD (63) $\pi$ -QD (14)	$\sigma$ (Si)-QD (79)	$\sigma$ (Si)-QD (22) $\pi$ - $\pi^*$ (22) $\pi$ -QD (16)
Phenylacetylene					
	S1	S2	S3	S4	S5
Si <sub>10</sub> H <sub>16</sub>	$\pi$ - $\pi^*$ (84)	$\pi$ - $\pi^*$ (89)	$\sigma$ (Si)- $\pi^*$ (75) $\pi$ - $\pi^*$ (9)	$\pi$ -QD (73)	$\pi$ - $\pi^*$ (74)
Si <sub>14</sub> H <sub>20</sub>	$\pi$ - $\pi^*$ (83)	$\pi$ - $\pi^*$ (87)	$\sigma$ (Si)- $\pi^*$ (74) $\pi$ - $\pi^*$ (6)	$\pi$ -QD (71)	$\pi$ -QD (43) $\pi$ - $\pi^*$ (32)
Si <sub>26</sub> H <sub>32</sub>	$\pi$ - $\pi^*$ (70) $\sigma$ (Si)- $\pi^*$ (10)	$\pi$ - $\pi^*$ (80) $\pi$ -QD (6) $\sigma$ (Si)- $\pi^*$ (5)	$\pi$ -QD (42) $\sigma$ (Si)-QD (37)	$\sigma$ (Si)-QD (10) $\pi$ -QD (27)	$\sigma$ (Si)-QD (49) $\sigma$ (Si)- $\pi^*$ (56) $\sigma$ (Si)-QD (7)
Naphthalene					
	S1	S2	S3	S4	S5
Si <sub>10</sub> H <sub>16</sub>	$\pi$ - $\pi^*$ (80) $\pi$ -QD (6)	$\pi$ - $\pi^*$ (86)	$\pi$ -QD (85)	$\pi$ - $\pi^*$ (79)	$\pi$ -QD (63)
Si <sub>14</sub> H <sub>20</sub>	$\pi$ - $\pi^*$ (78) $\pi$ -QD (8)	$\pi$ - $\pi^*$ (76) $\pi$ -QD (11)	$\sigma$ (Si)-QD (7) $\pi$ -QD (81)	$\pi$ -QD (6) $\pi$ - $\pi^*$ (70)	$\sigma$ (Si)-QD (12) $\pi$ -QD (58) $\sigma$ (Si)-QD (16)
Si <sub>26</sub> H <sub>32</sub>	$\pi$ - $\pi^*$ (57) $\pi$ -QD (25)	$\pi$ -QD (62) $\pi$ - $\pi^*$ (27)	$\pi$ -QD (54) $\sigma$ (Si)-QD (7)	$\pi$ -QD (48) $\sigma$ (Si)-QD (25)	$\sigma$ (Si)- $\pi^*$ (6) $\pi$ -QD (50) $\sigma$ (Si)-QD (21)
2-ethynynaphthalene					
	S1	S2	S3	S4	S5
Si <sub>10</sub> H <sub>16</sub>	$\pi$ - $\pi^*$ (68) $\pi$ -QD (13)	$\pi$ - $\pi^*$ (85)	$\pi$ - $\pi^*$ (66) $\pi$ -QD (17) $\sigma$ (Si)- $\pi^*$ (6)	$\sigma$ (Si)- $\pi^*$ (72) $\pi$ - $\pi^*$ (8)	$\pi$ -QD (70) $\sigma$ (Si)-QD (19)
Si <sub>14</sub> H <sub>20</sub>	$\pi$ - $\pi^*$ (77) $\pi$ -QD (7)	$\pi$ - $\pi^*$ (83)	$\pi$ - $\pi^*$ (70) $\pi$ -QD (8)	$\sigma$ (Si)- $\pi^*$ (75) $\pi$ - $\pi^*$ (7)	$\pi$ -QD (64) $\sigma$ (Si)-QD (12)
Si <sub>26</sub> H <sub>32</sub>	$\pi$ - $\pi^*$ (69) $\pi$ -QD (12)	$\pi$ - $\pi^*$ (80) $\pi$ -QD (8)	$\pi$ -QD (46) $\sigma$ (Si)-QD (27)	$\pi$ -QD (25) $\sigma$ (Si)-QD (25) $\sigma$ (Si)- $\pi^*$ (9)	$\pi$ - $\pi^*$ (24) $\pi$ -QD (21) $\sigma$ (Si)- $\pi^*$ (24)
2-hexylthiophene					
	S1	S2	S3	S4	S5
Si <sub>10</sub> H <sub>16</sub>	$\pi$ -QD (86) $\pi$ - $\pi^*$ (6)	$\pi$ - $\pi^*$ (68) $\pi$ -QD (14)	$\pi$ - $\pi^*$ (53) $\pi$ -QD (22)	$\pi$ -QD (62) $\pi$ - $\pi^*$ (13)	$\pi$ -QD (76)
Si <sub>14</sub> H <sub>20</sub>	$\pi$ -QD (93)	$\pi$ - $\pi^*$ (50) $\pi$ -QD (35)	$\pi$ -QD (85)	$\pi$ -QD (85)	$\pi$ - $\pi^*$ (48) $\pi$ -QD (39)
Si <sub>26</sub> H <sub>32</sub>	$\pi$ -QD (65) $\pi$ - $\pi^*$ (16)	$\pi$ -QD (73)	$\pi$ -QD (79)	$\pi$ -QD (69)	$\pi$ -QD (71) $\sigma$ (Si)-QD (13)
2-ethynyl-5-hexylthiophene					
	S1	S2	S3	S4	S5
Si <sub>10</sub> H <sub>16</sub>	$\pi$ - $\pi^*$ (87)	$\pi$ - $\pi^*$ (79)	$\pi$ -QD (82) $\sigma$ (Si)-QD (8)	$\pi$ - $\pi^*$ (83)	$\sigma$ (Si)- $\pi^*$ (80) $\pi$ - $\pi^*$ (9)
Si <sub>14</sub> H <sub>20</sub>	$\pi$ - $\pi^*$ (82)	$\pi$ - $\pi^*$ (48) $\pi$ -QD (40)	$\pi$ -QD (81)	$\pi$ - $\pi^*$ (71)	$\sigma$ (Si)- $\pi^*$ (81) / $\pi$ - $\pi^*$ (7)
Si <sub>26</sub> H <sub>32</sub>	$\pi$ - $\pi^*$ (87)	$\pi$ -QD (53) $\pi$ - $\pi^*$ (16) $\sigma$ (Si)-QD (6)	$\pi$ -QD (71) $\sigma$ (Si)-QD (17)	$\pi$ -QD (64) $\sigma$ (Si)-QD (26)	$\pi$ -QD (42) $\sigma$ (Si)-QD (41)

Occupied orbitals: While  $\pi$  bonding orbitals of the organic molecules are the energetically highest occupied orbitals at small cluster sizes,  $\sigma(\text{Si})$  orbitals emerge at large cluster sizes in their relative energy alignment replacing most of the  $\pi$  bonding orbitals. This effect shows in the nature of the electronic transitions where the excitations increasingly originate from  $\sigma(\text{Si})$  orbitals with growing cluster size (see table S3). This appears consistent with the experimental picture of a band-gap originating in the Si quantum dot. Further it is expected that the  $\sigma(\text{Si})$ -QD transitions will show large oscillator strengths and appear bright, which is a size behaviour rigorously shown experimentally.<sup>[1],[2]</sup>

Energetic alignment of the lowest QD state: Due to the large band-gap at the small cluster sizes, the  $\pi$  orbitals of the organic molecules affect the energetic alignment of the first appearing QD state directly. Therefore, a dependency on the different functionalizations on its relative energetic positions at the same cluster size is seen. However, this size effect gradually decreases already for the small model clusters studied here. The associated energy divergence of the first QD state changes from 0.4 eV for  $\text{Si}_{10}\text{H}_{16}$  to 0.2 eV for  $\text{Si}_{26}\text{H}_{32}$ , approaching the behaviour expected for a large SiNC, namely a constant band gap for the same cluster size (compare table S2).

Energetic alignment of  $\pi^*$  excited states:  $\pi^*$  states appearing as the lowest excited states S1 and S2 at small cluster sizes shift towards and through the lowest lying QD state with increasing size of the model clusters. In the case of the aryl functionalizations shown on the left of Fig. S7, the originally dominating  $\pi^*$  character of these states disappears with larger cluster size as a strong mixing with QD states is observed for the electronic transitions. Consistent for all aryl functionalizations, this mixing can be understood as a degeneracy of the  $\pi^*$  and QD transitions indicating the  $\pi^*$  transitions to absorb into the QD band. In contrast to this, the alkynyl(aryl) functionalizations shown on the right of Fig. S7 do not show such a mixing for the lowest (S1)  $\pi^*$  states. Here the electronic transitions appear consistently as pure (> 75% and also bright)  $\pi^*$  transitions which we attribute to a strong coupling of the  $\pi^*$  alkynyl antibonding LUMO and associated orbitals to the SiNC QD core states.

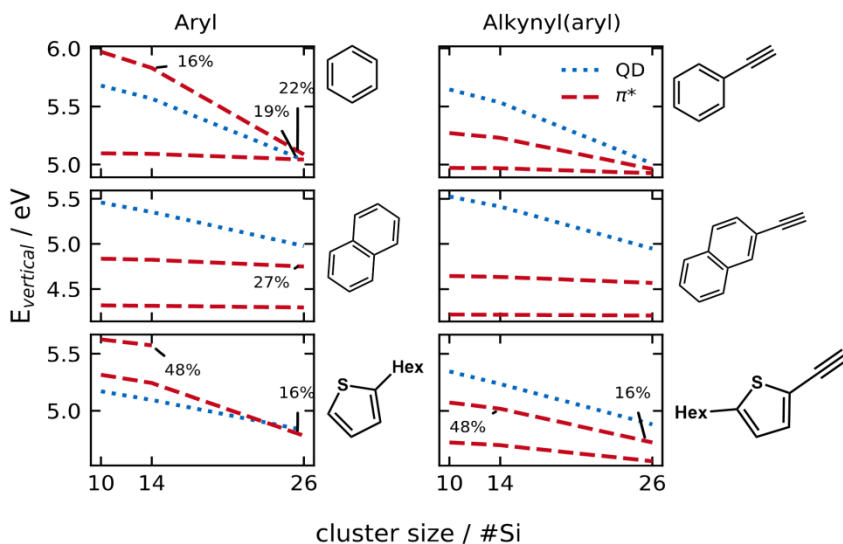


**Figure S7.** Energetic alignment with cluster size of selected excited states including the two lowest lying states including  $\pi^*$  character (red) and the lowest lying QD state (blue) for phenyl (top), naphthalene (center) and 2-hexylthiophene (bottom) derived organic molecules. On the left side the aryl and on the right the alkynyl(aryl) functionalizations are depicted. The contribution of  $\pi^*$  character to the electronic transitions is indicated in percentage if below 50% (compare table S3).

The aryl functionalizations only show one  $\pi^*$  orbital with a weak coupling to the SiNC (see Fig. S8) while other  $\pi^*$  orbitals are solely located on the organic molecule and are only found at a considerable higher energy. Alkynyl(aryl) functionalizations in contrast show three  $\pi^*$  orbitals (including a distinctive  $\pi^*$  alkynyl anti-bonding LUMO) which contribute substantially to the observed  $\pi^*$  transitions as shown in Fig. S8. The combined strong coupling to the SiNC is likely the cause for the persistence of the  $\pi^*$  states remaining energetically below the lowest lying QD state.

Albeit the trends seem persistent, the  $\pi^*$  states of naphthalene and 2-ethynyl naphthalene are not energetically aligned yet with the QD states at the here computed cluster sizes which is owed to the extended conjugated  $\pi$  system appearing at a specifically low energy. For naphthalene, this also results in an accidental degeneracy of a  $\pi$ - $\pi^*$  (27%) and a  $\pi$ -QD (62%) transition in the second excited state S2 leading to a comparably high oscillator strength of 0.2. Going to larger cluster sizes, a similar behaviour observed for phenyl and phenylacetylene is also expected for naphthalene and 2-ethynyl naphthalene.

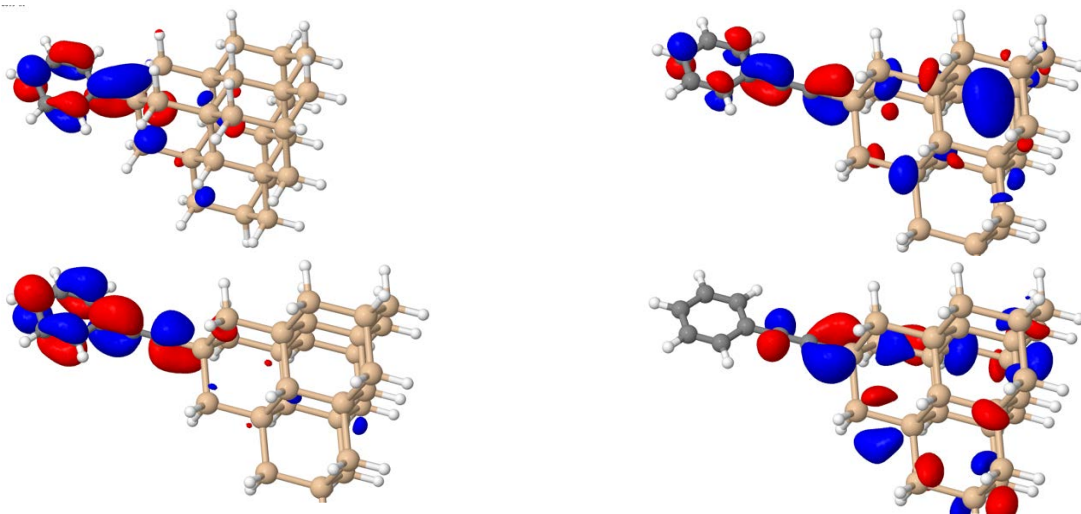


**Figure S8.** Relevant  $\pi^*$  orbitals found in model clusters functionalized with aryl and alkynyl(aryl) for the example of phenyl-Si<sub>26</sub>H<sub>31</sub> and phenylacetylene-Si<sub>26</sub>H<sub>31</sub>. The weakly coupling  $\pi^*$  orbital of phenyl-Si<sub>26</sub>H<sub>31</sub> which is the primarily involved orbital in all  $\pi^*$  transitions is shown in the top left. The strongly and weakly coupling LUMO  $\pi^*$  orbital for phenylacetylene-Si<sub>26</sub>H<sub>31</sub> are shown in the top right and bottom left respectively and the strongly coupling  $\delta^*$  orbital of phenylacetylene-Si<sub>26</sub>H<sub>31</sub> is shown in the bottom right. All three  $\pi^*$  orbital are found with varying contributions in all alkynyl(aryl)  $\pi^*$  transitions.

Based on the given electronic picture an explanation for the experimentally observed long lifetime of the excited states can be proposed. Considering the proposed absorption/emission mechanism (see main text), an initial excitation to the conduction band (here the QD\* states) would result in an immediate electronic relaxation to the SiNC conduction band edge. From here a direct non-radiative relaxation to the  $\pi^*$  in-gap state could be unlikely as the majorly contributing  $\pi^*$  LUMO shows a relative weak coupling to the QD\* states. Instead a mediated transition *via* a more strongly coupling excited state with  $\pi^*$  character located within the conduction band edge is suggested. This transiting state would introduce a barrier for the relaxation process to the in-gap state and thus account for the observed life-times. Additionally, the transition from the QD state to the  $\pi^*$  in-gap state involves a change in electron momentum. In that, the localization of the aromatic groups most probably yields interface states with no momentum at the  $\Gamma$ -point since effects evident for lateral interactions which could account for electronic momentum do not become apparent in the experiment. In contrast to that, quasi-indirect or indirect band gaps in SiNC imply an electronic momentum after excitation.<sup>[3]-[5]</sup> Thus, a conservation of momentum for a transition from QD state to the interface state would also involve phonon scattering. Although, molecular vibrations could facilitate the latter, the additional electronic barrier compensates this effect and thus leads to long lifetimes. These would be comparable to the lifetimes in aryl functionalizations which also

exhibit a barrier in emission due to the necessary momentum conservation in the mentioned quasi-indirect of indirect band gaps.

Based on the described size effects, the appearance of the bright  $\pi^*$  states originating from the alkynyl-bond interface states strongly coupling to the QD states is expected to be consistent for large SiNC. Thus, they likely present the origin of experimentally observed in-gap states.

**Basis set validation:** All excited state calculations are performed with TURBOMOLE's def2-SV(P) basis set to exploit the fast integration procedures<sup>[6]</sup> for the excited state calculations of the rather large clusters. To ensure a correct description of the electronic correlation, the basis set was benchmarked against the correlation-consistent cc-pVDZ Dunning basis set for the Si<sub>10</sub>H<sub>16</sub> clusters. As shown in table S4 and S5, electronic transitions are quantitatively coinciding and only slight differences in oscillator strengths are seen when compared to table S2 and S3.

**Table S4.** Vertical excitation energies in eV and oscillator strength (in parenthesis) of the first five excited states (S1-S5) for all calculated organic molecules on the Si<sub>10</sub>H<sub>16</sub> diamond model cluster calculated with the cc-pVDZ basis set.

	Phenyl				
	S1	S2	S3	S4	S5
Si <sub>10</sub> H <sub>16</sub>	5.038 (0.001)	5.620 (0.000)	5.846 (0.563)	5.950 (0.002)	6.044 (0.036)
	Phenylacetylene				
	S1	S2	S3	S4	S5
Si <sub>10</sub> H <sub>16</sub>	4.907 (0.001)	5.144 (1.022)	5.403 (0.002)	5.577 (0.006)	5.598 (0.008)
	Naphthalene				
	S1	S2	S3	S4	S5
Si <sub>10</sub> H <sub>16</sub>	4.255 (0.002)	4.716 (0.088)	5.385 (0.000)	5.568 (2.185)	5.807 (0.002)
	2-ethynyl-naphthalene				
	S1	S2	S3	S4	S5
Si <sub>10</sub> H <sub>16</sub>	4.153 (0.002)	4.530 (0.527)	5.173 (1.552)	5.266 (0.002)	5.448 (0.004)
	2-hexylthiophene				
	S1	S2	S3	S4	S5
Si <sub>10</sub> H <sub>16</sub>	5.079 (0.001)	5.177 (0.625)	5.526 (0.111)	5.550 (0.006)	5.643 (0.052)
	2-ethynyl-5-hexylthiophene				
	S1	S2	S3	S4	S5
Si <sub>10</sub> H <sub>16</sub>	4.591 (1.075)	4.896 (0.003)	5.251 (0.001)	5.360 (0.093)	5.404 (0.003)

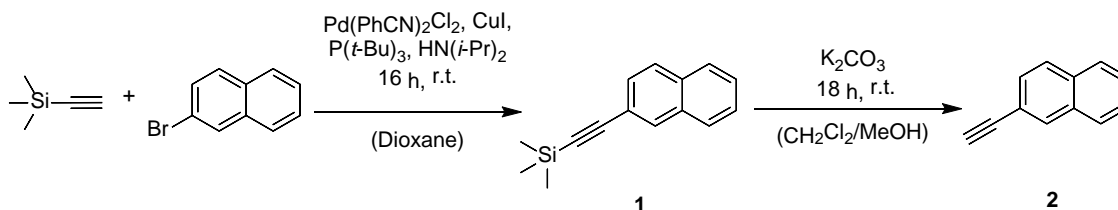


**Table S5.** Character of the electronic transitions with their respective share in percentage (in parenthesis) of the first five excited states (S1-S5) for all calculated organic molecules on the Si<sub>10</sub>H<sub>16</sub> diamond model cluster calculated with the cc-pVDZ basis set.

	Phenyl				
Si <sub>10</sub> H <sub>16</sub>	S1 π-π* (73)	S2 π-QD (80)	S3 π-π* (85)	S4 π-QD (68)	S5 π-QD (70)
	Phenylacetylene				
Si <sub>10</sub> H <sub>16</sub>	S1 π-π* (82)	S2 π-π* (89)	S3 π-π* (76)	S4 π-QD (85)	S5 π-π* (60) π-QD (11)
	Naphthalene				
Si <sub>10</sub> H <sub>16</sub>	S1 π-π* (83)	S2 π-π* (86)	S3 π-QD (79)	S4 π-π* (85)	S5 π-QD (61)
	2-ethynyl-naphthalene				
Si <sub>10</sub> H <sub>16</sub>	S1 π-π* (81)	S2 π-π* (86)	S3 π-π* (83)	S4 π-π* (73)	S5 π-QD (72)
	2-hexylthiophene				
Si <sub>10</sub> H <sub>16</sub>	S1 π-QD (85)	S2 π-π* (72)	S3 π-π* (73)	S4 π-QD (76)	S5 π-π* (70)
	2-ethynyl-5-hexylthiophene				
Si <sub>10</sub> H <sub>16</sub>	S1 π-π* (88)	S2 π-QD (70)	S3 π-QD (83)	S4 π-π* (71)	S5 π-π* (81)

## Synthesis of Conjugated Organic Molecules

### 2-Ethynyl-naphthalene<sup>[7]</sup>



**(1) 2-(trimethylsilyl)ethynyl-naphthalene:** 3.00 g 2-bromonaphthalene (14.5 mmol, 1.00 eq.), 2.46 mL ethynyltrimethylacetylene (1.71 g, 17.4 mmol, 1.20 eq.) and 2.45 mL diisopropylamine (1.76 g, 17.4 mmol, 1.20 eq.) are dissolved in dioxane (10 mL) and the mixture is degassed. 166 mg bis(benzonitrile)palladium(II)chloride (435 μmol, 0.03 eq.), 211 μL tri-*tert*-butylphosphine (176 mg, 869 μmol, 0.06 eq.) and 55.2 mg copper(I)iodide (290 μmol, 0.02 eq.) are added. The reaction mixture is stirred over night at room temperature, filtered over Celite and the solvent is removed *in vacuo*. The residue is dissolved in CH<sub>2</sub>Cl<sub>2</sub> (50 mL) and extracted with saturated NH<sub>4</sub>Cl solution (3 × 30 mL). The aqueous layers are extracted with CH<sub>2</sub>Cl<sub>2</sub> (30 mL) and the combined organic layers are washed with brine (50 mL), dried over Na<sub>2</sub>SO<sub>4</sub>, filtered and the solvent is removed *in vacuo*. The crude product is purified *via* column chromatography eluting with pentane to yield 2.04 g of the desired product (9.09 mmol, 63%) as a brown oil. *R*<sub>f</sub> = 0.38 (Pentane) [UV].

<sup>1</sup>H-NMR (CDCl<sub>3</sub>, 300 K, 360 MHz): δ (ppm) = 8.03 – 7.97 (m, 1H, C-1-H), 7.87 – 7.72 (m, 3H, C-4-H, C-6-H, C-9-H), 7.56 – 7.44 (m, 3H, C-3-H, C-7-H, C-8-H), 0.29 (s, 9H, Si(CH<sub>3</sub>)<sub>3</sub>).

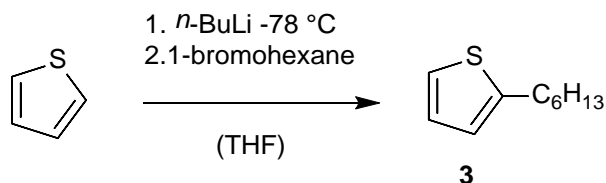
<sup>13</sup>C NMR (CDCl<sub>3</sub>, 300K, 101 MHz): δ (ppm) = 133.1 (s, C-Ar), 133.0 (s, C-Ar), 132.2 (d, C-Ar), 128.7 (d, C-Ar), 128.0 (d, C-Ar), 127.9 (d, C-Ar), 127.9 (d, C-Ar), 126.9 (d, C-Ar), 126.6 (d, C-Ar), 120.5 (s, C-2), 105.6 (s, C-1'), 94.7 (s, C-2'), 0.17 (s, 3C, Si(CH<sub>3</sub>)<sub>3</sub>).

**(2) 2-Ethynynaphthalene:** 2-(trimethylsilyl)ethynynaphthalene (**1**) (2.00 g, 9.00 mmol) is dissolved in CH<sub>2</sub>Cl<sub>2</sub> (30 mL) and MeOH (30 mL). 2.48 g potassium carbonate (18 mmol, 2.00 eq.) is added and the reaction mixture is stirred over night at room temperature. After the addition of water (50 mL), the organic layer is separated and extracted with saturated NH<sub>4</sub>Cl solution (3 × 20 mL). The aqueous layers are extracted with CH<sub>2</sub>Cl<sub>2</sub> (40 mL) and the combined organic layers are washed with brine (20 mL), dried over Na<sub>2</sub>SO<sub>4</sub>, filtered and the solvent is removed *in vacuo*. The crude product is purified *via* column chromatography eluting with pentane to yield 1.23 g (8.08 mmol, 91%) as a slightly yellow solid. *R*<sub>f</sub> = 0.31 (Pentane) [UV].

<sup>1</sup>H-NMR (CDCl<sub>3</sub>, 300 K, 360 MHz): δ (ppm) = 8.06 (s, 1H, C-1-H), 7.89 – 7.76 (m, 3H, C-4-H, C-6-H, C-9-H), 7.60 – 7.47 (m, 3H, C-3-H, C-7-H, C-8-H), 3.18 (s, 1H, C-2'-H).

<sup>13</sup>C NMR (CDCl<sub>3</sub>, 300K, 101 MHz): δ (ppm) = 133.12 (s, C-Ar), 132.91 (s, C-Ar), 132.42 (d, C-Ar), 128.65 (d, C-Ar), 128.14 (d, C-Ar), 127.89 (d, C-Ar), 127.88 (d, C-Ar), 127.02 (d, C-Ar), 126.73 (d, C-Ar), 119.46 (s, C-2), 84.13 (s, C-1'), 77.6 (d, C-2').

## 2-Hexylthiophene

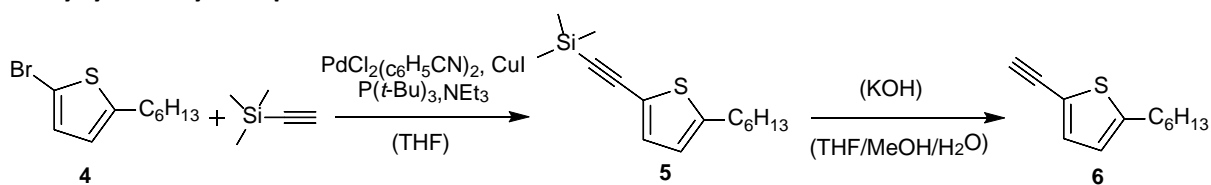


2-hexylthiophene was synthesized via a literature known process.<sup>[8]</sup> 10.0 g (119 mmol, 1.00 eq.) thiophene is dissolved in dry toluene (1.00 M) under argon atmosphere. It was cooled to -78 °C and 47.5 mL *n*-BuLi (2.5 M in hexane, 119 mmol, 1.00 eq.) was added dropwise in 30 minutes. The reaction mixture was stirred for 2 more hours at -78 °C and 15.8 mL (18.6 g, 119 mmol, 1 eq.) 1-bromohexane was added dropwise. The reaction mixture is then slowly brought to room temperature under constant stirring and continued to stir for 16 hours. The reaction was quenched by the addition of water, and the water phase was extracted with diethylether thrice. The organic phases are dried on MgSO<sub>4</sub>, filtered and its volume was reduced under reduced pressure. The purification was achieved through a distillation under reduced pressure (10<sup>-1</sup> mbar; 45 °C) and 15.08 g (89.6 mmol, 75 %) product (**3**) was achieved as a colorless liquid.

<sup>1</sup>H-NMR (300 MHz, Chloroform-*d*): δ[ppm] = 7.13 (dd, 3*J* = 5.2 Hz, 4*J* = 1.2 Hz, 1H), 6.94 (dd, 3*J* = 5.1, 3.4 Hz, 1H), 6.81 (vdq, 3*J* = 3.4 Hz, 4*J* = 1.1 Hz, 1H), 2.76 (t, 3*J* = 7.5 Hz, 2H), 1.63 (vp, *J* = 7.6 Hz, 2H), 1.48 – 1.27 (m, 6H), 0.88 (t, <sup>3</sup>*J* = 6.7 Hz, 3H).

<sup>13</sup>C-NMR (75 MHz, Chloroform-*d*): δ[ppm] = 146.0 (s), 126.7 (s), 124.0 (s), 122.8 (s), 31.9 (s), 31.7 (s), 30.1 (s), 29.0 (s), 22.7 (s), 14.2 (s).

## 2-Ethynyl-5-Hexyl Thiophene<sup>[9]</sup>



**(4) 2-bromo-5-hexylthiophene:** 13.7 g (81.3 mmol, 1 eq.) 2-hexylthiophene (**3**) is dissolved in 1:1 mixture of acetic acid and chloroform (0.08 M) and 14.5 g (81.3 mmol, 1 eq.) N-bromosuccinimide is added. The reaction mixture is stirred for 24 hours at room temperature. Saturated aqueous NaHCO<sub>3</sub> solution was added, the organic phase was washed 2 times with NaHCO<sub>3</sub> and once with brine. It was dried over MgSO<sub>4</sub>, and filtered. 19.5 g (78.7 mmol, 97 %) product (**4**) was obtained in the form of a yellow liquid.

<sup>1</sup>H-NMR (300 MHz, Chloroform-*d*): δ[ppm] = 6.84 (d, <sup>3</sup>J = 3.6 Hz, 1H), 6.53 (dt, <sup>3</sup>J = 3.6 Hz, 4J = 1.0 Hz, 1H), 2.73 (t, <sup>3</sup>J = 7.6 Hz, 1H), 1.62 (vp, <sup>3</sup>J = 7.8 Hz, 2H), 1.41 – 1.21 (m, 6H), 0.88 (t, <sup>3</sup>J = 6.8 Hz, 3H).

<sup>13</sup>C-NMR (75 MHz, Chloroform-*d*): δ[ppm] = 147.8 (s), 129.5 (s), 124.5 (s), 108.7 (s), 31.7 (s), 31.6 (s), 30.5 (s), 28.8 (s), 22.7 (s), 14.2 (s).

**(5) 2-(trimethylsilyl)ethynyl-5-hexylthiophene:** 1.00 g (4.05 mmol, 1 eq.) 2-Bromo,5-hexylthiophene (**4**), 1.12 mL (710 mg, 8.1 mmol, 2 eq.) ethynyltrimethylsilane, 2.24 mL (1.64 g, 16.2 mmol, 4 eq.) triethylamine and 121 μL (1 M in toluene, 121 μmol, 1 mol%) PtBu<sub>3</sub> are dissolved in 14 mL dry THF. The reaction mixture was degassed 3 times with freeze-thaw cycles. 140 mg (121 μmol, 3 mol%) PdCl<sub>2</sub>(PhCN)<sub>2</sub> and 15.4 mg (80.9 μmol, 2 mol%) CuI weighed in a glovebox, and added to the reaction and stirred overnight. The reaction mixture was diluted dichloromethane and saturated NH<sub>4</sub>Cl solution was added. The resulting suspension was centrifuged (9000 rpm, 2 min) and the organic phase (supernatants) were washed 3 times with saturated aqueous NH<sub>4</sub>Cl, dried over MgSO<sub>4</sub>, filtered and its volume was reduced under vacuum. The purification was achieved by column chromatography with pentane. 875 mg product (**5**) (3.31 mmol, 82 %) was obtained as a yellow liquid. R<sub>f</sub> = 0.46 (Pentane)

<sup>1</sup>H-NMR (300 MHz, Chloroform-*d*): δ[ppm] = 7.05 (d, 3J = 3.6 Hz, 1H), 6.61 (dt, 3J = 3.6 Hz, 4J = 0.9 Hz, 1H), 2.76 (t, 3J = 7.5 Hz, 1H), 1.63 (vp, 3J = 7.5 Hz, 2H), 1.41 – 1.22 (m, 6H), 0.88 (t, 3J = 6.7 Hz, 3H), 0.23 (s, 9H).

<sup>13</sup>C NMR (75 MHz, Chloroform-*d*) δ: [ppm] = 148.6 (s), 132.9 (s), 124.1 (s), 120.5 (s), 98.3 (s), 97.8 (s), 31.7 (s), 31.7 (s), 30.3 (s), 28.8 (s), 22.7 (s), 14.2 (s), 0.1(s, 3C).

**(6) 2-ethynyl-5-hexylthiophene:** 0.77 g (2.9 mmol, 1 eq.) 2-(trimethylsilyl)ethynyl-5-hexylthiophene (**5**) was dissolved in THF/MeOH/H<sub>2</sub>O (7/7/1) and 814 mg (14.5 mmol, 5 eq.) KOH was added. The reaction mixture was stirred for 2 hours at room temperature. The reaction mixture was diluted in dichloromethane and washed thrice with distilled water. The organic phase was dried over MgSO<sub>4</sub>, filtered and its volume was reduced. The purification was achieved by a column chromatography with pentane.

<sup>1</sup>H NMR (300 MHz, Chloroform-*d*): δ[ppm] = 7.09 (d, 3J = 3.6 Hz, 1H), 6.63 (dt, 3J = 3.6 Hz, 4J = 1.0 Hz, 1H), 3.29 (s, 1H), 2.77 (t, 3J = 7.6 Hz, 2H), 1.65 (vp, 3J = 7.6 Hz, 2H), 1.43 – 1.21 (m, 6H), 0.89 (t, 3J = 6.7 Hz, 3H).

<sup>13</sup>C NMR (75 MHz, Chloroform-d): δ[ppm] = 148.8 (s), 133.3 (s), 124.1 (s), 119.3 (s), 80.5 (s), 77.4 (s), 31.7 (s; 2C), 30.3 (s), 28.8 (s), 22.7 (s), 14.2 (s).

R<sub>f</sub> = 0.53 (Pentane)

## References

- [1] Y. Yu, G. Fan, A. Fermi, R. Mazzaro, V. Morandi, P. Ceroni, D.-M. Smilgies and B. A. Korgel, *J. Phys. Chem. C*, 2017, **121**(41), 23240.
- [2] C. M. Hessel, D. Reid, M. G. Panthani, M. R. Rasch, B. W. Goodfellow, J. Wei, H. Fujii, V. Akhavan and B. A. Korgel, *Chem. Mater.*, 2012, **24**(2), 393.
- [3] B. G. Lee, J.-W. Luo, N. R. Neale, M. C. Beard, D. Hiller, M. Zacharias, P. Stradins and A. Zunger, *Nano Letters*, 2016, **16**(3), 1583.
- [4] H. Li, Z. Wu, T. Zhou, A. Sellinger and M. T. Lusk, *Phys. Chem. Chem. Phys.*, 2014, **16**(36), 19275.
- [5] J. A. Kelly and J. G. C. Veinot, *ACS Nano*, 2010, **4**(8), 4645.
- [6] A. Schäfer, H. Horn and R. Ahlrichs, *J. Chem. Phys.*, 1992, **97**(4), 2571.
- [7] T. Hundertmark, A. F. Littke, S. L. Buchwald and G. C. Fu, *Org. Lett.*, 2000, **2**(12), 1729.
- [8] B. Wex, F. M. Jradi, D. Patra and B. R. Kaafarani, *Tetrahedron*, 2010, **66**(45), 8778.
- [9] S. Rondeau-Gagné, C. Curutchet, F. Grenier, G. D. Scholes and J.-F. Morin, *Tetrahedron*, 2010, **66**(23), 4230.

## 4.4 The Influence of Surface Functionalization Methods on the Performance of Silicon Nanocrystal LEDs

In the last decade, several groups demonstrated that SiNCs could be used as the active emissive material in hybrid organic/inorganic LEDs.<sup>10,199</sup> Despite significant research efforts focusing on the optimization of device efficiencies, expectations could still not be met.<sup>200</sup> One of the reasons behind this result is the low conductivity of SiNC thin films and limited charge transfer to and from SiNCs. To date, there are almost no reports in literature which aim to address these issues by controlling the surface chemistry of SiNCs. Almost all of these publications utilized decyl/dodecyl functionalized SiNCs prepared *via* thermally initiated hydrosilylation.<sup>29,30,199</sup> Only Ozin *et al.* stated that these groups may hinder the charge transport by creating an insulating layer and replaced them with allyl benzene groups.<sup>18</sup> They reported that the devices exhibited enhanced properties due to increased packing of SiNCs due to  $\pi$ - $\pi$  stacking and greater electronic coupling between SiNCs in the active layer. However, it is important to note that in the case of allylbenzene functionalization the aromatic ring is not in conjugation with the SiNC core, due to saturated C – C bridge in between.

In our work, we aimed to study the influence of different surface functionalization methods on the efficiency of LEDs. For this purpose, we functionalized SiNCs with hexyl surface groups *via* hydrosilylation (HS) and by using organolithium reagents (OLR). LEDs were built by utilizing these SiNCs. Our analysis showed that devices utilizing SiNCs functionalized with OLR exhibited lower turn-on voltages, higher luminance and external quantum efficiencies compared to those obtained from the HS method. These improvements were attributed to the less dense and monolayer surface coverage of the SiNCs obtained by the OLR method, as well as their higher absolute quantum yield based on detailed characterization of these SiNCs.

**Manuscript:**

**The Influence of Surface Functionalization Methods on the  
Performance of Silicon Nanocrystal LEDs**

<b>Status</b>	Published online on April 16, 2018
<b>Journal</b>	<i>Nanoscale</i> , 2018, Volume 10, 10337-10342.
<b>Publisher</b>	Royal Society of Chemistry
<b>DOI</b>	10.1039/C7NR09525B
<b>Authors</b>	Arzu Angı, <sup>†</sup> Marius Loch, <sup>†</sup> Regina Sinelnikov, Jonathan G. C. Veinot, Markus Becherer, Paolo Lugli, Bernhard Rieger

<sup>†</sup> These authors contributed equally to this work.

Angı *et al.* *Nanoscale*, **2018**, Advance Article – Reproduced by permission of The Royal Society of Chemistry.



Cite this: *Nanoscale*, 2018, **10**, 10337

Received 21st December 2017,  
Accepted 14th April 2018

DOI: 10.1039/c7nr09525b

rsc.li/nanoscale

## The influence of surface functionalization methods on the performance of silicon nanocrystal LEDs†

Arzu Angi,<sup>‡a</sup> Marius Loch,<sup>‡b</sup> Regina Sinelnikov,<sup>ib</sup> Jonathan G. C. Veinot,<sup>ib</sup> Markus Becherer,<sup>ib</sup> Paolo Lugli<sup>ib</sup> and Bernhard Rieger<sup>ib</sup>\*<sup>a</sup>

The influence of silicon nanocrystal (SiNC) surface characteristics obtained from different functionalization methods on the performance of LEDs was investigated. The surface of SiNCs was functionalized with hexyl chains via hydrosilylation (HS) or with organolithium reagents (OLR) and resulting SiNCs were incorporated as the emissive layer in hybrid organic/inorganic LEDs. Devices utilizing SiNCs functionalized with OLR consistently exhibited lower turn-on voltages, higher luminances and external quantum efficiencies compared to those obtained from the HS method. These improvements were attributed to the less dense and monolayer surface coverage of the SiNCs obtained by the OLR method, as well as their higher absolute quantum yield.

Silicon nanocrystals (SiNCs) have emerged as a promising class of quantum dots due to their unique optoelectronic properties.<sup>1,2</sup> When the dimensions of SiNCs are reduced below the Bohr radius of an exciton in Si (~4.5 nm),<sup>3</sup> they start to exhibit photoluminescence (PL)<sup>4,5</sup> at wavelengths that are tunable by controlling their size<sup>6–10</sup> and surface chemistry.<sup>11–13</sup> In addition to PL, beneficial properties of SiNCs such as elemental abundance, bio-compatibility<sup>14</sup> and solution processability triggered the design of several prototype applications including sensors,<sup>15–17</sup> solar cells,<sup>18–21</sup> bio-markers<sup>14,22</sup> and light emitting diodes (LEDs).<sup>23–32</sup> Due to their relatively low toxicity,<sup>1</sup> SiNCs are particularly appealing in comparison to II–VI and IV–VI quantum dots (e.g. CdSe, PbS) commonly employed in optoelectronic devices.<sup>33,34</sup>

The surface of SiNCs is commonly functionalized with organic molecules to facilitate their use in the aforementioned applications by preventing surface oxidation, achieving colloidal stability and tuning their optoelectronic properties.<sup>5,12</sup> Radical hydrosilylation (HS) is one of the most frequently employed methods for the surface functionalization of hydride-terminated SiNCs. In this method, organic molecules are grafted to the surface through Si–C bonds formed via the reaction of surface silyl radicals with terminal alkenes or alkynes (Fig. 1a).<sup>35</sup> These silyl radicals can be created at elevated temperatures ( $T \geq 150$  °C)<sup>36</sup> or using radical initiators such as azobisisobutyronitrile (AIBN).<sup>37</sup> Despite being able to yield a high surface coverage, HS has some disadvantages including oligomerization of the ligands on the surface of SiNCs at elevated temperatures.<sup>36</sup> These surface characteristics may decrease the efficiency of SiNCs in optoelectronic devices by forming an insulating barrier and hindering charge transport.<sup>28</sup>

We recently exploited an alternative method to functionalize hydride-terminated SiNCs at room temperature by using organolithium reagents (OLR).<sup>38</sup> This reaction proceeds via a mechanism in which surface Si–Si bonds cleave due to an attack of the organolithium reagent (R–Li, R = alkyl), yielding Si–R bonds and neighboring Si–Li surface species. Following acid workup, Si–Li groups are quenched to yield surface Si–H species (Fig. 1b).<sup>39</sup> Owing to its mechanism, the OLR method

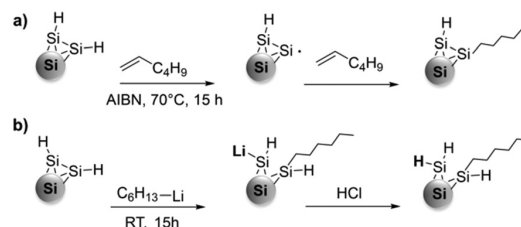


Fig. 1 Simplified representation of the mechanisms of the surface functionalization methods utilized in this work: (a) hydrosilylation with 1-hexene, initiated by AIBN. (b) Organolithium reagents with *n*-hexyllithium.

<sup>a</sup>WACKER-Lehrstuhl für Makromolekulare Chemie, Technische Universität München, Lichtenbergstraße 4, 85747, Catalysis Research Center, Ernst-Otto-Fischer-Straße 1, 85748 Garching, Germany. E-mail: rieger@tum.de

<sup>b</sup>Institute for Nanoelectronics, Technische Universität München, Theresienstrasse 90, 80333 Munich, Germany. E-mail: marius.loch@tum.de

<sup>c</sup>Department of Chemistry, University of Alberta, 11227 Saskatchewan Drive, Edmonton, Alberta, T6G 2G2, Canada

<sup>d</sup>Faculty of Science and Technology, Free University of Bozen-Bolzano, Universitätsplatz 5, 39100 Bolzano, Italy

† Electronic supplementary information (ESI) available: Experimental details, TEM UV-VIS spectroscopy and DLS data. See DOI: 10.1039/c7nr09525b

‡ These authors contributed equally to this work.

offers the advantage of functionalizing SiNCs under mild conditions while assuring defined monolayer coverage.

Several reports have demonstrated hybrid organic/inorganic LEDs utilizing SiNCs as the active emitting material (SiNC-LEDs). Efficiencies of SiNC-LEDs were improved by optimizing device architecture and their color could be tuned utilizing SiNCs with different sizes.<sup>24,26,29</sup> In addition, effects of SiNC size distribution<sup>30</sup> and layer thickness<sup>23</sup> on device performance were also studied. However, despite the well-known influence of SiNC surface chemistry on material properties,<sup>11,12,40</sup> reports studying the impact of the SiNC surface on SiNC-LED performance are rare. Most reports to date employed SiNCs functionalized with long alkyl chains *via* thermally induced HS.<sup>23–31</sup> So far, only Ozin *et al.* demonstrated that changing decyl surface groups to allyl benzene improved the efficiency of the devices due to enhanced charge transport and packing density.<sup>28</sup>

In this work, the influence of surface functionalization methods on the performance of SiNC-LEDs was investigated for the first time. For this purpose, SiNCs were functionalized with hexyl groups *via* HS (HS-SiNCs) and OLR (OLR-SiNCs) approaches. Detailed characterization of resulting SiNCs revealed that OLR method yielded a lower degree of surface coverage and higher quantum yield (QY) of the SiNCs. The LEDs built with OLR-SiNCs showed higher brightness and efficiency compared to those utilizing HS-SiNCs. Besides, when OLR method was employed, SiNC-LEDs showed a lower turn-on voltage indicating a lower resistance of the active layer. We suggest that these outcomes stem from the differing surface characteristics resulting from the surface functionalization methods, even when the same surface group is employed. Both the lower surface coverage, which improves the transport of charge carriers, and increased QY obtained by the OLR method increases the overall device efficiency.

## Results and discussion

### Surface functionalization of SiNCs and their properties

SiNCs were synthesized *via* thermolysis of hydrogen silsesquioxane (HSQ), which yields SiNCs embedded in a SiO<sub>2</sub> matrix. Free-standing, hydride-terminated SiNCs ( $d \sim 3.1$  nm, size distributions are given in ESI†) were obtained by etching this SiNC/SiO<sub>2</sub> composite with an ethanol : water : HF (1 : 1 : 1) mixture and final extraction into toluene.<sup>41</sup>

To study the impact of surface functionalization methods on the LED efficiency, surface functionalization of SiNCs was performed with hexyl chains *via* HS and OLR. For this purpose, freshly etched SiNCs from (600 mg Si/SiO<sub>2</sub> composite) were dispersed in 4 ml dry toluene. In the OLR method, 2 ml of this SiNC dispersion was reacted with *n*-hexyllithium (0.2 mmol, 2.3 M) for 15 hours at room temperature. HS was performed by reacting the remaining SiNCs with 1-hexene (0.4 ml) in the presence of AIBN (10 mg) at 70 °C for 15 hours.

Fourier transform infrared (FTIR) spectroscopy was utilized to interrogate the presence of surface groups associated with target ligands after the functionalization. In both cases, the

presence of hexyl chains was indicated by strong C–H and C–C stretching bands at *ca.* 2980–2835 and 1450 cm<sup>-1</sup>, respectively (Fig. 2). For both samples minor surface oxidation was observed as evidenced by the Si–O band at 1050 cm<sup>-1</sup>. Hydride terminated SiNCs show only Si–H bands, at 2100, 906, and 660 cm<sup>-1</sup>.<sup>38</sup> The most significant difference between the FTIR spectra of the SiNCs is the greater intensity of the Si–H band at 2100 cm<sup>-1</sup> relative to the C–H signal in the case of the OLR method. This observation is consistent with the accepted reaction mechanism (*vide supra*), as hydride groups are not consumed, but indeed formed upon quenching of Si–Li groups during workup. In the case of HS, the intensity of Si–H band is much lower, as hydride groups are consumed during the course of the reaction. Secondly, a higher surface coverage with HS method may also result in a lower Si–H signal relative to alkyl chains. Oligomerization of 1-hexene was excluded by Yang *et al.*,<sup>37</sup> who showed that oligomerization of unsaturated molecules was minimized in HS reactions initiated by AIBN.

To estimate the degree of surface coverage, thermogravimetric analysis (TGA) measurements were performed on SiNCs functionalized with both methods after 15-hour reaction time (Fig. 3). TGA data revealed 26.7% and 39.3% weight loss for OLR and HS reactions, respectively. These results are con-

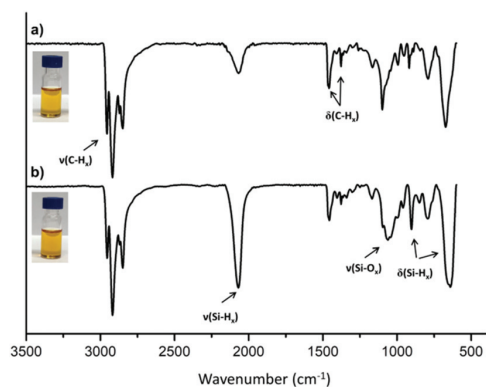


Fig. 2 FTIR spectra of SiNCs functionalized (a) with 1-hexene *via* HS, (b) with *n*-hexyllithium *via* OLR method. Images of SiNC solutions in toluene after functionalizing with respective methods are given in the inset. Both methods yield stable colloidal dispersions of SiNCs in toluene.

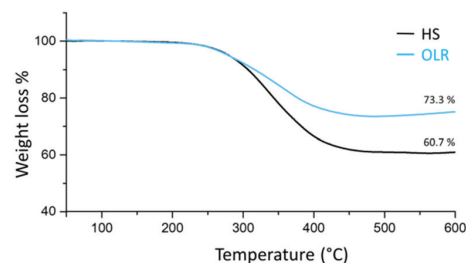


Fig. 3 TGA analysis of SiNCs functionalized with hexyl surface groups *via* OLR and HS methods after 15 hours reaction time.



sistent with the FTIR data, indicating a higher surface coverage is obtained with HS in comparison to the OLR method.

Transmission Electron Microscopy (TEM) images of SiNCs functionalized with both methods yielded a similar size distribution centred at  $3.1 \pm 0.2$  nm and  $3.1 \pm 0.2$  nm, for HS and OLR methods, respectively (ESI Fig. S1 and S2†). It is important to note that it is experimentally challenging to accurately measure the size of small SiNCs in TEM due to low atomic weight of silicon yielding a lower contrast.<sup>42</sup> In addition, dynamic light scattering (DLS) in toluene revealed mean hydrodynamic radii of SiNCs as  $2.5 \pm 0.3$  nm for HS and  $2.4 \pm 0.2$  nm for OLR (ESI Table S1†). Both DLS and TEM measurements confirmed that the size of the SiNCs was not altered by the surface functionalization method, *i.e.*, differences in observed properties must stem from the surface functionalization methods.

PL peak-wavelength of SiNCs was found at 684 nm, irrespective of the functionalization method (Fig. 5a). Slight broadening of the PL curve at the low energy side of the spectra was observed with HS-SiNCs as shown by full width at half maximum (FWHM) analysis (ESI Fig. S4†). Even though it is frequently correlated to size distribution of the samples,<sup>42</sup> surface characteristics can also alter the emission profile of SiNCs.<sup>43</sup> Absolute quantum yield of SiNCs, which describes the number of photons emitted per photons absorbed,<sup>44</sup> can be influenced by surface functionalization methods.<sup>12,45</sup> In our work, QY of OLR-SiNCs was found as  $22 \pm 1.0\%$ , whereas it was  $17 \pm 0.3\%$  in the case of HS-SiNCs. Increased QY of OLR-SiNCs can be attributed to the removal of surface defects and dark states<sup>45,46</sup> *via* surface restructuring during the course of the reaction.<sup>42</sup> As similar size and size distributions were found for SiNCs functionalized with both methods *via* DLS and TEM techniques, the differences in the optical properties of the SiNCs were attributed to altered surface characteristics.

### SiNC-LED device architecture

SiNC-LEDs with a device design as depicted in Fig. 4a were fabricated. The design consists of a compact SiNC layer with a thickness of 35 nm (spin coated from  $10 \text{ mg ml}^{-1}$  solutions in toluene) as the emitter material. This layer is sandwiched

between two metal electrodes, one with high work function (WF) for hole injection (indium tin oxide (ITO),  $\sim 120$  nm) and one with low WF for electron injection (Ca,  $\sim 20$  nm and Al  $\sim 100$  nm). The ITO layer is transparent and allows detection of the light produced by the device. Additional blocking layers were inserted between the electrodes and the SiNC layer to confine charges in the SiNCs and thus facilitate radiative recombination and avoid charge leakage. Poly[*N,N'*-bis(4-butylphenyl)-*N,N'*-bisphenylbenzidine] (PolyTPD,  $\sim 10$  nm) serves as hole-transport/electron-blocking layer (HTL/EBL) and ZnO ( $\sim 25$  nm) as electron-transport/hole-blocking layer (ETL/HBL). Proper alignment of energy levels of all layers is required to achieve efficient charge transport. An energy diagram of the stack is shown in Fig. 4b, where the energy levels of transport layers were taken from literature.<sup>24,28,31</sup>

Valence band (VB) and conduction band (CB) of SiNCs were estimated with the following formula<sup>47</sup> which describes the broadening of the band gap as a function of the particle diameter ( $\Delta E_g(d)$ ) in crystalline semiconductors, due to the quantum confinement effect:

$$\Delta E_g(d) = \frac{3.74}{(d/\text{nm})^{1.39}} \text{ eV}$$

with  $d = 3.1$  nm, this results in a band gap widening of  $\Delta E_g = 0.77$  eV. Energy levels of SiNCs were found by distributing this widening to the band edges of bulk silicon in a ratio of  $\Delta_{\text{VB}}/\Delta_{\text{CB}} = 2/1$ , as described by Buuren *et al.*<sup>48</sup> This calculation yielded VB and CB of SiNCs as  $E_{\text{VB}} = 3.79$  eV and  $E_{\text{CB}} = 5.68$  eV.

During operation under forward bias, electrons are injected from the low WF Ca/Al electrode and holes from the high WF ITO side. Both blocking layers have favorable energy levels for blocking charges leaving the SiNC layer, while posing only very small barriers for injection into SiNC. A layer of Poly(3,4-ethylenedioxythiophene)-poly(styrenesulfonate) (PEDOT:PSS,  $\sim 20$  nm) eases the energetic transition from ITO into PolyTPD. A scanning electron microscope (SEM) image of the stack shows that all layers are spatially well-defined and in good agreement with the nominal layer structure (Fig. 4c). Although PolyTPD and SiNCs were both spin coated from the same solvent, the SiNC layer can be clearly distinguished from the

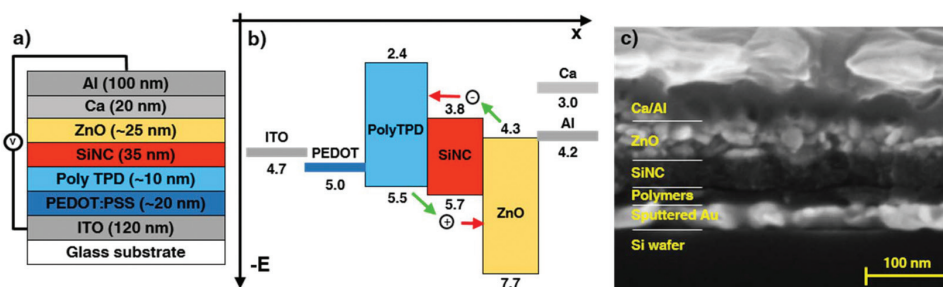


Fig. 4 Device architecture. (a) Schematic representation of the layer stack, (b) proposed energy level diagram of the layers utilized in the stack (eV), (c) cross sectional SEM image of the stack. The glass substrate was replaced by an Au coated Si wafer to have a more conductive substrate during SEM imaging.

underlying polymer layers with no visible intermixing. This is also confirmed by the complete lack of polyTPD emission from the devices (*vide infra*).

### Spectral properties of SiNC-LEDs

The electroluminescence (EL) spectra of LEDs utilizing SiNCs functionalized *via* both methods are shown in Fig. 5a. The EL curves are almost identical to the PL curves and their peak-maxima are found at 694 nm. There are no traces of blue emission from the PolyTPD layer in the EL spectra, implying that the emission originates only from the SiNCs. This indicates that the SiNC film is fully closed without pinholes and charge recombination is well confined within the SiNC layer. The emitted red light can be easily seen with the naked eye under ambient lighting conditions (Fig. 5b and c).

### Current–luminance–voltage (*J–L–V*) characteristics of SiNC-LEDs

To assess the device performances, luminance and current density of the SiNC-LEDs were measured while sweeping the applied voltage (Fig. 6a and b). Since EL spectra were virtually identical for both devices, a direct comparison based on lumi-

nance measurements was possible. Additionally, the external quantum efficiency (EQE) was calculated from the luminance data assuming Lambertian emission and using a weighted average of the emission spectrum (Fig. 6c).

In the *J–L–V* characteristics, the OLR-SiNC device showed a typical diode shape with exponential rise of current and luminance after reaching the turn-on threshold at a very low voltage of 2.5 V. The HS-SiNC device showed a higher turn-on voltage of 3.5 V and a much lower and more linear current draw. As both layers have the same thickness, this reveals a higher resistance of the HS-SiNC film.

The OLR-SiNC-LED reached a maximum luminance of 16.5  $\text{Cd m}^{-2}$  while the HS-SiNC device only went up to 4.8  $\text{Cd m}^{-2}$ . This lower luminance cannot be compensated by the lower current draw as EQE of HS-SiNC device was also lower. The EQE represents the photons emitted per electrons injected. The EQE of the OLR-SiNC-LED was higher than the HS-SiNC device's over the entire operating range, with a three times higher peak value of  $1.8 \times 10^{-2}\%$  vs.  $6.0 \times 10^{-3}\%$  (Fig. 6c). At the current density of 80  $\text{mA cm}^{-2}$ , where the HS-SiNC-LED showed the highest efficiency, luminance (7.8 vs. 4.3  $\text{Cd m}^{-2}$ ) and EQE ( $1.3 \times 10^{-2}$  vs.  $6.0 \times 10^{-3}\%$ ) of the OLR device were still twice as high.

The lower electrical resistivity and the higher EQE of the OLR-SiNC-LEDs are consistent with the surface characteristics obtained *via* the OLR method. OLR functionalization yields a lower degree of surface coverage than HS, which decreases the amount of insulating organic material on the surface of SiNCs. This may increase the electronic coupling between SiNCs, which leads to improved charge transport and lower film resistivity. Besides, it may facilitate charge injection into the SiNCs, so that more electrons can recombine radiatively. Together with the higher QY of the OLR-SiNC, these characteristics enhance the EQE of the devices.

It is important to note that preparing conductive films of SiNCs is one of the biggest challenges for the development of high efficiency SiNC-LEDs. Lower inherent conductivity of SiNCs and insulating organic surface groups are two major reasons for this drawback. However, the surface of SiNCs has to be functionalized to prevent oxidation, achieve colloidal stability and homogenous films. Therefore, employing surface functionalization methods which yield less dense surface cov-

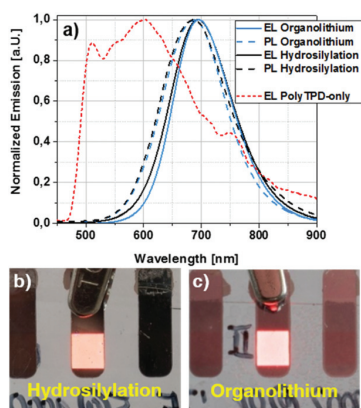


Fig. 5 (a) PL of SiNCs in toluene and EL of SiNC-LEDs built with SiNCs functionalized *via* HS and OLR methods. A representative SiNC-LED built with SiNCs prepared with (b) HS (c) OLR.

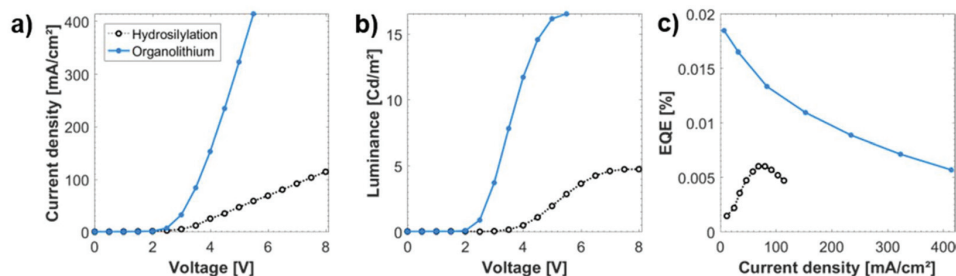


Fig. 6 Current–luminance–voltage characterization of SiNC-LEDs (a) current density vs. voltage, (b) luminance vs. voltage data and (c) EQE calculated from current and luminance data assuming Lambertian emission.

erage with monolayers appears to be a suitable strategy to increase the efficiency of SiNC-LEDs.

## Conclusions

In this work, the influence of surface characteristics of SiNCs on the performance of SiNC-LEDs was investigated. SiNCs were functionalized with hexyl groups by hydrosilylation (HS) and with organolithium reagents (OLR). Both methods yielded SiNCs with identical size and PL maxima, but the OLR method resulted in a less dense surface coverage and higher absolute quantum yield of SiNCs. The LEDs built with OLR-SiNCs showed lower turn-on voltages and more than 3 times higher absolute brightness compared to HS-SiNC-LEDs. OLR-SiNC-LEDs had also a higher EQE over the entire operating range, with a three times higher peak value of  $1.8 \times 10^{-2}\%$  vs.  $6.0 \times 10^{-3}\%$ .

The observed improvements in the performance of SiNC-LEDs with the OLR method can be attributed to a combined effect of reduced surface coverage and increased absolute quantum yield of SiNCs. These outcomes show that properties of SiNCs can be altered by surface functionalization techniques even with identical surface groups. The presented results underline the importance of surface characteristics on the performance of SiNC optoelectronic devices.

## Conflicts of interest

There are no conflicts to declare.

## Acknowledgements

B. Rieger, J. G. C. Veinot, M. Becherer and P. Lugli acknowledge the funding from DFG IRTG (2022) and NSERC CREATE programs for Alberta/TU München International Graduate School. A. Angi is thankful for the funding from Studienstiftung des Deutschen Volkes. R. Sinelnikov acknowledges the funding from AITF. Ignaz Höhle and Tobias Helbich are thanked for valuable discussions. Robin Nagel is thanked for assistance with SEM images. Philipp Altmann was thanked for his help with quantum yield measurements.

## References

- X. Cheng, S. B. Lowe, P. J. Reece and J. J. Gooding, *Chem. Soc. Rev.*, 2014, **43**, 2680–2700.
- M. Dasog, J. Kehrle, B. Rieger and J. G. C. Veinot, *Angew. Chem., Int. Ed.*, 2016, **55**, 2322–2339.
- E. G. Barbagiovanni, D. J. Lockwood, P. J. Simpson and L. V. Goncharova, *J. Appl. Phys.*, 2012, **111**, 34307.
- L. T. Canham, *Appl. Phys. Lett.*, 1990, **57**, 1046–1048.
- V. Singh, Y. Yu, Q.-C. Sun, B. Korgel and P. Nagpal, *Nanoscale*, 2014, **6**, 14643–14647.
- W. Sun, C. Qian, X. S. Cui, L. Wang, M. Wei, G. Casillas, A. S. Helmy and G. A. Ozin, *Nanoscale*, 2016, **8**, 3678–3684.
- C. M. Hessel, D. Reid, M. G. Panthani, M. R. Rasch, B. W. Goodfellow, J. Wei, H. Fujii, V. Akhavan and B. A. Korgel, *Chem. Mater.*, 2012, **24**, 393–401.
- O. Wolf, M. Dasog, Z. Yang, I. Balberg, J. G. C. Veinot and O. Millo, *Nano Lett.*, 2013, **13**, 2516–2521.
- G. Ledoux, O. Guillois, D. Porterat, C. Reynaud, F. Huisken, B. Kohn and V. Paillard, *Phys. Rev. B: Condens. Matter Mater. Phys.*, 2000, **62**, 15942–15951.
- T. Y. Kim, C. Huh, N. M. Park, C. J. Choi and M. Suemitsu, *Nanoscale Res. Lett.*, 2012, **7**, 634.
- A. Angi, R. Sinelnikov, A. Meldrum, J. G. C. Veinot, I. Balberg, D. Azulay, O. Millo and B. Rieger, *Nanoscale*, 2016, **8**, 7849–7853.
- M. Dasog, G. B. De los Reyes, L. V. Titova, F. A. Hegmann and J. G. C. Veinot, *ACS Nano*, 2014, **8**, 9636–9648.
- Z. Zhou, R. T. Anderson, H. Li, J. Bell, Y. Yang, B. P. Gorman, S. Pylypenko, M. T. Lusk and A. Sellinger, *Nano Lett.*, 2015, **15**, 3657–3663.
- A. Fucikova, J. Valenta, I. Pelant, M. H. Kalbacova, A. Broz, B. Rezek, A. Kromka and Z. Bakaeva, *RSC Adv.*, 2014, **4**, 10334–10342.
- J. Zhang and S.-H. Yu, *Nanoscale*, 2014, **6**, 4096.
- C. M. Gonzalez, M. Iqbal, M. Dasog, D. G. Piercey, R. Lockwood, T. M. Klapötke and J. G. C. Veinot, *Nanoscale*, 2014, **6**, 2608–2612.
- Z. H. Zhang, R. Lockwood, J. G. C. Veinot and A. Meldrum, *Sens. Actuators, B*, 2013, **181**, 523–528.
- C.-Y. Liu, Z. C. Holman and U. R. Kortshagen, *Nano Lett.*, 2009, **9**, 449–452.
- C. Y. Liu and U. R. Kortshagen, *Nanoscale Res. Lett.*, 2010, **5**, 1253–1256.
- C.-Y. Liu and U. R. Kortshagen, *Nanoscale*, 2012, **4**, 3963.
- V. Svrcek, T. Yamanari, D. Mariotti, S. Mitra, T. Velusamy and K. Matsubara, *Nanoscale*, 2015, **7**, 11566–11574.
- A. Shiohara, S. Prabakar, A. Faramus, C.-Y. Hsu, P.-S. Lai, P. T. Northcote and R. D. Tilley, *Nanoscale*, 2011, **3**, 3364.
- K. Y. Cheng, R. Anthony, U. R. Kortshagen and R. J. Holmes, *Nano Lett.*, 2010, **10**, 1154–1157.
- K.-Y. Cheng, R. Anthony, U. R. Kortshagen and R. J. Holmes, *Nano Lett.*, 2011, **11**, 1952–1956.
- C.-C. C. Tu, L. Tang, J. Huang, A. Voutsas and L. Y. Lin, *Appl. Phys. Lett.*, 2011, **98**, 213102.
- D. P. Puzzo, E. J. Henderson, M. G. Helander, Z. Wang, G. A. Ozin and Z. Lu, *Nano Lett.*, 2011, **11**, 1585–1590.
- R. J. Anthony, K.-Y. Cheng, Z. C. Holman, R. J. Holmes and U. R. Kortshagen, *Nano Lett.*, 2012, **12**, 2822–2825.
- M. L. Mastronardi, E. J. Henderson, D. P. Puzzo, Y. Chang, Z. Bin Wang, M. G. Helander, J. Jeong, N. P. Kherani, Z. Lu and G. A. Ozin, *Small*, 2012, **8**, 3647–3654.
- F. Maier-Flaig, J. Rinck, M. Stephan, T. Bocksrocker, M. Bruns, C. Kübel, A. K. Powell, G. A. Ozin and U. Lemmer, *Nano Lett.*, 2013, **13**, 475–480.

- 30 F. Maier-Flaig, C. Kübel, J. Rinck, T. Bocksrocker, T. Scherer, R. Prang, A. K. Powell, G. A. Ozin and U. Lemmer, *Nano Lett.*, 2013, **13**, 3539–3545.
- 31 B. Ghosh, Y. Masuda, Y. Wakayama, Y. Imanaka, J. I. Inoue, K. Hashi, K. Deguchi, H. Yamada, Y. Sakka, S. Ohki, T. Shimizu and N. Shirahata, *Adv. Funct. Mater.*, 2014, **24**, 7151–7160.
- 32 Y. Xin, K. Nishio and K. Saitow, *Appl. Phys. Lett.*, 2015, **106**, 201102.
- 33 Y. Shirasaki, G. J. Supran, M. G. Bawendi and V. Bulović, *Nat. Photonics*, 2013, **7**, 13–23.
- 34 B. S. Mashford, M. Stevenson, Z. Popovic, C. Hamilton, Z. Zhou, C. Breen, J. Steckel, V. Bulovic, M. Bawendi, S. Coe-Sullivan and P. T. Kazlas, *Nat. Photonics*, 2013, **7**, 407–412.
- 35 J. M. Buriak, *Chem. Rev.*, 2002, **102**, 1271–1308.
- 36 Z. Yang, M. Iqbal, A. R. Dobbie and J. G. C. Veinot, *J. Am. Chem. Soc.*, 2013, **135**, 17595–17601.
- 37 Z. Yang, C. M. Gonzalez, T. K. Purkait, M. Iqbal, A. Meldrum and J. G. C. Veinot, *Langmuir*, 2015, **31**, 10540–10548.
- 38 I. M. D. Höhle, A. Angi, R. Sinelnikov, J. G. C. Veinot and B. Rieger, *Chem. – Eur. J.*, 2015, **21**, 2755–2758.
- 39 J. H. Song and M. J. Sailor, *J. Am. Chem. Soc.*, 1998, **120**, 2376–2381.
- 40 A. Shiohara, S. Hanada, S. Prabakar, K. Fujioka, T. H. Lim, K. Yamamoto, P. T. Northcote and R. D. Tilley, *J. Am. Chem. Soc.*, 2010, **132**, 248–253.
- 41 C. M. Hessel, E. J. Henderson and J. G. C. Veinot, *Chem. Mater.*, 2006, **18**, 6139–6146.
- 42 Y. Yu, G. Fan, A. Fermi, R. Mazzaro, V. Morandi, P. Ceroni, D.-M. Smilgies and B. A. Korgel, *J. Phys. Chem. C*, 2017, **121**, 23240–23248.
- 43 K. Dohnalová, T. Gregorkiewicz and K. Kúsová, *J. Phys.: Condens. Matter*, 2014, **26**, 173201.
- 44 C. Würth, M. Grabolle, J. Pauli, M. Spieles and U. Resch-Genger, *Nat. Protoc.*, 2013, **8**, 1535–1550.
- 45 M. A. Islam, M. H. Mobarok, R. Sinelnikov, T. K. Purkait and J. G. C. Veinot, *Langmuir*, 2017, **33**, 8766–8773.
- 46 I. Sychugov, R. Juhasz, J. Linnros and J. Valenta, *Phys. Rev. B: Condens. Matter Mater. Phys.*, 2005, **71**, 115331.
- 47 C. Delerue, G. Allan and M. Lannoo, *Phys. Rev. B: Condens. Matter Mater. Phys.*, 1993, **48**, 11024–11036.
- 48 T. van Buuren, L. Dinh, L. Chase, W. Siekhaus and L. Terminello, *Phys. Rev. Lett.*, 1998, **80**, 3803–3806.

## Supporting Information

# The influence of surface functionalization methods on the performance of silicon nanocrystal LEDs

Arzu Angi,<sup>a,†</sup> Marius Loch,<sup>b,†,\*</sup> Regina Sinelnikov,<sup>c</sup> Jonathan G. C. Veinot,<sup>c</sup> Markus Becherer,<sup>b</sup> Paolo Lugli,<sup>d</sup> Bernhard Rieger<sup>a,\*</sup>

<sup>a</sup> WACKER-Lehrstuhl für Makromolekulare Chemie, Technische Universität München, Lichtenbergstraße 4, 85747; Catalysis Research Center, Ernst-Otto-Fischer-Straße 1, 85748 Garching, Germany

<sup>b</sup> Institute for Nanoelectronic, Technische Universität München, Theresienstrasse 90, 80333 Munich, Germany

<sup>c</sup> Department of Chemistry, University of Alberta, 11227 Saskatchewan Drive, Edmonton, Alberta, T6G 2G2, Canada .

<sup>d</sup> Faculty of Science and Technology, Free University of Bozen-Bolzano, Universitätsplatz 5, 39100 Bolzano, Italy

\*Corresponding authors: Marius Loch, E-mail: marius.loch@tum.de, Bernhard Rieger, E-mail: rieger@tum.de

† These authors contributed equally to this work.

### Content

1	Analytical Data.....	2
1.1	Dynamic Light Scattering (DLS).....	2
1.2	TEM Images .....	2
1.3	UV-VIS Spectroscopy .....	3
1.4	Full Width Half Maximum (FWHM) Analysis .....	4
2	Experimental Details .....	4
2.1	Synthetic and Preparative Techniques .....	4
2.2	Characterization Methods .....	5
	References.....	6

# 1 Analytical Data

## 1.1 Dynamic Light Scattering (DLS)

**Table S1.** DLS data of SiNCs functionalized with hexyl groups *via* hydrosilylation (HS) and with organolithium reagents (OLR). Mean and standard values calculated over 5 measurements were listed. Every data point was obtained as the mean value of 10 acquisitions. Measurements were performed at room temperature in toluene.

Surface Functionalization	Organolithium Reagents		Hydrosilylation	
	Hydrodynamic Radius (nm)	Polydispersity (%)	Hydrodynamic Radius (nm)	Polydispersity (%)
1.	2.0	34.8	2.5	37.3
2.	2.4	31.2	2.9	31.1
3.	2.5	31.6	2.6	34.4
4.	2.6	34.9	2.2	31.8
5.	2.5	36.3	2.3	28.2
Average	2.4	33.8	2.5	32.6
Standard deviation	0.2	2.0	0.3	3.1

## 1.2 TEM Images

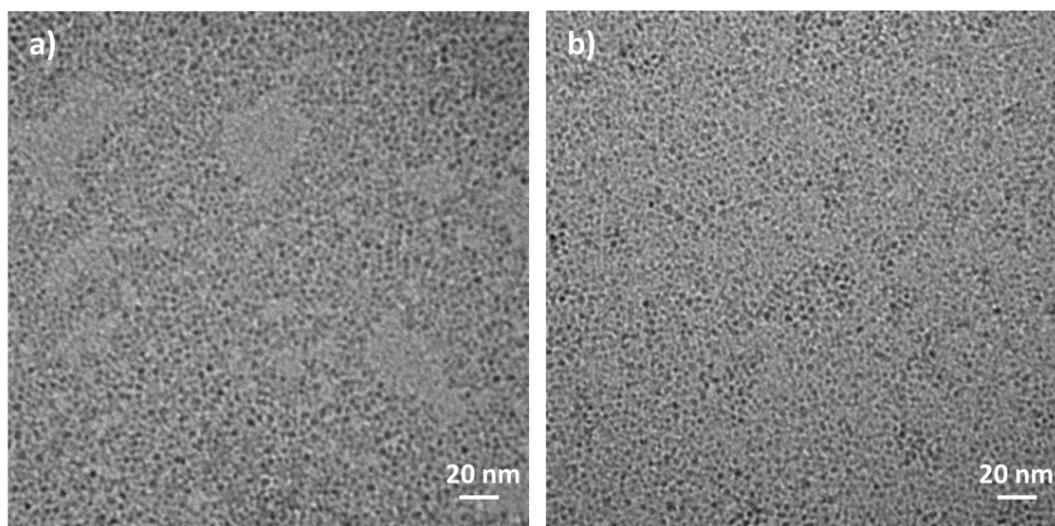


**Figure S1.** Bright field TEM images of SiNCs functionalized with a) *n*-hexyllithium *via* OLR, b) 1-hexene *via* HS method.

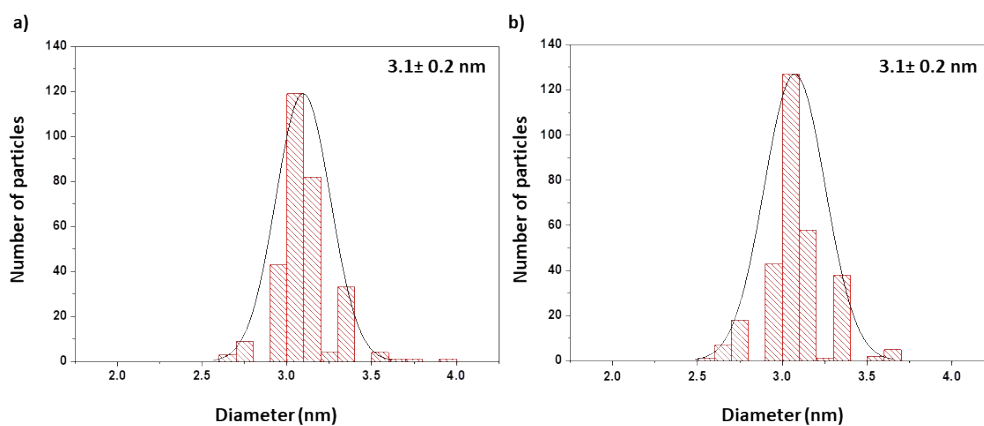


**Figure S2.** Size distributions of SiNCs functionalized with a) *n*-hexyllithium *via* OLR, b) 1-hexene *via* HS method found by counting 300 SiNCs. Mean and standard deviation of the distributions are given in the inset.

### 1.3 UV-VIS Spectroscopy

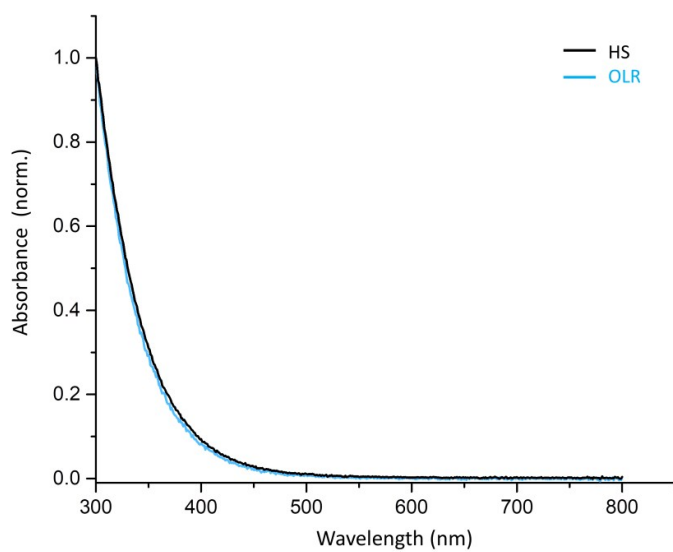


**Figure S3.** UV-Vis spectroscopy data of SiNCs functionalized with hexyl groups *via* OLR and HS methods. Absorption data is normalized at 300 nm.

## 1.4 Full Width Half Maximum (FWHM) Analysis

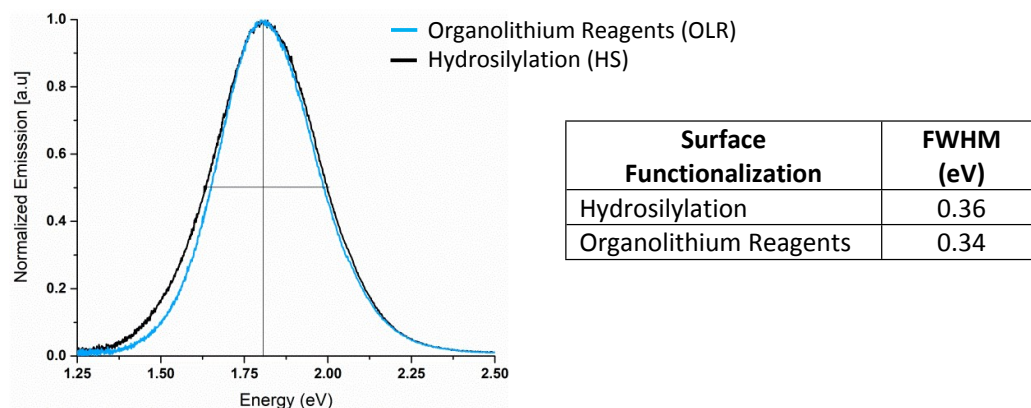


**Figure S4.** FWHM analysis on PL data obtained for SiNCs functionalized with OLR and HS methods. FWHM values of 0.34 eV and 0.36 eV were found for OLR-SiNCs and HS-SiNCs, respectively.

## 2 Experimental Details

### 2.1 Synthetic and Preparative Techniques

**General information and materials:** Surface functionalization of SiNCs was performed with standard Schlenk and glovebox techniques. All chemicals were used as received, unless stated otherwise. *n*-hexyllithium (2.3 M, in hexane), 1-hexene, 49% HF solution, 1,2-Dichlorobenzene and ZnO nanoparticle solution (Nanograde N-10X) were purchased from Sigma Aldrich. AIBN was bought from Fluka. Dry solvents were obtained from a MBraun SPS 800 solvent purification system with Argon 5.0 as the operating gas. PEDOT:PSS solution was purchased from Heraeus, Germany (Clevios P VP Al 4083), PolyTPD from Solaris Chem Inc., Canada.

**Preparation of oxide-embedded SiNCs:** Polymeric hydrogen silsesquioxane (HSQ) was synthesized based on a literature known procedure.<sup>1</sup> HSQ (7 g) was weighed in a quartz reaction boat, heated from ambient to a peak processing temperature of 1100 °C at 18 °C/min in a Nabertherm RD 30/200/11 furnace with quartz working tube under an atmosphere consisting 5% H<sub>2</sub> and 95% N<sub>2</sub>. The sample was kept at 1100 °C for 1 h. After cooling to room temperature, the resulting solid was ground into a fine brown powder using mortar and pestle. The composite was dispersed in ethanol and further ground in a shaker for 24h with high-purity silica beads using a WAB Turbula mixer. The resulting SiNC/SiO<sub>2</sub> composite was dried *in vacuo*.

**Liberation of hydride-terminated SiNCs:** 300 mg of the SiNC/SiO<sub>2</sub> composite was transferred to an ethylene-tetrafluoroethylene (ETFE) beaker equipped with a Teflon-coated stir bar. Ethanol (3 mL) and water (3 mL) were then added, and stirred to form a brown suspension, followed by addition of 3 mL of 49% HF aqueous solution. After 30 min of etching, the color of the suspension turned to yellow. Hydride-terminated SiNCs were subsequently extracted from the aqueous layer into *ca.* 30 mL of toluene by multiple (*i.e.*, 3 × 10 mL) extractions. The SiNC toluene suspension was centrifuged in an ETFE-centrifuge tube at 9000 rpm for 4 mins. Extracted particles were re-dispersed in 5 ml dry toluene and centrifuged once more to remove any residual water/ethanol.



**Surface functionalization of SiNCs with organolithium reagents:** Freshly etched hydride-terminated SiNCs (from 300 mg Si/SiO<sub>2</sub> composite) were dispersed in 2 mL of a dry toluene in a Schlenk flask equipped with a stir bar. The dispersion was degassed *via* three freeze-thaw cycles. *n*-hexyllithium (0.2 mmoles from 2.3 M solution) was then added. Upon addition, the color of the reaction mixture turned dark brown. The reaction was run for 15 hours under an argon atmosphere at room temperature and terminated by precipitation of the functionalized SiNCs from a 5 mL 1:1 ethanol-methanol mixture, acidified with HCl conc. (0.2 mL). Obtained SiNCs were centrifuged at 9000 rpm for 6 minutes and the sediment was re-dispersed in minimum amount of toluene. The precipitation-centrifugation-redispersion cycle was performed two more times from toluene and ethanol-methanol. Finally, functionalized SiNCs were dispersed in toluene and filtered through a 0.45 μm PTFE syringe filter.

**Surface functionalization of SiNCs *via* hydrosilylation:** Freshly etched hydride-terminated SiNCs (from 300 mg Si/SiO<sub>2</sub> composite) were dispersed in 2 mL of a dry toluene in a Schlenk flask equipped with a stir bar. 10 mg AIBN and 0.4 mL 1-hexene were added and the reaction mixture was degassed *via* three freeze-thaw cycles. This reaction mixture was heated at 70 °C for 15 hours. At the end of the reaction, purification was achieved by precipitating the functionalized SiNCs from a 5 mL 1:1 ethanol-methanol mixture. SiNCs were then centrifuged at 9000 rpm for 6 minutes and the sediment was re-dispersed in a minimum amount of toluene. The precipitation-centrifugation-redispersion cycle was performed two more times from toluene and ethanol-methanol. Finally, functionalized SiNCs were dispersed in toluene and filtered through a 0.45 μm PTFE syringe filter.

**Device fabrication:** Glass substrates with pre-patterned ITO films (120 nm, 15 Ω/square) were cleaned by successive sonication in lab detergent, acetone, and isopropanol (IPA) and subsequent rinsing with deionized water. PEDOT:PSS solution (Clevios P VP Al 4083, filtered with a 0.45 μm RC filter and diluted with two parts IPA) was spin coated on top at 3000 rpm for 30 sec. Afterwards, the substrates were transferred into a nitrogen-filled glove box and all following steps were done under inert atmosphere. The PEDOT:PSS film was heated on a hot plate at 140°C for 10 minutes to evaporate any remaining solvent before the deposition of subsequent layers. PolyTPD solution was prepared with 5 mg/mL in 1,2-Dichlorobenzene and stirred for 30 minutes at 60°C. It was then spun on top of the PEDOT:PSS layer at 4000 rpm for 30 seconds and dried at 140°C for 10 minutes. SiNC were spun coated from toluene solution with different concentrations and speeds and heated at 140°C for 10 minutes. The ZnO nanoparticle solution was diluted to 1 wt.-% in IPA, spin coated at 3000 rpm for 30 sec and heated at 140°C for 10 minutes. A top electrode consisting of 20 nm calcium and 100 nm aluminum was deposited by thermal resistive evaporation under vacuum (10<sup>-6</sup> mbar) using a shadow mask. The active area of the devices is determined by the overlap of top and bottom electrodes and amounts to 9 mm<sup>2</sup>. Finally, the finished devices were encapsulated using a thin glass sheet and a two component epoxy resin (Araldite 2011).

## 2.2 Characterization Methods

**Characterization of SiNCs:** FTIR spectra were collected with a Bruker Vertex 70 FTIR using a Platinum ATR from Bruker. PL spectra were measured with an AVA-Spec 2048 from Avantes using a Prizmatix (LED Current controller) as light source. Samples were excited with a 365 nm source. UV-Vis Spectroscopy was performed with a Varian Cary 50 Scan Spectrometer within the 200-800 nm range. Absolute quantum yield of SiNCs was measured with Hamamatsu Absolute PL Quantum Yield C11347 spectrometer. Every measurement was obtained over ten acquisitions. Mean and standard deviation values were calculated over three measurements. Dynamic light scattering measurements were done with a Dyna Pro NanoStar from Wyatt with toluene as solvent. Every measurement was obtained over ten acquisitions. Mean and standard deviation values were calculated over five measurements. TGA analysis was performed with a Netzsch TG 209 F1 Libramachine at a heating rate of 10 K/min in an

argon flow of 20 mL/min (Ar 4.8) in platinum pans. Bright field TEM images were obtained using a JEOL-2012 electron microscope equipped with LaB<sub>6</sub> filament and operated at an accelerating voltage of 200 kV. Particle size distribution was calculated by counting at least 200 particles using ImageJ software (Version 1.49).

**Device characterization:** Film thickness was measured with a Bruker Dektak XT profilometer by preparing single films on a glass substrate and scratching it with a scalpel. Scanning electron microscope images were taken with a Carl Zeiss NVision40 field-emission scanning electron microscope. The luminance-current-voltage-characteristics were measured using a Keithley 2602 sourcemeter and a MAVO-SPOT 2 USB luminance meter. The EL spectrum was measured with an AVANTES SenseLine CCD spectrometer with integrated monochromator (ULS2048x64 TEC). EQE was calculated from the luminance data assuming lambertian emission and using a weighted average of the emission spectrum to determine the dominant emission wavelength for conversion with the luminous efficiency function. All characterization steps were performed in ambient conditions.

## References

- 1 H. M. Bank, M. E. Cifuentes, E. M. Theresa, *United States Pat.*, 1991, 5.010.159.

## 4.5 Dissipative Self-Assembly of Photoluminescent Silicon Nanocrystals

In dissipative self-assembly (DSA), precursors are converted into self-assembling building blocks in a reaction network in which a source of energy such as a photon or a chemical fuel is irreversibly consumed. These self-assembling building blocks are unstable in their nature and thus, they spontaneously re-form their original precursor with time. Therefore, the lifetime of the building blocks is controlled by the kinetics of the coupled reaction network, which gives the associated supramolecular material temporal properties. For instance, properties of these materials can be controlled over space and time.<sup>33</sup> DSA processes take place in several natural and biological systems. Similar principles have been exploited to design man-made materials with extraordinary properties such as motility, self-healing and self-replication.<sup>201</sup>

Surface chemistry of SiNCs is well-developed.<sup>13</sup> However, the strategies to modify the surface of the SiNCs mostly rely on the formation of stable, covalent bonds. The static nature of these bonds does not allow for dynamic material properties that evolve over time or that adapt to environmental changes.

In this work, we aimed to present a chemical reaction network to achieve dissipative self-assembly of SiNCs. In this system, DSA of water soluble carboxylic acid functionalized SiNCs was induced when a chemical fuel was added. These assemblies were not stable and therefore disassembled when the system was out of fuel. Lifetimes of the assemblies could be tuned by the amount of fuel added. Such unique properties of DSA in combination with bio-compatibility and low-toxicity of SiNCs can pave the way to design biomedical applications with outstanding properties.

We demonstrated that SiNCs in the self-assembled state could not be up-taken by COS-7 mammalian cells due to their large size. However, as the assemblies fell apart in time, self-standing SiNCs formed, which were easily taken up. This principle can potentially be utilized to achieve time-delayed drug delivery systems which simultaneously offer the possibility for bioimaging, if the surface of SiNCs loaded with therapeutics.

**Manuscript:**

**Dissipative Self-Assembly of Photoluminescent Silicon Nanocrystals**

<b>Status</b>	Published online on July 24, 2018
<b>Journal</b>	<i>Angewandte Chemie International Edition</i> , 2018.
<b>Publisher</b>	John Wiley and Sons
<b>DOI</b>	10.1002/anie.201807937
<b>Authors</b>	Raphael K. Grötsch, <sup>†</sup> Arzu Angi, <sup>†</sup> Yonatan G. Mideksa, Caren Wanzke, Marta Tena-Solsona, Matthias J. Feige, Bernhard Rieger, Job Boekhoven

<sup>†</sup> These authors contributed equally to this work.

Reprinted with the permission of *John Wiley and Sons* with the license number 4453860509457.

## Dissipative Self-Assembly of Photoluminescent Silicon Nanocrystals

Raphael K. Grötsch<sup>+</sup>, Arzu Angi<sup>+</sup>, Yonatan G. Mideksa, Caren Wanzke, Marta Tena-Solsona, Matthias J. Feige, Bernhard Rieger, and Job Boekhoven\*

**Abstract:** Solutions of silicon nanocrystals (SiNCs) are used in a diverse range of applications because of their tunable photoluminescence, biocompatibility, and the abundance of Si. In dissipative supramolecular materials, self-assembly of molecules or nanoparticles is driven by a chemical reaction network that irreversibly consumes fuel. The properties of the emerging structures are controlled by the kinetics of the underlying chemical reaction network. Herein, we demonstrate the dissipative self-assembly of photoluminescent SiNCs driven by a chemical fuel. A chemical reaction induces self-assembly of the water-soluble SiNCs. However, the assemblies are transient, and when the chemical reaction network runs out of fuel, the SiNCs disassemble. The lifetime of the assemblies is controlled by the amount of fuel added. As an application of the transient supramolecular material, we demonstrate that the platform can be used to control the delayed uptake of the nanocrystals by mammalian cells.

Silicon nanocrystals (SiNCs) have garnered significant attention<sup>[1]</sup> for their unique properties, which include size-dependent photoluminescence,<sup>[2]</sup> low-toxicity,<sup>[3]</sup> and biocompatibility.<sup>[4,5]</sup> Moreover, the elemental abundance of silicon favors the applications in sensors,<sup>[6]</sup> LEDs,<sup>[7]</sup> solar cells,<sup>[8]</sup> and bio-imaging.<sup>[9,10]</sup> The surface chemistry of SiNCs plays a critical role in these applications because it can alter the nanocrystal's natural properties.<sup>[11]</sup> Thus properties such as cytotoxicity,<sup>[12]</sup> photoluminescent emission quantum yield,<sup>[13]</sup> or emission wavelength,<sup>[14]</sup> can be tuned through functional-

ization of the SiNCs' surface. Strategies to modify the surface chemistry of the SiNCs rely on the formation of stable, covalent bonds. The static nature of these bonds does not allow for dynamic material properties that evolve or that adapt to environmental changes.

In contrast, dissipative supramolecular materials are intrinsically dynamic, and their function can be controlled over space and time.<sup>[15]</sup> For these materials, the self-assembly of molecules is coupled to (photo)chemical reaction networks. In these chemical reaction networks, an activation reaction activates a precursor, which enables the precursor to undergo self-assembly. The reaction can only occur at the expense of a source of energy, typically a photon or a chemical fuel, and is irreversible. That is, the activation reaction “burns” a source of energy to activate a precursor for self-assembly. The activated product can then self-assemble to form a supramolecular material. However, the product is metastable and spontaneously deactivates into the original precursor via the deactivation reaction. The dissipative self-assembly implies that the supramolecular material is dynamic and forms in response to energy. Man-made examples of dissipative self-assembly include the ATP-fueled assembly of amphiphiles into temporary nanoreactors,<sup>[16]</sup> the formation of transient self-healing hydrogels driven by the hydrolysis of methylating agents,<sup>[17]</sup> the carbodiimide-driven formation of colloids that can deliver hydrophobic agents,<sup>[18]</sup> among others.<sup>[19,20]</sup> In the context of the dissipative assembly of nanoparticles, researchers have described the light-driven self-assembly of silver and gold nanoparticles into self-erasing inks,<sup>[21]</sup> and the dynamic pH controlled clustering of gold nanoparticles.<sup>[22]</sup> Another example used methylating agents to drive the assembly of colloids.<sup>[20]</sup>

Herein, we describe a new chemical reaction network that drives the dissipative self-assembly of SiNCs (Figure 1a). We show that the emerging clusters of SiNCs change size predictably over time and that the emerging materials can be re-used in multiple cycles. We use the evolving size of the SiNC clusters to delay the uptake of the SiNCs by mammalian fibroblasts-like cells. The combined experiments open a platform that could deliver therapeutics with a delayed and regulated uptake kinetics.

We functionalized SiNCs with 5-hexenoic acid to make them water-soluble (the precursor in Figure 1a). An acid-titration experiment revealed their pK<sub>a</sub> to be approximately 6.9 (Figure S11 in the Supporting Information). The SiNCs were dissolved in a buffer at a final surface-bound carboxylic acid concentration of 5 mM. The buffer we used was a 200 mM 2-(*N*-morpholino)ethanesulfonic acid (MES) buffer with 100 mM *N*-hydroxysuccinimide (NHS) at pH 6.5 in water. At this pH, more than half of the carboxylic groups on the SiNCs were deprotonated. As a result, the electrostatic

[\*] R. K. Grötsch,<sup>[†]</sup> C. Wanzke, Dr. M. Tena-Solsona, Prof. Dr. J. Boekhoven  
Department of Chemistry, Technische Universität München  
Lichtenbergstrasse 4, 85748 Garching (Germany)  
E-mail: job.boekhoven@tum.de

A. Angi,<sup>[†]</sup> Prof. Dr. B. Rieger  
WACKER-Lehrstuhl für Makromolekulare Chemie  
Technische Universität München  
Lichtenbergstrasse 4, 85748 Garching (Germany)  
and  
Catalysis Research Center  
Ernst-Otto-Fischer-Strasse 1, 85748 Garching (Germany)

Y. G. Mideksa, Prof. Dr. M. J. Feige  
Center for Integrated Protein Science at the Department of  
Chemistry, Technische Universität München  
Lichtenbergstrasse 4, 85748 Garching (Germany)

R. K. Grötsch,<sup>[†]</sup> Y. G. Mideksa, C. Wanzke, Dr. M. Tena-Solsona,  
Prof. Dr. M. J. Feige, Prof. Dr. J. Boekhoven  
Institute for Advanced Study, Technische Universität München  
Lichtenbergstrasse 2a, 85748 Garching (Germany)

[†] These authors contributed equally to this work.

Supporting information and the ORCID identification number(s) for the author(s) of this article can be found under:  
<https://doi.org/10.1002/anie.201807937>.

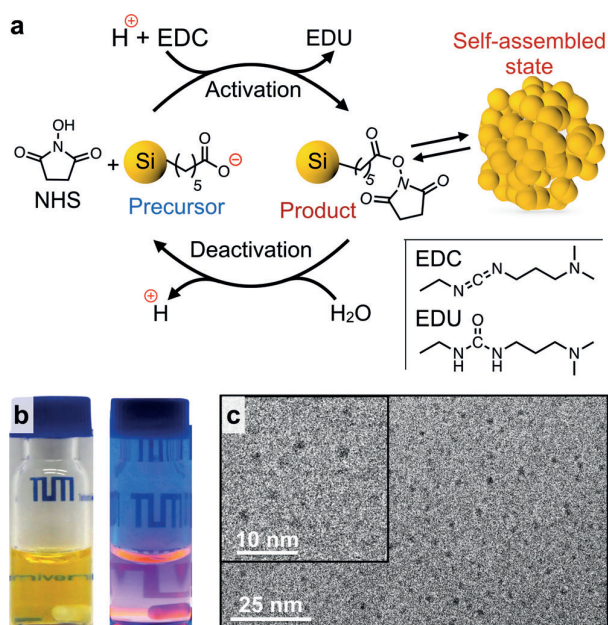


**Figure 1.** a) Schematic representation of the chemical reaction network. Carboxylate surface groups on the SiNCs react with EDC and NHS to form a transient NHS ester. The loss of surface charges induced the temporary self-assembly of SiNCs. b) Photographs of a solution of the precursor in MES buffer under visible (left) and UV (365 nm, right) light. c) Cryo-TEM images of the precursor solution.

stabilization achieved by these charges made the SiNCs well-soluble in the buffer. Indeed, dissolution of the SiNCs in the buffer yielded a yellow transparent colloidal solution (Figure 1b). Under UV irradiation the yellow solution emitted red light, strongly indicating that the SiNCs maintained their intrinsic photoluminescence. The emission was further verified in a spectrophotometer, which showed a photoluminescent emission maximum at 681 nm when irradiated with 365 nm UV light (Figure SI2). We determined the hydrodynamic diameter of the SiNCs to be  $(5.5 \pm 1.1)$  nm by dynamic light scattering (Table SI1). Cryogenic transmission electron microscopy (cryo-TEM) corroborated the successful synthesis of the SiNCs and their homogeneous dissolution. From the micrographs, we determined their diameter to be  $(3.6 \pm 0.5)$  nm (Figure 1c, Figure SI3b). Finally, UV/Vis spectra of the SiNCs showed absorption at wavelengths shorter than 400 nm (Figure SI4).

The carboxylic acid functionalized SiNCs served as the precursors in the chemical reaction network we introduce herein (Figure 1a). In the activation reaction, the carboxylate groups on the SiNC surface were converted into the corresponding NHS-esters by the irreversible consumption of 1-ethyl-3-(3-dimethylaminopropyl) carbodiimide (EDC). In the deactivation reaction, the NHS esters hydrolyzed back to their initial carboxylate state. The cycle could only operate for as long as EDC was present because the activation irreversibly consumed EDC. Moreover, the loss of electrostatic stabilization upon the conversion of the precursor induced assembly of the SiNCs into clusters. Taken together,

the irreversible consumption of EDC induced the transient assembly of the SiNCs.

We studied the kinetics of the aforementioned reaction network. The SiNCs solution was fueled with a 7 mM solution of EDC, and the evolution of the concentration of EDC was monitored via high-pressure liquid chromatography (HPLC, Figure 2a). The concentration of EDC decreased to less than

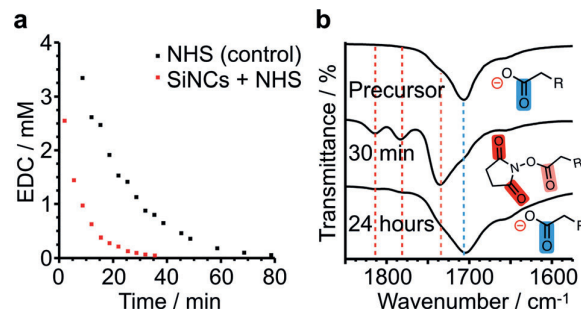


**Figure 2.** a) The EDC concentration as a function of time. The red markers correspond to the addition of 7 mM EDC to a solution of SiNCs in MES-buffer (200 mM) and NHS (100 mM), the black markers show the same experiment without the SiNCs as a control. b) FTIR spectra of the precursor SiNCs; 30 min and 24 h after addition of 7 mM EDC. Dashed lines from left to right: 1814, 1784, 1738, 1706  $\text{cm}^{-1}$  ( $R = (\text{CH}_2)_4\text{-SiNC}$ ).

3 mM within the first minute, after which it further decayed exponentially. No substantial amount of EDC was detected after 35 min. The initial rapid decay was likely a result of a reaction of EDC with NHS.<sup>[23]</sup> This hypothesis was further corroborated by a similar rapid decrease in the EDC concentration in a control experiment without the SiNCs (Figure 2a). The EDC decay rate was higher in the presence of SiNCs than in the control reaction. This accelerated decay served as a good indicator of the reaction between the carbodiimide and the carboxylate surface groups of SiNCs.

We monitored the surface groups of the SiNCs in response to EDC by Fourier-transform infrared (FTIR) spectroscopy (Figure 2b, see Figure SI5 for full spectra). Before the addition of EDC, the spectrum of the SiNCs showed a  $\text{C}=\text{O}$  band at  $1706 \text{ cm}^{-1}$ , which corresponds to the carboxylic acid groups.<sup>[24,25]</sup> Upon the addition of 7 mM EDC, the peak at  $1706 \text{ cm}^{-1}$  weakened to a small shoulder and three new peaks arose at  $1814 \text{ cm}^{-1}$ ,  $1784 \text{ cm}^{-1}$  and  $1738 \text{ cm}^{-1}$ , which correspond to  $\nu_s(\text{C}=\text{O}, \text{NHS ester})$ ,  $\nu_s(\text{C}=\text{O} \text{ NHS imide})$ , and to  $\nu_s(\text{C}=\text{O} \text{ NHS-imide})$ , respectively. Importantly, 24 h after the addition of EDC, the NHS-ester peaks mostly disappeared, whereas the carboxylic acid peak at  $1706 \text{ cm}^{-1}$  recovered (Figure 2b). This result is a good indication that the NHS ester is transient and hydrolyzes to the original precursor. The combined results demonstrate that the carboxylic acids on the SiNCs' surface were transiently converted into their corresponding NHS ester at the expense of EDC.

The initially yellow clear solution became turbid upon the addition of EDC. Moreover, the turbid solution became transparent over the course of hours, pointing to an assembly and disassembly process of the SiNCs. We used time-lapse photography to follow the changes in turbidity over time

(Figure 3a). An EDC concentration of at least 6.5 mM was required to induce a noticeable increase in turbidity. When the EDC concentration was 6.5 mM, the increase in turbidity persisted for more than 4 h. Moreover, we observed that, with

observed a homogeneous photoluminescent solution, reminiscent of the solution shown in the micrographs collected before the addition of EDC (Figure 3g). Moreover, cryo-TEM images of SiNC solutions after the reaction cycle revealed a size distribution of SiNCs ( $d = 3.6 \pm 0.7$  nm) similar to that before the addition of EDC (Figure 1c, Figure S13). Unfortunately, cryo-TEM on the samples during the cycle proved challenging probably because of the size of the clusters. Instead, we used confocal microscopy and found clusters of the particles of tens of microns in all three dimensions (Figure S18).

The possibility of inducing transient assembly of the SiNCs in consecutive cycles was also tested. The first reaction cycle was initiated with the addition of 7 mM EDC. After the solution had lost its turbidity, the next cycle was started by addition of a new batch of 7 mM EDC. The turbidity measurements showed that the cycles could be repeated as many as three times. However, the third cycle showed signs of fatigue, that is, the maximum turbidity the sample reached was only 59% of the value compared to the first cycle. All three cycles showed

lifetimes of approximately 6.2 h (Figure 3c). Two possible reasons could explain the fatigue: The reaction between the carboxylic acids and EDC can yield N-acylurea<sup>[24]</sup> as a stable side product that cannot revert to the precursor state, or the waste product 1-[3-(Dimethylamino)propyl]-3-ethylurea (EDU) interferes with the assembly process. We only observed minimal amounts of the N-acylurea by FTIR after three cycles (Figure S19). In contrast, we found that addition of EDU affected the cycle drastically, which would explain the fatigue after three cycles (Figure S110). Performing the experiment under argon to limit SiNC oxidation did not change the fatigue (Figure S111).

From these experiments, we conclude that EDC induced the transient assembly of the SiNCs into clusters. The lifetime of these assemblies is tunable, and the assembly–disassembly process can be repeated several times. Encouraged by these results, we began exploring the properties of these SiNC assemblies for potential future biomedical applications. Recent work has shown that SiNCs are readily taken up by cells, likely through passive diffusion of the relatively small particles.<sup>[4,9]</sup> We wondered whether we could delay such passive uptake by the transient clustering of the SiNCs. Our rationale was that the particle clusters might not be taken up because of their large size. However, as the clusters disassemble the SiNC precursors become available for passive uptake (Figure 4a).

To test the delayed uptake of the particles, we confirmed the uptake of SiNCs by a mammalian cell line by incubating COS-7 fibroblast-like cells with the SiNCs for 9 h. In these experiments, the SiNCs were added to cells in a mixture of phosphate-buffered saline (PBS, see Supporting Information

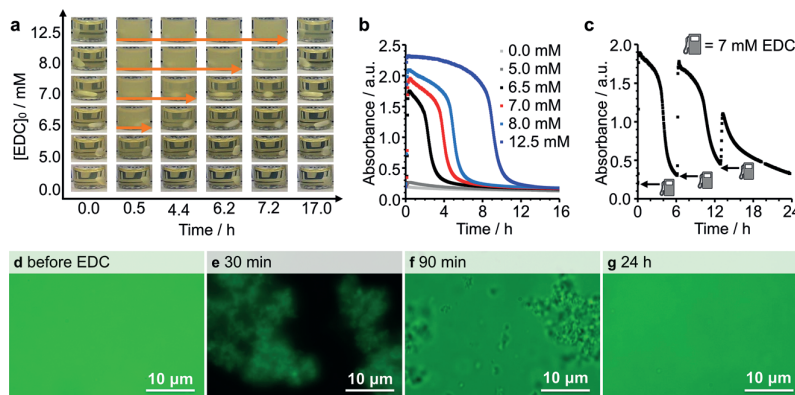


**Figure 3.** a) Photographs of SiNC solutions with different initial EDC concentrations over time; each column represents a different time point. b) Absorbance at 500 nm over time as a quantification of turbidity induced by the addition of different concentrations of EDC (0.0, 5.0, 6.5, 7.0, 8.0, and 12.5 mM). c) Three consecutive additions of 7 mM EDC to the same SiNC solution. Turbidity was monitored via UV/Vis spectrophotometry (absorbance at 500 nm). d)–g) Fluorescent micrographs acquired before (d) and 30 min (e), 90 min (f) and, 24 h (g) after the addition of 7 mM EDC. The intrinsic fluorescence of the SiNCs was measured.

increasing EDC concentration, the samples remained turbid longer. For example, with 12.5 mM EDC, which corresponds to a 2.5-fold excess of fuel over the surface-bound carboxylates, the turbidity persisted approximately 17 h. When a 20-fold excess of fuel was added, the solutions remained turbid for longer than 2 days (Figure S16).

We quantified the transient turbidity by measuring the absorbance at 500 nm in a UV/Vis spectrophotometer. When EDC was added to the samples, the turbidity increased in the first 30 min to a maximum, then decreased to its original level (Figure 3b). To quantify the lifetime of the increased turbidity, we set an arbitrary absorbance threshold at 0.27 absorbance units. Above this threshold, the sample was considered turbid; below the threshold, it was considered transparent. We found that the lifetime of the turbidity increased linearly with increasing EDC concentration between 6.5 to 12.5 mM (Figure S17).

We used the intrinsic photoluminescence of the SiNCs in combination with fluorescence microscopy to study the nature of the turbidity in greater detail. Before the addition of EDC, fluorescence microscopy revealed a homogeneous fluorescent solution without evidence of assemblies. In contrast, 30 min after the addition of 7 mM EDC, we observed bright fluorescent clusters of tens of micrometers, whereas the surrounding solution showed no fluorescent emission (Figure 3d,e). From the lack of fluorescence in the surrounding solution, we concluded that most of the SiNCs had been incorporated into the clusters. After 90 min, we observed smaller clusters and the surrounding solution started to emit light again (Figure 3f). These observations point toward the disassembly of the clusters into the SiNCs. After 24 h, we

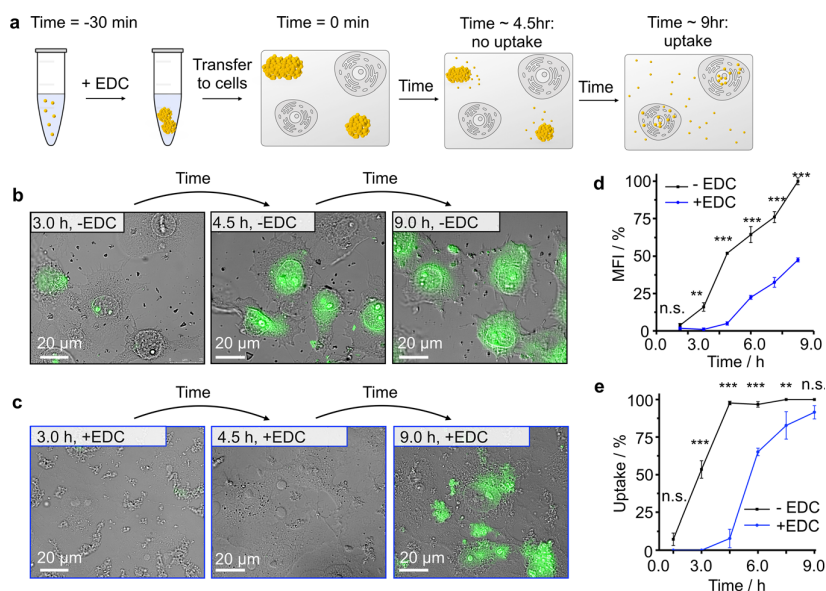


**Figure 4.** a) Schematic overview of the experiment. For the control experiment, no EDC is added (-EDC). The delayed uptake (4.5 h) depends on the amount of EDC added to the particles in the first step. b), c) Fluorescence micrographs of cells incubated with the SiNC solution without EDC (b) and with EDC (c) for 3.0, 4.5, and 9.0 h. d) Mean fluorescence intensity of the nucleus as a function of time for cells incubated with SiNCs and SiNCs + 9 mM EDC. The highest uptake after 9 hours is set to 100%. e) Percentage of cells that have taken up a significant amount of SiNCs, that is, with a nucleus intensity above the threshold level of 50 a.u. Error bars depict  $\pm$  standard deviation of the mean for  $n \geq 3$ , and two-way analysis of variance (ANOVA) with a Bonferroni post-test is used between the with and without EDC at each time point. \*\* and \*\*\* represent a  $P$  value  $< 0.01$  and  $< 0.001$ , respectively.

for details) and MES. At intervals of 1.5 h, the cells were thoroughly washed and tested for uptake of the SiNCs by live-cell fluorescence microscopy. We measured the mean fluorescence intensity of the nuclei of the cells. After the first 1.5 h, the mean fluorescence intensity was similar to an untreated control sample. In contrast, after 3.0 h, the cells were brighter than those of an untreated control sample (Figure 4b, Figures SII13,14). Moreover, the fluorescence intensity continued to increase with increasing incubation time (Figure 4d). To quantify the fraction of cells that had taken up SiNCs, we set a threshold value fluorescence intensity (see Supporting Information). Above this value, we considered the cell had taken up a significant amount of SiNCs (Figure 4e). The quantification of the uptake followed a similar trend over time: In the first 1.5 h, only a small fraction of the cells had taken up particles, whereas all cells had taken up after 4.5 h.

In a second experiment, the uptake of the SiNCs fueled by EDC was tested. The assembly of SiNCs was initiated by the addition of 9 mM EDC. After 30 min, the turbid solution with the SiNC clusters was added to the cells. It should be clarified that after 30 min, most of the EDC had reacted (Figure 2) and the cells were thus only exposed to minimal amounts of EDC. The lack of EDC after 30 min also implies that the growth of the clusters is likely minimal and the material properties are dominated by the hydrolysis and disassembly kinetics. We determined the lifetime of the metastable clusters to be 6 h in the presence of cell media but in the absence of cells

(Figure SII15). In the first hours of the experiment with cells, we did not observe an increase in the mean fluorescence intensity of the cells (Figure 4d). Only after 6 h, did we start to see an increase in fluorescence of the nuclei compared to the control without SiNCs. Moreover, the fraction of cells that had taken up SiNCs had also drastically increased compared to earlier time points (Figure 4e). The mean fluorescence of the cells continued to increase with time, and the number of cells that had taken up SiNCs reached greater than 90% after 9.0 h of incubation. We also confirmed the viability of the COS-7 cells in the conditions we used in these experiments (Figure SII12). Finally, we confirmed the observed differences in uptake profile were not a result of the EDU, the waste product of the reaction cycle (Figure SII16).

When we compare the evolution of the uptake by the cells of the SiNC treated or not treated with EDC, a picture emerges that confirms our hypothesis. It becomes apparent that the cells cannot take up the clusters, because after 4.5 h there was an insignificant uptake when EDC was added, whereas

all cells had taken up SiNCs in the experiment without EDC. This comparison points to inhibition of uptake when the SiNCs are assembled into a cluster. After 6.0 h, that is, when the clusters are disassembling (Figure SII15), we observed uptake of the SiNCs, which points to a mechanism in which the cells take up the SiNCs that have been released from the clusters. Because of the dissipative chemistry, this release of the SiNCs is delayed and so is the uptake. The fraction of cells with particles reaches similar levels as the experiments without EDC only after 9.0 h.

In conclusion, we demonstrated the dissipative self-assembly of SiNCs driven by EDC as chemical fuel. The SiNCs assembled into clusters of tens of micrometers. By varying the amount of EDC, we tuned the lifetime of SiNC clusters between 4 h and 2 days. A biological application of the transient character of SiNC clusters was explored. We showed that the time of uptake of the SiNCs by COS-7 cells could be delayed with our dissipative self-assembled system. We foresee that such dissipative supramolecular materials, whether SiNCs or other types of nanoparticles, could be used in the future to engineer materials that can delay the delivery of therapeutics into or inside cells.

## Acknowledgements

This work was supported by the Technische Universität München—Institute for Advanced Study, funded by the



German Excellence Initiative and the European Union Seventh Framework Programme under grant agreement N° 291763 and the International Research Training Group ATUMS (IRTG 2022). A.A. acknowledges funding from Studienstiftung des deutschen Volkes. M.T.-S. acknowledges the European Union's Horizon 2020 Research and Innovation program for the Marie Skłodowska Curie Fellowship under grant agreement N° 747007.

### Conflict of interest

The authors declare no conflict of interest.

**Keywords:** cellular uptake · chemical reaction network · dissipative self-assembly · non-equilibrium self-assembly · silicon nanocrystals

- 
- [1] M. Dasog, J. Kehrlé, B. Rieger, J. G. C. Veinot, *Angew. Chem. Int. Ed.* **2016**, *55*, 2322; *Angew. Chem.* **2016**, *128*, 2366.
- [2] a) C. M. Hessel, D. Reid, M. G. Panthani, M. R. Rasch, B. W. Goodfellow, J. Wei, H. Fujii, V. Akhavan, B. A. Korgel, *Chem. Mater.* **2012**, *24*, 393; b) O. Wolf, M. Dasog, Z. Yang, I. Balberg, J. G. C. Veinot, O. Millo, *Nano Lett.* **2013**, *13*, 2516.
- [3] a) Q. Wang, Y. Bao, X. Zhang, P. R. Coxon, U. A. Jayasooriya, Y. Chao, *Adv. Healthcare Mater.* **2012**, *1*, 189; b) X. Cheng, S. B. Lowe, P. J. Reece, J. J. Gooding, *Chem. Soc. Rev.* **2014**, *43*, 2680; c) N. H. Alsharif, C. E. M. Berger, S. S. Varanasi, Y. Chao, B. R. Horrocks, H. K. Datta, *Small* **2009**, *5*, 221.
- [4] F. Erogbogbo, K.-T. Yong, I. Roy, G. Xu, P. N. Prasad, M. T. Swihart, *ACS Nano* **2008**, *2*, 873.
- [5] H. Nishimura, K. Ritchie, R. S. Kasai, M. Goto, N. Morone, H. Sugimura, K. Tanaka, I. Sase, A. Yoshimura, Y. Nakano et al., *J. Cell. Biol.* **2013**, *202*, 967.
- [6] C. M. Gonzalez, M. Iqbal, M. Dasog, D. G. Piercey, R. Lockwood, T. M. Klapötke, J. G. C. Veinot, *Nanoscale* **2014**, *6*, 2608.
- [7] a) F. Maier-Flaig, J. Rinck, M. Stephan, T. Bocksrocker, M. Bruns, C. Kübel, A. K. Powell, G. A. Ozin, U. Lemmer, *Nano Lett.* **2013**, *13*, 475; b) A. Angi, M. T. Loch, R. Sinelnikov, J. Veinot, M. Becherer, P. Lugli, B. Rieger, *Nanoscale* **2018**, *10*, 10337.
- [8] M. Dutta, L. Thirugnanam, P. van Trinh, N. Fukata, *ACS Nano* **2015**, *9*, 6891.
- [9] J. H. Warner, A. Hoshino, K. Yamamoto, R. D. Tilley, *Angew. Chem. Int. Ed.* **2005**, *44*, 4550; *Angew. Chem.* **2005**, *117*, 4626.
- [10] B. F. P. McVey, R. D. Tilley, *Acc. Chem. Res.* **2014**, *47*, 3045.
- [11] K. Dohnalová, T. Gregorkiewicz, K. Kůsová, *J. Phys. Condens. Matter* **2014**, *26*, 173201.
- [12] a) S. Bhattacharjee, I. M. C. M. Rietjens, M. P. Singh, T. M. Atkins, T. K. Purkait, Z. Xu, S. Regli, A. Shukaliak, R. J. Clark, B. S. Mitchell et al., *Nanoscale* **2013**, *5*, 4870; b) A. Shiohara, S. Hanada, S. Prabakar, K. Fujioka, T. H. Lim, K. Yamamoto, P. T. Northcote, R. D. Tilley, *J. Am. Chem. Soc.* **2010**, *132*, 248.
- [13] M. A. Islam, M. H. Mobarok, R. Sinelnikov, T. K. Purkait, J. G. C. Veinot, *Langmuir* **2017**, *33*, 8766.
- [14] a) A. Angi, R. Sinelnikov, A. Meldrum, J. G. C. Veinot, I. Balberg, D. Azulay, O. Millo, B. Rieger, *Nanoscale* **2016**, *8*, 7849; b) M. Dasog, G. B. De los Reyes, L. V. Titova, F. A. Hegmann, J. G. C. Veinot, *ACS Nano* **2014**, *8*, 9636.
- [15] a) S. A. P. van Rossum, M. Tena-Solsona, J. H. van Esch, R. Eelkema, J. Boekhoven, *Chem. Soc. Rev.* **2017**, *46*, 5519; b) A. Sorrenti, J. Leira-Iglesias, A. J. Markvoort, T. F. A. de Greef, T. M. Hermans, *Chem. Soc. Rev.* **2017**, *46*, 5476; c) R. Merindol, A. Walther, *Chem. Soc. Rev.* **2017**, *46*, 5588; d) F. Della Sala, S. Neri, S. Maiti, J. L.-Y. Chen, L. J. Prins, *Curr. Opin. Biotechnol.* **2017**, *46*, 27; e) R. Grötsch, J. Boekhoven, *Unique properties of Supramolecular Biomaterials through Non-equilibrium Self-assembly in Self-assembling Biomaterials*, Woodhead Publishing, Oxford, **2018**; f) B. Rieß, J. Boekhoven, *ChemNanoMat* **2018**, <https://doi.org/10.1002/cnma.201800169>.
- [16] S. Maiti, I. Fortunati, C. Ferrante, P. Scrimin, L. J. Prins, *Nat. Chem.* **2016**, *8*, 725.
- [17] a) J. Boekhoven, W. E. Hendriksen, G. J. M. Koper, R. Eelkema, J. H. van Esch, *Science* **2015**, *349*, 1075; b) J. Boekhoven, A. M. Brizard, K. N. K. Kowligi, G. J. M. Koper, R. Eelkema, J. H. van Esch, *Angew. Chem. Int. Ed.* **2010**, *49*, 4825; *Angew. Chem.* **2010**, *122*, 4935.
- [18] a) M. Tena-Solsona, B. Rieß, R. K. Grötsch, F. C. Löhner, C. Wanzke, B. Käsdorf, A. R. Bausch, P. Müller-Buschbaum, O. Lieleg, J. Boekhoven, *Nat. Commun.* **2017**, *8*, 15895; b) B. Rieß, C. Wanzke, M. Tena-Solsona, R. K. Grötsch, C. Maity, J. Boekhoven, *Soft Matter* **2018**, *14*, 4852.
- [19] a) A. Sorrenti, J. Leira-Iglesias, A. Sato, T. M. Hermans, *Nat. Commun.* **2017**, *8*, 15899; b) C. G. Pappas, I. R. Sasselli, R. V. Ulijn, *Angew. Chem. Int. Ed.* **2015**, *54*, 8119; *Angew. Chem.* **2015**, *127*, 8237.
- [20] B. G. P. van Ravensteijn, W. E. Hendriksen, R. Eelkema, J. H. van Esch, W. K. Kegel, *J. Am. Chem. Soc.* **2017**, *139*, 9763.
- [21] R. Klajn, P. J. Wesson, K. J. M. Bishop, B. A. Grzybowski, *Angew. Chem. Int. Ed.* **2009**, *48*, 7035; *Angew. Chem.* **2009**, *121*, 7169.
- [22] L. Heinen, A. Walther, *Chem. Sci.* **2017**, *8*, 4100.
- [23] K. A. Totaro, X. Liao, K. Bhattacharya, J. I. Finneman, J. B. Sperry, M. A. Massa, J. Thorn, S. V. Ho, B. L. Pentelute, *Bioconjugate Chem.* **2016**, *27*, 994.
- [24] S. Sam, L. Touahir, J. Salvador Andresa, P. Allongue, J.-N. Chazalviel, A. C. Gouget-Laemmel, C. Henry de Villeneuve, A. Moraillon, F. Ozanam, N. Gabouze et al., *Langmuir* **2010**, *26*, 809.
- [25] C. Wang, Q. Yan, H.-B. Liu, X.-H. Zhou, S.-J. Xiao, *Langmuir* **2011**, *27*, 12058.

Manuscript received: July 11, 2018

Accepted manuscript online: July 24, 2018

Version of record online: ■ ■ ■ ■ ■ ■ ■ ■ ■ ■

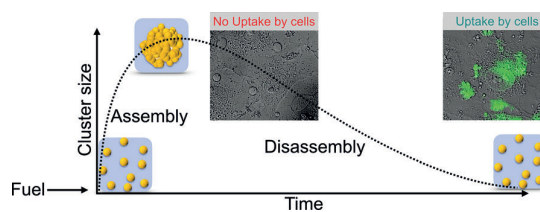
## Communications



## Self-Assembly

R. K. Grötsch, A. Angi, Y. G. Mideksa,  
C. Wanzke, M. Tena-Solsona, M. J. Feige,  
B. Rieger, J. Boekhoven\* — ■■■■—■■■■

Dissipative Self-Assembly of  
Photoluminescent Silicon Nanocrystals



**Come together:** The dissipative self-assembly of silicon nanocrystals (SiNCs) is coupled to a fuel-driven chemical reaction network, thereby enabling kinetic control over the self-assembled struc-

tures. For example, the amount of fuel determines the lifetime of the assemblies. Using this mechanism, the uptake of SiNCs by cells could be delayed.

## Supporting Information

### **Dissipative Self-Assembly of Photoluminescent Silicon Nanocrystals**

*Raphael K. Grötsch<sup>+</sup>, Arzu Angi<sup>+</sup>, Yonatan G. Mideksa, Caren Wanzke, Marta Tena-Solsona, Matthias J. Feige, Bernhard Rieger, and Job Boekhoven\**

anie\_201807937\_sm\_miscellaneous\_information.pdf

# Supporting Information

## Table of Content

1.	Supplementary Tables.....	2
	Dynamic light scattering .....	2
2.	Supplementary Figures .....	3
	Titration of SiNC .....	3
	Photoluminescence Spectroscopy.....	4
	Cryogenic-Transmission Electron Microscopy (cryo-TEM).....	5
	UV/VIS Spectroscopy .....	6
	Fourier-transform Infrared Spectroscopy.....	7
	Time-lapse Photography .....	8
	Lifetime against concentration EDC .....	9
	Confocal fluorescent microscopy.....	10
	Fourier-transform Infrared Spectroscopy.....	11
	UV/Vis as a function of time with different EDU concentrations .....	12
	UV/Vis as a function of time under Argon atmosphere.....	13
	Microscopy of COS-7cells .....	15
	UV/Vis as a function of time under cell-experiment conditions .....	16
	Viability assay.....	14
3.	Materials.....	18
4.	Experimental Details.....	18
	References .....	23

## 1. Supplementary Tables

### Dynamic light scattering

**Table SI1.** Hydrodynamic diameter and PDI data of SiNCs obtained by dynamic light scattering in MES buffered aqueous solution.

	Hydrodynamic Diameter (nm)	PDI (%)
	5.0	30
	6.2	22
	5.7	24
	4.0	24
	5.9	30
	6.0	29
	4.2	24
	7.7	26
	5.2	28
	5.0	40
Mean Diameter	5.5 ± 1.1	
Mean PDI		28 ± 5

## 2. Supplementary Figures

### Titration of SiNC

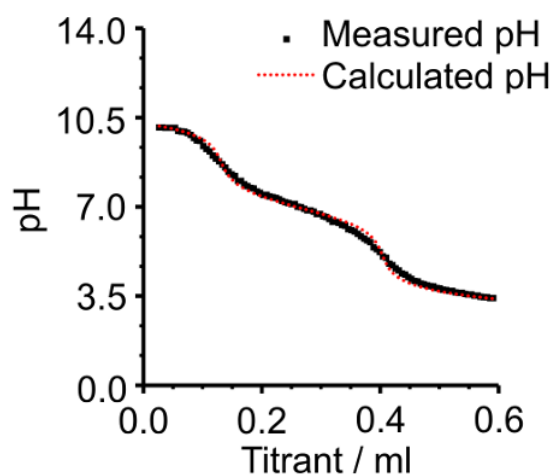
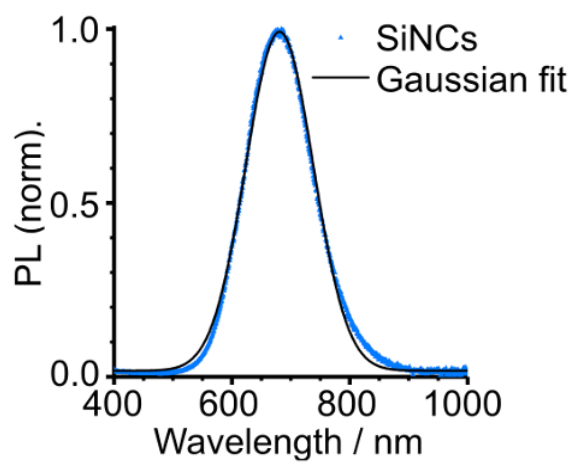


**Figure S11.** Plot of the pH value as a function of the titrant (0.01 M HCl) of a SiNC batch. The black curve indicates the measured values, whereas the red markers the fitted values by HySS 2009. Based on the fit, we calculated a  $pK_a$  of 6.9 of the surface bound carboxylates. The total amount of acid in the sample was calculated to be 2.6  $\mu$ moles.

## Photoluminescence Spectroscopy



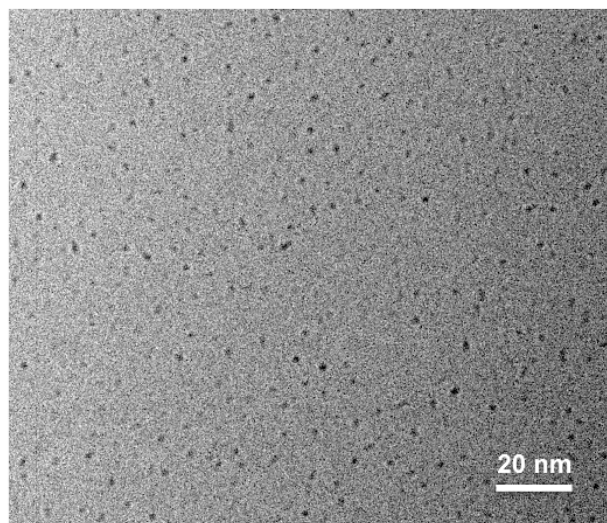
model	Gauss
	$y=y_0 +$
equation	$(A/(w*\sqrt{\pi/2})) * \exp(-2*((x-x_c)/w)^2)$
$y_0$	$0.0179 \pm 0.0008$
$x_c$	$680.8 \pm 0.1$
$w$	$114.6 \pm 0.3$
$A$	$139.9 \pm 0.4$
$R^2(\text{COD})$	$0.997$

**Figure S12.** Photoluminescence (PL) of SiNCs in MES buffered aqueous solution (100 mM NHS, Ex. 365 nm).

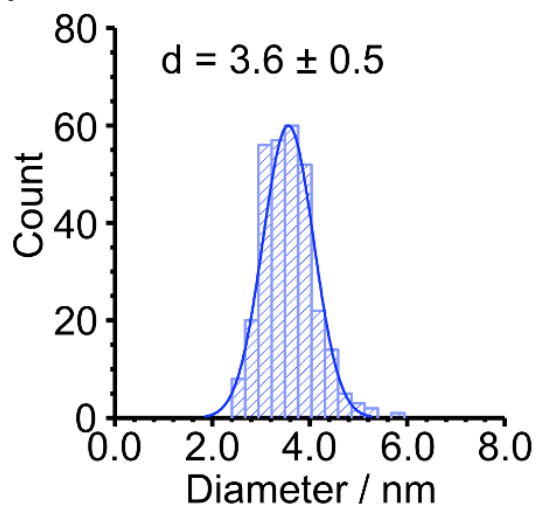
## Cryogenic-Transmission Electron Microscopy (cryo-TEM)

The analysis of the cryo-TEM pictures and the resulting data depiction followed the guidelines of Murphy and Buriak.<sup>[1]</sup> We measured 300 particles for the size distribution and applied Scott's rule for the bin width in histograms of a normal distribution.

**a**



**b**



**c**

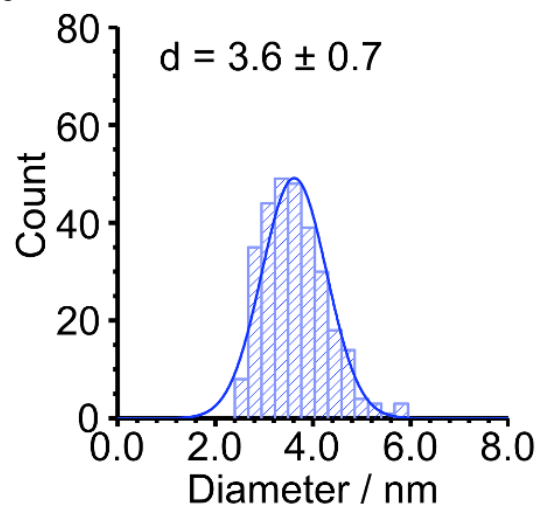


**Figure S13.** **a)** Cryo-TEM micrographs of SiNCs 24 h after EDC addition. **b,c)** Histograms of the distribution of the SiNC diameters before (b) and 24 h after (c) 7 mM EDC addition.



## UV/VIS Spectroscopy

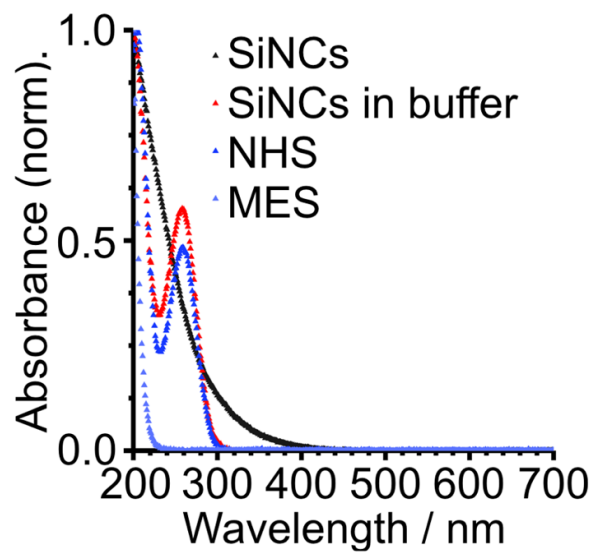


**Figure S14.** UV-Vis spectra of SiNCs in water ( $\text{pH} = 6.5$ ), SiNCs in buffer (MES, NHS,  $\text{pH} = 6.5$ ), NHS, and MES. Absorbance is normalized to 1 at 200 nm.

## Fourier-transform Infrared Spectroscopy

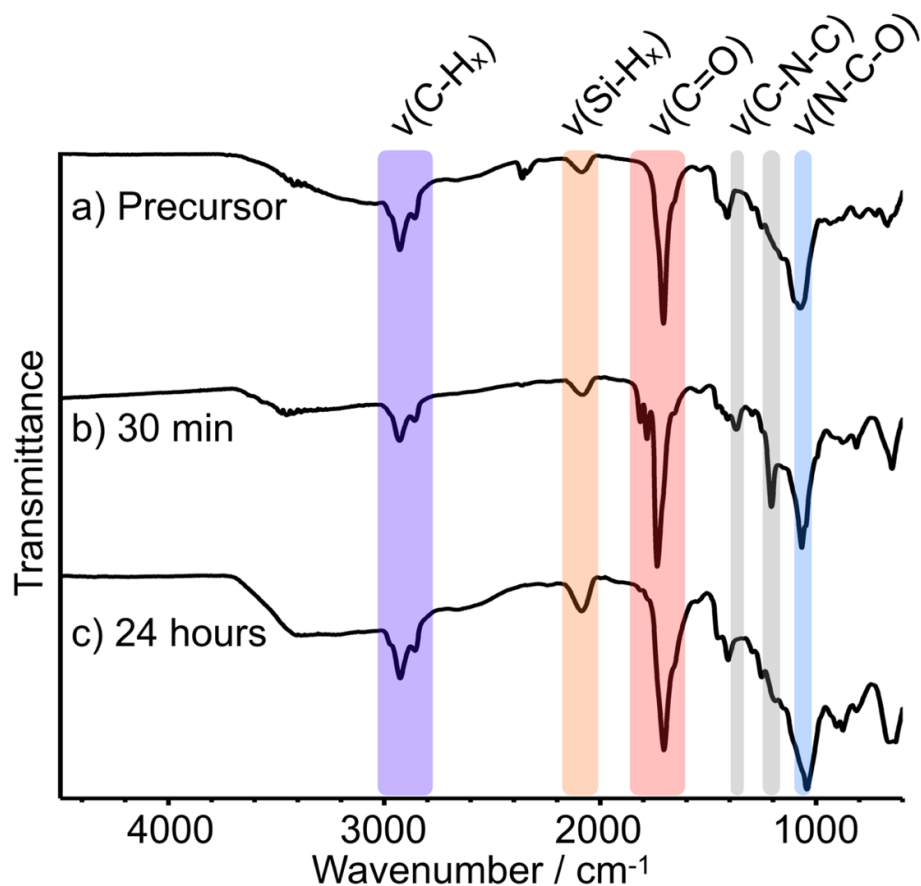


**Figure S15.** FTIR spectra of SiNCs. a) FTIR spectrum of the precursor solution before addition of EDC. Si-H<sub>x</sub> peaks at ~2100, 906 and 660 cm<sup>-1</sup>; broad Si-O band centered at 1050 cm<sup>-1</sup>, hexanoic acid functionalized SiNCs alkyl peaks between 2825-2955 cm<sup>-1</sup> (C-H<sub>2</sub> and C-H<sub>3</sub>), at 1450 cm<sup>-1</sup> and 1408 cm<sup>-1</sup> (C-H δ-deformation); Carbonyl peak at 1705 cm<sup>-1</sup> (C=O) together with a broad O-H peak between 3500-2500 cm<sup>-1</sup>. b) FTIR spectrum of the precursor solution 30 min after 7 mM EDC addition. The NHS ester additional peaks appear at 1814, 1784, and 1738 cm<sup>-1</sup> originating from the carbonyl groups of the NHS ester. In addition, characteristic signals of the succinimide cycle were observed at 1370 cm<sup>-1</sup> vs(C-N-C), 1206 cm<sup>-1</sup> vs(C-N-C), and 1065 cm<sup>-1</sup> vs(N-C-O). c) FTIR spectrum 24 hours after EDC addition. The signals of SiNCs with hexanoic acid surface groups have reappeared.

## Time-lapse Photography

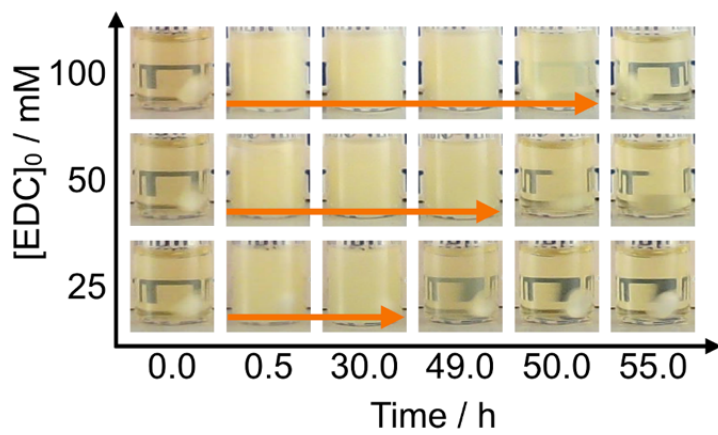


**Figure SI6.** Photographs at different points in time during a dissipative cycle initiated by addition of 25, 50 and 100 mM of EDC to SiNC solutions.

## Lifetime against concentration EDC

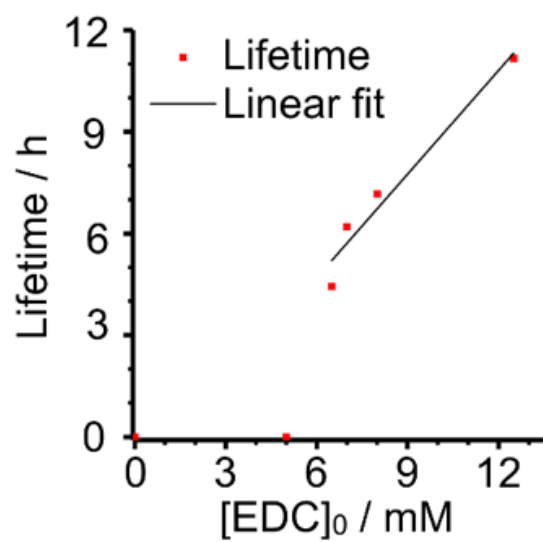


**Figure S17.** The lifetime of the transient SINC clusters as a function of the initial EDC concentration added. The lifetime was determined by UV-Vis spectroscopy.

## Confocal fluorescent microscopy

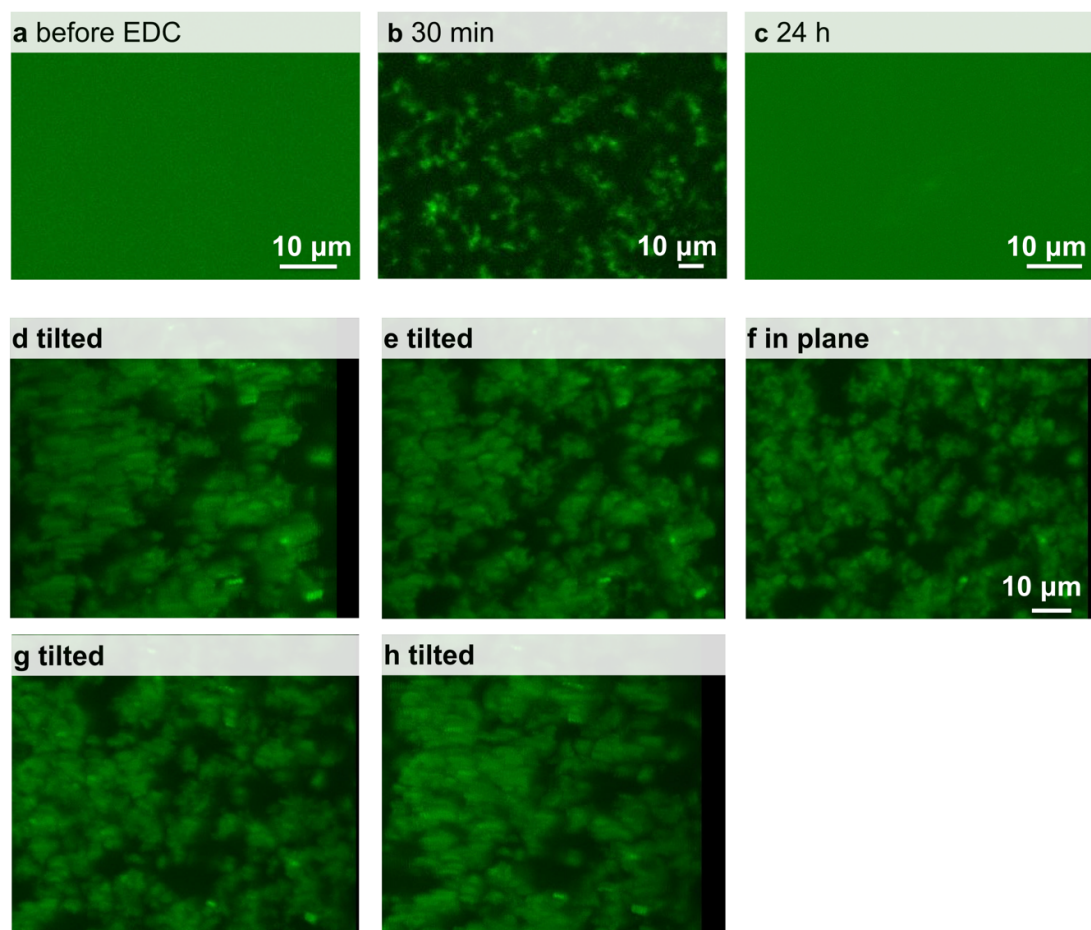


**Figure S18.** Fluorescent micrographs acquired before (a) and 30 min (b) and, 24 h (c) after the addition of 7 mM EDC. d-h) 3D projection of the clusters.

## Fourier-transform Infrared Spectroscopy

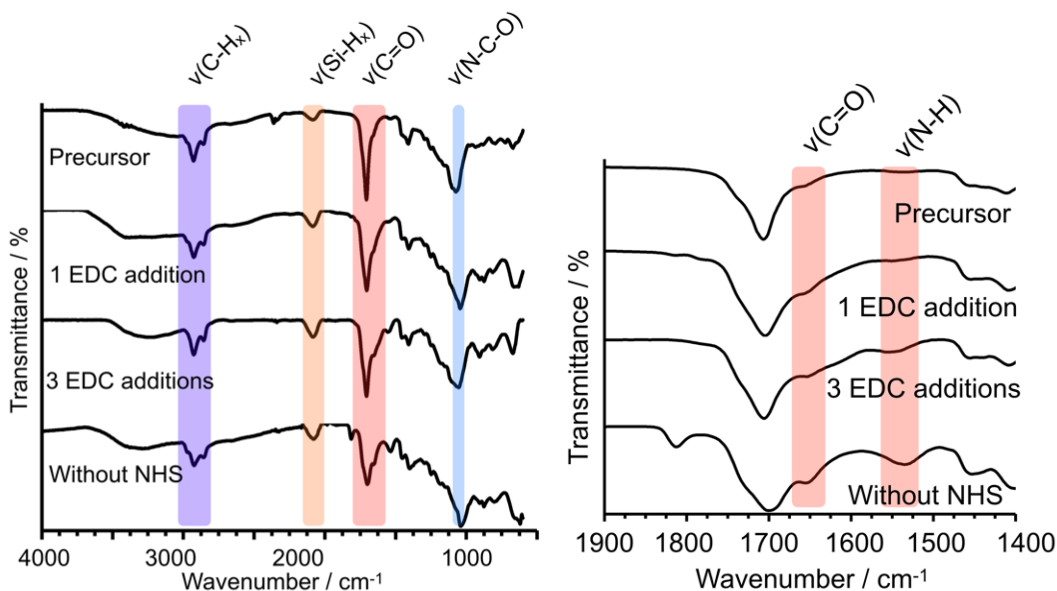


**Figure S19.** FTIR spectra of SiNC Precursor. **Precursor**) FTIR spectrum of the precursor solution before addition of EDC. Si-H<sub>x</sub> peaks at ~2100, 906 and 660 cm<sup>-1</sup>; broad Si-O band centered at 1050 cm<sup>-1</sup>, hexanoic acid functionalized SiNCs alkyl peaks between 2825-2955 cm<sup>-1</sup> (C-H<sub>2</sub> and C-H<sub>3</sub>), at 1450 cm<sup>-1</sup> and 1408 cm<sup>-1</sup> (C-H δ-deformation); Carbonyl peak at 1705 cm<sup>-1</sup> (C=O) together with a broad O-H peak between 3500-2500 cm<sup>-1</sup>. **1 EDC addition**) FTIR spectrum of the precursor solution 24 h after 7 mM EDC addition. Slightly broadened peaks compared to the precursor spectra. **3 EDC additions**) FTIR spectrum of the precursor solution 24 h after the third 7 mM EDC addition. Slightly broadened peaks compared to the precursor spectra and new peaks at 1650 and 1535 cm<sup>-1</sup>, which we assigned to v(amide C=O) and v(amide N-H) of N-Acylurea. **Without NHS**) FTIR spectrum 24 hours after EDC addition to Precursor solution without NHS. In the spectra without NHS we see peaks at 1650 and 1535 cm<sup>-1</sup>, which we assigned to v(amide C=O) and v(amide N-H) of N-Acylurea. Another peak appears at 1815 cm<sup>-1</sup>, which we assigned to anhydride formation. In addition, the carbonyl peak at 1705 cm<sup>-1</sup> is also measured.

## UV/Vis as a function of time with different EDU concentrations

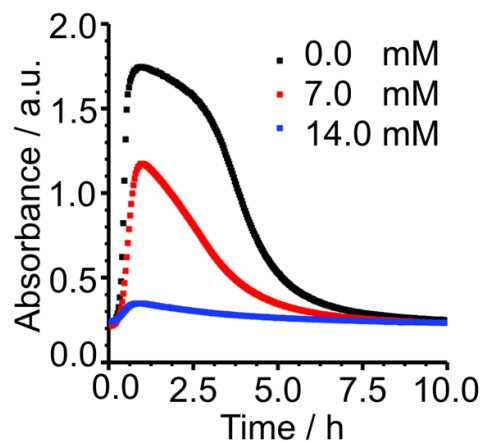


**Figure SI10.** UV-Vis absorbance at 500 nm as a function of time as a quantification of turbidity induced by addition of 7 mM EDC. The turbidity is a measure for cluster formation. The different EDU concentrations (black 0.0 mM, red 7.0 and blue 14.0 mM) represent the waste accumulation for the cycle experiment after 0, 1 and 2 cycles. EDU decreases the UV absorbance drastically with increasing concentration.

## UV/Vis as a function of time under Argon atmosphere

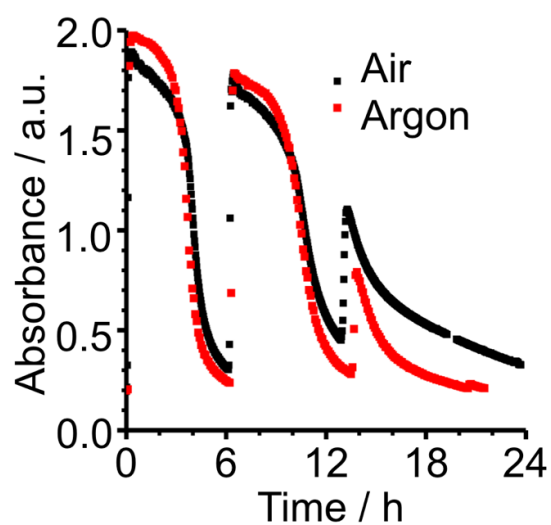


**Figure SI11.** UV-Vis absorbance at 500 nm as a function of time as a quantification of turbidity induced by addition of 7 mM EDC. The turbidity is a measure for cluster formation. The argon sample was synthesized and measured under argon atmosphere with degassed solvents. The air sample was synthesized as described.



## Viability assay

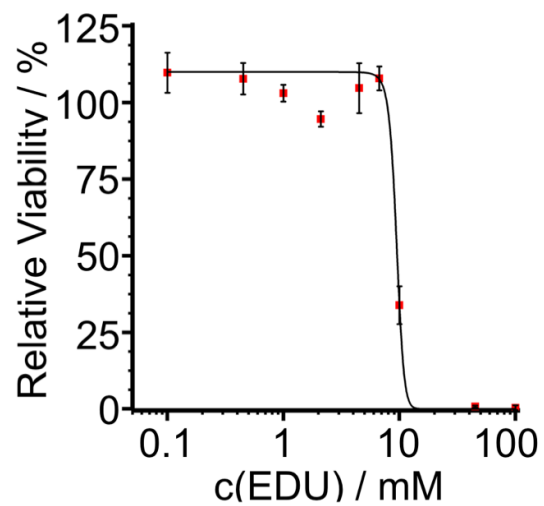


**Figure S112.** Viability assay. Relative viability against EDU concentration. After 6.7 mM EDU viability starts to decrease.  $IC_{50}$ : 9.5 mM EDU.

## Microscopy of COS-7 cells

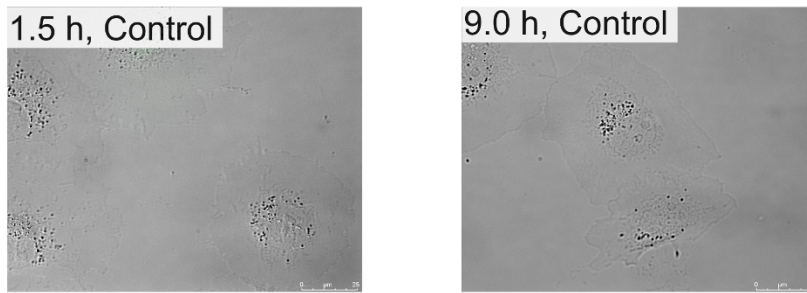


**Figure SI13: Fluorescence microscopy images of COS-7 cells.** Cells incubated without SiNCs as a control experiment.

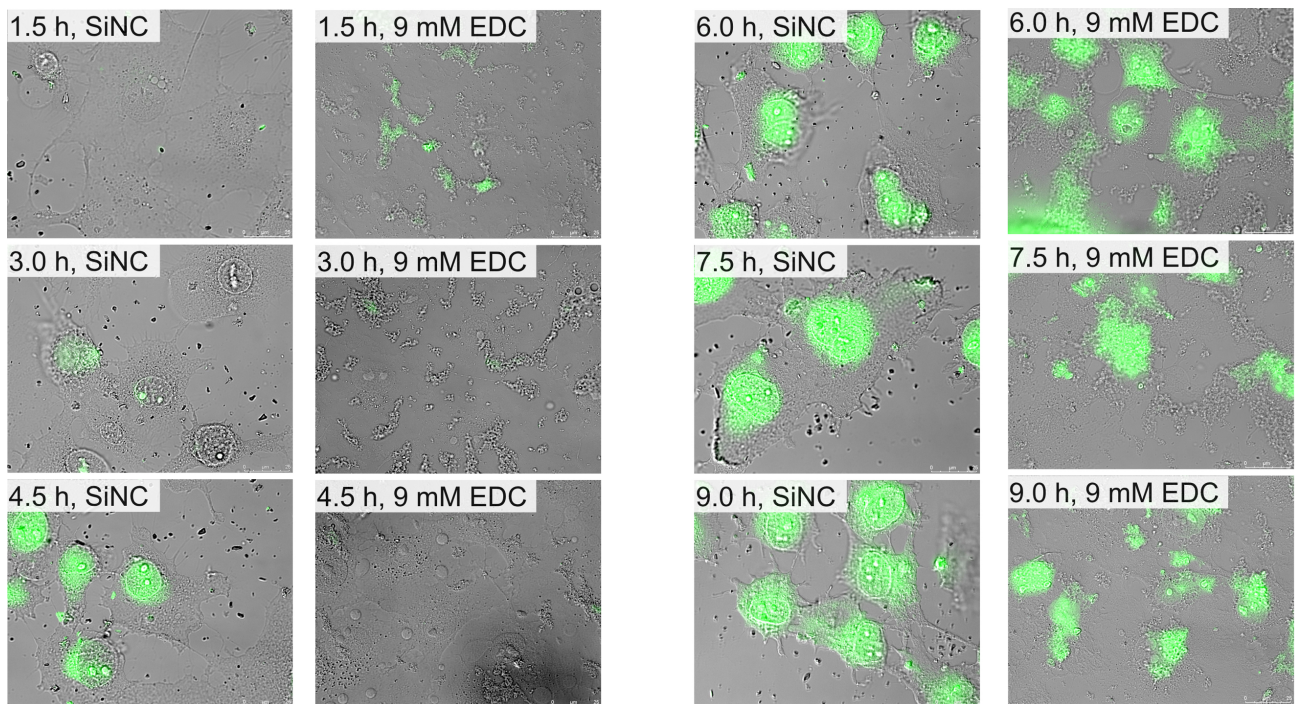


**Figure SI14: Fluorescence microscopy images of COS-7 cells.** Cells incubated with SiNCs. In the left column, cells are incubated with untreated SiNCs. In the right column cells are incubated with SiNCs that have been treated with 9 mM EDC for 30 minutes prior to the incubation.

We chose a threshold of 50 a.u. above the background for the mean fluorescent intensity to count cells with a significant uptake of SiNCs.

## UV/Vis as a function of time under cell-experiment conditions

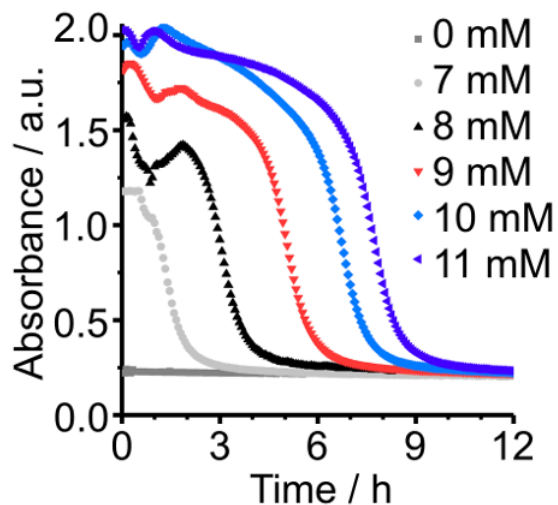


**Figure SI15.** UV-Vis absorbance at 500 nm as a function of time as a quantification of turbidity induced by addition of different concentrations of EDC (0.0, 7.0, 8.0, 9.0, 10.0, and 11.0). The turbidity is a measure for cluster formation. The conditions were used to mimic the cell experiment's environment, i.e., EDC was added 30 min prior to mixing the SiNC cluster solution with PBS in a 1 to 1 ration. The experiment was carried out at 25°C for the first 30 min and then continued at 37°C.

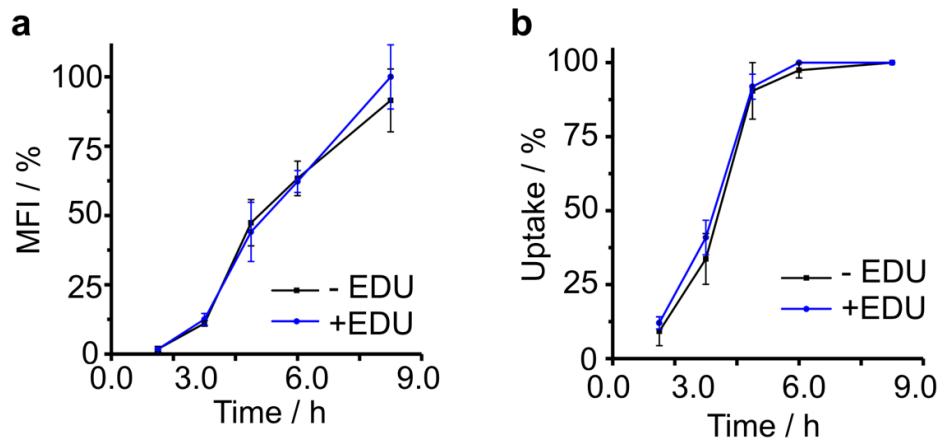


**Figure SI16.** a) Mean fluorescence intensity of the nucleus as a function of time for cells incubated with SiNCs and SiNCs + 9 mM EDU. The highest uptake after 9 hours is set to 100%. b) Percentage of cells that have taken up a significant amount of SiNCs, i.e., with a nucleus intensity above the threshold level of 10 a.u.. Both experiments show that the presence of EDU does not change the uptake of the SiNCs

### 3. Materials

5-Hexenoic acid, hydrofluoric acid (HF, 48%) ethanol, N-Hydroxysuccinimide (NHS), 1-ethyl-3-(3-dimethylaminopropyl)carbodiimide (EDC), and 2-(N-morpholino) ethanesulfonic acid (MES) were purchased from Sigma-Aldrich. Azobisisobutyronitrile (AIBN) was bought from Fluka. All chemicals were used without further purification, except for NHS which was recrystallized twice. Dry toluene was obtained from a MBraun SPS 800 solvent purification system with Argon 5.0 as the operating gas. Water was obtained from a Milli-Q water purifier system.

### 4. Experimental Details

**Synthesis of the SiNC/SiO<sub>2</sub> composite.** The SiNCs were prepared via thermolysis of polymeric hydrogen silsesquioxane (HSQ) which was synthesized following a literature procedure.<sup>[2]</sup> After the synthesis, HSQ (7 g) was weighed in a quartz reaction boat, placed in to a Nabertherm RD 30/200/11 furnace with quartz working tube and heated from room temperature to a peak processing temperature of 1100 °C with 18 °C/min heating rate in a slightly reducing atmosphere (5% H<sub>2</sub>/95% N<sub>2</sub>). The sample was kept at 1100 °C for 1 h. A brown solid was obtained and ground into a fine powder using a mortar and pestle. Then the composite was shaken in ethanol for 24h with high-purity silica beads using a WAB Turbula mixer for further grinding. The resulting SiNC/SiO<sub>2</sub> composite was dried in vacuo and stored in glass vials.

**Liberation of Hydride-Terminated SiNCs.** Free-standing, hydride terminated SiNCs with an average diameter of  $3.6 \pm 0.5$  nm are obtained upon etching this composite with an ethanol:water:HF (1:1:1) mixture and final extraction into toluene. 150 mg of the SiNC/SiO<sub>2</sub> composite was weighed into an ethylene-tetrafluoroethylene beaker equipped with a Teflon-coated stir bar. Ethanol (1.5 mL) and water (1.5 mL) were then

added, and stirred to form a brown suspension. 1.5 ml 49% HF aqueous solution was added, and the composite is etched for 30 min. Hydride-terminated SiNCs were subsequently extracted from the aqueous layer into ca. 15 mL of toluene by multiple (i.e., 3 × 5 mL) extractions. The SiNC-toluene suspension was centrifuged in an ETFE-centrifuge tube at 9000 rpm for 5 mins. To remove any residual water/ethanol, extracted particles dispersed in 5 ml dry toluene and centrifuged once more.

**Surface Functionalization of SiNCs.** Freshly etched, hydride-terminated SiNCs were dispersed in 0.5 ml dry toluene and transferred to a Schlenk flask equipped with a stirring bar. 10 mg AIBN was dissolved in 0.5 ml dry toluene and added to the reaction flask. Upon addition of 0.3 ml 5-hexenoic acid, the reaction mixture was degassed 3 times via freeze-thaw cycles. The flask was filled with argon and placed in a 70°C oil bath for 16 hours. At the end of the reaction, functionalized SiNCs were purified by 3 centrifugation/dispersion cycles with ethanol and pentane. Resulting SiNCs were readily dispersible in ethanol.

**Determination of the concentration of surface bonded –COOH groups.** A fraction of 10% of the obtained SiNCs was dispersed in water and the pH was set to pH 10.5 by addition of concentration NaOH. It was titrated against HCl (0.01 M) to determine the pKa and the number of carboxylates on the SiNC surface in the sample (See Fig. S11).

**Reaction conditions for the dynamic self-assembly.** The remaining fraction (90%) of the SiNCs were dispersed in degassed MES Buffer (0.2 M, pH = 6.5) with 100mM NHS to yield a 5 mM solution of carboxylates surface groups. SiNC solution referred from here on has this concentration.

All measurements and reactions were performed with freshly synthesized SiNCs and under stirring with 600 rpm if not stated otherwise.

**Photoluminescence spectroscopy (PL).** PL spectra were measured with an AVA-Spec 2048 from Avantes using a Prizmatix (LED Current controller) as the light source.

**Dynamic light scattering (DLS).** DLS measurements were performed using a Zetasizer Nano ZS from Malvern with a laser wavelength of 633 nm. The SiNCs solutions were measured using disposable cuvettes (PS). Each measurement consisted of 6 acquisitions with an acquisition time of 20 s.

**Cryogenic-Transmission Electron Microscopy (cryo-TEM).** Samples for cryo-TEM were prepared as described above. Shortly before imaging, the samples were diluted a 20-fold to decrease the density of SiNCs in the micrographs. Cryo-TEM imaging was performed on a Tecnai Spirit microscope (FEI/Thermo Fisher) operating at 120 kV. The grids (C-Flat R1.2/1.3, 400 mesh, Cu) were freshly glow-discharged for 90 seconds prior to use. Preparation of the grids was performed in a FEI/Thermo Fisher Vitrobot at 25 °C with the relative humidity set to 100%. The sample was incubated for 30 seconds on the grid, blotted for 2 seconds (blotting force set to -1) and then directly plunged into liquid ethane that was pre-cooled by liquid nitrogen. The cryo-TEM grids were transferred and stored in liquid nitrogen, and when needed, placed into a Gatan cryo-transfer-specimen holder to insert into the microscope. The specimen temperature was maintained at -170 °C during the data collection. The images were recorded in a low-dose mode on a CCD camera.

**Fourier-Transform Infrared Spectroscopy (FTIR).** FTIR spectra were obtained of the SiNCs. First, the SiNCs were isolated by acidifying the reaction solution of the samples before or after a cycle. To isolate the SiNCs during a cycle, EDC was added and the SiNCs were allowed to aggregate into their clusters. Then the aggregated SiNCs were centrifuged, the supernatant was removed and the SiNCs were redispersed in

ethanol/pentane. The centrifugation and dispersion steps were performed three times to obtain a pellet of precipitated particles. The SiNCs were then dried on the measurement-crystal of the Bruker Vertex 70 FTIR using a Platinum ATR from Bruker.

In order to obtain information on the interaction of the surface –COOH groups with EDC and NHS, two control experiments were performed. First, only NHS was added to the SiNCs solution. In the absence of the EDC, NHS does not react with the surface as the spectrum of SiNCs only exhibit signals correlated to hexanoic acid groups. In the second experiment, only EDC was added to the SiNCs solution. In this case, first O-Acylurea forms as the –OH of the carboxyl group adds to EDC. O-Acylurea then can yield 2 different products: i.) An anhydride due to a reaction with a neighboring carboxyl group ii.) N-acylurea via intramolecular rearrangement of an acyl functionality. The bands in FTIR spectrum may relate to the formation of N-acylurea, as the signals at  $1727\text{ cm}^{-1}$  vs(C=O, N-acylurea),  $1647\text{ cm}^{-1}$  vs(C=O, peptide (amide I) and  $1531\text{ cm}^{-1}$  (peptide N-H bending (amide II)). At the same time, the peak at  $1815\text{ cm}^{-1}$  can also be assigned to anhydride C=O. Both possible products seem to coexist at the surface of SiNCs.

**High Pressure Liquid Chromatography (HPLC).** The kinetics of the chemical reaction networks were monitored over time by means of analytical HPLC (HPLC, Thermofisher Dionex Ultimate 3000, Hypersil Gold 250 x 4.8 mm, 25°C). A 400  $\mu\text{L}$  sample was prepared as described above, filtered with a 25 mm syringe filter (w/200  $\mu\text{m}$  polyethersulfone) and placed into a screw cap HPLC vial. Every 10 minutes, samples of the freshly filtered solutions were directly injected without further dilution, and all compounds involved were separated using a linear gradient water: ACN from 100:0 to 70:30. Calibration curves for EDC ( $\lambda = 220\text{ nm}$ ) were performed in duplicate in order to quantify the compound over time.



**Time-lapse photography.** In a 1 ml HPLC vial 600  $\mu$ l of SiNC solution were stirred in front of a camera. A picture was taken every two minutes. EDC (1 M water solution) was added according to the concentrations of each sample.

**Fluorescent Microscopy.** For each time (before EDC, 30, 90 min, 24h), a fresh aliquot (20  $\mu$ L) of the sample was placed on a microscope slide, covered with a 12 mm diameter coverslip and imaged within the first minute. A Leica DMI8 inverted wide-field microscope (100x objective) with DIC and GFP filters (Exc. BP 470/40; Em. BP 525/50; DC 495) was used.

**Confocal Fluorescence Microscopy.** Confocal fluorescence microscopy was performed on a Leica SP5 confocal microscope using a 63x oil immersion objective. Samples were prepared as described above for the fluorescent microscopy. 20  $\mu$ L (timepoints: before EDC, 30 min, 24 h after) of the sample was deposited in a circle of grease on the glass slide and covered with a 12 mm diameter coverslip. Samples were excited with 543 nm laser and imaged at 580-700 nm.

**Cell-based experiments.** COS-7 cells were grown in Dulbecco's Modified Eagle's Medium (DMEM) containing L-Ala-L-Gln (AQmedia, Sigma-Aldrich) supplemented with 10% (v/v) fetal bovine serum (Biochrom) and a 1% (v/v) antibiotic-antimycotic solution (25  $\mu$ g/ml amphotericin B, 10 mg/ml streptomycin, and 10,000 units of penicillin) at 37°C in a humidified 5% CO<sub>2</sub> atmosphere. 24 hours prior to the experiments, cells were seeded at 80% confluency on a  $\mu$ -slide 8-well plate (ibidi) and further incubated at 37°C with 5% CO<sub>2</sub>. Either SiNC or self-assembled SiNC (i.e. SiNC incubated with 9mM EDC for 30 minutes) were added to cells in a 1:1 dilution with DPBS and incubated for the indicated time points. Cells treated with only DPBS served as a control to estimate viability, stress levels and the background fluorescence. After addition of SiNC, cells were washed twice with DMEM without phenol red (Gibco) containing 10% (v/v) fetal

bovine serum, 2 mM Glutamax™ (Gibco), pyruvate and 25 mM HEPES. Cells were then monitored on a 37°C-heated stage using a Leica DMI8 inverted wide-field microscope (63x objective) with DIC and GFP filters ( $\lambda_{\text{exc}}$ . BP 470/40;  $\lambda_{\text{em}}$ . BP 525/50; DC 495).

To quantify the cell uptake of the SiNCs the mean fluorescence of the nucleus was measured. A threshold values of 50 a.u. above the background fluorescence of the control cells was chosen as significant uptake. Above this value, the cell was consider to have taken up SiNCs.

**Viability Assay.** COS-7 cells were incubated at 37°C with 5% CO<sub>2</sub> for 9 hours in PBS/MES-buffer with different EDU concentrations (0.0, 0.1, 0.45, 1.0, 2.1, 4.5, 6.7, 10.0, 45.0, 100.0 mM). The media was exchanged for DMEM with 0.5 mg/ml Methylthiazolyldiphenyl-tetrazolium bromide (MTT) as a yellow dye that is converted into a water insoluble formazan. After three hours the media is exchanged for DMSO to liberate the formazan crystals and 30 min later the absorbance is measured at 570 nm (background (630 nm) subtracted).

## 5. References

- [1] a) S. L. Anderson, E. J. Lubber, B. C. Olsen, J. M. Buriak, Chem. Mater. **2016**, 28, 5973; b) C. J. Murphy, J. M. Buriak, Chem. Mater. **2015**, 27, 4911.
- [2] H. M. Bank, M. E. Cifuentes, E. M. Theresa, United States Pat. **1991**, 5.

## 5 Summary and Outlook

In the first project of this PhD thesis, surface functionalization of hydride-terminated SiNCs using organolithium and Grignard reagents was presented. This reaction is suggested to proceed through the cleavage of surface Si – Si bonds due to the nucleophilic attack of organolithium reagents. As a result, a Si – C bond is formed, neighboring to Si – Li groups which can be quenched by electrophiles. This reaction is capable of functionalizing SiNCs at room temperature in short reaction times. With this method, aryl and alkynyl(aryl) conjugated molecules could be directly grafted to the surface of SiNCs. We observed that the PL of SiNCs could be red-shifted between 685-800 nm solely *via* surface functionalization with different alkynyl(aryl) (phenylacetylene, 2-ethynyl-naphthalene, 2-ethynyl-5-hexylthiophene) surface groups. Tunneling spectra showed the presence of in-gap states for every alkynyl(aryl) functionalized SiNC. Therefore, the observed PL red-shifts were attributed to an emission pathway involving these in-gap states that decreased the effective band gap for recombination. To be able to explain the mechanism behind this observation, *ab-initio* calculations on model Si clusters were performed. The results suggested that the in-gap states originated as interface states from excited electronic antibonding ( $\pi^*$ ) states located on the alkynyl bond which strongly couple to the SiNC. These outcomes provided a likely mechanism for the observed PL shifts with alkynyl(aryl) surface groups: Excitation of the QD core states is followed by non-radiative relaxation to bright  $\pi^*$  interface states (in-gap state) which are conjugated with the alkynyl(aryl) moiety. This transfer likely occurs *via* an electronic barrier surpassing a second, dark  $\pi^*$  state also originating from the triple bond, which interacts directly with the SiNC states. A subsequent transition to the ground state then accounts for the red-shifted PL emission.

The influence of surface characteristics obtained by different functionalization methods on the performance of Si-LEDs was studied. We found that hexyl functionalized SiNCs prepared with organolithium reagents have lower surface coverage and a higher QY than the ones functionalized *via* hydrosilylation. As a result, LEDs built on SiNCs functionalized with organolithium reagents exhibited lower turn-on voltages, higher luminance and external quantum efficiencies. These improvements were attributed to the less dense and monolayer surface coverage, which reduced the resistance of the SiNCs films. Higher absolute quantum yield observed for SiNCs prepared with organolithium reagents was also beneficial.

In the last project, dissipative self-assembly of SiNCs was studied. In this system, upon addition of a chemical fuel, free-standing SiNCs started to assemble into clusters. These assemblies were not stable and therefore they reverted back to single SiNCs when the whole fuel was consumed. Lifetimes of the assemblies could be tuned by the amount of fuel added and several cycles could have been induced. We utilized this system to demonstrate time-delayed uptake of SiNCs by COS-7 cells. This principle can potentially pave the way to time-delayed drug delivery systems which simultaneously offer the possibility for bioimaging.

The results presented in this PhD thesis broaden the understanding on the effects of aromatic surface groups on optical properties and electronic structure of SiNCs. As a next step, the influence of conjugated surface groups on the electronic properties (*i.e.*, charge transport rate and mechanism) of SiNCs could be investigated. Establishing such a relationship through systematic electronic measurements would be a very important step to tune the SiNC properties to facilitate high efficiency target devices.

In this work, the performance of Si-LEDs was improved by functionalizing the SiNCs with organolithium reagents which offer favorable surface characteristics such as lower barrier for charge transfer and high quantum yield. Instead of hexyl groups, SiNCs functionalized with conjugated surface groups could be utilized. Performance of such devices could be compared to ones with hexyl functionalized SiNCs, to observe the influence of conjugation on the device efficiency.

Time-delayed uptake of SiNCs was achieved through dissipative self-assembly induced by a chemical fuel. As a next step, the surface of SiNCs can be decorated with therapeutics or other biologically active materials, to test drug-delivery mechanisms.

## Bibliography

1. Dasog, M.; Kehrle, J.; Rieger, B.; Veinot, J. G. C. Silicon Nanocrystals and Silicon-Polymer Hybrids: Synthesis, Surface Engineering, and Applications. *Angew. Chem. Int. Ed.* **2016**, *55*, 2322–2339.
2. Barbagioanni, E. G.; Lockwood, D. J.; Simpson, P. J.; Goncharova, L. V. Quantum Confinement in Si and Ge Nanostructures. *J. Appl. Phys.* **2012**, *111*, 034307.
3. Wolf, O.; Dasog, M.; Yang, Z.; Balberg, I.; Veinot, J. G. C.; Millo, O. Doping and Quantum Confinement Effects in Single Si Nanocrystals Observed by Scanning Tunneling Spectroscopy. *Nano Lett.* **2013**, *13*, 2516–2521.
4. Wen, X.; Zhang, P.; Smith, T. A.; Anthony, R. J.; Kortshagen, U. R.; Yu, P.; Feng, Y.; Shrestha, S.; Coniber, G.; Huang, S. Tunability Limit of Photoluminescence in Colloidal Silicon Nanocrystals. *Sci. Rep.* **2015**, *5*, 12469.
5. Dasog, M.; De los Reyes, G. B.; Titova, L. V.; Hegmann, F. A.; Veinot, J. G. C. Size vs Surface: Tuning the Photoluminescence of Freestanding Silicon Nanocrystals Across the Visible Spectrum via Surface Groups. *ACS Nano* **2014**, *8*, 9636–9648.
6. Zhou, T.; Anderson, R. T.; Li, H.; Bell, J.; Yang, Y.; Gorman, B. P.; Pylypenko, S.; Lusk, M. T.; Sellinger, A. Bandgap Tuning of Silicon Quantum Dots by Surface Functionalization with Conjugated Organic Groups. *Nano Lett.* **2015**, *15*, 3657–3663.
7. Dohnalová, K.; Gregorkiewicz, T.; Kůsová, K. Silicon quantum dots: Surface matters. *J. Phys.: Condens. Matter.* **2014**, *26*, 173201.
8. Erogbogbo, F.; Yong, K.-T.; Roy, I.; Xu, G.; Prasad, P. N.; Swihart, M. T. Biocompatible Luminescent Silicon Quantum Dots for Imaging of Cancer Cells. *ACS Nano* **2008**, *2*, 873–878.
9. Liu, J.; Erogbogbo, F.; Yong, K.-T.; Ye, L.; Liu, J.; Hu, R.; Chen, H.; Hu, Y.; Yang, Y.; Yang, J. *et al.* Assessing Clinical Prospects of Silicon Quantum Dots: Studies in Mice and Monkeys. *ACS Nano* **2013**, *7*, 7303–7310.
10. Maier-Flaig, F.; Rinck, J.; Stephan, M.; Bocksrocker, T.; Bruns, M.; Kübel, C.; Powell, A. K.; Ozin, G. A.; Lemmer, U. Multicolor Silicon Light-Emitting Diodes (SiLEDs). *Nano Lett.* **2013**, *13*, 475–480.
11. Dutta, M.; Thirugnanam, L.; van Trinh, P.; Fukata, N. High Efficiency Hybrid Solar Cells Using Nanocrystalline Si Quantum Dots and Si Nanowires. *ACS Nano* **2015**, *9*, 6891–6899.
12. Gonzalez, C. M.; Veinot, J. G. C. Silicon Nanocrystals for the Development of Sensing Platforms. *J. Mater. Chem. C* **2016**, *4*, 4836–4846.
13. Cheng, X.; Lowe, S. B.; Reece, P. J.; Gooding, J. J. Colloidal Silicon Quantum Dots: From Preparation to the Modification of Self-Assembled Monolayers (SAMs) for Bio-Applications. *Chem. Soc. Rev.* **2014**, *43*, 2680–2700.

14. Yang, Z.; Gonzalez, C. M.; Purkait, T. K.; Iqbal, M.; Meldrum, A.; Veinot, J. G. C. Radical Initiated Hydrosilylation on Silicon Nanocrystal Surfaces: An Evaluation of Functional Group Tolerance and Mechanistic Study. *Langmuir* **2015**, *31*, 10540–10548.
15. Yang, Z.; Iqbal, M.; Dobbie, A. R.; Veinot, J. G. C. Surface-induced Alkene Oligomerization: Does Thermal Hydrosilylation Really Lead to Monolayer Protected Silicon Nanocrystals? *J. Am. Chem. Soc.* **2013**, *135*, 17595–17601.
16. Reboredo, F. A.; Galli, G. Theory of Alkyl-Terminated Silicon Quantum Dots. *J. Phys. Chem. B* **2005**, *109*, 1072–1078.
17. Li, Q. S.; Zhang, R. Q.; Niehaus, T. A.; Frauenheim, T.; Lee, S. T. Theoretical Studies on Optical and Electronic Properties of Propionic-Acid-Terminated Silicon Quantum Dots. *J. Chem. Theory Comput.* **2007**, *3*, 1518–1526.
18. Mastronardi, M. L.; Henderson, E. J.; Puzzo, D. P.; Chang, Y.; Wang, Z. B.; Helander, M. G.; Jeong, J.; Kherani, N. P.; Lu, Z.; Ozin, G. A. Silicon Nanocrystal OLEDs: Effect of Organic Capping Group on Performance. *Small* **2012**, *8*, 3647–3654.
19. Li, Q. S.; Zhang, R. Q.; Lee, S. T.; Niehaus, T. A.; Frauenheim, T. Optimal Surface Functionalization of Silicon Quantum Dots. *J. Chem. Phys.* **2008**, *128*, 244714.
20. Dung, M. X.; Tung, D. D.; Jeong, S.; Jeong, H.-D. Tuning optical properties of Si quantum dots by  $\pi$ -conjugated capping molecules. *Chem. Asian J.* **2013**, *8*, 653–664.
21. Buriak, J. M. Organometallic Chemistry on Silicon and Germanium Surfaces. *Chem. Rev.* **2002**, *102*, 1271–1308.
22. Nadler, E. B.; Rappoport, Z. Hexamethyldisilane as a Source of Both Trimethylsilyl and Pentamethyldisilyl Anions. Formation of a Substituted Pentamethyldisilyl Stable Enol. *Tetrahedron Lett.* **1990**, *31*, 555–558.
23. Song, J. H.; Sailor, M. J. Functionalization of Nanocrystalline Porous Silicon Surfaces with Aryllithium Reagents: Formation of Silicon–Carbon Bonds by Cleavage of Silicon–Silicon Bonds. *J. Am. Chem. Soc.* **1998**, *120*, 2376–2381.
24. Song, J. H.; Sailor, M. J. Reaction of Photoluminescent Porous Silicon Surfaces with Lithium Reagents To Form Silicon–Carbon Bound Surface Species. *Inorg. Chem.* **1999**, *38*, 1498–1503.
25. Höhlein, I. M. D.; Angi, A.; Sinelnikov, R.; Veinot, J. G. C.; Rieger, B. Functionalization of Hydride-Terminated Photoluminescent Silicon Nanocrystals with Organolithium Reagents. *Chem. Eur. J.* **2015**, *21*, 2755–2758.
26. Angi, A.; Sinelnikov, R.; Meldrum, A.; Veinot, J. G. C.; Balberg, I.; Azulay, D.; Millo, O.; Rieger, B. Photoluminescence Through In-gap States in Phenylacetylene Functionalized Silicon Nanocrystals. *Nanoscale* **2016**, *8*, 7849–7853.
27. Banin, U.; Millo, O. Tunneling and Optical Spectroscopy of Semiconductor Nanocrystals. *Annu. Rev. of Phys. Chem.* **2003**, *54*, 465–492.

28. Angi, A.; Sinelnikov, R.; Heenen, H.; Meldrum, A.; Veinot, J.; Scheurer, C.; Reuter, K.; Ashkenazi, O.; Azulay, D.; Balberg, I. *et al.* The influence of Conjugated Alkynyl(aryl) Surface Groups on the Optical Properties of Silicon Nanocrystals: Photoluminescence Through In-gap States. *Nanotechnology*, DOI: 10.1088/1361-6528/aac9ef.
29. Cheng, K.-Y.; Anthony, R.; Kortshagen, U. R.; Holmes, R. J. Hybrid Silicon Nanocrystal-Organic Light-Emitting Devices for Infrared Electroluminescence. *Nano Lett.* **2010**, *10*, 1154–1157.
30. Puzzo, D. P.; Henderson, E. J.; Helander, M. G.; Wang, Z.; Ozin, G. A.; Lu, Z. Visible Colloidal Nanocrystal Silicon Light-Emitting Diode. *Nano Lett.* **2011**, *11*, 1585–1590.
31. Anthony, R. J.; Cheng, K.-Y.; Holman, Z. C.; Holmes, R. J.; Kortshagen, U. R. An All-Gas-Phase Approach for the Fabrication of Silicon Nanocrystal Light-Emitting Devices. *Nano Lett.* **2012**, *12*, 2822–2825.
32. A. Angi, M. Loch, R. Sinelnikov, J. G. C. Veinot, M. Becherer, P. Lugli, B. Rieger. Effect of Surface Functionalization Methods on Performance of Silicon Nanocrystal LEDs. *Nanoscale* **2018**, *10*, 10337–10342.
33. van Rossum, S. A. P.; Tena-Solsona, M.; van Esch, J. H.; Eelkema, R.; Boekhoven, J. Dissipative Out-of-Equilibrium Assembly of Man-made Supramolecular Materials. *Chem. Soc. Rev.* **2017**, *46*, 5519–5535.
34. Tena-Solsona, M.; Rieß, B.; Grötsch, R. K.; Löhrer, F. C.; Wanzke, C.; Käsdorf, B.; Bausch, A. R.; Müller-Buschbaum, P.; Lieleg, O.; Boekhoven, J. Non-equilibrium Dissipative Supramolecular Materials With a Tunable Lifetime. *Nat. Commun.* **2017**, *8*, 15895.
35. Richard P. Feynman. There is Plenty of Room at the Bottom. *Eng. Sci.* **1960**, *22*, 22–36.
36. Kroto, H. W.; Heath, J. R.; O'Brien, S. C.; Curl, R. F.; Smalley, R. E. C60: Buckminsterfullerene. *Nature* **1985**, *318*, 162–163.
37. Iijima, S.; Ichihashi, T. Single-Shell Carbon Nanotubes of 1-nm Diameter. *Nature* **1993**, *363*, 603–605.
38. Brus, L. E. A Simple Model for the Ionization Potential, Electron Affinity, and Aqueous Redox Potentials of Small Semiconductor Crystallites. *J. Chem. Phys.* **1983**, *79*, 5566–5571.
39. Brus, L. E. Electron–Electron and Electron-Hole Interactions in Small Semiconductor Crystallites: The Size Dependence of the Lowest Excited Electronic State. *J. Chem. Phys.* **1984**, *80*, 4403–4409.
40. Alivisatos, A. P. Semiconductor Clusters, Nanocrystals, and Quantum Dots. *Science* **1996**, *271*, 933–937.
41. Takagahara, T.; Takeda, K. Theory of the Quantum Confinement Effect on Excitons in Quantum Dots of Indirect-Gap Materials. *Phys. Rev. B* **1992**, *46*, 15578–15581.



42. Mazzaro, R.; Romano, F.; Ceroni, P. Long-Lived Luminescence of Silicon Nanocrystals: From Principles to Applications. *Phys. Chem. Chem. Phys.* **2017**, *19*, 26507–26526.
43. Kairdolf, B. A.; Smith, A. M.; Stokes, T. H.; Wang, M. D.; Young, A. N.; Nie, S. Semiconductor Quantum Dots for Bioimaging and Biodiagnostic Applications. *Annu. Rev. Anal. Chem.* **2013**, *6*, 143–162.
44. Reed; Randall; Aggarwal; Matyi; Moore; Wetsel. Observation of Discrete Electronic States in a Zero-Dimensional Semiconductor Nanostructure. *Phys. Rev. Lett.* **1988**, *60*, 535–537.
45. Ekimov, A. I.; Efros, A.; Onushchenko, A. A. Quantum Size Effect in Semiconductor Microcrystals. *Solid State Commun.* **1985**, *56*, 921–924.
46. Mansur, H. S. Quantum Dots and Nanocomposites. *Wiley Interdiscip. Rev. Nanomed. Nanobiotechnol.* **2010**, *2*, 113–129.
47. Smith, A. M.; Nie, S. Semiconductor Nanocrystals: Structure, Properties, and Band Gap Engineering. *Acc. Chem. Res.* **2010**, *43*, 190–200.
48. Habas, S. E.; Platt, H. A. S.; van Hest, M. F. A. M.; Ginley, D. S. Low-Cost Inorganic Solar Cells: From Ink to Printed Device. *Chem. Rev.* **2010**, *110*, 6571–6594.
49. Schlamp, M. C.; Peng, X.; Alivisatos, A. P. Improved Efficiencies in Light Emitting Diodes Made with CdSe(CdS) Core/Shell Type Nanocrystals and a Semiconducting Polymer. *J. Appl. Phys.* **1997**, *82*, 5837–5842.
50. Freeman, R.; Willner, I. Optical Molecular Sensing with Semiconductor Quantum Dots (QDs). *Chem. Soc. Rev.* **2012**, *41*, 4067–4085.
51. Frasco, M. F.; Chaniotakis, N. Semiconductor Quantum Dots in Chemical Sensors and Biosensors. *Sensors* **2009**, *9*, 7266–7286.
52. Medintz, I. L.; Uyeda, H. T.; Goldman, E. R.; Mattoussi, H. Quantum Dot Bioconjugates for Imaging, Labelling and Sensing. *Nat. Mater.* **2005**, *4*, 435–446.
53. Ledentsov, N. N.; Ustinov, V. M.; Shchukin, V. A.; Kop'ev, P. S.; Alferov, Z. I.; Bimberg, D. Quantum Dot Heterostructures: Fabrication, Properties, Lasers. *Semiconductors* **1998**, *32*, 343–365.
54. Li, L.-S.; Alivisatos, A. P. Semiconductor Nanorod Liquid Crystals and Their Assembly on a Substrate. *Adv. Mater.* **2003**, *15*, 408–411.
55. Godt, J.; Scheidig, F.; Grosse-Siestrup, C.; Esche, V.; Brandenburg, P.; Reich, A.; Groneberg, D. A. The Toxicity of Cadmium and Resulting Hazards for Human Health. *J. Occup. Med. Toxicol.* **2006**, *1*, 22.
56. Chelikowsky, J. R.; Cohen, M. L. Electronic Structure of Silicon. *Phys. Rev. B* **1974**, *10*, 5095–5107.
57. Canham, L. T. Silicon Quantum Wire Array Fabrication by Electrochemical and Chemical Dissolution of Wafers. *Appl. Phys. Lett.* **1990**, *57*, 1046–1048.

58. Pi, X. D.; Liptak, R. W.; Nowak, J. D.; Wells, N. P.; Carter, C. B.; Campbell, S. A.; Kortshagen, U. Air-Stable Full-Visible-Spectrum Emission From Silicon Nanocrystals Synthesized by an All-Gas-Phase Plasma Approach. *Nanotechnology* **2008**, *19*, 245603.
59. Pucker, G.; Serra, E.; Jestin, Y. Silicon Quantum Dots for Photovoltaics: A Review, Quantum Dots - A Variety of New Applications, Ed: Dr. Ameenah Al-Ahmadi, InTech, **2012**.
60. McVey, B. F. P.; Tilley, R. D. Solution Synthesis, Optical Properties, and Bioimaging Applications of Silicon Nanocrystals. *Acc. Chem. Res.* **2014**, *47*, 3045–3051.
61. Švrček, V.; Rehspringer, J.-L.; Gaffet, E.; Slaoui, A.; Muller, J.-C. Unaggregated Silicon Nanocrystals Obtained by Ball Milling. *J. Cryst. Growth* **2005**, *275*, 589–597.
62. Heintz, A. S.; Fink, M. J.; Mitchell, B. S. Mechanochemical Synthesis of Blue Luminescent Alkyl/Alkenyl-Passivated Silicon Nanoparticles. *Adv. Mater.* **2007**, *19*, 3984–3988.
63. Mangolini, L. Synthesis, Properties, and Applications of Silicon Nanocrystals. *J. Vac. Sci. Technol. B* **2013**, *31*, 20801.
64. Heinrich, J. L.; Curtis, C. L.; Credo, G. M.; Sailor, M. J.; Kavanagh, K. L. Luminescent Colloidal Silicon Suspensions From Porous Silicon. *Science* **1992**, *255*, 66–68.
65. Kang, Z.; Tsang, C. H. A.; Zhang, Z.; Zhang, M.; Wong, N.-b.; Zapien, J. A.; Shan, Y.; Lee, S.-T. A Polyoxometalate-Assisted Electrochemical Method for Silicon Nanostructures Preparation: From Quantum Dots to Nanowires. *J. Am. Chem. Soc.* **2007**, *129*, 5326–5327.
66. Sato, K.; Tsuji, H.; Hirakuri, K.; Fukata, N.; Yamauchi, Y. Controlled Chemical Etching for Silicon Nanocrystals with Wavelength-Tunable Photoluminescence. *Chem. Commun.* **2009**, 3759–3761.
67. Werwa, E.; Seraphin, A. A.; Chiu, L. A.; Zhou, C.; Kolenbrander, K. D. Synthesis and Processing of Silicon Nanocrystallites Using a Pulsed Laser Ablation Supersonic Expansion Method. *Appl. Phys. Lett.* **1994**, *64*, 1821–1823.
68. Patrone, L.; Nelson, D.; Safarov, V. I.; Sentis, M.; Marine, W.; Giorgio, S. Photoluminescence of Silicon Nanoclusters with Reduced Size Dispersion Produced by Laser Ablation. *J. Appl. Phys.* **2000**, *87*, 3829–3837.
69. Shimizu-Iwayama, T.; Fujita, K.; Nakao, S.; Saitoh, K.; Fujita, T.; Itoh, N. Visible Photoluminescence in Si<sup>+</sup>-Implanted Silica Glass. *J. Appl. Phys.* **1994**, *75*, 7779–7783.
70. Mutti, P.; Ghislotti, G.; Bertoni, S.; Bonoldi, L.; Cerofolini, G. F.; Meda, L.; Grilli, E.; Guzzi, M. Room-Temperature Visible Luminescence From Silicon Nanocrystals in Silicon Implanted SiO<sub>2</sub> Layers. *Appl. Phys. Lett.* **1995**, *66*, 851–853.
71. Min, K. S.; Shcheglov, K. V.; Yang, C. M.; Atwater, H. A.; Brongersma, M. L.; Polman, A. Defect-Related Versus Excitonic Visible Light Emission From Ion Beam Synthesized Si Nanocrystals in SiO<sub>2</sub>. *Appl. Phys. Lett.* **1996**, *69*, 2033–2035.

72. Lalic, N.; Linnros, J. Light Emitting Diode Structure Based on Si Nanocrystals Formed by Implantation Into Thermal Oxide. *J. Lumin.* **1998**, *80*, 263–267.
73. Li, X.; He, Y.; Talukdar, S. S.; Swihart, M. T. Process for Preparing Macroscopic Quantities of Brightly Photoluminescent Silicon Nanoparticles with Emission Spanning the Visible Spectrum. *Langmuir* **2003**, *19*, 8490–8496.
74. Li, X.; He, Y.; Swihart, M. T. Surface Functionalization of Silicon Nanoparticles Produced by Laser-Driven Pyrolysis of Silane followed by HF–HNO<sub>3</sub> Etching. *Langmuir* **2004**, *20*, 4720–4727.
75. Hua, F.; Swihart, M. T.; Ruckenstein, E. Efficient surface grafting of luminescent silicon quantum dots by photoinitiated hydrosilylation. *Langmuir* **2005**, *21*, 6054–6062.
76. Mangolini, L.; Thimsen, E.; Kortshagen, U. High-Yield Plasma Synthesis of Luminescent Silicon Nanocrystals. *Nano Lett.* **2005**, *5*, 655–659.
77. Kortshagen, U. Nonthermal Plasma Synthesis of Semiconductor Nanocrystals. *J. Phys. D: Appl. Phys.* **2009**, *42*, 113001.
78. Swihart, M. T. Electron Affinities of Selected Hydrogenated Silicon Clusters (Si<sub>x</sub>H<sub>y</sub>, x = 1–7, y = 0–15) from Density Functional Theory Calculations. *J. Phys. Chem. A* **2000**, *104*, 6083–6087.
79. Jurbergs, D.; Rogojina, E.; Mangolini, L.; Kortshagen, U. Silicon Nanocrystals with Ensemble Quantum Yields Exceeding 60%. *Appl. Phys. Lett.* **2006**, *88*, 233116.
80. Heath, J. R. A Liquid-Solution-Phase Synthesis of Crystalline Silicon. *Science* **1992**, *258*, 1131–1133.
81. Baldwin, R. K.; Pettigrew, K. A.; Ratai, E.; Augustine, M. P.; Kauzlarich, S. M. Solution Reduction Synthesis of Surface Stabilized Silicon Nanoparticles. *Chem. Commun.* **2002**, 1822–1823.
82. Arul Dhas, N.; Raj, C. P.; Gedanken, A. Preparation of Luminescent Silicon Nanoparticles: A Novel Sonochemical Approach. *Chem. Mater.* **1998**, *10*, 3278–3281.
83. Wilcoxon, J. P.; Samara, G. A.; Provencio, P. N. Optical and Electronic Properties of Si Nanoclusters Synthesized in Inverse Micelles. *Phys. Rev. B* **1999**, *60*, 2704–2714.
84. Tilley, R. D.; Yamamoto, K. The Microemulsion Synthesis of Hydrophobic and Hydrophilic Silicon Nanocrystals. *Adv. Mater.* **2006**, *18*, 2053–2056.
85. Bley, R. A.; Kauzlarich, S. M. A Low-Temperature Solution Phase Route for the Synthesis of Silicon Nanoclusters. *J. Am. Chem. Soc.* **1996**, *118*, 12461–12462.
86. Yang, C.-S.; Bley, R. A.; Kauzlarich, S. M.; Lee, H. W. H.; Delgado, G. R. Synthesis of Alkyl-Terminated Silicon Nanoclusters by a Solution Route. *J. Am. Chem. Soc.* **1999**, *121*, 5191–5195.
87. Mayeri, D.; Phillips, B. L.; Augustine, M. P.; Kauzlarich, S. M. NMR Study of the Synthesis of Alkyl-Terminated Silicon Nanoparticles From the Reaction of SiCl<sub>4</sub> with the Zintl Salt, NaSi. *Chem. Mater.* **2001**, *13*, 765–770.

88. Baldwin, R. K.; Pettigrew, K. A.; Garno, J. C.; Power, P. P.; Liu, G.-y.; Kauzlarich, S. M. Room Temperature Solution Synthesis of Alkyl-Capped Tetrahedral Shaped Silicon Nanocrystals. *J. Am. Chem. Soc.* **2002**, *124*, 1150–1151.
89. Zou, J.; Baldwin, R. K.; Pettigrew, K. A.; Kauzlarich, S. M. Solution Synthesis of Ultrastable Luminescent Siloxane-Coated Silicon Nanoparticles. *Nano Lett.* **2004**, *4*, 1181–1186.
90. Pettigrew, K. A.; Liu, Q.; Power, P. P.; Kauzlarich, S. M. Solution Synthesis of Alkyl- and Alkyl/Alkoxy-Capped Silicon Nanoparticles via Oxidation of Mg 2 Si. *Chem. Mater.* **2003**, *15*, 4005–4011.
91. Manhat, B. A.; Brown, A. L.; Black, L. A.; Ross, J. B. A.; Fichter, K.; Vu, T.; Richman, E.; Goforth, A. M. One-step Melt Synthesis of Water Soluble, Photoluminescent, Surface-Oxidized Silicon Nanoparticles for Cellular Imaging Applications. *Chem. Mater.* **2011**, *23*, 2407–2418.
92. Liu, S.-M.; Sato, S.; Kimura, K. Synthesis of Luminescent Silicon Nanopowders Redispersible to Various Solvents. *Langmuir* **2005**, *21*, 6324–6329.
93. Liu, S.-M.; Yang, S.; Sato, S.; Kimura, K. Enhanced Photoluminescence from Si Nano-organosols by Functionalization with Alkenes and Their Size Evolution. *Chem. Mater.* **2006**, *18*, 637–642.
94. Hessel, C. M.; Henderson, E. J.; Veinot, J. G. C. Synthesis, Surface Functionalization, and Properties of Freestanding Silicon Nanocrystals. *Chem. Mater* **2006**, *18*, 6139–6146.
95. H. M. Bank, M. E. Cifuentes, E. M. Theresa. *United States Pat.* **1991**, *5.010.159*.
96. Hühlein, I. M. D. New Methods for the Surface Functionalization of Photoluminescent Silicon Nanocrystals. PhD Dissertation, Technical University of Munich, Germany, 2015.
97. Yang, C.-C.; Chen, W.-C. The Structures and Properties of Hydrogen Silsesquioxane (HSQ) Films Produced by Thermal Curing. *J. Mater. Chem.* **2002**, *12*, 1138–1141.
98. Hessel, C. M.; Reid, D.; Panthani, M. G.; Rasch, M. R.; Goodfellow, B. W.; Wei, J.; Fujii, H.; Akhavan, V.; Korgel, B. A. Synthesis of Ligand-Stabilized Silicon Nanocrystals with Size-Dependent Photoluminescence Spanning Visible to Near-Infrared Wavelengths. *Chem. Mater.* **2012**, *24*, 393–401.
99. Yang, Z.; Dobbie, A. R.; Cui, K.; Veinot, J. G. C. A Convenient Method for Preparing Alkyl-Functionalized Silicon Nanocubes. *J. Am. Chem. Soc.* **2012**, *134*, 13958–13961.
100. Steinert, M.; Acker, J.; Oswald, S.; Wetzig, K. Study on the Mechanism of Silicon Etching in HNO<sub>3</sub> -Rich HF/HNO<sub>3</sub> Mixtures. *J. Phys. Chem. C* **2007**, *111*, 2133–2140.
101. Kang, J. K.; Musgrave, C. B. The Mechanism of HF/H<sub>2</sub>O Chemical Etching of SiO<sub>2</sub>. *J. Chem. Phys.* **2002**, *116*, 275.
102. Trucks; Raghavachari; Higashi; Chabal. Mechanism of HF Etching of Silicon Surfaces: A Theoretical Understanding of Hydrogen Passivation. *Phys. Rev. Lett.* **1990**, *65*, 504–507.

103. Weinberger, B. R.; Peterson, G. G.; Eschrich, T. C.; Krasinski, H. A. Surface Chemistry of HF Passivated Silicon: X-ray Photoelectron and Ion Scattering Spectroscopy Results. *J. Appl. Phys.* **1986**, *60*, 3232–3234.
104. Pereira, R. N.; Rowe, D. J.; Anthony, R. J.; Kortshagen, U. Oxidation of Freestanding Silicon Nanocrystals Probed with Electron spin Resonance of Interfacial Dangling Bonds. *Phys. Rev. B* **2011**, *83*, 155327.
105. Dasog, M.; Bader, K.; Veinot, J. G. C. Influence of Halides on the Optical Properties of Silicon Quantum Dots. *Chem. Mater.* **2015**, *27*, 1153–1156.
106. Barrelet, C. J.; Robinson, D. B.; Cheng, J.; Hunt, T. P.; Quate, C. F.; Chidsey, C. E. D. Surface Characterization and Electrochemical Properties of Alkyl, Fluorinated Alkyl, and Alkoxy Monolayers on Silicon. *Langmuir* **2001**, *17*, 3460–3465.
107. Bley, R. A.; Kauzlarich, S. M.; Davis, J. E.; Lee, H. W. H. Characterization of Silicon Nanoparticles Prepared from Porous Silicon. *Chem. Mater.* **1996**, *8*, 1881–1888.
108. Kelly, J. A.; Shukaliak, A. M.; Fleischauer, M. D.; Veinot, J. G. C. Size-Dependent Reactivity in Hydrosilylation of Silicon Nanocrystals. *J. Am. Chem. Soc.* **2011**, *133*, 9564–9571.
109. Stewart, M. P.; Buriak, J. M. Exciton-Mediated Hydrosilylation on Photoluminescent Nanocrystalline Silicon. *J. Am. Chem. Soc.* **2001**, *123*, 7821–7830.
110. Sun, Q.-Y.; Smet, L. C. P. M. de; van Lagen, B.; Giesbers, M.; Thüne, P. C.; van Engelenburg, J.; Wolf, F. A. de; Zuilhof, H.; Sudhölter, E. J. R. Covalently Attached Monolayers on Crystalline Hydrogen-Terminated Silicon: Extremely Mild Attachment by Visible Light. *J. Am. Chem. Soc.* **2005**, *127*, 2514–2523.
111. Yang, Z.; los Reyes, G. B. de; Titova, L. V.; Sychugov, I.; Dasog, M.; Linnros, J.; Hegmann, F. A.; Veinot, J. G. C. Evolution of the Ultrafast Photoluminescence of Colloidal Silicon Nanocrystals with Changing Surface Chemistry. *ACS Photonics* **2015**, *2*, 595–605.
112. Nelles, J.; Sendor, D.; Ebbers, A.; Petrat, F. M.; Wiggers, H.; Schulz, C.; Simon, U. Functionalization of Silicon Nanoparticles via Hydrosilylation with 1-Alkenes. *Colloid. Polym. Sci.* **2007**, *285*, 729–736.
113. Höhle, I. M. D.; Kehrle, J.; Helbich, T.; Yang, Z.; Veinot, J. G. C.; Rieger, B. Diazonium Salts as Grafting Agents and Efficient Radical-Hydrosilylation Initiators for Freestanding Photoluminescent Silicon Nanocrystals. *Chem. Eur. J.* **2014**, *20*, 4212–4216.
114. Helbich, T.; Kloberg, M. J.; Sinelnikov, R.; Lyuleeva, A.; Veinot, J. G. C.; Rieger, B. Diaryliodonium Salts as Hydrosilylation Initiators for the Surface Functionalization of Silicon Nanomaterials and Their Collaborative Effect as Ring Opening Polymerization Initiators. *Nanoscale* **2017**, *9*, 7739–7744.
115. Mobarok, M. H.; Purkait, T. K.; Islam, M. A.; Miskolzie, M.; Veinot, J. G. C. Instantaneous Functionalization of Chemically Etched Silicon Nanocrystal Surfaces. *Angew. Chem. Int. Ed.* **2017**, *56*, 6073–6077.

116. Islam, M. A.; Mobarok, M. H.; Sinelnikov, R.; Purkait, T. K.; Veinot, J. G. C. Phosphorus Pentachloride Initiated Functionalization of Silicon Nanocrystals. *Langmuir* **2017**, *33*, 8766–8773.
117. Tilley, R. D.; Warner, J. H.; Yamamoto, K.; Matsui, I.; Fujimori, H. Micro-Emulsion Synthesis of Monodisperse Surface Stabilized Silicon Nanocrystals. *Chem. Comm.* **2005**, *14*, 1833–1835.
118. Warner, J. H.; Hoshino, A.; Yamamoto, K.; Tilley, R. D. Water-Soluble Photoluminescent Silicon Quantum Dots. *Angew. Chem. Int. Ed.* **2005**, *44*, 4550–4554.
119. Purkait, T. K.; Iqbal, M.; Wahl, M. H.; Gottschling, K.; Gonzalez, C. M.; Islam, M. A.; Veinot, J. G. C. Borane-Catalyzed Room-Temperature Hydrosilylation of Alkenes/Alkynes on Silicon Nanocrystal Surfaces. *J. Am. Chem. Soc.* **2014**, *136*, 17914–17917.
120. Holland, J. M.; Stewart, M. P.; Allen, M. J.; Buriak, J. M. Metal Mediated Reactions on Porous Silicon Surfaces. *J. Solid State Chem.* **1999**, *147*, 251–258.
121. Yang, Z.; Wahl, M. H.; Veinot, J. G. Size-Independent Organosilane Functionalization of Silicon Nanocrystals Using Wilkinson's Catalyst. *Can. J. Chem.* **2014**, *92*, 951–957.
122. Liao, Y.-C.; Roberts, J. T. Self-Assembly of Organic Monolayers on Aerosolized Silicon Nanoparticles. *J. Am. Chem. Soc.* **2006**, *128*, 9061–9065.
123. Mangolini, L.; Kortshagen, U. Plasma-Assisted Synthesis of Silicon Nanocrystal Inks. *Adv. Mater.* **2007**, *19*, 2513–2519.
124. Jariwala, B. N.; Dewey, O. S.; Stradins, P.; Ciobanu, C. V.; Agarwal, S. In Situ Gas-Phase Hydrosilylation of Plasma-Synthesized Silicon Nanocrystals. *ACS Appl. Mater. Interfaces* **2011**, *3*, 3033–3041.
125. Rogozhina, E.; Belomoin, G.; Smith, A.; Abuhassan, L.; Barry, N.; Akcakir, O.; Braun, P. V.; Nayfeh, M. H. Si–N linkage in Ultrabright, Ultrasmall Si Nanoparticles. *Appl. Phys. Lett.* **2001**, *78*, 3711–3713.
126. Bell, J. P.; Cloud, J. E.; Cheng, J.; Ngo, C.; Kodambaka, S.; Sellinger, A.; Ratanathanawongs Williams, S. K.; Yang, Y. N-Bromosuccinimide-Based Bromination and Subsequent Functionalization of Hydrogen-Terminated Silicon Quantum Dots. *RSC Adv.* **2014**, *4*, 51105–51110.
127. Pavesi, L.; Lockwood, D. J. *Silicon Fundamentals for Photonics Applications, In: Silicon Photonics*; Springer-Verlag Berlin: Heidelberg, 2004.
128. Furukawa, S.; Miyasato, T. Three-Dimensional Quantum Well Effects in Ultrafine Silicon Particles. *Jpn. J. Appl. Phys.*, *27*, L2207.
129. Furukawa, S.; Miyasato, T. Quantum Size Effects on the Optical Band Gap of Microcrystalline Si. *Phys. Rev. B* **1988**, *38*, 5726–5729.
130. Takagi, H.; Ogawa, H.; Yamazaki, Y.; Ishizaki, A.; Nakagiri, T. Quantum Size Effects on Photoluminescence in Ultrafine Si Particles. *Appl. Phys. Lett.* **1990**, *56*, 2379–2380.

131. Hybertsen, M. S. Absorption and Emission of Light in Nanoscale Silicon Structures. *Phys. Rev. Lett.* **1994**, *72*, 1514–1517.
132. Kovalev, D.; Heckler, H.; Ben-Chorin, M.; Polisski, G.; Schwartzkopff, M.; Koch, F. Breakdown of the k Conservation Rule in Si Nanocrystals. *Phys. Rev. Lett.* **1998**, *81*, 2803–2806.
133. Daldosso, N.; Pavesi, L. Nanosilicon Photonics. *Laser & Photon. Rev.* **2009**, *3*, 508–534.
134. Mastronardi, M. L.; Maier-Flaig, F.; Faulkner, D.; Henderson, E. J.; Kubel, C.; Lemmer, U.; Ozin, G. A. Size-Dependent Absolute Quantum Yields for Size-Separated Colloidally-Stable Silicon Nanocrystals. *Nano Lett.* **2012**, *12*, 337–342.
135. Wang, Y.; Herron, N. Nanometer-Sized Semiconductor Clusters: Materials Synthesis, Quantum Size Effects, and Photophysical Properties. *J. Phys. Chem.* **1991**, *95*, 525–532.
136. Shiohara, A.; Hanada, S.; Prabakar, S.; Fujioka, K.; Lim, T. H.; Yamamoto, K.; Northcote, P. T.; Tilley, R. D. Chemical Reactions on Surface Molecules Attached to Silicon Quantum Dots. *J. Am. Chem. Soc.* **2010**, *132*, 248–253.
137. Dasog, M.; Yang, Z.; Regli, S.; Atkins, T. M.; Faramus, A.; Singh, M. P.; Muthuswamy, E.; Kauzlarich, S. M.; Tilley, R. D.; Veinot, J. G. C. Chemical Insight Into the Origin of Red and Blue Photoluminescence Arising From Freestanding Silicon Nanocrystals. *ACS Nano* **2013**, *7*, 2676–2685.
138. Yu, Y.; Fan, G.; Fermi, A.; Mazzaro, R.; Morandi, V.; Ceroni, P.; Smilgies, D.-M.; Korgel, B. A. Size-Dependent Photoluminescence Efficiency of Silicon Nanocrystal Quantum Dots. *J. Phys. Chem. C* **2017**, *121*, 23240–23248.
139. Zhou, Z.; Brus, L.; Friesner, R. Electronic Structure and Luminescence of 1.1- and 1.4-nm Silicon Nanocrystals: Oxide Shell versus Hydrogen Passivation. *Nano Lett.* **2003**, *3*, 163–167.
140. Scheres, L.; Rijksen, B.; Giesbers, M.; Zuilhof, H. Molecular Modeling of Alkyl and Alkenyl Monolayers on Hydrogen-Terminated Si(111). *Langmuir* **2011**, *27*, 972–980.
141. M. V. Wolkin, J. Jorne, P. M. Fauchet, G. Allan, C. Delerue. Electronic States and Luminescence in Porous Silicon Quantum Dots: The Role of Oxygen. *Phys. Rev. Lett.* **1999**, *82*, 197–200.
142. Chen, C.-L.; Zeng, J.; Bao, N.; Dai, H.; Gu, H.-Y. Oxygen Backed Silicon Hydride in Correlation with the Photoluminescence of Silicon Nano-Crystals. *RSC Adv.* **2017**, *7*, 44655–44658.
143. Mastronardi, M. L.; Chen, K. K.; Liao, K.; Casillas, G.; Ozin, G. A. Size-Dependent Chemical Reactivity of Silicon Nanocrystals with Water and Oxygen. *J. Phys. Chem. C* **2014**, *119*, 826–834.
144. Lockwood, R.; Yang, Z.; Sammynaiken, R.; Veinot, J. G. C.; Meldrum, A. Light-Induced Evolution of Silicon Quantum Dot Surface Chemistry—Implications for Photoluminescence, Sensing, and Reactivity. *Chem. Mater.* **2014**, *26*, 5467–5474.

145. los Reyes, G. B. de; Dasog, M.; Na, M.; Titova, L. V.; Veinot, J. G. C.; Hegmann, F. A. Charge Transfer State Emission Dynamics in Blue-Emitting Functionalized Silicon Nanocrystals. *Phys. Chem. Chem. Phys.* **2015**, *17*, 30125–30133.
146. Wang, L.; Li, Q.; Wang, H.-Y.; Huang, J.-C.; Zhang, R.; Chen, Q.-D.; Xu, H.-L.; Han, W.; Shao, Z.-Z.; Sun, H.-B. Ultrafast Optical Spectroscopy of Surface-Modified Silicon Quantum Dots: Unraveling the Underlying Mechanism of the Ultrabright and Color-Tunable Photoluminescence. *Light Sci. Appl.* **2015**, *4*, e245.
147. Li, Q.; Luo, T.-Y.; Zhou, M.; Abroshan, H.; Huang, J.; Kim, H. J.; Rosi, N. L.; Shao, Z.; Jin, R. Silicon Nanoparticles with Surface Nitrogen: 90% Quantum Yield with Narrow Luminescence Bandwidth and the Ligand Structure Based Energy Law. *ACS Nano* **2016**, *10*, 8385–8393.
148. Le, T.-H.; Jeong, H.-D. The Effects of Electronic Coupling Between Capping Molecules and Quantum Dots on the Light Absorption and Emission of Octyl, Styryl, and 4-Ethynylstyryl Terminated Silicon Quantum Dots. *Phys. Chem. Chem. Phys.* **2014**, *16*, 18821–18826.
149. Li, H.; Wu, Z.; Zhou, T.; Sellinger, A.; Lusk, M. T. Tailoring the Optical Gap of Silicon Quantum Dots Without Changing Their Size. *Phys. Chem. Chem. Phys.* **2014**, *16*, 19275–19281.
150. Abdelhameed, M.; Martir, D. R.; Chen, S.; Xu, W. Z.; Oyeneye, O. O.; Chakrabarti, S.; Zysman-Colman, E.; Charpentier, P. A. Tuning the Optical Properties of Silicon Quantum Dots via Surface Functionalization with Conjugated Aromatic Fluorophores. *Sci. Rep.* **2018**, *8*, 3050.
151. Sommer, A.; Cimpean, C.; Kunz, M.; Oelsner, C.; Kupka, H. J.; Kryschi, C. Ultrafast Excitation Energy Transfer in Vinylpyridine Terminated Silicon Quantum Dots. *J. Phys. Chem. C* **2011**, *115*, 22781–22788.
152. Groenewegen, V.; Kuntermann, V.; Haarer, D.; Kunz, M.; Kryschi, C. Excited-State Relaxation Dynamics of 3-Vinylthiophene-Terminated Silicon Quantum Dots. *J. Phys. Chem. C* **2010**, *114*, 11693–11698.
153. Bhattacharjee, S.; Rietjens, I. M. C. M.; Singh, M. P.; Atkins, T. M.; Purkait, T. K.; Xu, Z.; Regli, S.; Shukaliak, A.; Clark, R. J.; Mitchell, B. S. *et al.* Cytotoxicity of Surface-Functionalized Silicon and Germanium Nanoparticles: The Dominant Role of Surface Charges. *Nanoscale* **2013**, *5*, 4870–4883.
154. Tu, C.; Ma, X.; House, A.; Kauzlarich, S. M.; Louie, A. Y. PET Imaging and Biodistribution of Silicon Quantum Dots in Mice. *ACS Med. Chem. Lett.* **2011**, *2*, 285–288.
155. McVey, B. F. P.; Prabakar, S.; Gooding, J. J.; Tilley, R. D. Solution Synthesis, Surface Passivation, Optical Properties, Biomedical Applications, and Cytotoxicity of Silicon and Germanium Nanocrystals. *ChemPlusChem* **2016**, 60–73.
156. Gonzalez, C. M.; Iqbal, M.; Dasog, M.; Piercey, D. G.; Lockwood, R.; Klapötke, T. M.; Veinot, J. G. C. Detection of High-Energy Compounds Using Photoluminescent Silicon Nanocrystal Paper Based Sensors. *Nanoscale* **2014**, *6*, 2608–2612.



157. Campos, B. B.; Algarra, M.; Alonso, B.; Casado, C. M.; Jiménez-Jiménez, J.; Rodríguez-Castellón, E.; Esteves da Silva, J. C. G. Fluorescent Sensor for Cr(VI) Based in Functionalized Silicon Quantum Dots with Dendrimers. *Talanta* **2015**, *144*, 862–867.
158. Zhang, J.; Yu, S.-H. Highly Photoluminescent Silicon Nanocrystals for Rapid, Label-Free and Recyclable Detection of Mercuric Ions. *Nanoscale* **2014**, *6*, 4096–4101.
159. Zhao, J.; Deng, J.; Yi, Y.; Li, H.; Zhang, Y.; Yao, S. Label-Free Silicon Quantum Dots as Fluorescent Probe for Selective and Sensitive Detection of Copper Ions. *Talanta* **2014**, *125*, 372–377.
160. Ban, R.; Zheng, F.; Zhang, J. A Highly Sensitive Fluorescence Assay for 2,4,6-trinitrotoluene Using Amine-Capped Silicon Quantum Dots as a Probe. *Anal. Methods* **2015**, *7*, 1732–1737.
161. Lou, Y.; Zhao, Y.; Chen, J.; Zhu, J.-J. Metal Ions Optical Sensing by Semiconductor Quantum Dots. *J. Mater. Chem. C* **2014**, *2*, 595–613.
162. Wu, P.; Zhao, T.; Wang, S.; Hou, X. Semiconductor Quantum Dots-Based Metal Ion Probes. *Nanoscale* **2014**, *6*, 43–64.
163. Yi, Y.; Deng, J.; Zhang, Y.; Li, H.; Yao, S. Label-Free Si Quantum Dots as Photoluminescence Probes for Glucose Detection. *Chem. Commun.* **2013**, *49*, 612–614.
164. Zhang, X.; Chen, X.; Kai, S.; Wang, H.-Y.; Yang, J.; Wu, F.-G.; Chen, Z. Highly Sensitive and Selective Detection of Dopamine Using One-Pot Synthesized Highly Photoluminescent Silicon Nanoparticles. *Anal. Chem.* **2015**, *87*, 3360–3365.
165. Zhang, Z. H.; Lockwood, R.; Veinot, J.; Meldrum, A. Detection of Ethanol and Water Vapor with Silicon Quantum Dots Coupled to an Optical Fiber. *Sens. Actuator. B: Chem.* **2013**, *181*, 523–528.
166. Lin, J.; Wang, Q. Role of Novel Silicon Nanoparticles in Luminescence Detection of a Family of Antibiotics. *RSC Adv.* **2015**, *5*, 27458–27463.
167. Yi, Y.; Zhu, G.; Liu, C.; Huang, Y.; Zhang, Y.; Li, H.; Zhao, J.; Yao, S. A Label-Free Silicon Quantum Dots-Based Photoluminescence Sensor for Ultrasensitive Detection of Pesticides. *Anal. Chem.* **2013**, *85*, 11464–11470.
168. Priolo, F.; Gregorkiewicz, T.; Galli, M.; Krauss, T. F. Silicon Nanostructures for Photonics and Photovoltaics. *Nat. Nanotechnol.* **2014**, *9*, 19–32.
169. Yoshikawa, K.; Kawasaki, H.; Yoshida, W.; Irie, T.; Konishi, K.; Nakano, K.; Uto, T.; Adachi, D.; Kanematsu, M.; Uzu, H. *et al.* Silicon Heterojunction Solar Cell with Interdigitated Back Contacts for a Photoconversion Efficiency Over 26%. *Nat. Energy* **2017**, *2*, 17032.
170. Shockley, W.; Queisser, H. J. Detailed Balance Limit of Efficiency of p-n Junction Solar Cells. *J. Appl. Phys.* **1961**, *32*, 510–519.
171. Pi, X.; Li, Q.; Li, D.; Yang, D. Spin-Coating Silicon-Quantum-Dot Ink to Improve Solar Cell Efficiency. *Sol. Energy Mater. Sol. Cells* **2011**, *95*, 2941–2945.

172. Švrček, V.; Slaoui, A.; Muller, J.-C. Silicon Nanocrystals as Light Converter for Solar Cells. *Thin Solid Films* **2004**, *451-452*, 384–388.
173. Cho, E.-C.; Park, S.; Hao, X.; Song, D.; Conibeer, G.; Park, S.-C.; Green, M. A. Silicon Quantum Dot/Crystalline Silicon Solar Cells. *Nanotechnology* **2008**, *19*, 245201.
174. Basu, I.; Mandali, A. K.; Samanta, P. K.; Kumar, V.; Hussain, M. A.; Abhilash; Kumar, A.; Shashank, S.; Singh, S. K.; Anubhav, K. Hot Carrier Solar Cell (HCSC): A New Generation Nano-Structured Solar Cell. In *2017 8th Industrial Automation and Electromechanical Engineering Conference (IEMECON)*, 16-18 August, 2017, Sasin Graduate Institute of Business Administration of Chulalongkorn University, Bangkok, Thailand; Chakrabarti, S., Saha, H. N., Eds.; IEEE: [Piscataway, NJ], 2017; pp 297–299.
175. Aliberti, P.; Shrestha, S. K.; Teuscher, R.; Zhang, B.; Green, M. A.; Conibeer, G. J. Study of Silicon Quantum Dots in a SiO<sub>2</sub> Matrix for Energy Selective Contacts Applications. *Sol. Energy Mater. Sol. Cells* **2010**, *94*, 1936–1941.
176. Shrestha, S. K.; Aliberti, P.; Conibeer, G. J. Energy Selective Contacts for Hot Carrier Solar Cells. *Sol. Energy Mater. Sol. Cells* **2010**, *94*, 1546–1550.
177. Conibeer, G. J.; Jiang, C.-W.; König, D.; Shrestha, S.; Walsh, T.; Green, M. A. Selective Energy Contacts for Hot Carrier Solar Cells. *Thin Solid Films* **2008**, *516*, 6968–6973.
178. Saeed, S.; Jong, E. M. L. D. de; Dohnalova, K.; Gregorkiewicz, T. Efficient Optical Extraction of Hot-Carrier Energy. *Nat. Commun.* **2014**, *5*, 4665.
179. Beard, M. C.; Knutsen, K. P.; Yu, P.; Luther, J. M.; Song, Q.; Metzger, W. K.; Ellingson, R. J.; Nozik, A. J. Multiple Exciton Generation in Colloidal Silicon Nanocrystals. *Nano Lett.* **2007**, *7*, 2506–2512.
180. Trinh, M. T.; Limpens, R.; Boer, W. D. A. M. de; Schins, J. M.; Siebbeles, L. D. A.; Gregorkiewicz, T. Direct Generation of Multiple Excitons in Adjacent Silicon Nanocrystals Revealed by Induced Absorption. *Nat. Photonics* **2012**, *6*, 316–321.
181. Niesar, S.; Fabian, W.; Petermann, N.; Herrmann, D.; Riedle, E.; Wiggers, H.; Brandt, M. S.; Stutzmann, M. Efficiency Enhancement in Hybrid P3HT/Silicon Nanocrystal Solar Cells. *Green* **2011**, *1*, 339–352.
182. Liu, C.-Y.; Holman, Z. C.; Kortshagen, U. R. Hybrid Solar Cells From P3HT and Silicon Nanocrystals. *Nano Lett.* **2009**, *9*, 449–452.
183. Niesar, S.; Dietmueller, R.; Nesswetter, H.; Wiggers, H.; Stutzmann, M. Silicon/Organic Semiconductor Heterojunctions for Solar Cells. *Phys. Status Solidi (a)* **2009**, *295*, 2775–2781.
184. Liu, C.-Y.; Holman, Z. C.; Kortshagen, U. R. Optimization of Si NC/P3HT Hybrid Solar Cells. *Adv. Funct. Mater.* **2010**, *20*, 2157–2164.
185. Islam, M. A.; Purkait, T. K.; Mobarok, M. H.; Hoehlein, I. M. D.; Sinelnikov, R.; Iqbal, M.; Azulay, D.; Balberg, I.; Millo, O.; Rieger, B. *et al.* Grafting Poly(3-hexylthiophene) from Silicon Nanocrystal Surfaces: Synthesis and Properties of a

Functional Hybrid Material with Direct Interfacial Contact. *Angew. Chem. Int. Ed.* **2016**, *55*, 7393–7397.

186. Li, Z. F.; Ruckenstein, E. Water-Soluble Poly(acrylic acid) Grafted Luminescent Silicon Nanoparticles and Their Use as Fluorescent Biological Staining Labels. *Nano Lett.* **2004**, *4*, 1463–1467.

187. Alsharif, N. H.; Berger, C. E. M.; Varanasi, S. S.; Chao, Y.; Horrocks, B. R.; Datta, H. K. Alkyl-Capped Silicon Nanocrystals Lack Cytotoxicity and Have Enhanced Intracellular Accumulation in Malignant Cells via Cholesterol-Dependent Endocytosis. *Small* **2009**, *5*, 221–228.

188. Zhai, Y.; Dasog, M.; Snitynsky, R. B.; Purkait, T. K.; Aghajamali, M.; Hahn, A. H.; Sturdy, C. B.; Lowary, T. L.; Veinot, J. G. C. Water-Soluble Photoluminescent d-Mannose and l-Alanine Functionalized Silicon Nanocrystals and Their Application to Cancer Cell Imaging. *J. Mater. Chem. B* **2014**, *2*, 8427–8433.

189. Zhong, Y.; Peng, F.; Bao, F.; Wang, S.; Ji, X.; Yang, L.; Su, Y.; Lee, S.-T.; He, Y. Large-Scale Aqueous Synthesis of Fluorescent and Biocompatible Silicon Nanoparticles and Their Use as Highly Photostable Biological Probes. *J. Am. Chem. Soc.* **2013**, *135*, 8350–8356.

190. He, Y.; Zhong, Y.; Peng, F.; Wei, X.; Su, Y.; Lu, Y.; Su, S.; Gu, W.; Liao, L.; Lee, S.-T. One-Pot Microwave Synthesis of Water-Dispersible, Ultraphoto- and pH-Stable, and Highly Fluorescent Silicon Quantum Dots. *J. Am. Chem. Soc.* **2011**, *133*, 14192–14195.

191. Zhong, Y.; Peng, F.; Wei, X.; Zhou, Y.; Wang, J.; Jiang, X.; Su, Y.; Su, S.; Lee, S.-T.; He, Y. Microwave-Assisted Synthesis of Biofunctional and Fluorescent Silicon Nanoparticles Using Proteins as Hydrophilic Ligands. *Angew. Chem. Int. Ed.* **2012**, *51*, 8485–8489.

192. Erogbogbo, F.; Yong, K.-T.; Roy, I.; Hu, R.; Law, W.-C.; Zhao, W.; Ding, H.; Wu, F.; Kumar, R.; Swihart, M. T. *et al.* In Vivo Targeted Cancer Imaging, Sentinel Lymph Node Mapping and Multi-Channel Imaging with Biocompatible Silicon Nanocrystals. *ACS Nano* **2011**, *5*, 413–423.

193. Tu, C.; Ma, X.; Pantazis, P.; Kauzlarich, S. M.; Louie, A. Y. Paramagnetic, Silicon Quantum Dots for Magnetic Resonance and Two-Photon Imaging of Macrophages. *J. Am. Chem. Soc.* **2010**, *132*, 2016–2023.

194. Cheng, X.; Hinde, E.; Owen, D. M.; Lowe, S. B.; Reece, P. J.; Gaus, K.; Gooding, J. J. Enhancing Quantum Dots for Bioimaging using Advanced Surface Chemistry and Advanced Optical Microscopy: Application to Silicon Quantum Dots (SiQDs). *Adv. Mater.* **2015**, *27*, 6144–6150.

195. Joo, J.; Liu, X.; Kotamraju, V. R.; Ruoslahti, E.; Nam, Y.; Sailor, M. J. Gated Luminescence Imaging of Silicon Nanoparticles. *ACS Nano* **2015**, *9*, 6233–6241.

196. Ji, X.; Peng, F.; Zhong, Y.; Su, Y.; Jiang, X.; Song, C.; Yang, L.; Chu, B.; Lee, S.-T.; He, Y. Highly Fluorescent, Photostable, and Ultrasmall Silicon Drug Nanocarriers for

- Long-Term Tumor Cell Tracking and In-Vivo Cancer Therapy. *Adv. Mater.* **2015**, *27*, 1029–1034.
197. Jambois, O.; Rinnert, H.; Devaux, X.; Vergnat, M. Photoluminescence and Electroluminescence of Size-Controlled Silicon Nanocrystallites Embedded in SiO<sub>2</sub> Thin Films. *J. Appl. Phys.* **2005**, *98*, 46105.
198. Cho, K. S.; Park, N.-M.; Kim, T.-Y.; Kim, K.-H.; Sung, G. Y.; Shin, J. H. High Efficiency Visible Electroluminescence From Silicon Nanocrystals Embedded in Silicon Nitride Using a Transparent Doping Layer. *Appl. Phys. Lett.* **2005**, *86*, 71909.
199. Cheng, K.-Y.; Anthony, R.; Kortshagen, U. R.; Holmes, R. J. High-Efficiency Silicon Nanocrystal Light-Emitting Devices. *Nano Lett.* **2011**, *11*, 1952–1956.
200. Maier-Flaig, F.; Kübel, C.; Rinck, J.; Bocksrocker, T.; Scherer, T.; Prang, R.; Powell, A. K.; Ozin, G. A.; Lemmer, U. Looking Inside a Working SiLED. *Nano Lett.* **2013**, *13*, 3539–3545.
201. Klajn, R.; Wesson, P. J.; Bishop, K. J. M.; Grzybowski, B. A. Writing Self-Erasing Images Using Metastable Nanoparticle "Inks". *Angew. Chem. Int. Ed.* **2009**, *48*, 7035–7039.